TESIS DE LA UNIVERSIDAD
DE ZARAGOZA

2020

79

José Antonio Altabas Navarro

Directly Phase Modulated Transmitters and Coherent Recivers for Future Passive Optical Networks (PON)

Departamento
Ingeniería Electrónica y Comunicaciones

Director/es
Garcés Gregorio, Juan Ignacio
Lázaro Villa, José Antonio

ISSN 2254-7606

Prensas de la Universidad
Universidad Zaragoza

ISSN 2254-7606

Universidad Zaragoza
1542

Tesis Doctoral

DIRECTLY PHASE MODULATED TRANSMITTERS AND COHERENT RECIVERS FOR FUTURE PASSIVE OPTICAL NETWORKS (PON)

Autor

José Antonio Altabas Navarro

Director/es

Garcés Gregorio, Juan Ignacio
Lázaro Villa, José Antonio

UNIVERSIDAD DE ZARAGOZA
Ingeniería Electrónica y Comunicaciones

2020

UNIVERSIDAD DE ZARAGOZA
Departamento de Ingeniería Electrónica y Comunicaciones

ESCUELA DE INGENIERÍA Y ARQUITECTURA

PHD THESIS

Directly Phase Modulated Transmitters and Coherent Receivers for Future Passive Optical Networks (PON)

Transmisores Modulados Directamente en Fase y Receptores Coherentes para Futuras Redes Ópticas Pasivas (PON)

Author:
José Antonio Altabás Navarro
Supervisors:
Prof. Ignacio Garcés Gregorio
Prof. José Antonio Lázaro Villa

Zaragoza, October 10, 2019

To my parents
A mis padres

Acknowledgments

First of all, I would like to thank my supervisors, Profesor Ignacio Garcés Gregorio and Professor José Antonio Lázaro Villa. Thank you for all the support and the advises that you have given me along the thesis. Your guide through all these years has lead me to this day and I will thank you for it forever.

I would also thank to my colleagues David, Jesus, Carlos and Samael for all the time that we have spent together in the laboratory and outside of it. An special thank to David for being like a third supervisor of my thesis. I would also thank to all my GTF colleagues for their help and support during this years.

I would also like to express my gratitude to Idelfonso, Juan Jose and Jesper for giving me the opportunity to experience a different way of work in an international environment.

I would like to acknowledge the Spanish Ministry of Education, Culture and Sports through FPU grant (FPU-13/00620), the Spanish Ministry of Economy and Competitive through the research projects muCORE (TEC2013-46917-C2-2-R), SUNSET (TEC2014-59583-C2-1-R), FOANT (TEC2017-85752-R) and ALLIANCE (TEC2017-90034-C2-2-R) and the Spanish Diputacion General de Aragon through the grants T25 and T20_17R.

I would like to thank to all my friends from Torres de Berrellén, for being there to when I have needed you in the good and in the not that good moments. Thank you for your support all this time. Also, I would like to thank to my friends from Copenhaguen for all the support that they have given me every time that I have gone and specially in the last months after I moved in there.

Finally, I would like to thank to my family for accompanying me on the long road that has taken me to this point. I would like to especially thank my parents, Manuel and Encarna, for all the sacrifices that have been done to offer me the best opportunities and for the education that you have give me. There are not enough words to thank you everything. I also would like to remember my grandparents, who are not with me anymore but they will be always on my thoughts.

Finalmente, me gustaría agradecer a mi familia por acompañarme en el largo camino que me ha llevado hasta aquí. Me gustaría agradecer especialmente a mis padres, Manuel y Encarna, por todos los sacrificios que se han hecho para ofrecerme las mejores oportunidades *y por la educación que me han brindado. No hay suficientes palabras para agradecerle todo. También me gustaría recordar a mis abuelos, que ya no están conmigo, pero siempre estarán en mis pensamientos.*

Abstract

During the recent years, data traffic over optical access networks has grown exponentially due to new services such as cloud computing, video streaming, virtual and augmented reality, internet of things (IoT) and the converged optical and wireless networks for the 5G paradigm. These new services toughen the requirements of optical access networks, as can be higher data rates, longer reach and higher number of users. In order to address these requirements, this thesis has researched, developed and analyzed new transmitter and receiver technologies for two types of optical access networks that the research community has pointed as a possible candidates: ultra dense wavelength division multiplexing (uDWDM) networks and time and wavelength division multiplexing (TWDM) networks as the NG-PON2 networks and beyond.

uDWDM networks are based on relative low data rates, lower than 2.5 Gbps, which are fully dedicated to the final users. These relative low data rates are wavelength multiplexed using narrow frequency slots, as 12.5 GHz or 6.25 GHz. In this thesis, directly phase modulated transmitters are proposed as potential candidates for these uDWDM networks. Specifically, 1 Gbps directly phase modulated distributed feedback laser (DFBs); 1 Gbps directly phase modulated reflective semiconductor optical amplifier (RSOAs) pumped by vertical cavity surface emitting laser (VCSELs); and 1.25 Gbps and 2.5 Gbps directly phase modulated VCSELs are proposed. These directly phase modulated emitted signals are received using a single photodiode (PD) heterodyne receiver in order to keep the cost as low as possible. The combination of these directly phase modulated transmitters with single PD heterodyne receivers has been probed as a promising candidate for optical access networks based on uDWDM technologies. These combinations provide sensitivities that range between -39.5 dBm and -52 dBm, which can be translated into power budgets between 38.5 dB and 51 dB and therefore into splitting ratios from 128 to 1024 after 50 km SSMF transmission.

Additionally, the links formed by 1 Gbps directly phase modulated DFBs or 1 Gbps directly phase modulated RSOAs pumped by VCSELs with a single PD heterodyne receiver are used as the uplink in bidirectional channels. These uplinks are combined with downlinks formed by Nyquist-DPSK signals generated using a Mach-Zehnder modulator (MZM) and received with a single PD heterodyne receiver. As part of the bidirectional channel analysis, the feasibility of using low cost local oscillators (LOs), as DFBs or VCSELs, in the single PD heterodyne

receiver has been studied. These bidirectional channels are also promising candidates for the future uDWDM networks because this thesis has proved that they may provide a full-duplex 1 Gbps communication link using frequency slots as small as 6.25 GHz or 5 GHz. These bidirectional channels exhibit power budgets from 37 dB to 42 dB and so the possibility of using splitting ratios of 128 or 256 after 50 km SSMF transmission.

This thesis has also researched and developed quasicoherent receivers for NG-PON2 networks and beyond. This type of networks are based on high data rate links, as 10 Gbps for NG-PON2 networks and 25 Gbps for networks beyond NG-PON2, in a multiwavelength environment where the users are multiplexed in time and wavelength (TWDM). The quasicoherent receiver uses the coherent amplification due to heterodyne reception in such a way that the sensitivity of the receiver is improved in comparison with the direct detection schemes. The quasicoherent receiver shows a polarization independent operation which is an important feature for coherent receivers. Additionally, the quasicoherent receiver is colorless because it allows to select the operation channel without optical filters by tuning the wavelength of the LO. The 10 Gbps quasicoherent receiver has exhibited a sensitivity of -35.2 dBm, which will allow to have a power budget of 35.64 dB and a splitting ratio of 128 after 20 km SSMF transmission.

The combination of the quasicoherent receiver with FFE/DFE equalizers allows to overcome the chromatic dispersion of C-band wavelength and permits a 25 Gbps link over 20 km SSMF. The 25 Gbps quasicoherent receiver with a high performance FFE/DFE equalization shows a best sensitivity of -30.5 dBm and it leads to a power budget of 25 dB. If the low complexity FFE/DFE equalizer is employed the sensitivity drops to -27 dBm and the power budget also drops to 23 dBm. In both cases, the 25 Gbps quasicoherent receiver with FFE/DFE equalization allows a splitting ratio of 32 after 20 km SSMF transmission.

Resumen y Conclusiones

Resumen

En los últimos años, el trafico de dato transmitido en las redes ópticas de acceso ha crecido exponencialmente debido a nuevos servicios como pueden ser la computación en la nube, el video online, la realidad virtual y aumentada, el internet de las cosas (IoT) y la convergencia entre las redes ópticas y redes inalámbricas en el paradigma del 5G. Estos nuevos servicios endurecen los requerimientos de las redes ópticas de acceso, como pueden ser unas tasas de datos mas altas, un mayor alcance y un mayor numero de usuarios. Para abordar estos requerimientos, esta tesis ha investigado, desarrollado y analizado nuevas tecnologías para transmisores y receptores orientados a dos tipos de redes ópticas de acceso que la comunidad científica ha identificado como posibles candidatas. Estos dos tipos de redes ópticas son las redes uDWDM y las redes TWDM como las redes NG-PON2 y sus evoluciones.

Las redes uDWDM están basadas en la transmisión de tasas de datos relativamente bajas, por debajo de 2.5 Gbps, que son dedicadas en su totalidad a los usuarios finales. Estas tasas de datos relativamente bajas son multiplexadas en longitud de onda usando intervalos frecuenciales estrechos, del orden de 12.5 GHz o 6.25 GHz. En esta tesis, transmisores modulados directamente en fase se han propuesto como posibles candidatos para estas redes uDWDM. En concreto, se han propuesto un DFB modulado directamente en fase con una tasa de datos de 1 Gbps; un RSOA bombeado por VCSEL y modulado directamente en fase con una tasa de datos de 1 Gbps; y un mboxVCSEL modulado directamente en fase con una tasa de datos de 1.25 Gbps y 2.5 Gbps. Estas señales moduladas directamente en fase son recibidos con un receptor heterodino con un único PD para mantener el coste tan bajo como sea posible. La combinación de estos transmisores modulados directamente en fase con el receptor heterodino con un único PD ha sido probada como unos candidatos muy prometedores para las redes ópticas de acceso basadas en redes uDWDM. Estas combinaciones proveen de sensibilidades que varían entre -39.5 dBm y -52 dBm, que se traducen en balances de potencia que van desde 38.5 dB a 51 dB y por lo tanto en ratios de división o numero de usuarios de entre 128 y 1024 después de una transmisión de 50 km a través de SSMF.

Además, los links de 1 Gbps formados por la modulación directa de DFBs o de RSOAs bombeados por VCSELs y el receptor heterodino con un único PD son usados como enlace de

subida en canales bidireccionales. Estos enlaces de subida son combinados con enlaces de bajada basados en Nyquist-DPSK generada con un MZM y recibidos con un receptor heterodino de un único PD. Como parte de análisis de los canales bidireccionales, se ha analizado el estudio de la viabilidad del uso de LOs de bajo coste, como DFBs o VCSELs, em los receptores heterodinos con un único PD. Estos canales bidireccionales son también unos candidatos prometedores para las futuras redes uDWDM, ya que en esta tesis se ha probado que pueden proveer enlaces full-duplex de 1 Gbps usando intervalos frecuenciales tan pequeños como 6.25 GHz o 5 GHz. Estos canales bidireccionales tienen balances de potencia que van desde 37 dB a 42 dB y tienen posibles ratios de división de 128 o 256 después de una transmisión de 50 km a través de SSMF.

Esta tesis también ha investigado y desarrollado receptores quasicoherentes para redes NG-PON2 y sus evoluciones. Este tipo de redes esta basadas en altas tasas de datos, como 10 Gbps para redes NG-PON2 y 25 Gbps para las futuras evoluciones de NG-PON2, en entornos multi longitud de onda donde los usuarios son multiplexados en tiempo y longitud de onda (TWDM). El receptor quasicoherente usa la amplificación coherente gracias a la recepción heterodina y por tanto la sensibilidad del receptor es mejorada en comparación con los esquemas de detección directa. El receptor quasicoherente es independiente a la polarización, lo cual es una característica importante para los receptores coherentes. Además, el receptor quasicoherente permite seleccionar el canal de trabajo sin la necesidad de filtros ópticos y es un receptor independiente de la longitud de onda debido a que el canal de trabajo se puede elegir ajustando la longitud de onda del LO. El receptor quasicoherente de 10 Gbps muestra una sensibilidad -35.2 dBm y por tanto permite un balance de potencias de 35.64 dB y un ratio de división de 128 después de una transmisión de 40 km a través de SSMF.

La combinación del receptor quasicoherente con un ecualizador FFE/DFE permite combatir la dispersión cromática de la banda C y conseguir un link de 25 Gbps con un alcance de 40 km a través de SSMF. El receptor quasicoherente a 25 Gbps con ecualización FFE/DFE muestra una mejor sensibilidad de -30.5 dBm con el llamado ecualizador de altas prestaciones, lo que lleva a un balance de potencias de25 dB. Si se utilizada el llamado ecualizador de baja complejidad, la sensibilidad cae a -27 dBm y el balance de potencias cae a 23 dBm. En ambos casos, el receptor quasicoherente a 25 Gbps con ecualización FFE/DFE permite un ratio de división de 32 después de una transmisión de 20 km a través de SSMF.

En conclusión, esta tesis ha presentado transmisores (DFB, RSOA y VCSEL) modulados directamente en fase combinados con un receptor heterodino con un único PD como potenciales candidatos para las redes uDWDM. Esta tesis también ha presentados los receptores quasicoherentes como unos candidatos muy prometedores para las redes NG-PON2 y sus futuras evoluciones.

Conclusiones

En esta tesis, han sido investigados y desarrollados receptores y transmisores para la siguiente generación de redes ópticas de acceso. Buscando el cumplimiento de los requerimientos de estas futuras redes ópticas de acceso, tales como incrementar el alcance, incrementar el número de usuarios, incrementar la capacidad total de la red y reducir la latencia de la misma, pero manteniendo el coste tan bajo como sea posible, la tesis se ha centrado en dos tipos diferentes de redes ópticas pasivas: redes con multiplexación ultradensa en longitud de onda (uDWDM) y redes de acceso NG-PON2 y sus evoluciones.

En esta tesis se han investigado técnicas uDWDM que se basan en canales super estrechos contenidos en intervalos frecuenciales de 12.5 GHz o 6.25 GHz y que son asignados en exclusiva al usuario final. Este concepto se conoce como longitud de onda para el usuario (lambda-to-the-user) y generalmente requiere links con una relativa baja capacidad, en el rango de 1 Gbps, 1.25 Gbps o 2.5 Gbps, pero completamente dedicado al usuario final. Las redes de acceso NG-PON2 y sus evoluciones siguen el camino marcado por los actuales estándares, que se basan en links entre las oficinas centrales y los usuarios utilizando señales moduladas en intensidad (IM) y multiplexadas en tiempo (TDM). Las redes de acceso NG-PON2 y sus evoluciones incrementan la tasa de datos a 10 Gbps o 25 Gbps de los actuales 1.25 Gbps y 2.5 Gbps. Adicionalmente, introducen el concepto de multiplexación en tiempo y longitud de onda (TWDM), donde los usuarios finales son multiplexados en tiempo y longitud de onda simultáneamente.

Los transmisores modulados directamente en fase han sido investigados y desarrollados durante esta tesis para abordar los requerimientos de las redes uDWDM. En concreto, tres transmisores modulados directamente en fase han sido investigados: un transmisor de 1 Gbps basado en un DFB; un transmisor de 1 Gbps basado en un RSOA bombeado con un VCSEL; y un transmisor de 1.25 Gbps y 2.5 Gbps basado en un VCSEL. Estos transmisores modulados directamente en fase permiten incrementar la capacidad total de la red porque debido a que están modulados en fase, pueden transmitir la misma o una mayor tasa de datos con un espectro más compacto manteniendo un bajo coste. Además, un receptor heterodino basado en un único fotodiodo (PD) ha sido implementado evaluando su desempeño cuando se utilizan diferentes osciladores locales tales como DFBs o VCSELs. Este tipo de receptor permite la selección de un único canal de las redes uDWDM sin necesidad de filtros ópticos y permiten incrementar el alcance y el numero de usuarios de la red debido a la amplificación coherente de las señales recibidas. La combinación de estos transmisores modulados directamente en fase con el receptor heterodino basado en un único PD permite obtener altos balances de potencias que van desde 38.5 dB a 51 dB y que por tanto permiten ratios de división o numero de usuarios que van desde los 128 a los 1024. Por lo tanto, la viabilidad de utilizar DFBs, RSOAs y VCSELs modulados directamente en fase combinados con receptores heterodinos con un único PD han sido demostrados y son potentes candidatos para las futuras redes ópticas de acceso basadas en técnicas uDWDM.

Links con 1 Gbps de tasa de datos basado en la modulación directa de fase de DFBs o RSOAs bombeados con VCSELs han sido utilizados como links de subida en canales bidireccionales. Como canales de bajada de estos canales bidireccionales, se han utilizado modulaciones diferenciales de pase con conformado de pulso Nyquist (Nyquist-DPSK) generadas con un modulador Mach-Zehnder (MZM). Estos canales bidireccionales permiten obtener 1 Gbps full-duplex entre la oficina central y el usuario contenidos en intervalos frecuenciales tan pequeños como 6.25 GHz o 5 GHz. La modulación directa en fase del VCSEL permite obtener tasas de datos de 1.25 Gbps o 2.5 Gbps con un espectro compacto usando el transmisor mas barato posible. Estos canales bidireccionales proveen de un balance de potencia de 42 dB en el caso de usar DFBs y de 37 dB en el caso de usar RSOAs y que por tanto proveen de ratios de división de 256 y 128, respectivamente. Por lo tanto, la viabilidad de los canales bidireccionales contenidos en intervalos frecuenciales ultra estrechos, así como su contribución al incremento de la capacidad total de las futuras redes ópticas de acceso basadas en técnicas uDWDM.

En esta tesis, se ha desarrollado un receptor quasicoherente de 10 Gbps que permite abordar los requerimientos de las redes de acceso NG-PON2. Los receptores quasicoherentes utilizan la amplificación coherente para incrementar la sensibilidad del receptor ante señales IM, alcanzando balances de potencias de 35.64 dB. Esto permite incrementar el alcance y el ratio de división de la red, en este caso a 40 km y 128 usuarios con 10 Gbps por longitud de onda. El receptor quasicoherente también permite la operación multi longitud de onda sin necesidad de filtrado óptico. Esta operación multi longitud de onda es un requerimiento de las redes de acceso NG-PON2, donde cuatro longitudes de onda son multiplexadas con una tasa de datos de 10 Gbps por longitud de onda. Por lo tanto, el receptor quasicoherente ha sido desarrollado y probado durante esta tesis, convirtiéndolo en un atractivo candidato para las redes de acceso NG-PON2.

En esta tesis también se ha presentado un receptor quasicoherente de 25 Gbps combinado con un ecualizador FFE/DFE para abordar los requerimientos de las futuras evoluciones de las redes de acceso NG-PON2. Este receptor permite transmitir en banda C con suficiente sensibilidad gracias a la amplificación coherente y con un alcance remarcable superando los limites que impone la dispersión cromática. Este receptor quasicoherente de 25 Gbps provee de un balance de potencias tan alto como 23 dB después de una transmisión de 20 km sobre fibra óptica estándar (SSMF), lo cual se traduce en que puede dar servicio a 32 usuarios. La capacidad de operación multi longitud de onda en banda C de este receptor quasicoherente permitirá su uso en redes DWDM siguiendo el camino marcado por las redes NG-PON2 pero a una mayor tasa de datos. Por lo tanto, la combinación del receptor quasicoherente con la ecualización FFE/DFE ha sido probada y muestra unos resultados muy prometedores para las futuras evoluciones de las redes de acceso NG-PON2.

Contents

Acknowledgments **i**

Abstract **iii**

Resumen y Conclusiones **v**

1 List of Publications **1**

2 Introduction **9**

2.1 Basic PON technologies . . . 10

2.1.1 TDM PON . . . 12

2.1.2 WDM PON . . . 13

2.1.3 TWDM PON . . . 14

2.2 Advanced PON Technologies . . . 15

2.2.1 Advanced WDM PONs . . . 15

2.2.1.1 DWDM PON . . . 15

2.2.1.2 uDWDM PON . . . 19

2.2.2 Advanced Modulation Formats . . . 20

2.2.3 Coherent Technologies for PON . . . 27

2.2.4 Relation with the published works that are part of the compendium . . 36

3 Published works **39**

3.1 Paper I . . . 41

3.2 Paper II . . . 55

3.3 Paper III . . . 61

3.4 Paper IV . . . 67

3.5 Paper V . . . 75

4 Report **81**

4.1 Research objectives . . . 81

4.2 Methodology . . . 81

4.2.1 Directly-phase modulated transmitters . . . 82
4.2.2 Single PD heterodyne receivers for DPSK signals . . . 91
4.2.3 Quasi-coherent receiver . . . 96
4.3 Main contributions . . . 98
4.3.1 Phase modulated uDWDM access networks . . . 99
4.3.2 Intensity modulated optical access networks for NG-PON2 and beyond 107

5 Conclusions 113

List of Acronyms 137

List of Figures 145

List of Tables 147

A PON standards 149
A.1 ITU-T . . . 149
A.1.1 B-PON . . . 149
A.1.2 G-PON . . . 151
A.1.3 XG-PON . . . 153
A.1.4 NG-PON2 . . . 155
A.1.5 XGS-PON . . . 158
A.2 IEEE . . . 160
A.2.1 1G-EPON . . . 160
A.2.2 10G-EPON . . . 162
A.3 Future standard PON . . . 163

B Additional published works 165
B.1 Paper I . . . 167
B.2 Paper II . . . 173

C Description of Compendium Articles 179

Chapter 1

List of Publications

Reproduced articles

The articles included on the compendium are enlisted below:

1. Section 3.1: J. A. Altabas, D. Izquierdo, J. A. Lazaro, A. Lerin, F. Sotelo, and I. Garces, "1Gbps full-duplex links for ultra-dense-WDM 6.25GHz frequency slots in optical metro-access networks," *Optics Express*, vol. 24, no. 1, pp. 555–565, 2016

2. Section 3.2: J. A. Altabas, D. Izquierdo, J. A. Lazaro, and I. Garces, "Cost-Effective Transceiver Based on an RSOA and a VCSEL for Flexible uDWDM Networks," *IEEE Photonics Technology Letters*, vol. 28, no. 10, pp. 1111–1114, 2016

3. Section 3.3: J. A. Altabas, D. Izquierdo, J. A. Lazaro, and I. Garces, "Chirp-based direct phase modulation of VCSELs for cost-effective transceivers," *Optics Letters*, vol. 42, no. 3, pp. 583–586, 2017

4. Section 3.4: J. A. Altabas, G. Silva Valdecasa, L. F. Suhr, M. Didriksen, J. A. Lazaro, I. Garces, I. Tafur Monroy, A. T. Clausen, and J. B. Jensen, "Real-Time 10 Gbps Polarization Independent Quasicoherent Receiver for NG-PON2 Access Networks," *Journal of Lightwave Technology*, vol. 37, no. 2, pp. 651–656, 2019

5. Section 3.5: J. A. Altabas, L. F. Suhr, G. Silva Valdecasa, J. A. Lazaro, I. Garces, J. B. Jensen, and A. T. Clausen, "25Gbps Quasicoherent Receiver for Beyond NG-PON2 Access Networks," in *2018 European Conference on Optical Communication (ECOC)*, (Rome, Italy), p. We2.70, 2018

The following articles are considered relevant enough for being included as annex of the thesis even if they are excluded of the compendium:

1. Appendix B.1: J. A. Altabas, D. Izquierdo, J. Lazaro, and I. Garces, "1Gbps full-duplex 5GHz frequency slots uDWDM flexible Metro/Access Networks based on VCSEL-RSOA transceiver," in *2016 OptoElectronics and Communications Conference - International Conference on Photonics in Switching (OECC/PS)*, (Niigata, Japan), pp. WA1–5, 2016

2. Appendix B.2: J. A. Altabas, D. Izquierdo, J. A. Lazaro, and I. Garces, "1.25-2.5Gbps cost-effective transceiver based on directly phase modulated VCSEL for flexible access networks," in *2017 Optical Fiber Communications Conference and Exhibition (OFC)*, (Los Angeles, CA, USA), p. Th1K.4, 2017

Full list of publications

The journal articles, the conference contributions, book chapters and patents related with the thesis are enlisted below:

Journal articles

1. J. A. Altabas, D. Izquierdo, J. A. Lazaro, A. Lerin, F. Sotelo, and I. Garces, "1Gbps full-duplex links for ultra-dense-WDM 6.25GHz frequency slots in optical metro-access networks," *Optics Express*, vol. 24, no. 1, pp. 555–565, 2016

2. J. A. Altabas, D. Izquierdo, J. A. Lazaro, and I. Garces, "Cost-Effective Transceiver Based on an RSOA and a VCSEL for Flexible uDWDM Networks," *IEEE Photonics Technology Letters*, vol. 28, no. 10, pp. 1111–1114, 2016

3. R. Puerta, S. Rommel, J. A. Altabas, L. Pyndt, R. Idrissa, A. K. Sultanov, J. J. Vegas Olmos, and I. Tafur Monroy, "Multiband carrierless amplitude/phase modulation for ultra-wideband high data rate wireless communications," *Microwave and Optical Technology Letters*, vol. 58, no. 7, pp. 1603–1607, 2016

4. J. A. Altabas, D. Izquierdo, J. A. Lazaro, and I. Garces, "Chirp-based direct phase modulation of VCSELs for cost-effective transceivers," *Optics Letters*, vol. 42, no. 3, pp. 583–586, 2017

5. S. Sarmiento, J. A. Altabas, D. Izquierdo, I. Garces, S. Spadaro, and J. A. Lazaro, "Cost-Effective DWDM ROADM Design for Flexible Sustainable Optical Metro–Access Networks," *Journal of Optical Communications and Networking*, vol. 9, no. 12, pp. 1116–1124, 2017

6. J. A. Altabas, S. Rommel, R. Puerta, D. Izquierdo, J. I. Garces, J. A. Lazaro, J. J. V. Olmos, and I. T. Monroy, "Nonorthogonal Multiple Access and Carrierless Amplitude

Phase Modulation for Flexible Multiuser Provisioning in 5G Mobile Networks," *Journal of Lightwave Technology*, vol. 35, no. 24, pp. 5456–5463, 2017

7. J. A. Altabas, G. Silva Valdecasa, L. F. Suhr, M. Didriksen, J. A. Lazaro, I. Garces, I. Tafur Monroy, A. T. Clausen, and J. B. Jensen, "Real-Time 10 Gbps Polarization Independent Quasicoherent Receiver for NG-PON2 Access Networks," *Journal of Lightwave Technology*, vol. 37, no. 2, pp. 651–656, 2019

8. S. Sarmiento, J. A. Altabas, S. Spadaro, and J. A. Lazaro, "Experimental Assessment of 10 Gbps 5G Multicarrier Waveforms for High-Layer Split u-DWDM-PON-Based Fronthaul," *Journal of Lightwave Technology*, vol. 37, no. 10, pp. 2344–2351, 2019

International conference contributions

1. J. A. Altabas, J. A. Lazaro, F. Sotelo, and I. Garces, "Experimental Demonstration of Bandwidth Reduction using Nyquist Shaped PSK for Flexible udWDM," in *2015 Conference on Lasers and Electro-Optic (CLEO: 2015)*, (San Jose, CA, USA), p. JTh2A.70, 2015

2. J. A. Altabas, F. Sotelo, J. A. Lazaro, and I. Garces, "Experimental Bandwidth Optimization for Flexible PON Using Nyquist Shaped PSK," in *2015 Conference on Lasers and Electro-Optics Europe - European Quantum Electronics Conference (CLEO/Europe-EQEC)*, (Munich, Germany), pp. CI–2.4 SUN, 2015

3. J. A. Altabas, P. Arribas, D. Izquierdo, F. Sotelo, A. Lerin, J. M. Fabrega, J. A. Lazaro, I. Garces, and G. Junyent, "Survey of Faster-Than-Nyquist for Flexible Passive Optical Networks," in *2015 International Conference on Transparent Optical Networks (ICTON)*, (Budapest, Hungary), p. Mo.D1.3, 2015

4. J. A. Altabas, D. Izquierdo, F. Sotelo, I. Garces, J. A. Lazaro, A. Lerin, S. Spadaro, and G. Junyent, "Experimental demonstration of flex-grid udWDM with 6.25GHz full-duplex frequency slots for Metro/Access & Data Centers," in *2015 International Conference on Photonics in Switching (PS)*, (Florence, Italy), p. SC3, 2015

5. J. A. Altabas, D. Izquierdo, J. Lazaro, and I. Garces, "1Gbps full-duplex 5GHz frequency slots uDWDM flexible Metro/Access Networks based on VCSEL-RSOA transceiver," in *2016 OptoElectronics and Communications Conference - International Conference on Photonics in Switching (OECC/PS)*, (Niigata, Japan), pp. WA1–5, 2016

6. J. A. Altabas, D. Izquierdo, A. Pascual, S. Sarmiento, J. A. Lazaro, I. Garces, and A. Villafranca, "Design of flexible udWDM Metro-Access Network Devices assisted by High

Resolution Complex Spectroscopy," in *2016 International Conference on Transparent Optical Networks (ICTON)*, (Trento, Italy), p. Tu.D2.5, 2016

7. J. A. Lazaro, S. Spadaro, J. Perello, J. Gene, J. A. Altabas, A. Pages, D. Careglio, P. Barlet-Ros, A. Cabellos, and J. Sole-Pareta, "SUNSET: Sustainable network infrastructure enabling the future Digital Society," in *2016 International Conference on Transparent Optical Networks (ICTON)*, (Trento, Italy), p. Tu.C3.3, 2016

8. S. Sarmiento, R. Montero, J. A. Altabas, D. Izquierdo, F. Agraz, A. Pages, J. Perello, J. Gene, M. Alonso, A. Pascual, I. Garces, S. Spadaro, and J. A. Lazaro, "SDN-enabled flexible optical node designs and transceivers for sustainable metro-access networks convergence," in *2016 International Conference on Transparent Optical Networks (ICTON)*, (Trento, Italy), p. Th.A1.4, 2016

9. J. A. Altabas, D. Izquierdo, J. A. Lazaro, and I. Garces, "1.25-2.5Gbps cost-effective transceiver based on directly phase modulated VCSEL for flexible access networks," in *2017 Optical Fiber Communications Conference and Exhibition (OFC)*, (Los Angeles, CA, USA), p. Th1K.4, 2017

10. J. A. Altabas, D. Izquierdo, A. Lopez, M. A. Losada, J. Mateo, J. A. Lazaro, and I. Garces, "MultiCAP modulation for high spectral efficiency transmission over SI-POF," in *2017 Conference on Lasers and Electro-Optics Europe - European Quantum Electronics Conference (CLEO/Europe-EQEC)*, (Munich, Germany), pp. CI–4.5 SUN, 2017

11. L. Nadal, J. M. Fabrega, J. A. Altabas, D. Izquierdo, F. J. Vilchez, M. S. Moreolo, J. A. Lazaro, and I. Garces, "Transparent service delivery in elastic metro/access networks with cost-effective programmable transceivers," in *2017 International Conference on Transparent Optical Networks (ICTON)*, (Girona, Spain), p. Tu.C2.5, 2017

12. J. A. Altabas, S. Rommel, R. Puerta, D. Izquierdo, I. Garces, J. A. Lazaro, J. J. Vegas Olmos, and I. Tafur Monroy, "Non-Orthogonal Multiple Access and Carrierless Amplitude Phase Modulation for 5G Mobile Networks," in *2017 European Conference on Optical Communication (ECOC)*, (Gothenburg, Sweden), p. Tu.1.B.2, 2017

13. J. A. Altabas, G. Silva Valdecasa, M. Didriksen, J. A. Lazaro, I. Garces, I. Tafur Monroy, and J. B. Jensen, "Real-time 10Gbps polarization independent quasicoherent receiver for NG-PON2 access networks," in *2018 Optical Fiber Communications Conference and Exhibition (OFC)*, (San Diego, CA, USA), p. Th1A.3, 2018

14. J. A. Lazaro, M. Coves, S. Sarmiento, J. A. Altabas, and A. Lerin, "5G Connected Vehicles Supported by Optical Fiber Access," in *2018 International Conference on Transparent Optical Networks (ICTON)*, (Bucharest, Romania), p. Mo.B5.3, 2018

15. J. A. Altabas, D. Izquierdo, M. A. Losada, J. Clemente, S. Sarmiento, J. Mateo, J. A. Lazaro, and I. Garces, "Experimental demonstration of multiband CAP modulation for SI-POF links," in *2018 International Conference on Plastic Optical Fibers (POF)*, (Seattle, WA, USA), p. P19, 2018

16. S. Sarmiento, A. Gran, J. A. Altabas, M. Scalabroni, S. Spadaro, I. Garces, and J. A. Lazaro, "Experimental Assessment of 5-10Gbps 5G Multicarrier Waveforms with Intensity-Modulation Direct-Detection for PONs," in *2018 Photonics in Switching and Computing (PSC)*, (Limassol, Cyprus), p. Fr1C.5, 2018

17. J. A. Altabas, L. F. Suhr, G. Silva Valdecasa, J. A. Lazaro, I. Garces, J. B. Jensen, and A. T. Clausen, "25Gbps Quasicoherent Receiver for Beyond NG-PON2 Access Networks," in *2018 European Conference on Optical Communication (ECOC)*, (Rome, Italy), p. We2.70, 2018

18. J. Clemente, D. Izquierdo, P. J. Reyes-Iglesias, A. Ortega-Monux, J. A. Altabas, I. Molina-Fernandez, G. Wanguemert-Perez, J. de Oliva-Rubio, and I. Garces, "Experimental Demonstration of Colorless Operation of an Integrated 120 Coherent Receiver," in *2018 European Conference on Optical Communication (ECOC)*, (Rome, Italy), p. We3H.2, 2018

19. D. Izquierdo, J. A. Altabas, P. Millan, J. Clemente, J. A. Lazaro, S. Rommel, R. Puerta, J. J. Vegas Olmos, I. Tafur Monroy, and I. Garces, "Non-Orthogonal Multiple Access based on Carrierless Amplitude Phase format for coherent PON flexible resource provisioning," in *2019 Conference on Lasers and Electro-Optics Europe - European Quantum Electronics Conference (CLEO/Europe-EQEC)*, (Munich, Germany), pp. CI–P.15 SUN, 2019

20. S. Sarmiento, J. A. Altabas, S. Spadaro, and J. A. Lazaro, "From 4.2Gbps Asymmetrical Clipping (ACO)-OFDM to 8.7Gbps Layered ACO-FBMC with Intensity-Modulation Direct-Detection for PONs," in *2019 Conference on Lasers and Electro-Optics Europe - European Quantum Electronics Conference (CLEO/Europe-EQEC)*, (Munich, Germany), pp. CI–P.13 SUN, 2019

21. S. Sarmiento, J. M. Delgado Mendinueta, J. A. Altabas, S. Spadaro, S. Shinada, H. Furukawa, J. J. Vegas Olmos, J. A. Lazaro, and N. Wada, "Experimental Investigation of 50–90 Gb/s IM-DD NOMA-CAP Modulation for Short Range Optical Transmission Applications," in *2019 OptoElectronics and Communications Conference (OECC) - International Conference on Photonics in Switching and Computing (PSC)*, (Fukuoka, Japan), pp. TuF3–5, 2019

22. J. A. Altabas, D. Izquierdo, J. Clemente, S. Sarmiento, G. Silva Valdecasa, M. Squartecchia, L. F. Suhr, O. Gallardo, A. Lopez, M. Á. Losada, J. Mateo, J. B. Jensen, J. A. Lazaro, and I. Garces, "Advanced Technologies for Coherent Access Networks," in *2019 International Conference on Transparent Optical Networks (ICTON)*, (Agnes, France), p. Th.B1.4, 2019

23. S. Sarmiento, J. M. Delgado Mendinueta, J. A. Altabas, S. Spadaro, S. Shinada, H. Furukawa, J. J. Vegas Olmos, J. A. Lazaro, and N. Wada, "Optical power budget enhancement in 50 Gb/s IM-DD PONs with NOMA CAP modulation and SOA-based amplification," in *2019 International Conference on Transparent Optical Networks (ICTON)*, (Agnes, France), p. We.D1.3, 2019

24. D. Izquierdo, J. A. Altabas, J. Clemente, P. Millan, J. A. Lazaro, S. Rommel, R. Puerta, J. J. Vegas Olmos, I. Tafur Monroy, and I. Garces, "Flexible resource provisioning of coherent PONs based on Non-Orthogonal Multiple Access and CAP signals," in *2019 European Conference on Optical Communication (ECOC)*, (Dublin, Ireland), p. M.1.F.3, 2019

25. S. Sarmiento, J. M. Delgado Mendinueta, J. A. Altabas, S. Spadaro, S. Shinada, H. Furukawa, J. J. Vegas Olmos, J. A. Lazaro, and N. Wada, "Split-Enabled 490 Gb/s Optical Interconnect with Direct Detection NOMA-CAP and 7-core Multi-Core Fibre," in *2019 European Conference on Optical Communication (ECOC)*, (Dublin, Ireland), p. P32, 2019

National conference contributions

1. J. A. Altabas, P. Arribas, F. Sotelo, D. Izquierdo, J. A. Lazaro, and I. Garces, "Analysis of Advanced Coherent Modulation Formats for Optical Flexible Metro-Access Networks," in *2015 IX Reunión Española de Optoelectrónica (OPTOEL)*, (Salamanca, Spain), pp. PO–SIII–34, 2015

2. J. D. Sarmiento-Merenguel, A. Ortega-Moñix, R. Hallir, C. A. Alonso-Ramos, P. Reyes-Iglesias, I. Molina-Fernandez, I. Garces-Gregorio, and J. A. Altabas-Navarro, "Monolithically integrated DP-QPSK receiver without polarization beam splitters," in *2015 IX Reunión Española de Optoelectrónica (OPTOEL)*, (Salamanca, Spain), pp. PO–SII–23, 2015

3. D. Izquierdo, R. Martinez, J. A. Altabas, and I. Garces, "Transceptor Sintonizable de Coste Reducido Basado en VCSEL para Redes Opticas udWDM Flexibles Metropolitanas y de Acceso," in *2016 IV Congreso Nacional de I+D en Defensa y Seguridad (DESE I+D)*, (San Javier, Spain), pp. II–B–157, 2016

4. J. A. Altabas, D. Izquierdo, M. Chueca, C. Seron, J. Cebollada, S. Sarmiento, J. A. Lazaro, and I. Garces, "Transceptores ópticos coherentes para las redes ópticas de acceso futuras," in *2017 X Reunión Española de Optoelectrónica (OPTOEL)*, (Santiago de Compostela, Spain), pp. S.1–055, 2017

5. G. Ramos, J. A. Altabas, D. Izquierdo, A. Lopez, M. A. Losada, J. Clemente, S. Sarmiento, J. Mateo, J. A. Lazaro, and I. Garces, "Bit and Power Loaded Multiband Carrierless Amplitude Phase Modulation for High Capacity POF Links," in *2019 XI Reunión Española de Optoelectrónica (OPTOEL)*, (Zaragoza, Spain), p. SP3.COM04, 2019

6. D. Izquierdo, J. A. Altabas, J. Clemente, P. Millan, J. A. Lazaro, S. Rommel, R. Puerta, J. J. Vegas Olmos, I. Tafur Monroy, I. Salinas, and I. Garces, "Distribución flexible de recursos en redes PON coherentes combinando NonOrthogonal Multiple Access y formatos CAP," in *2019 XI Reunión Española de Optoelectrónica (OPTOEL)*, (Zaragoza, Spain), p. SP3.COM06, 2019

Book chapters

1. J. A. Altabas, S. Sarmiento, and J. A. Lazaro, "Passive Optical Networks: Introduction," in *Wiley Encyclopedia of Electrical and Electronics Engineering* (J. G. Webster, ed.), pp. 1–20, John Wiley & Sons, Inc., 2018

Patents

1. J. A. Altabas Navarro, I. Tafur Monroy, S. Rommel, R. Puerta, J. J. Vegas Olmos, D. Izquierdo Nuñez, J. I. Garces Gregorio, and J. A. Lazaro Villa, "WO2018138254 -Constellation Multiplexing and Non-Orthogonal Multiple Access Based on Carrierless Amplitude Phase Modulation," 2018

Finally, the rest of the journal articles, the conference contributions, book chapters and patents with low relation with the thesis are enlisted below:

1. Z. Franco, F. Sotelo, S. Gómez-De Pedro, J. A. Altabas, M. Puyol, D. Izquierdo, J. Alonso, and I. Garcés, "Nanosecond fluorescence lifetime low-cost system for sensor applications," in *2014 Transfrontier Meeting of Sensors and Biosensors (TMSB)*, (Barcelona, Spain), 2014

2. Z. Franco, F. Sotelo, S. Gómez-De Pedro, J. A. Altabas, M. Puyol, D. Izquierdo, J. Alonso, and I. Garcés, "Nanosecond fluorescence lifetime low-cost sensor," in *2014 IEEE Sensors*, (Valencia. Spain), pp. A1L–B.3, 2014

3. J. A. Lazaro, J. Gonzalez, J. A. Altabas, and A. Lerin, “Graphene Silicon ring resonators for wavelength routers in Photonic Network-on-Chip,” in *2015 Conference on Lasers and Electro-Optics Europe - European Quantum Electronics Conference (CLEO/Europe-EQEC)*, (Munich, Germany), pp. JSIV–2.4 SUN, 2015

4. Z. Franco, F. Sotelo, S. Gomez-de Pedro, J. A. Altabas, M. Puyol, D. Izquierdo, J. Alonso, and I. Garces, “Low-cost measurement system for nanosecond fluorescence lifetime sensors,” in *2015 IX Reunión Española de Optoelectrónica (OPTOEL)*, (Salamanca, Spain), pp. PO–SIII–18, 2015

5. J. A. Lazaro, J. Gonzalez, J. A. Altabas, and A. Lerin, “Graphene Silicon ring resonators for wavelength routers in Photonic Network-on-Chip,” in *2015 International Conference on Transparent Optical Networks (ICTON)*, (Budapest, Hungary), p. Th.B5.2, 2015

6. J. A. Lazaro Villa, A. Lerin de la Santisima Trinidad, and J. A. Altabas Navarro, “ES2597577 - Device and System for Modulating the Phase of an Optical Signal, Based on Graphene and/or Carbon-Based Nanostructured Materials,” 2017

Chapter 2

Introduction

Current telecommunication networks can be divided on three levels: core, metropolitan and access network.

Core networks are the higher level of the telecommunication networks and are based on long-haul and submarine links. This kind of network holds a high amount of traffic due to the intercontinental and international connections. The main research interest on this networks is to increase the total transmitted data rate employing wavelength division multiplexing (WDM) [48], spatial division multiplexing (SDM) [49,50], coherent technologies, advanced modulation formats with high spectral efficiency [51] and the best available transmitters, receivers and amplifiers [52].

The intermediate level of the current telecommunication networks are the metropolitan networks. They cover extended areas between core networks and access networks and support different functionalities as traffic grooming and multiplexing. This kind of networks also manage a high volume of data traffic, so network managing technologies are continuously improving in these networks, including new concepts such as: software defined networks and network function virtualization (SDN/NFV) [53], elastic optical networks [54] and network slicing [55].

Finally, access networks are the last level of the current networks, also called last-mile networks from the operator point of view or first-mile networks form the user point of view. However, nowadays optical fiber communications and passive optical networks (PON) in particular have extended the last-mile concept towards 20-60 km, as it will be further developed along the text. Access networks connect the central office (CO), placed at the edge of a metropolitan network, with the end users [56]. Access networks can be based on copper, including twisted pair and coaxial cables, wireless and fiber technology.

PON are a kind of access network that have allowed high bit rates delivered to many users, which are the base of the modern communications network and the information society. They are based on a point-to-multipoint communication through a fully passive optical distribution network (ODN), i.e. a fully optical fiber based network without active or electronic components between CO and user. Multiple users will communicate with the CO sharing the available

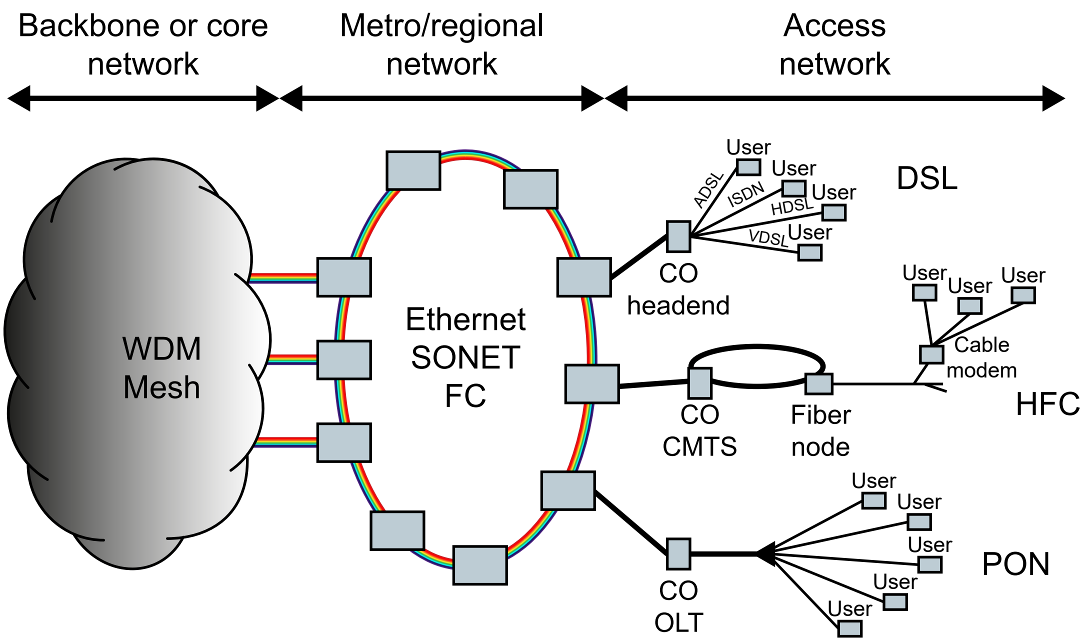

Figure 2.1: Current telecommunication networks.

resources of the network. If resource sharing is done in the time domain, the PON will be named as time division multiplexed PON (TDM-PON). On the contrary, if resource sharing is done in the wavelength domain, it will be named wavelength division multiplexed PON (WDM-PON). There are also hybrid approaches for resource sharing as time and wavelength division multiplexed PON (TWDM-PON), where the time and the wavelength resources are shared simultaneously. This PhD thesis is related to the research and development of new technologies able to improve current PON technologies or to create new and future access technologies based on optical fibers, which are expected to hold the new 5G paradigm. In the rest of the introduction a brief explanation about the basic PON technologies will be given and the new PON research tendencies will be addressed, including their relationship with the different research publications that are part of this compendium.

2.1 Basic PON technologies

Commonly, fiber access networks, also denoted as fiber-to-the-x (FTTx), are reduced to the concept of PON because it is the most extended technology, but the FFTx concept is much broader [56]. The 'x' of FFTx denotes all the different types of FFTx networks classified according to its application scenario [57]:

- *Fiber-to-the-business* (FTTB) and *Fiber-to-the-office* (FTTO): They are applied to optical fiber networks that connect directly the CO with the business office.

- *Fiber-to-the-home* (FTTH): This fiber access network connects the CO with the user's house. The FTTH usually requires a smaller bandwidth than the FTTB.

- *Fiber-to-the-curb* (FTTC) and *Fiber-to-the-neighborhood* (FTTN): The FTTC and FTTN connects the CO with an optical network unit (ONU) placed far of the final users, which are connected with other type of the access technology. Their difference is based on the distance, FTTC distances will be below 300 m while the FTTN will be around 1000 m.

- *Fiber-to-the-antenna* (FTTA): It connects the CO, which has base station functionalities, with the mobile radio remote units (RRU) and antennas.

- *Fiber-to-the-premises* (FTTP) and Fiber-to-the-user (FTTU): They denote jointly the FTTB and FTTH.

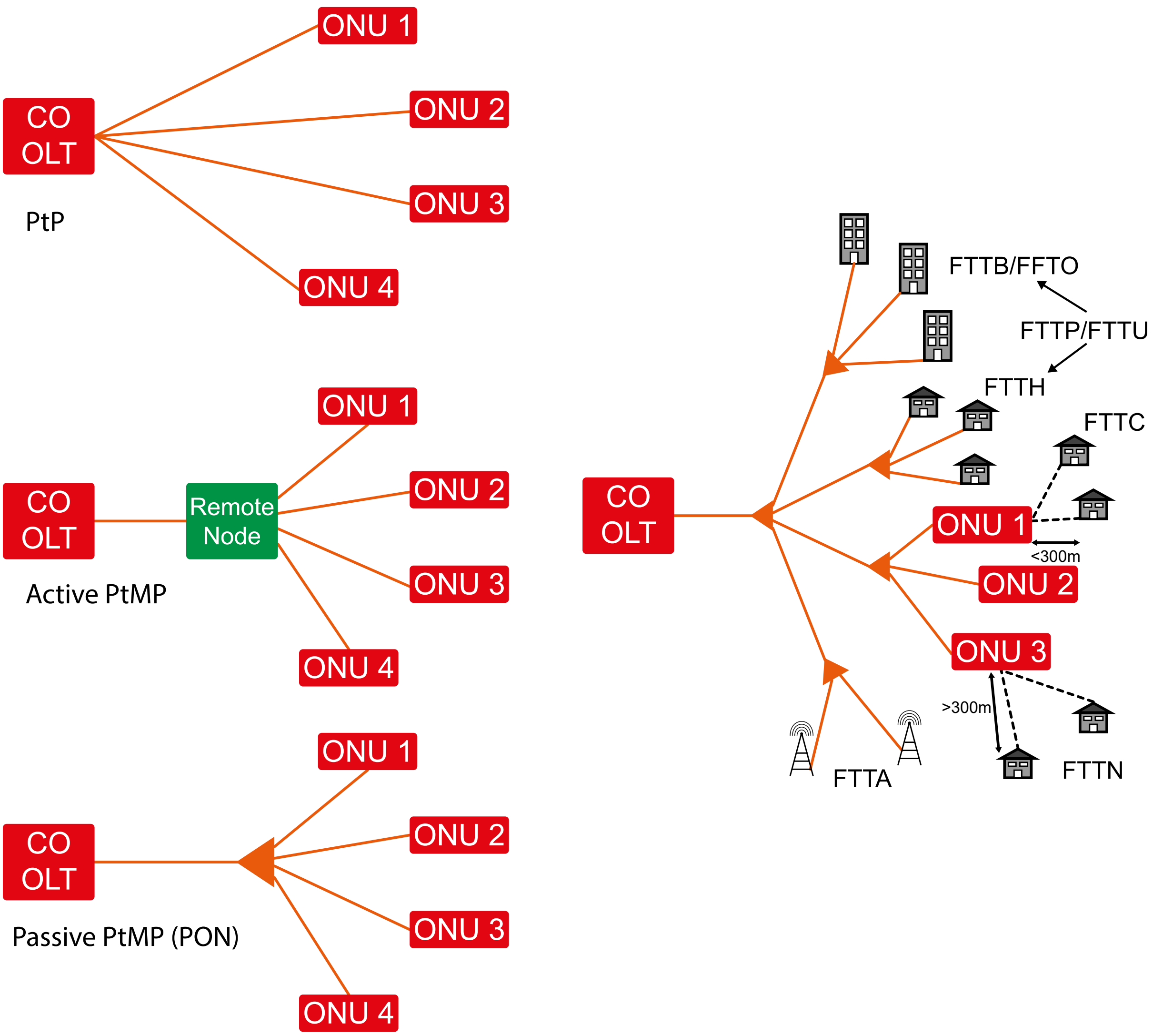

Figure 2.2: FTTx concept.

FTTH can be based on single fiber as point-to-point (PtP) links or on shared fiber as point-to-multipoint (PtMP) links [57,58]. The FTTx based on single fiber PtP links increases the cost in comparison with the one based on shared fiber PtMP, so PtP links are much less deployed [58]. The PtMP FTTx includes a remote note (RN) in order to distribute the signal among the users. This RN can be an active Ethernet switch or a passive splitter, which leads the FFTx to a PON [57, 58]. The difference between the different types of FFTx can be seen in Figure 2.2. The PON concept has several advantages over the active switches: PONs have a lower deployment and maintenance cost than the active optical networks, PONs have a higher reliability because they do not use active or electronic components in the ODN and are easy to upgrade [58]. This thesis is focused on PONs as a specific case of the FTTx networks and they are broadly described in the following sections.

2.1.1 TDM PON

TDM-PON stands for time division multiplexing PON and it is the most common architecture for this kind of network. Its main characteristic is that it shares the network resources on the time domain: in the downlink, the CO, also named optical line terminator (OLT), multiplexes the different users over different time slots, as can be seen in Figure 2.3.a, and sends the information to the network in a continuous stream of data. The complete signal, i.e. the signal carrying all the multiplexed time slots, is transmitted though the fully passive ODN to all the users. The RN of the TDM-PON ODN is a power splitter, which distributes the signals between all the users. Each user has a network terminal called ONU, which selects the time slot that contains the relevant information for the user, and dismisses the rest of the information contained in the other time slots. In the uplink, a time division multiple access (TDMA) strategy must be implemented to manage the access of the ONU to a shared ODN, as can be seen in Figure 2.3.b. Each ONU must transmit its information in an assigned time slot in such a way that collisions with the rest of the users' information are avoided. A common problem of optical networks is that optical data collisions cannot be detected, so it is mandatory to avoid them.

There are many other characteristics that are part of a typical PON architecture, like the use of different wavelengths for up and downstream in order to avoid unwanted reflections by optical filtering of the signals, the tight optical budget restrictions that arise from the division of the optical power among the different users, the adoption of a dynamic bandwidth allocation (DBA) strategy to include variable length time slots in the transmission or the use of modern digital encryption and error correction codes to stand for a secure and error free data transmission. A complete analysis of a typical TDM-PON can be found here [40].

As it has been explained, the TDM-PON concept is the most common approach among the PON standards. These standards have been included as an appendix in this work, where several of them have been analyzed: B-PON standard (subsection A.1.1), G-PON standard (subsection A.1.2), XG-PON standard (subsection A.1.3), XGS-PON standard (subsection A.1.5), 1G-EPON standard (subsection A.2.1) and 10G-EPON standard (subsection A.2.2) are based on TDM-PON.

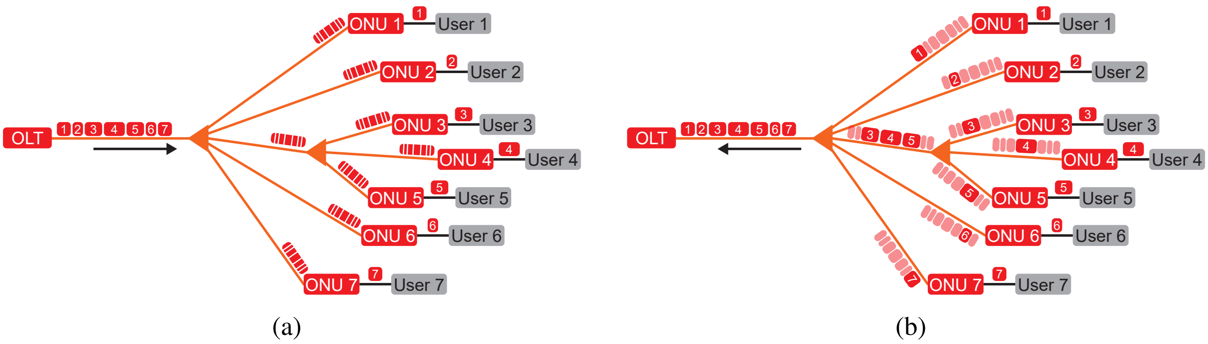

Figure 2.3: TDM-PON network: (a) downlink, (b) uplink.

2.1.2 WDM PON

Another approach for sharing the available resources of an optical access network is the so called Wavelength Division Multiplexing PON or WDM-PON. In WDM-PON, the communication between the different ONUs and the OLT is multiplexed over different wavelengths. In the downlink, the OLT modulates the wavelengths that are necessary to establish a communication with the ONUs and multiplexes these wavelengths before they are sent through the ODN, as can be seen in Figure 2.4.a. The ONUs also multiplex their data streams communication between them and the OLT using different wavelengths, in such a way that often a TDM approach is not needed any more. This type of access to the medium is known as wavelength division multiple access (WDMA), as is shown in Figure 2.4.b. Therefore, WDM-PON can be considered as a multiple PtP link over different wavelength through the same fiber.

The ODN can employ a power splitter as RN, similar to the case shown in Figure 2.3, and so the ONUs have to select the wavelength channel for their link (Figure 2.3.a). Likewise, a wavelength multiplexer/demultiplexer or wavelength router can be employed as RN, and so the ONUs only receive their wavelength channel. If the ODN is based on a power splitter or a wavelength router [59], the WDM-PON will have flexible channel allocation for each ONU-OLT communication, whereas if the RN is a wavelength multiplexer/demultiplexer the wavelength channel allocation will be selected when the ODN is deployed and will not be possible a flexible reallocation of the wavelengths in case of failure of one of the channels.

In any case, the WDM-PON concept is less flexible and much more expensive that the TDM-PON, so WDM-PON is less common than TDM-PON among the PON standards. WDM-PON are only considered on PtP WDM PON of NG-PON2 standard (subsection A.1.4) or in proprietary optical access networks, which are not based on the current standards. Additionally, international telecommunication union - telecommunication standardization sector (ITU-T) proposed the recommendation G.9802 for WDM-PON, entitled as Multiple-wavelength passive optical networks (MW-PONs) [60]. However, WDM-PON architectures have been extensively used in research, and some approaches will be shown in subsection 2.2.1.

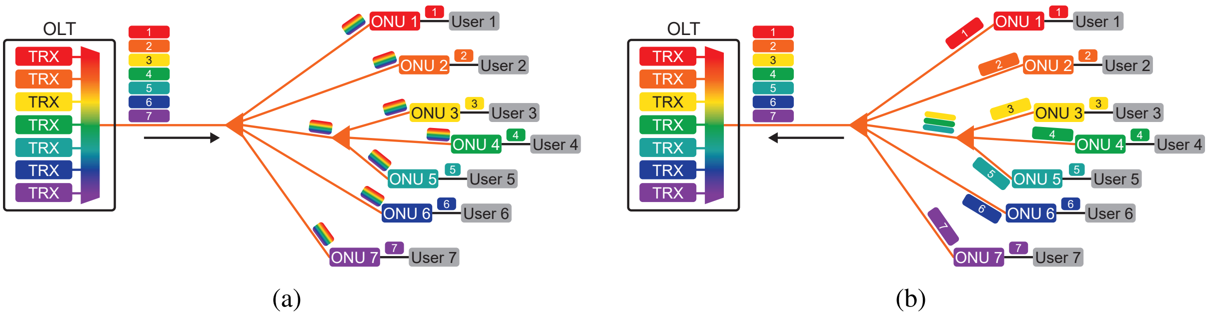

Figure 2.4: WDM-PON network: (a) downlink, (b) uplink.

2.1.3 TWDM PON

The TWDM-PON concept is a hybrid case of the previous approaches (TDM-PON and WDM-PON). This approach combines the sharing of the resources over time and wavelength simultaneously. The downlink channel multiplexes the different users' data using time division multiplexing over different wavelengths that are also multiplexed. Therefore, the OLT assigns a specific time slot of a specific wavelength to each user. Each ONU will extract the information of that time slot of its wavelength channel. This TWDM downlink is depicted in Figure 2.5.a. In the uplink, the ONU will transmit on the assigned time slot of the assigned wavelength channel avoiding the collision between the different users. This technique is denoted as time and wavelength-division multiple access (TWDMA) and it is shown in Figure 2.5.b. Additionally, DBA techniques can also be implemented on both TWDM and TWDMA techniques.

The ODN in a TWDM-PON can be based on power splitters as RN, which provides fully flexibility for resource assignation. However, it also can be based on wavelength multiplexer/demultiplexers or wavelength routers as main RN, which reduces the flexible resources assignment and behaves as a combination of several TDM-PON.

The TWDM-PON approach has been introduced as part of the NG-PON2 standard [61] (subsection A.1.4) and it is considered for future standards (section A.3) as the natural extension of the current TDM-PON standards. In addition, most of the international projects cited on subsubsection 2.2.1.1 for the description of the recent research of dense WDM (DWDM) access networks, consider the TDM over each wavelength as a proper solution for increasing the number of users. Therefore, most of the international projects cited on subsubsection 2.2.1.2

could be included also in this section.

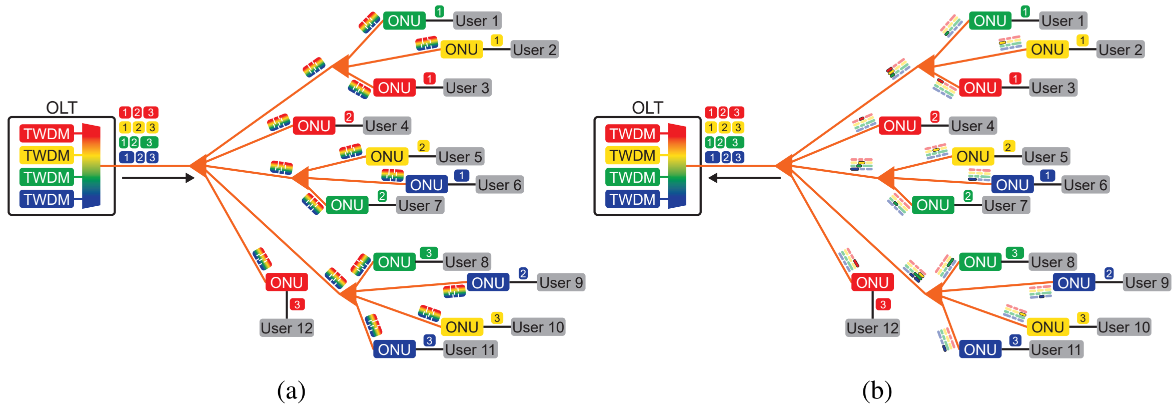

Figure 2.5: TWDM-PON network: (a) downlink, (b) uplink.

2.2 Advanced PON Technologies

The evolution of optical access networks is increasing their requirements in terms of data rate, reach and splitting ratio. The different PON types have been analyzed in the previous section. The evolution of the PON standards have been described in Appendix A showing how the data rate per channel and the number of channels are continuously increasing.

Therefore, new approaches are required in order to fulfil this data rate growth with an increment of the channel density while keeping or increasing the reach and the number of users that the PON is able to serve. These new approaches are based on the development of extreme dense wavelength multiplexing strategies to increase the number of users, the employment of new modulation formats, which allow to increase the spectral efficiency and the data rate, and the use of coherent technologies to increase the data rate and the available optical power budget i.e. reach and splitting ratios.

In this section, the newest research approaches for improvement of PONs in terms of reach, splitting ratio and data rate will be shown and the publications used in the compendium will be placed in the context of the last research results.

2.2.1 Advanced WDM PONs

2.2.1.1 DWDM PON

The most basic way of applying the WDM concept is through what is called coarse WDM [62]. Coarse WDM (CWDM) consists of 18 wavelength channels where the different users or links are multiplexed. In this technology, the optical spectrum is divided in two regions: 1310 nm and 1550 nm region. The 1310 nm region covers the wavelengths from 1270 nm to 1450 nm, i.e. O and E bands, while the 1550 nm region covers the wavelength range between 1470 nm to 1610 nm, i.e. S, C and L bands. The wavelength channels are spaced over a 20 nm grid and so the transmitters do not need to be thermally stabilized. This concept can be applied for PON as it has been employed in several standards for multiplexing the uplink and the downlink, as it is in B-PON, G-PON, G-EPON, XG-PON, 10G-EPON and XGS-PON, where the uplink is placed in the 1310 nm region and the downlink is placed in the 1550 nm region.

The natural evolution of the WDM concept is the reduction of the space between channels in order to improve the spectral efficiency. This evolution leads to the concept named as DWDM. In DWDM systems, the wavelength spacing between channels is reduced to 100GHz or 50GHz, as is indicated on the ITU-T recommendation [62]. This DWDM concept was initially applied for long haul links due to its capability to multiplex several wavelengths in the C band (up to 88 channels) and amplify them using Erbium doped fiber amplifiers (EDFAs). Recently, the DWDM concept has been extended to other bands, like E and L bands, thanks to the development of new broadband amplifiers [52]. The main difference between coarse and dense WDM PON in terms of the wavelength bands and the PON deployment is shown in Figure 2.6.

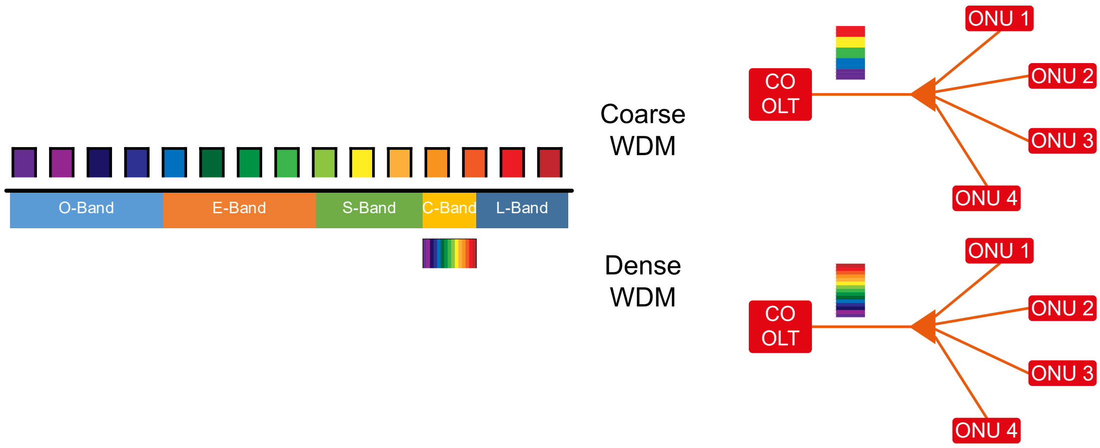

Figure 2.6: Difference between coarse and dense WDM-PON.

After the application of this DWDM concept for long haul links, the natural move has been to extend it to the access networks. Therefore, several research projects have been developed around this concept during the last years: PIEMAN, SARDANA, GigaWaM, OASE and DISCUS. In the following, their main features will be described:

- **Photonic integrated extended metro and access network - PIEMAN (2006-2009)**: This European Union (EU) FP6 project focused on the development of all-optical integrated metro and access network [63, 64]. They designed a simplified DWDM metro-access network with 32 wavelength spaced 50 GHz. They proposed 10 Gbps colorless ONU transceivers based on electro-absorption modulators (EAM) with semiconductor optical amplifiers (SOA) or low cost tunable lasers [63] and avalanche photodiodes (APD). They also proposed to reach 100km with amplified remote nodes [64] and splitting ratios of 512 employing TDM per wavelength. The basic PIEMAN system architecture is shown in Figure 2.7.

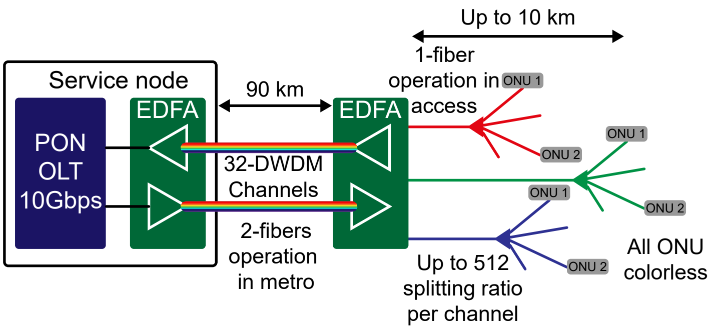

Figure 2.7: PIEMAN. [64]

- **Scalable advanced ring-based passive dense access network architecture - SARDANA (2008-2011)**: This EU FP7 project consisted of 100 GHz DWDM double-fiber ring with remote amplification with central pump [65–68]. The fiber ring is connected thought a remote note with single-fiber and single-wavelength tree, as can be seen in Figure 2.8. They proposed to employ 32 wavelengths for uplink and downlink and to serve up to 1024 users, which was multiplexed with TDM in each wavelength [66]. The proposed data rated for wavelength was 10 Gbps.

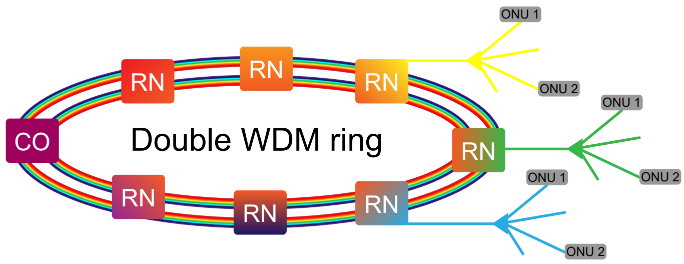

Figure 2.8: SARDANA. [66]

- **Giga bit access passive optical network using wavelength division multiplexing - GigaWaM (2008-2012)**: This EU FP7 project proposed a DWDM access network with 50 GHz channel spacing with 2.5 Gbps uplinks in the C-band and 10 Gbps downlinks in the L-band [69,70]. They GigaWaM basic architecture, shown in Figure 2.9, connects 64 end users multiplexed with a remote node based on arrayed waveguide grating (AWG). The OLT transceivers were based on vertical cavity surface emitting lasers (VCSEL) and photodiodes (PD) and the ONU transceivers were based on a modulated grating Y-branch lasers with a SOA (MGY-SOA) and a PD.

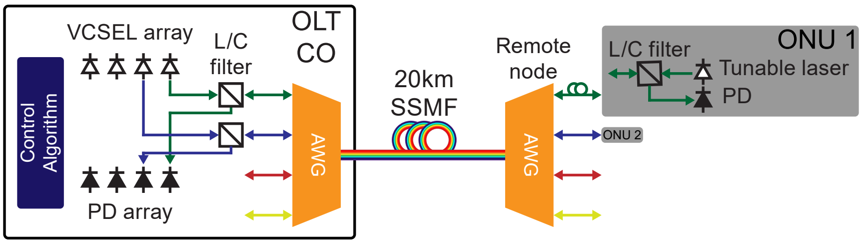

Figure 2.9: GigaWaM. [70]

- **Optical access seamless evolution - OASE (2010-2013)**: This EU FP7 project analyzed and proposed the migration paths from the deployed PON to the next generation optical access (NGOA) [71–74]. They proposed several types of NGOA among which are DWDM access networks, as can be seen in Figure 2.10. The ODN of this DWDM access network can be divided in: wavelength selected (WS) WDM, which are based on power splitters as distribution element of the ODN, wavelength routed (WR) WDM, which are based on WDM multiplexer as distribution element of the ODN.

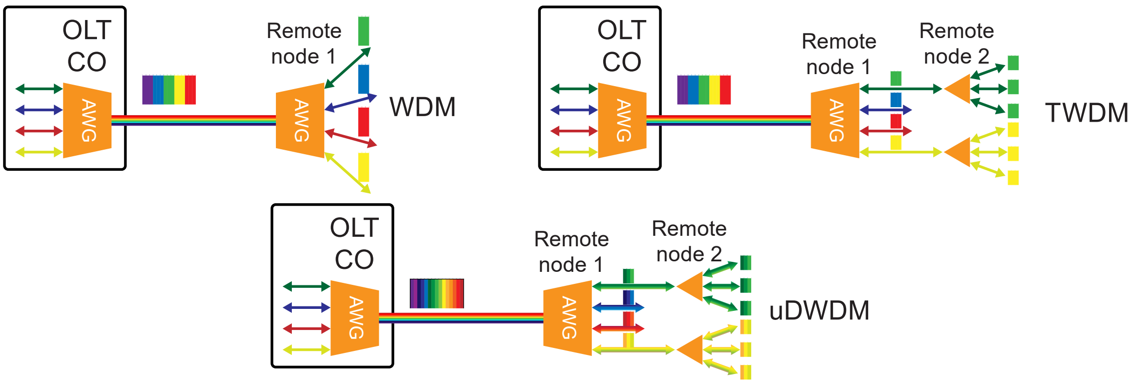

Figure 2.10: OASE. [71]

- **The distributed core for unlimited bandwidth supply for all users and services - DISCUS (2012-2015)**: This EU FP7 project looked for an end-to-end solution for ubiquitous broadband services [75–77]. This project combines a flat optical core network with a long reach passive optical network (LR-PON), shown in Figure 2.11, with high splitting ratios (up to 512). In addition, it combines 10 Gbps DWDM channels with dynamic reconfigurable TDM for end users with 100 Gbps dedicated channels for business application. They proposed amplified nodes with some functionalities that allows low-latency services [77].

In addition, ITU-T released the recommendation G.9802 - Multiple-wavelength passive optical networks (MW-PONs) [60] in 2015. This recommendation defines the WDM-PON architectures considering WS-WDM and WR-WDM ODNs, as it was done in the OASE project, and

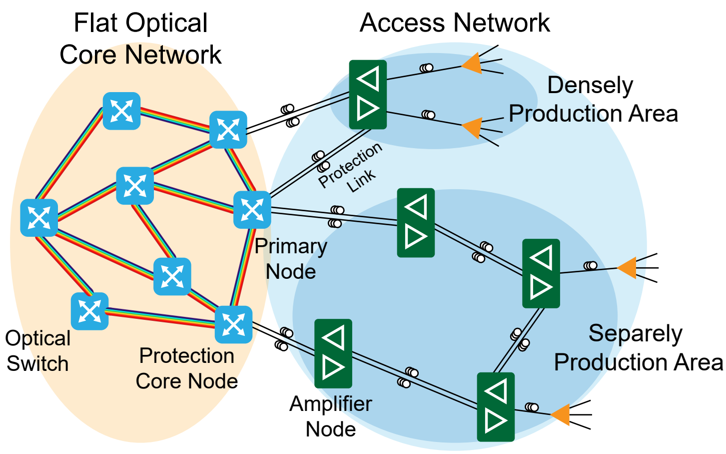

Figure 2.11: DISCUS. [76]

the different hybrid cases that could be considered. Finally, it establishes the recommendations for enhancement to XG-PON and 10G-EPON to a multi-wavelength PON.

2.2.1.2 uDWDM PON

After the development of DWDM systems, the natural step was reducing the channel bandwidth in order to increase the spectral efficiency and therefore, the transmitted data rate. The reduction of the channel bandwidth brought the concept of ultra-dense WDM networks (uDWDM) [62]. The G.694.1 standard considers channel bandwidths of 12.5GHz with a nominal central frequency granularity of 6.25GHz. The uDWDM concept was combined with the flex-grid concept in the high capacity networks like long-haul and metropolitan networks in order to increase the data rate and the flexible connection between nodes [78].

The next step for the uDWDM concept was its application to access networks. The uDWDM access networks brought the concept of lambda-to-the-user, which means that each user will have a dedicate wavelength channel. Figure 2.12 shows a comparative between a DWDM and uDWDM PON, showing the channel separation reduction.

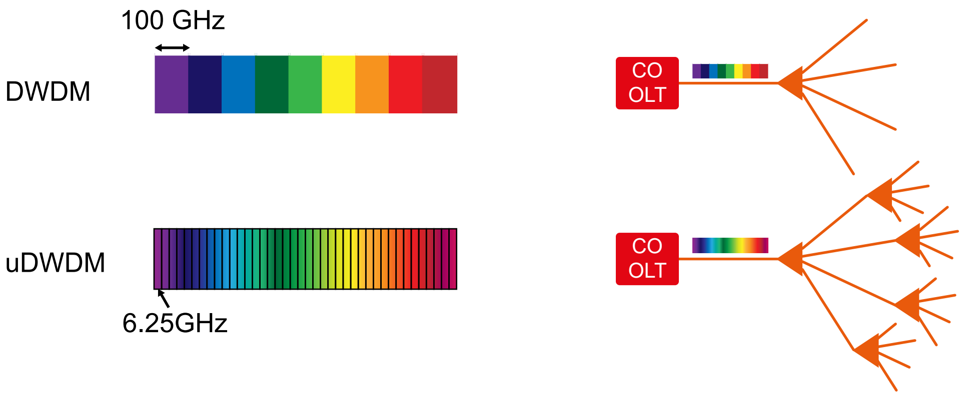

Figure 2.12: Difference between DWDM and uDWDM PON.

In the same way than DWDM PON, there are some international projects focused on the research of uDWDM access networks: OASE and COCONUT.

- **Optical access seamless evolution - OASE (2010-2013)**: This EU FP7 project has already been presented in the DWDM PON section but it also proposed the migration NGOA [71–74] based on uDWDM access networks, as can be seen in Figure 2.10. The uDWDM PON can be considered as a variant of the WS-WDM PON with ODN based on only power splitters or with hybrid ODN based on a combination of WDM multiplexers and power splitters [71].

- **Cost-effective coherent ultra-dense-WDM-PON for lambda-to-the-user access networks - COCONUT (2012-2016)**: This EU FP7 project proposes the use of coherent technologies as solution for the deployment of uDWDM access network [79–81]. This project employs coherent technologies for increasing the loss budget and the number of users of the network [79]. This project considered a wavelength channel spacing of 6.25 GHz and data rates between 1.25 Gbps and 10 Gbps, as is shown in Figure 2.13. The coherent technologies employed in this project will be described later on a specific section about coherent technologies applied to PON (subsection 2.2.3).

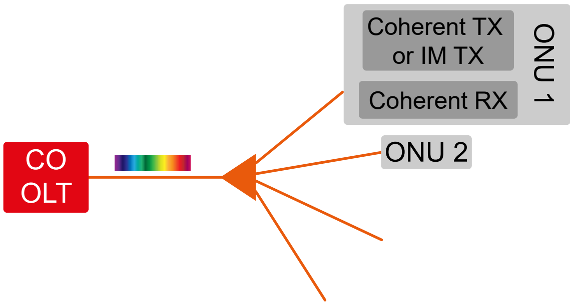

Figure 2.13: COCONUT. [81]

2.2.2 Advanced Modulation Formats

All the current standards have only considered the basic amplitude modulation of the transmitted signals, non-return to zero (NRZ) on-off keying (OOK) modulation, because it is the simplest format that allows direct intensity modulation (IM) with common and cost-effective lasers such as direct modulated lasers (DML) or externally modulated lasers (EML) and direct detection (DD) using photodetectors (PIN or APDs). Therefore, its main advantages are the easiness of implementation and the reduced cost, but this simplicity also leads to a low spectral efficiency. This low spectral efficiency, combined with the data rate increment needed for the future networks, cause a dramatic increase in the required bandwidth. This bandwidth increment leads to expensive electro-optical transmitters and receivers and a higher optical prower budget penalty due to the fiber dispersion. In addition, this low spectral efficiency is also critical when the wavelength channel spacing is reduced since it will limit the maximum data rate if this channel spacing becomes too small.

Therefore, the new standards committees and the researchers are considering new modulation formats. The most simple approach is to keep the IM and increase the modulation levels, obtaining modulations as duobinary (DB) or pulse amplitude modulation (PAM-N), which are being considered as a way to improve the spectral efficiency in optical networks.

The DB format is based on using a controlled intesymbolic interference (ISI) that allows to transmit a data rate using half of the bandwidth. If the DB signal is generated by three intensity levels, it will be denoted as electrical duobinary (EDB), but, if it is generated with three field levels, which leads to two intensity levels (encoding the third level using the phase of the high level), it will be denoted as optical duobinary (ODB).

The controlled ISI can be caused by a ”delay and add” filter before the optical transmission as is shown in Figure 2.14, where this filter adds the current bit with the previous one. In the case of the EDB, the controlled ISI can be generated using an electrical low-pass filter with $BW = 0.28R$, which can be implemented either in the transmitter or in the receiver [82]. The pre-coder implements a differential encoding in order to avoid the propagation of errors. In the case of the EDB, this precodification allows to decode the signal using two comparators for detecting the upper and lower level and then a XOR logical gate, as shown in Figure 2.14. In the case of the ODB, it is possible to decode the modulation using a simple NRZ detection, as shown in Figure 2.14.

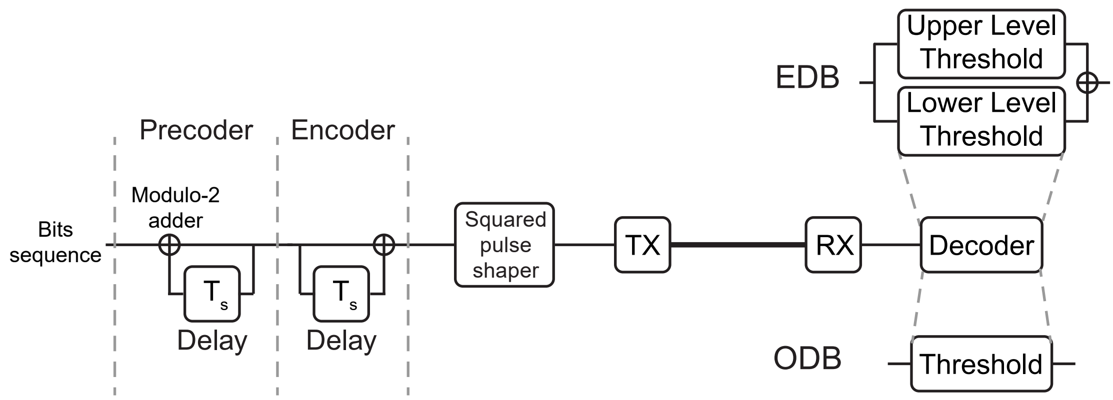

Figure 2.14: Duobinary.

The EDB is a pure IM with half of the bandwidth and so it can be transmitted and received with cost effective transmitters and receivers presenting a reduced bandwidth. The EDB increases the dispersion tolerance by a factor 2 but requires more sensitivity because of the three level signal at the receiver.

The ODB has to be generated with a Mach-Zehnder Modulator (MZM) at the null point or using a EML and a phase modulator. This increment of the transmitter complexity causes a reduction of the receiver complexity because it can be detected as a NRZ receiver. Therefore, it also has a higher dispersion tolerance but without a sensitivity reduction. The MZM can be replaced by a directly intensity modulated transmitter followed by a phase modulator after it [83]. Another alternative is to replace the MZM by a phase modulator and an optical filter [84]. These solutions for ODB are considered too expensive for access networks.

Additionally, more complex modulation formats with controlled ISI have been researched for optical access networks as [85], but their complexity and the reduction of sensitivity have stopped their possible deployment in access networks.

The PAM-N is also being considered for the next generation PON standards. PAM-N consists of encoding several bits in each symbol, which will have several intensity levels. The N order represents the number of levels of the transmitted signal with $N = 2^b$ and b being the number of bits per symbol. Although there has been some research with higher N order [86], the main research studies for the new PON standards have been focused on PAM-4 [82, 87]. PAM-4 can transmit a given data rate using half of the bandwidth. Thus, it can be performed with lower cost transmitters and receivers. PAM-4 will also have a dispersion tolerance 4 times better but the sensitivity will also be reduced because of the four levels of the received signals.

In Figure 2.15, the eye diagrams and spectra of the NRZ, EDB, ODB and PAM-4 are shown.

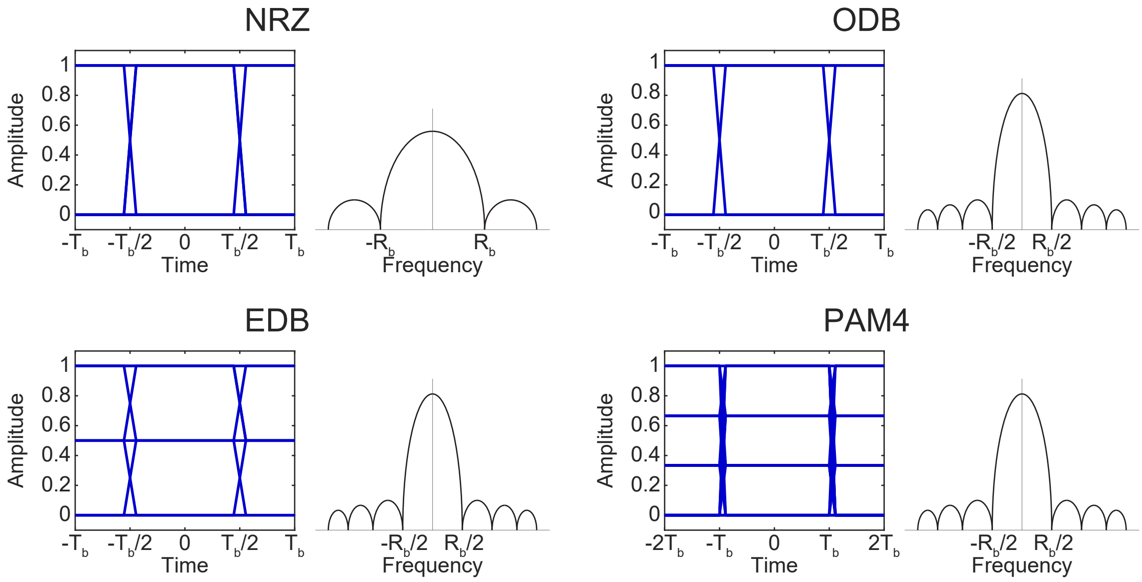

Figure 2.15: NRZ, EDB, ODB and PAM-4 optical power eye diagrams and spectrum with R_b data rate.

Other advanced optical phase modulation techniques as phase shift keying (M-PSK) or quadrature amplitude modulation (M-QAM) are also starting to be considered for PONs, specially from the research side. The main disadvantage of these modulation techniques is that they usually need coherent receiver technology, which is more expensive and much more complex than the conventional intensity modulation/direct detection (IM/DD), but the main advantage is that they can encode several bits in each level codified on the in-phase (I) and the quadrature (Q) components and that thanks to the coherent detection the sensitivity improves greatly. Therefore, these modulation formats allow to increase the spectral efficiency since there are several bits encoded on the same symbol and therefore the required bandwidth necessary for transmitting a given data rate decreases with $\log_2(2)$. In addition, these modulation formats are able to recover the phase and the amplitude of the optical signal and so lineal distortions as the chromatic dispersion (CD) can be compensated at the receiver.

The techniques for generation and reception of coherent technologies applied to PONs will be described on the subsection 2.2.3. Figure 2.16 shows some constellation diagrams that correspond with some of the M-PSK and M-QAM.

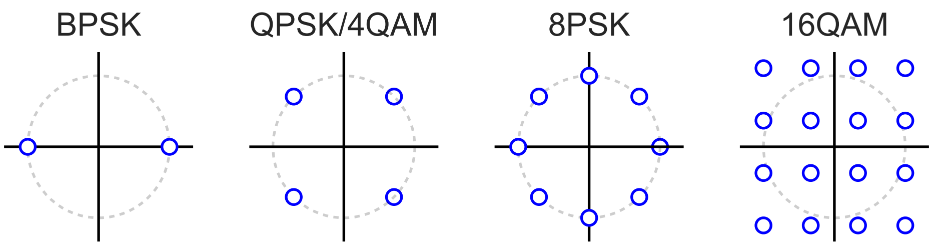

Figure 2.16: M-PSK and M-QAM constellations.

Finally, multicarrier modulations like discrete multitone (DMT), orthogonal frequency division multiplexing (OFDM) and multicarrier carrierless amplitude phase modulation (CAP) are also considered as possible solutions for future PONs.

The most basic multicarrier modulation is the DMT because it consists of transmitting the overall data rate in a set of narrow tributary signals. The reduced bandwidth of each tributary signal allows to transmit a high total data rate with long symbol periods. Therefore, the channel distortions have a reduced effect over the signal but has less spectral efficiency due to the spectral guard bands required to avoid the crosstalk between the bands.

The natural evolution of a DMT modulation is the OFDM. The OFDM eliminates the spectral guard bands because it avoids the subcarrier crosstalk by employing a set of orthogonal frequencies, as shown in Equation 2.1.

$$\int_0^T s_i(t)s_j(t)dt = 0 \tag{2.1}$$

where $s_i(t)$ represent each subcarrier with frequency f_i , for $i = 0, 1, 2, ..., N - 1$. Each subcarrier is modulated with a complex M-QAM symbol (A_i,B_i), as show in Equation 2.2.

$$s_i(t) = A_i \cos(2\pi f_i t) - B_i sin(2\pi f_i t) \tag{2.2}$$

Each subcarrier frequency has to fulfill the condition expressed in Equation 2.3 [REF97] in order to satisfy the condition of Equation 2.1.

$$f_i = \frac{i}{T} + f_{RF} \tag{2.3}$$

where the f_{RF} is the upconversion frequency that can be an intermediate radiofrequency carrier or an optical carrier. Therefore, the N OFDM subcarriers can partially overlap each other in the frequency domain without interfering and the OFDM signal can be expressed as Equation 2.4.

$$s_{OFDM}(t) = \sum_{i=0}^{N-1} A_i \cos(2\pi f_i t) - B_i sin(2\pi f_i t) \tag{2.4}$$

The OFDM signal can be rewritten as Equation 2.5, and so the inverse fast Fourier transform (iFFT) can be used in order to generate the symbols before the upconversion. Figure 2.17 shows the block diagram for OFDM generation. One of the blocks shown in the figure is the cyclic prefix (CP) addition. This CP consists of a temporal replica of the end part of the OFDM symbol at the beginning of it. The CP reduces the ISI and enables the frequency-domain equalization (FDE) [88, 89].

$$s_{OFDM}(t) = \mathbb{R}\left\{ e^{j2\pi f_{RF} t} \sum_{i=0}^{N-1} (A_i - jB_i)\, e^{j2\pi (i/T) t} \right\} \tag{2.5}$$

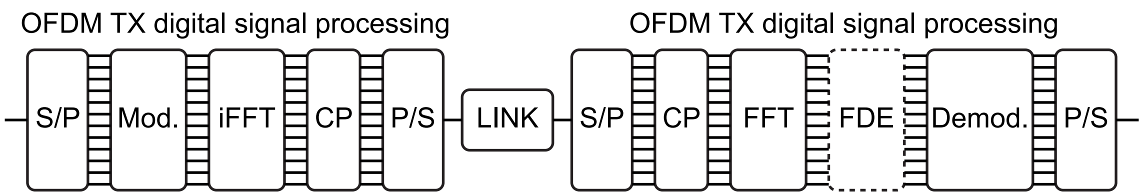

Figure 2.17: OFDM block diagram.

The main drawback of OFDM is the high peak to average power ratio (PAPR) caused by the constructive summation of the different subcarriers. This leads to an inefficient use of the electrical amplifiers and the electrical mixers and/or optical modulators.

The OFDM signal has to be adapted in order to be applied for optical access networks. The complex nature of the OFDM signal requires either the employment of expensive optical complex transmitters and receivers, i.e. coherent optical OFDM (CO-OFDM), or the development of some strategies to convert the OFDM signal in a real signal in order to use low cost intensity transmitters and DD receivers, i.e. IM and DD based devices (IM/DD OFDM).

The CO-OFDM can be generated modulating an external laser with an optical IQ modulator [90] or employing the technique named as all-optical OFDM (AO-OFDM) [91], where the subcarriers are optically generated, independently modulated and aggregated before their transmission as an optical OFDM signal. Both generation schemes are coherent signals, i.e. complex signals with information in the amplitude and the phase of the signal, and so they have to be recovered with a complex receiver. These OFDM techniques, since require a high complexity transmitter and receivers, are not suitable for PON.

The IM/DD OFDM is based on the direct IM of a transmitter, as a DML or EML, and DD with a PIN or an APD. Therefore, the IM/DD OFDM signal has to be real and positive. It is necessary to apply some techniques in order to obtain a real OFDM signal.

The first possible technique is the upconversion to an intermediate radiofrequency by means of an electrical IQ modulator. After this upconversion, the OFDM signal will be real as it is necessary for an IM/DD OFDM link [92]. Other possible technique for IM/DD OFDM is applying the Hermitian symmetry (complex conjugate symmetry) to the subcarriers before the iFFT, as is shown in Figure 2.18, to obtain the required real signal after it [93]. This technique also avoids the issues that cause IQ imbalances of the upconversion [88]. On the other hand, it is possible to generate the complex signal and intercalate the real and the imaginary part [11, 94], i.e. sending the real part of the symbol first and then sending the imaginary part of the symbol. After intercalating them, the transmitted OFDM signal will be real as it is required. One of the main drawback of all of these techniques is that the spectral efficiency falls to the half. In addition, other drawback that degrades the signal quality in the IM/DD OFDM is the CD that affects it because it is a double-sideband signal. This disadvantage may be solved converting it to a single-sideband signal [95].

Figure 2.18: Real OFDM: Hermitian.

These techniques allow to generate a real OFDM signal but it also has to be positive for achieving the compatibility with IM. The easiest way of obtaining a positive signal is applying a bias to the real signal, which is named as direct current (DC) biased optical OFDM (DCO-OFDM) [96]. This technique will generate a high optical carrier, which will degrade the optical signal-to-noise ratio (OSNR). The OSNR is also degraded because of the high PAPR of the OFDM signal and one of the solutions is clipping the signal [88]. The clipping technique can also be applied to eliminate the negative part of the signal, obtaining the required positive signal. This technique is named as asymmetrical clipped optical OFDM (ACO-OFDM) [96]. Its main drawback is that the asymmetrical clipping causes intercarrier interference (ICI). This causes that only half of the carriers can be used and so that the spectral efficiency is reduced to the half. In order to increase the spectral efficiency of the ACO-OFDM, some techniques as layered ACO-OFDM (LACO-OFDM) [97] and spectral and energy efficient OFDM (SEE-OFDM) are being proposed [98]. Another technique consists of obtaining the sign and the magnitude of each symbol and sending first the sign and after that the magnitude of them [99].

The OFDM signals with its different versions can be applied directly for the downlink in a PON. In the case of applying the OFDM concept to the uplink, it has to be adapted to multiple access to the medium. Therefore, the OFDM becomes in orthogonal frequency division multiple access (OFDMA) [100]. In OFDMA, each user only modulates some of the subcarriers before the iFFT, i.e. the unassigned subcarriers are turned off in order to the rest of the users can use them. The OFDMA operation in a PON uplink is schematically shown in Figure 2.19.

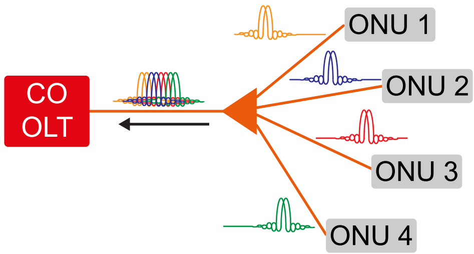

Figure 2.19: OFDMA.

The CAP modulation format [101, 102] is based on orthogonal filters, which are employed to generate the two components of the signal $h_I(t)$ and $h_Q(t)$, i.e. I and Q components. The CAP orthogonal filters are generated multiplying a pulse shaper ($p(t)$) with a cosine, in the case of the I filter, and with a sine, in the case of the Q filter, as can be seen in Equation 2.6. In order to demodulate the CAP signal, the matched filters will be used.

$$\begin{aligned} h_I(t) &= p(t)\cos(2\pi f_c t) \\ h_Q(t) &= p(t)\sin(2\pi f_c t) \end{aligned} \tag{2.6}$$

where f_c is the central frequency of the orthogonal filters. The pulse shaper $p(t)$ is usually a root raised cosine (RRC), which is described in Equation 2.7. The RRC has a reduced spectrum and so it allows to increase the spectral efficiency. In addition, the reception filtering with the RRC matched filters, and assuming a flat frequency response of channel, of raised cosine (RC), will provide a total frequency response of the system that minimizes the ISI [103].

$$p(t) = \begin{cases} \frac{1}{T}\left(1+\beta\left(\frac{4}{\pi}-1\right)\right), & t=0 \\ \frac{\beta}{T\sqrt{2}}\left(\left(1+\frac{2}{\pi}\right)\sin\left(\frac{\pi}{4\beta}\right)+\left(1-\frac{2}{\pi}\right)\cos\left(\frac{\pi}{4\beta}\right)\right), & t=\pm\frac{T}{4\beta} \\ \frac{1}{T}\frac{\sin\left(\pi\frac{t}{T}(1-\beta)\right)+4\beta\frac{t}{T}\cos\left(\pi\frac{t}{T}(1+\beta)\right)}{\pi\frac{t}{T}\left(1-\left(4\beta\frac{t}{T}\right)^2\right)}, & otherwise \end{cases} \tag{2.7}$$

where T is the symbol period and β is the roll of factor. One of the main drawbacks of CAP is the necessity of having a flat response channel. This drawback can be mitigated through a multiband operation with smaller band bandwidth. This multiband operation is named as multiCAP [104]. In order to obtain the multiCAP signal, a pair of orthogonal filters are designed for each band, following the Equation 2.8.

$$\begin{aligned} h_{I_i}(t) &= p(t)\cos(2\pi f_{c_i} t) \\ h_{Q_i}(t) &= p(t)\sin(2\pi f_{c_i} t) \end{aligned} \tag{2.8}$$

where f_{c_i} is the central frequency of each band. The difference between the central frequency of two adjacent bands has to be enough to avoid the overlap of the two bands and so to ensure the orthogonality between them [104]. An example of a time and frequency response of the multiCAP orthogonal filters is show in Figure 2.20.

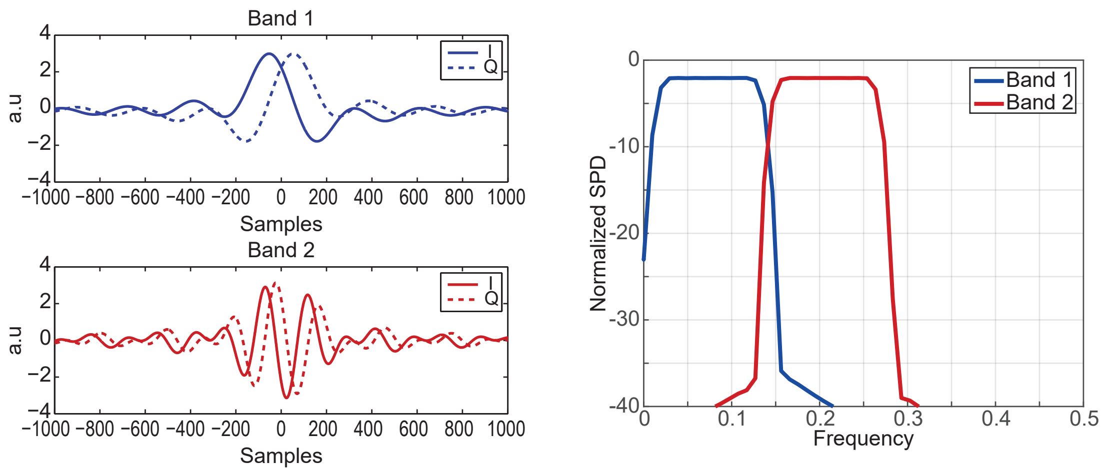

Figure 2.20: Time and frequency response of the multiCAP filters.

The multiCAP modulation format has been successfully employed in wireless and optical links achieving high data rates [105, 106]. In addition, the multiband operation of the mutliCAP modulation format allows to apply bit and power loading, maximizing the transmitted data rate [104].

2.2.3 Coherent Technologies for PON

A coherent optical communication can be defined as an optical link that transmits information employing the phase and the amplitude of the light. In general, the coherent receiver is based on the combination of the received signal with a local oscillator (LO) in the detector [107, 108]. Therefore, the information carried over the amplitude and phase can be extracted through the interference between the singal and the LO.

Coherent optical communications have been developed and applied in long haul links during the recent years. Long haul optical communications need high data rates with high spectral efficiencies, which can be achieved using the coherent optical communications technology since M-PSK and M-QAM modulation formats can be easily implemented and demodulated. In addition, the optical coherent reception provides a much higher sensitivity due to the mixing of the signal with the LO. Additionally, the coherent optical reception allows to equalize the lineal impairments because the received signal keeps the phase and amplitude information [108].

In the last years, the coherent technologies have started to be considered as an attractive candidate for the PON. The new generation PONs require higher reach and data rates that serves a higher number of users. The combination of these requirements with a reasonable cost only can be achieved using coherent technologies.

I will describe the generation of optical coherent signals, including some cost effective alternatives. The coherent signal that I have described previously requires to modulate the I and Q components of the light and so and IQ modulator is needed. The most common IQ modulator is based on two nested MZMs, as it is shown in Figure 2.21. Each Mach-Zehnder is employed to modulate each component and before they are joined, the Q component is 90º phase shifted.

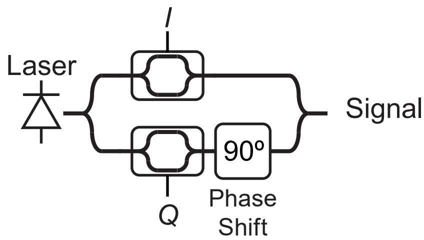

Figure 2.21: IQ modulator.

Additionally, a dual-polarization IQ signals allows to duplicate the data rate multiplexing two coherent signals over the two polarizations. The dual-polarization IQ modulator consists of two IQ modulators, which are joined employing a PBS , as is shown in Figure 2.22.

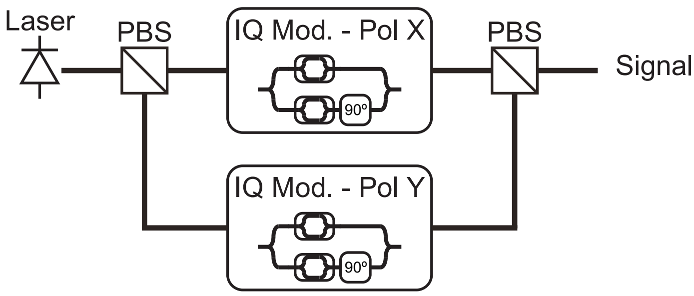

Figure 2.22: Dual-polarization IQ modulator.

During the recent years, directly-phase modulated cost-effective transceivers for coherent links have been intensely researched. The DMLs can be modulated with amplitude, phase or frequency depending on the pulse shape of the modulation signal, as is described on [109]. Recently, M-DPSK has been developed over directly phase modulated distributed feedback laser (DFBs) [109–113] and reflective semiconductor optical amplifier (RSOAs) [114, 115] in order to reduce the cost of the coherent signal generation. In addition, there have been some proposals to modulate FSK signals over DFBs [109, 116, 117] through the chirp caused by the power variations of the optical signal. All these techniques provide amplitude and phase modulation using only DMLs.

Next, the basic fundamentals of the coherent detection will be developed. The received signal (Equation 2.9) and the LO signal (Equation 2.10) can be expressed as:

$$\vec{E}_S(t) = |E_S(t)|\, e^{j(\omega_S t + \phi_S(t))} \hat{e}_S \tag{2.9}$$

$$\vec{E}_{LO}(t) = |E_{LO}|\, e^{j(\omega_{LO} t + \phi_{LO}(t))} \hat{e}_{LO} \tag{2.10}$$

where $|E_S(t)|$ is the amplitude of the received signal, ω_S is the frequency of the received signal, $\phi_S(t)$ is the phase of the received signal, $\hat{e}_S$ is the polarization vector of the received signal, $|E_{LO}|$ is the amplitude of the LO, ω_{LO} is the frequency of the LO, $\phi_{LO}(t)$ is the phase of the LO and $\hat{e}_{LO}$ is the polarization vector of the LO.

The interaction between the signal and the LO in a PD is necessary in a coherent receiver and requires an additional condition of polarization alignment between the signal and the LO, i.e. $\hat{e}_S = \hat{e}_{LO}$. This condition increases the complexity of coherent receivers because they need to include a polarization management system. Different coherent receivers will be described assuming a polarization alignment between the signal and the LO. Finally, it will be studied how the polarization management is addressed in a real coherent receiver.

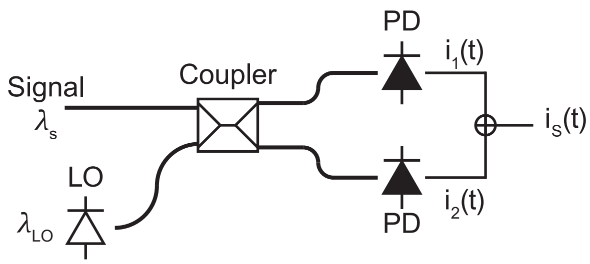

Figure 2.23: Coherent receiver based on 2x2 optical coupler.

The simplest coherent receiver is based on a 2x2 optical coupler and a balanced PD, as can be seen in Figure 2.23. This receiver joins the signal and the LO with the optical coupler, and the output fields can be obtained from the input fields through the Equation 2.11.

$$\begin{pmatrix} \vec{E}_1 \\ \vec{E}_2 \end{pmatrix} = \frac{1}{\sqrt{2}} \begin{pmatrix} 1 & j \\ j & 1 \end{pmatrix} \begin{pmatrix} \vec{E}_S \\ \vec{E}_{LO} \end{pmatrix} \tag{2.11}$$

where $\vec{E}_1$ and $\vec{E}_2$ are the two output signals of the 2x2 optical coupler. Each of the PDs generates a photocurrent proportional to the received optical power (the square of the optical field) and so the beating between the signal and the LO at each PD is obtained, following the Equations 2.12 and 2.13.

$$i_1(t) = \eta \left|\vec{E}_1\right|^2 = \eta \left(\underbrace{\frac{1}{2}|E_{LO}|^2}_{LO\ DD} + \underbrace{\frac{1}{2}|E_S(t)|^2}_{Signal\ DD} + \underbrace{|E_S(t)|\,|E_{LO}|\sin(2\pi\Delta f t + \Delta\phi(t))}_{Signal-LO\ beating} \right) \quad (2.12)$$

$$i_2(t) = \eta \left|\vec{E}_2\right|^2 = \eta \left(\underbrace{\frac{1}{2}|E_{LO}|^2}_{LO\ DD} + \underbrace{\frac{1}{2}|E_S(t)|^2}_{Signal\ DD} - \underbrace{|E_S(t)|\,|E_{LO}|\sin(2\pi\Delta f t + \Delta\phi(t))}_{Signal-LO\ beating} \right) \quad (2.13)$$

where $i_1(t)$ is the photocurrent of the first PD, $i_2(t)$ is the photocurrent of the second PD, η is the responsivity of the PD, $2\pi\Delta f = f_S - f_{LO}$ is the frequency difference between the signal and the LO and $\Delta\phi(t) = \phi_S(t) - \phi_{LO}$ is the phase difference between the signal and the LO.

Therefore, the information about the amplitude and the phase of the signal is kept after the PD. In addition, the PD also produces two extra terms related with the DD of the LO and the signal, as is indicated on Equations 2.12 and 2.13. The extra terms can be removed because the balanced configuration of both PDs subtracts the Equation 2.12 and Equation 2.13, as shown in Figure 2.23 and giving the photocurrent as shown in Equation 2.14.

$$i_S(t) = i_1(t) - i_2(t) = 2\eta\,|E_S(t)|\,|E_{LO}|\sin(2\pi\Delta f t + \Delta\phi(t)) \quad (2.14)$$

where $i_S(t)$ is the difference between the photocurrents of the PDs.

After the PD, the received signal is downcoverted to $2\pi\Delta f$ and, depending of its value, the receiver can be classified as heterodyne ($|2\pi\Delta f| >> BW$), homodyne ($|2\pi\Delta f| = 0$) or intradyne receiver ($|2\pi\Delta f| < BW$) as it is depicted in Figure 2.24.

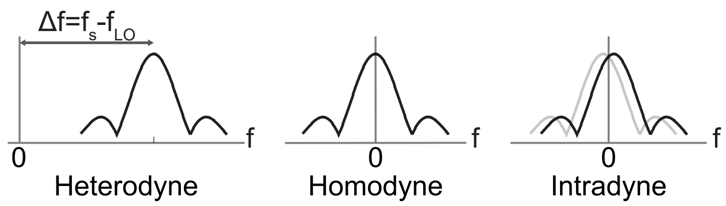

Figure 2.24: Heterodyne, homadyne and intradyne electrical spectra.

The coherent receiver, shown in Figure 2.23, is the basic heterodyne receiver and allows to recover the full information carried by the received signal. The electronic and/or digital signal processing (DSP) required to obtain the received data stream depends on the modulation format that is employed to transmit the signal. If the modulation format is an OOK or PAM-N, the data can be received employing an envelope detector since the information is carried only by the amplitude of the signal [118]. In the case of employing a differential PSK (DPSK), the data stream can be recovered multiplying the current symbol with the previous one [119–121]. In the case of employing non-differential PSK or QAM modulation formats, a phase-locked loop (PLL) [122] or complex demodulation algorithms [123] are required for obtain the I and Q components of the format. These reception techniques are summarized in Figure 2.25.

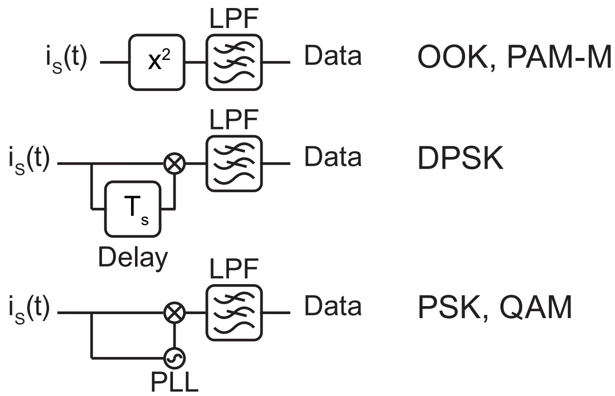

Figure 2.25: Heterodyne electical and digital receiver part.

A single PD version of this heterodyne receiver would be of interest for a reduced cost and more simple implementation. This has been one of the research results of this thesis and will be discused in detail in subsection 4.2.2.

If the coherent receiver described in Figure 2.23 is employed as homodyne receiver, i.e. the frequency difference ($2\pi\Delta f$) is 0, the received signal is converted directly to baseband although this receiver only will provide information about the I component as it is described in Equation 2.14. In order to receive the full information of the complex received signal, a phase-diversity homodyne receiver has to be implemented.

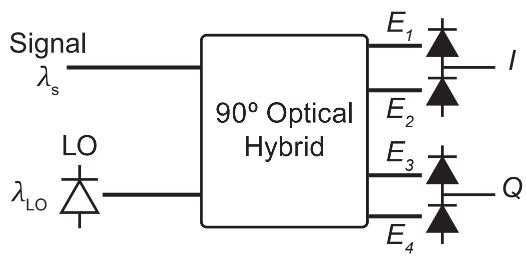

Figure 2.26: Phase-diversity homodyne coupler (90º hybrid).

The optical part of the phase-diversity homodyne receiver, also named as 90º hybrid, can be described by the Equation 2.15 [124], where the output fields are obtained from the input optical fields as can be seen in Figure 2.26.

$$\begin{pmatrix} \vec{E}_1 \\ \vec{E}_2 \\ \vec{E}_3 \\ \vec{E}_4 \end{pmatrix} = \frac{1}{2} \begin{pmatrix} 1 & 1 \\ 1 & -1 \\ 1 & j \\ 1 & -j \end{pmatrix} \begin{pmatrix} \vec{E}_S \\ \vec{E}_{LO} \end{pmatrix} \tag{2.15}$$

where $\vec{E}_1$, $\vec{E}_2$, $\vec{E}_3$ and $\vec{E}_4$ are the four output signals of the 90º hybrid. After the PDs reception, the I and Q components are described by Equation 2.16.

$$\begin{aligned} I(t) = i_1(t) - i_2(t) = \eta|E_1(t)|^2 - \eta|E_2(t)|^2 = \eta\,|E_S(t)|\,|E_{LO}|\cos(2\pi\Delta ft + \Delta\phi(t)) \\ Q(t) = i_3(t) - i_4(t) = \eta|E_3(t)|^2 - \eta|E_4(t)|^2 = \eta\,|E_S(t)|\,|E_{LO}|\,sin(2\pi\Delta ft + \Delta\phi(t)) \end{aligned} \tag{2.16}$$

where $I(t)$ and $Q(t)$ are the I and Q component signals and $i_1(t)$, $i_2(t)$, $i_3(t)$ and $i_4(t)$ are the photocurrents of the four PDs.

The condition for the frequency difference ($2\pi\Delta f$) to be 0, i.e. frequency lock between the received signal and the LO, together with the phase lock between the received signal and the LO can be achieved by an optical PLL (OPLL) [125–127]. The main drawback of the homodyne receivers comes from the necessity of implementing an OPLL, which increases dramatically its complexity.

The solution for this problem is the phase-diversity intradyne receiver. It is based in the same scheme shown in Figure 2.26 but they do not require $2\pi\Delta f$ to be 0. The intradyne receiver allows some frequency shift between the frequencies of the received signal and LO up to the electrical bandwidth BW. This frequency offset and the consequent phase unlocking can be solved by the DSP. DSP can be also used to improve other channel impairments.

Figure 2.27 shows the basic block diagram for the DSP of an intradyne receiver. The DSP can include the following blocks: IQ orthogonality, CD compensation, adaptative equalization, frequency offset compensation and phase compensation [108].

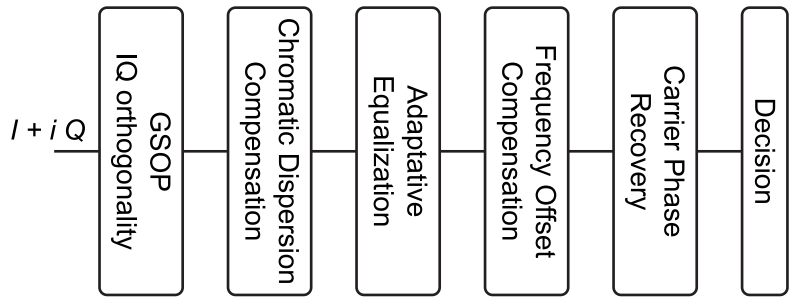

Figure 2.27: Digital signal processing of a coherent intradyne receiver.

The 3x3 couplers, also named as 120º hybrids, have been also proposed as an alternative to the 90º hybrids [128, 129]. The coherent receiver based on a 120º hybrid is shown in Figure 2.28.

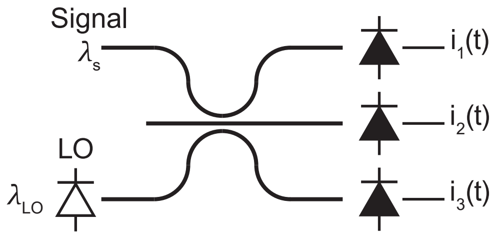

Figure 2.28: Coherent 3x3 receiver (120º hybrid).

This coherent receiver only requires two inputs, one for the received and other for the LO. The 120º hybrid operation is described by Equations 2.17 and 2.18 [128].

$$\begin{pmatrix} \vec{E}_1 \\ \vec{E}_2 \\ \vec{E}_3 \end{pmatrix} = \begin{pmatrix} a & b & b \\ b & a & b \\ b & b & a \end{pmatrix} \begin{pmatrix} \vec{E}_S \\ 0 \\ \vec{E}_{LO} \end{pmatrix} \tag{2.17}$$

where,

$$\begin{aligned} a &= \tfrac{2}{3}e^{j\frac{2\pi}{9}} + \tfrac{1}{3}e^{-j\frac{4\pi}{9}} \\ b &= \tfrac{1}{3}e^{-j\frac{4\pi}{9}} - \tfrac{1}{3}e^{j\frac{2\pi}{9}} \end{aligned} \tag{2.18}$$

After the 3x3 coupler, the three outputs are received with the three PDs obtaining the three photocurrents described in Equation 2.19.

$$\begin{aligned} i_1(t) &= \eta\left(\tfrac{1}{3}|E_{LO}|^2 + \tfrac{1}{3}|E_S(t)|^2 + \tfrac{2}{3}\,|E_S(t)|\,|E_{LO}|\cos\left(2\pi\Delta ft + \Delta\phi(t) + \tfrac{2\pi}{3}\right)\right) \\ i_2(t) &= \eta\left(\tfrac{1}{3}|E_{LO}|^2 + \tfrac{1}{3}|E_S(t)|^2 + \tfrac{2}{3}\,|E_S(t)|\,|E_{LO}|\cos\left(2\pi\Delta ft + \Delta\phi(t)\right)\right) \\ i_3(t) &= \eta\left(\tfrac{1}{3}|E_{LO}|^2 + \tfrac{1}{3}|E_S(t)|^2 + \tfrac{2}{3}\,|E_S(t)|\,|E_{LO}|\cos\left(2\pi\Delta ft + \Delta\phi(t) - \tfrac{2\pi}{3}\right)\right) \end{aligned} \tag{2.19}$$

Finally, the three photocurrents can be converted to the I and Q components following the Equation 2.20.

$$\begin{pmatrix} I(t) \\ Q(t) \end{pmatrix} = \begin{pmatrix} -\frac{1}{2} & 1 & -\frac{1}{2} \\ -\frac{\sqrt{3}}{2} & 0 & \frac{\sqrt{3}}{2} \end{pmatrix} \begin{pmatrix} i_1(t) \\ i_2(t) \\ i_3(t) \end{pmatrix} = \begin{pmatrix} \eta\,|E_{LO}|\,|E_S(t)|\cos\left(2\pi\Delta ft + \Delta\phi(t)\right) \\ \eta\,|E_{LO}|\,|E_S(t)|\sin\left(2\pi\Delta ft + \Delta\phi(t)\right) \end{pmatrix} \tag{2.20}$$

The described I and Q component extraction can be done after the digitalization of the three signals or by electrically reducing the digitalization process to only two signals, if the matrix is applied to the photocurrents by means of an analog electronic circuit. If the three signals are acquired, the matrix employed for extracting the I and Q component, which is shown in Equation 2.20, can be calibrated in order to compensate part of the receiver impairments [26] and reduce the interchannel interference.

Previously, it has been mentioned the necessity of a proper polarization alignment between the polarizations of both the signal and the LO. This requirement is not a trivial issue for coherent receivers because the polarization of the received signal varies randomly with time. A basic solution could be to include a polarization tracking system that makes the polarization of the LO to follow the polarization of the received signal [130].

However, the most common solution is to implement a polarization-diversity coherent receiver. This solution allows to avoid the polarization alignment issue and exploit the concept of polarization multiplexing. I will focus in the explanation of the polarization-diversity intradyne 90º hybrid receiver for describing this concept but it could be extended to the rest of the described receivers. This receiver is shown in Figure 2.29.

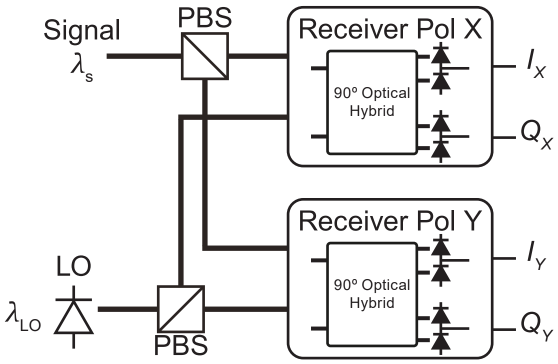

Figure 2.29: Polarization-diversity intradyne coupler (90º hybrid).

The polarization-diversity intradyne receiver duplicates the phase-diversity intradyne receiver, one for each of the orthogonal polarizations (X and Y polarization). A polarization beam splitter (PBS) separates the X and Y orthogonal polarizations of the received signal. The LO is aligned to a 45º polarization respect to the PBS main polarizations, which will be also splitted into the X and Y polarization by another PBS. Four signals (I_x, Q_x, I_y and Q_y) are generated after the PDs of the polarization-diversity intradyne receiver and they will be digitalized and processed in order to recover the signals carried by each polarization. The DSP is similar to the one used on the phase-diversity intradyne receiver for each polarization, but including an additional block to separate and recover the signals of each polarization [108]. The polarization recovering block is required because the polarization of the signal rotates due to the fiber propagation and the two orthogonal polarization will be mixed at the receiver. The summary of the DSP blocks of the polarization-diversity intradyne receiver is shown in Figure 2.30.

Polarization-diversity intradyne receivers based either on 90 hybrids [131] or on 120 hybrids [128] are extremely powerful receivers that allow to receive two signals multiplexed in polarization. The main drawback of this receiver is its complexity, its high cost and the fabrication impairments. Therefore, the polarization-diversity intradyne receiver is adequate for long-haul communications, but it is not suitable for cost-sensitive applications as PON.

The alternative to polarization-diversity receivers are polarization insensitive coherent receivers [132, 133]. This alternative will not allow to duplicate the data rate of the link through

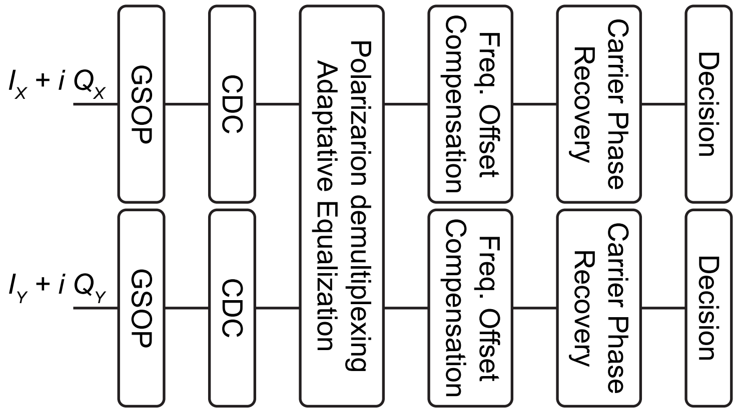

Figure 2.30: Digital signal processing of a coherent polarization-diversity intradyne receiver.

polarization multiplexing but it will allow to reduce the complexity and the cost of the coherent receiver for cost-sensitive applications. There are a lot of different options around the concept of polarization insensitive receiver for coherent communications depending on the link and modulation format of the received signal. Some of these alternatives will be described below.

The first polarization insensitive coherent receiver that will be described is based on a single PD heterodyne receiver [81, 134] and it was proposed for binary DPSK. This receiver includes a PBS after the coupler for detecting both polarizations. This receiver is described in subsection 4.2.2. On the other hand, some variations of this receiver for frequency shift keying (FSK) also have been proposed [135, 136].

The use of a 3x3 coupler combined with a PBS [137] is presented in Figure 2.31. This polarization insensitive coherent receiver has been designed for amplitude modulation signals as OOK or M-PAM. The PBS is used to split the LO in two polarizations (X and Y). The signal is connected to the upper input of the 3x3 coupler and the two outputs of the PBS are connected to the other two inputs of the 3x3 coupler. In addition, this receiver requires that the LO is frequency shifted by $0.9Rb$ in order to remove the interference of the DD signal. After the receiver, the 3 signals coming from the PDs are squared and added. This receiver can also be used for phase signals, but the 3 PD signals should be acquired without applying the squaring function [138] and a linear operation should be applied to obtain the I and Q signals and DD signal cancellation.

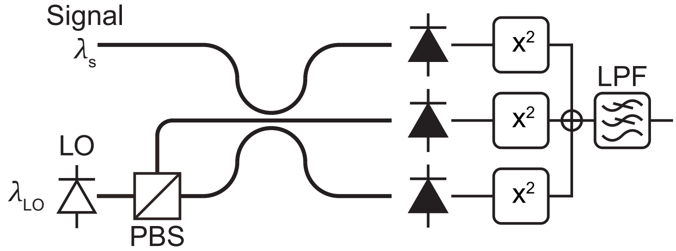

Figure 2.31: Ciaramella receiver.

Other alternative for obtaining a polarization insensitive link is to perform a polarization scrambling of the transmitted signal [112, 139], i.e. transmit the half of the symbol in each orthogonal polarization (X and Y). This coherent receiver will receive the signal partially aligned with the LO polarization in both halves of the period. In the worst of the cases, the LO polarization will be full aligned with the signal at least the half of the time. The reception can be implemented with a single-PD heterodyne receiver [139] or with a 120º intradyne receiver [112]. After the reception, both half periods will be added in order to maximize the received signal.

Finally, another alternative for polarization insensitive receivers are the so called Alamouti receivers [140, 141]. These receivers are based on a single polarization coherent receiver and are able to receive the signal independently of the state of the polarization of the signal and the LO thanks to the Alamouti polarization-time block code (PTBC). The PTBC requires a dual-polarization IQ modulator, which will be described lately. In addition, the PTBC has a 50% of redundancy so the spectral efficiency drops to half. The original Alamouti receiver employs an intradyne coherent receiver [140], as the one shown in Figure 2.26. Lately, the Alamouti receiver concept has been combined with the balanced PD heterodyne receiver [141], as shown in Figure 2.23, in order to simplify the receiver complexity.

2.2.4 Relation with the published works that are part of the compendium

I will summary the published works that are part of the compendium relating it with this introduction:

1. J. A. Altabas, D. Izquierdo, J. A. Lazaro, A. Lerin, F. Sotelo, and I. Garces, "1Gbps full-duplex links for ultra-dense-WDM 6.25GHz frequency slots in optical metro-access networks," *Optics Express*, vol. 24, no. 1, pp. 555–565, 2016 - section 3.1: In this article, the directly phase modulated DFB and the single PD heterodyne receiver with DFBs as LO are presented as feasible solution for transmitter and receiver in cost-effective ONUs. Their combination with a Nyquist-DPSK over MZM as downlink signal allows to generate a bidirectional channel with an occupied frequency slot of 6.25 GHz providing 1 Gbps for the uplink and for the downlink. This 6.25GHz bidirectional channel is ideal for uDWDM PON, as the one introduced in subsubsection 2.2.1.2. The directly phase modulated DFB generates an advanced modulation techniques, as it is the generated DSPK signal (subsection 2.2.2), using coherent technologies through the management of the chirp of the DFB (subsection 2.2.3). Additionally, the single PD heterodyne receiver is a coherent receiver applied for PON (subsection 2.2.3). Finally, the Nyquist pulse shaping (subsection 2.2.2) is applied to the downlink in order to fulfill the frequency slot target.

2. J. A. Altabas, D. Izquierdo, J. A. Lazaro, and I. Garces, “Cost-Effective Transceiver Based on an RSOA and a VCSEL for Flexible uDWDM Networks,” *IEEE Photonics Technology Letters*, vol. 28, no. 10, pp. 1111–1114, 2016 - section 3.2: In this article, a cost-effective ONU is proposed based on directly-phase modulated RSOA pumped with a VCSEL as transmitter. The same VCSEL is employed as LO of a single PD heterodyne receiver. This ONU combined with a Nyquist-DPSK over MZM as downlink allows to generate bidirectional channels that transmit 1 Gbps in each direction. This bidirectional channels only occupy frequency slots of 6.25 GHz or 5 GHz, which are also ideal for uDWDM PON (subsubsection 2.2.1.2). The NRZ-DSPK signal generated by the RSOA as uplink signal and the Nyquist-DPSK of the downlink are advanced modulation formats for PON (subsection 2.2.2). The directly phase modulation of a RSOA using its refractive index variation and the single PD heterodyne receiver with a VCSEL as LO are coherent technologies adapted to PON (subsection 2.2.3).

3. J. A. Altabas, D. Izquierdo, J. A. Lazaro, and I. Garces, “Chirp-based direct phase modulation of VCSELs for cost-effective transceivers,” *Optics Letters*, vol. 42, no. 3, pp. 583–586, 2017 - section 3.3: In this article, a 2.5 Gbps directly phase modulated VCSEL is presented. This direct phase modulation of VCSEL is gotten managing the chirp of the VCSEL (subsection 2.2.3). Additionally, a technique for obtaining the VCSEL chirp parameters for designing of the pulse shape, which is necessary for generating the DSPK with a direct modulation of a VCSEL (subsection 2.2.2 and subsection 2.2.3). This transmitter is a serious candidate for cost-effective transmitters in the uDWDM PON (subsubsection 2.2.1.2).

4. J. A. Altabas, G. Silva Valdecasa, L. F. Suhr, M. Didriksen, J. A. Lazaro, I. Garces, I. Tafur Monroy, A. T. Clausen, and J. B. Jensen, “Real-Time 10 Gbps Polarization Independent Quasicoherent Receiver for NG-PON2 Access Networks,” *Journal of Lightwave Technology*, vol. 37, no. 2, pp. 651–656, 2019 - section 3.4: This article presents a real-time polarization independent 10 Gbps quasicoherent receiver. This coherent receiver (subsection 2.2.3) has been adapted for receiving IM signals from the current standards (Appendix A). The quasicoherent receiver is designed to work in DWDM based PONs (subsubsection 2.2.1.1) without the necessity of optical filters, which makes it a perfect candidate for the NG-PON2 standard (subsection A.1.4).

5. J. A. Altabas, L. F. Suhr, G. Silva Valdecasa, J. A. Lazaro, I. Garces, J. B. Jensen, and A. T. Clausen, “25Gbps Quasicoherent Receiver for Beyond NG-PON2 Access Networks,” in *2018 European Conference on Optical Communication (ECOC)*, (Rome, Italy), p. We2.70, 2018 - section 3.5: This conference contribution explores the combination of the quasicoherent receiver with equalizers in order to receive 25 Gbps IM signals. Thus,

this contribution explores the adaptacion of advanced coherent technologies for PONs (subsection 2.2.3). The target of this 25 Gbps quasicoherent receiver is address the necessities of future access networks (section A.3) through single or multiwavelength channels (subsubsection 2.2.1.1).

Chapter 3

Published works

3.1 Paper I

1Gbps full-duplex links for ultra-dense-WDM 6.25GHz frequency slots in optical metro-access networks

J. A. Altabas, D. Izquierdo, J. A. Lazaro, A. Lerin, F. Sotelo, and I. Garces, "1Gbps full-duplex links for ultra-dense-WDM 6.25GHz frequency slots in optical metro-access networks," *Optics Express*, vol. 24, no. 1, pp. 555–565, 2016

1Gbps full-duplex links for ultra-dense-WDM 6.25GHz frequency slots in optical metro-access networks

Jose A. Altabas,[1,*] David Izquierdo,[1,2] Jose A. Lazaro,[3] Adolfo Lerin,[3] Felix Sotelo,[1] and Ignacio Garces[1]

[1]*Grupo de Tecnologías Fotónicas (GTF), Aragon Institute of Engineering Research (I3A), Universidad de Zaragoza, Mariano Esquillor ed. I + D + i, Zaragoza, 50018, Spain*
[2]*Centro Universitario de la Defensa (CUD), Academia General Militar, Carretera de Huesca s/n, Zaragoza, 50090, Spain*
[3]*Grupo de Comunicaciones Ópticas (GCO), Universitat Politècnica de Catalunya, Jordi Girona 31, Barcelona, 08034, Spain*
**jaltabas@unizar.es*

Abstract: 1Gbps full-duplex optical links for 6.25GHz ultra dense WDM frequency slots are demonstrated and optimized for cost-effective metro-access networks. The OLT-ONU downlinks are based on 1Gbps Nyquist-DPSK using MZM and single-detector heterodyne reception obtaining a sensitivity of −52dBm. The ONU-OLT uplinks are based on 1Gbps NRZ-DPSK by directly phase modulated DFB and also single-detector heterodyne reception obtaining same sensitivity of −52dBm. The power budget of full-duplex link is 43dB. These proposed links can provide service to 16 (32) users at each 100 (200) GHz WDM channel.

OCIS codes: (060.1660) Coherent communications; (060.2360) Fiber optics links and subsystems; (060.5060) Phase modulation.

References and links

1. H. Song, B. Kim, and B. Mukherjee, "Long-reach optical access networks: a survey of research challenges, demonstrations, and bandwidth assignment mechanisms," IEEE Comm. Surv. and Tutor. **12**(1), 112–123 (2010).
2. J. A. Lazaro, J. Prat, P. Chanclou, G. M. Tosi Beleffi, A. Teixeira, I. Tomkos, R. Soila, and V. Koratzinos, "Scalable extended reach PON," in *Optical Fiber Communication Conference/National Fiber Optic Engineers Conference*, OSA Technical Digest (CD) (Optical Society of America, 2008), paper OThL2.
3. W. Shieh, H. Bao, and Y. Tang, "Coherent optical OFDM: theory and design," Opt. Express **16**(2), 841–859 (2008).
4. J. A. Altabas, F. Sotelo, J. A. Lazaro, and I. Garces, "Experimental bandwidth optimization for flexible PON using Nyquist shaped PSK," in *2015 European Conference on Lasers and Electro-Optics - European Quantum Electronics Conference* (Optical Society of America, 2015), paper CI_2_4.
5. X. Liu, S. Chandrasekhar, and P. J. Winzer, "Digital signal processing techniques enabling multi-Tb/s superchannel transmission: an overview of recent advances in DSP-enabled superchannels," IEEE Signal Process. Mag. **31**(2), 16–24 (2014).
6. C. Kottke, K. Habel, M. H. Eiselt, H. Griesser, and J. P. Elbers, "Coherent subcarrier-WDM-PON system with SSB modulation and wavelength reuse," in *Optical Fiber Communication Conference/National Fiber Optic Engineers Conference 2013*, OSA Technical Digest (online) (Optical Society of America, 2013), paper OM2A.3.
7. R. S. Vodhanel, A. F. Elrefaie, M. Z. Iqbal, R. E. Wagner, J. Gimlett, and S. Tsuji, "Performance of directly modulated DFB lasers in 10-Gb/s ASK, FSK, and DPSK lightwave systems," J. Lightwave Technol. **8**(9), 1379–1386 (1990).
8. M. Funabashi, H. Nasu, T. Mukaihara, T. Kimoto, T. Shinagawa, T. Kise, K. Takaki, T. Takagi, M. Oike, T. Nomura, and A. Kasukawa, "Recent advances in DFB lasers for ultradense WDM applications," IEEE J. Sel. Top. Quantum Electron. **10**(2), 312–320 (2004).
9. J. Zhu, S. Pachnicke, M. Lawin, S. Mayne, A. Wonfor, R. V. Penty, R. Cush, R. Turner, P. Firth, M. Wale, I. H. White, and J.-P. Elbers, "First demonstration of a WDM-PON System using full C-band tunable SFP+ transceiver modules [Invited]," J. Opt. Commun. Netw. **7**(1), A28–A36 (2015).
10. I. N. Cano, A. Lerin, V. Polo, and J. Prat, "Direct phase modulation DFBs for cost-effective ONU transmitter in udWDM PONs," IEEE Photonics Technol. Lett. **26**(10), 973–975 (2014).
11. B. Glance, "Polarization independent coherent optical receiver," J. Lightwave Technol. **5**(2), 274–276 (1987).

#252375 Received 20 Oct 2015; revised 21 Dec 2015; accepted 22 Dec 2015; published 7 Jan 2016
(C) 2016 OSA 11 Jan 2016 | Vol. 24, No. 1 | DOI:10.1364/OE.24.000555 | OPTICS EXPRESS 555

12. ITU-T Rec., G.975.1: Forward error correction for high bit-rate DWDM submarine systems (2004).
13. ITU-T Rec., G.652: Characteristics of a single-mode optical fibre and cable (2009).
14. P. Gysel and R. K. Staubli, "Statistical properties of Rayleigh backscattering in single-mode fibres," J. Lightwave Technol. **8**(4), 561–567 (1990).

1. Introduction

The telecommunications scenario is quickly evolving during the last years. Growing cloud and multimedia streaming services are creating new communication frameworks, requiring flexible architectures in order to enable scalability while supporting a high level of dynamic connectivity. While the core remains as a multi-layer packet over optical network, metro networks are merging with access networks, as depicted in Fig. 1, and evolving towards an all-optical solution [1, 2]. In these networks, the Optical Line Terminal (OLT) acts just like another node in the metro network, while the users/subscribers are connected through a Passive Optical Network (PON), having a tree topology in Fig. 1, which is linked to the metro access through a Reconfigurable Optical Add-Drop Multiplexer (ROADM) node. Each PON uses a different WDM channel that is shared among all the subscribers connected through the same PON, using narrower ultra dense WDM (udWDM) channels for both up and down links, as is depicted in Fig. 1. Meanwhile, the metro network is transparent transmitting the entire optical spectrum within a given optical transmission band between the different nodes in such a way that each ROADM extracts the WDM channel of its child PON from the network. The connection between the OLT/Node and each user/subscriber ONU (Optical Network Unit) is established using a different udWDM channel or frequency slot for each user, which travels unalterable (without any wavelength conversion) in the entire merged network.

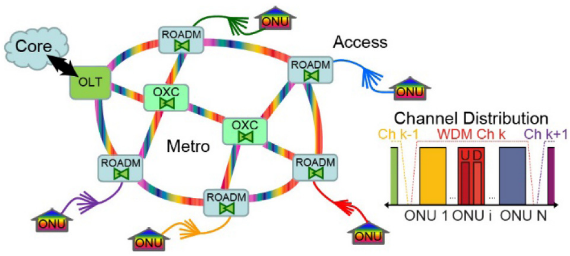

Fig. 1. All-optical access/metro network scenario. Inlet: proposed flexible udWDM full-duplex frequency slot division.

Additionally, the increasing traffic demand is pushing an even more efficient use of optical network resources by developing Elastic/Flexible Optical Networks and bandwidth optimization. Lately, this has been mainly done by several techniques, namely orthogonal frequency division multiplexing (OFDM) [3] and Nyquist pulse-shaping [4]. Both methods can be implemented using flexible digital transmitters and receivers [5] and require very sophisticated Digital Signal Processing (DSP), but are expected to give: the best performance and the highest flexibility in the near future; and also adaptive modulation format to ensure successful transmission under varying link conditions.

In this paper we propose a passive optical access network that uses 6.25GHz optical frequency slots for each user/subscriber where 1Gbps full-duplex channel are obtained for down (from OLT to ONU) and up (from ONU to OLT) streams using Differential Binary Phase Shift Keying (DPSK) modulation in a udWDM scheme. Using the proposed scheme in combination with Nyquist pulse shaping technique, 16 (32) frequency slots can be allocated within each ITU 100GHz (200GHz) wide WDM channel. The presented coherent links will allow an increment of the number of users of the current access networks. Therefore, the deployment and the maintenance costs of these networks will be shared by a greater number of users so the cost per user will be reduced.

#252375 Received 20 Oct 2015; revised 21 Dec 2015; accepted 22 Dec 2015; published 7 Jan 2016

Two different flexible digital transceivers (transmitter and receiver) have been developed and are presented in this paper. As flexible digital transceivers, the bit rate can be adapted to user's requirements. 1Gbps full-duplex channel has been detailed measured as a reference for testing minimum size of the frequency slots. The ONU transmitter is based on cost-effective light sources and uses NRZ pulse-shaping while the OLT uses an externally modulated tunable light source and Nyquist pulse-shaping technique to provide a higher spectral efficiency. Both OLT and ONU receivers are based on a reduced-complexity heterodyne receiver compatible with a polarization independent version.

2. Experimental setup

The experimental setup for the evaluation of the proposed merged network is depicted in Fig. 2, where an OLT can serve to several ONUs of a PON using phase modulation and coherent detection in udWDM full-duplex 1Gbps channels. We will show that it is possible to allocate 16 of those channels in a 100GHz wide ITU grid channel. The full-duplex link between OLT and an ONU of the PON will be evaluated for sensitivity measurements including additional ONU implemented for interchannel interference measurements.

The OLT transmitter is based on an external cavity, 100kHz linewidth, Tuneable Laser Source (TLS), modulated by a Mach-Zehnder Modulator (MZM). The TLS is used to adjust its wavelength inside the frequency slot for these measurements, but a wavelength thermally-tunable Distributed Feedback Laser (DFB) can be used instead of the TLS. The MZM is set at the minimum transmission point for phase modulation and is thermally controlled to ensure its stability. In this configuration, the OLT would need as many transmitters as served ONUs, but this configuration can be simplified combining several user downstream data by electrical subcarrier division multiplexing previous to its optical modulation by a high bandwidth I/Q modulator [6].

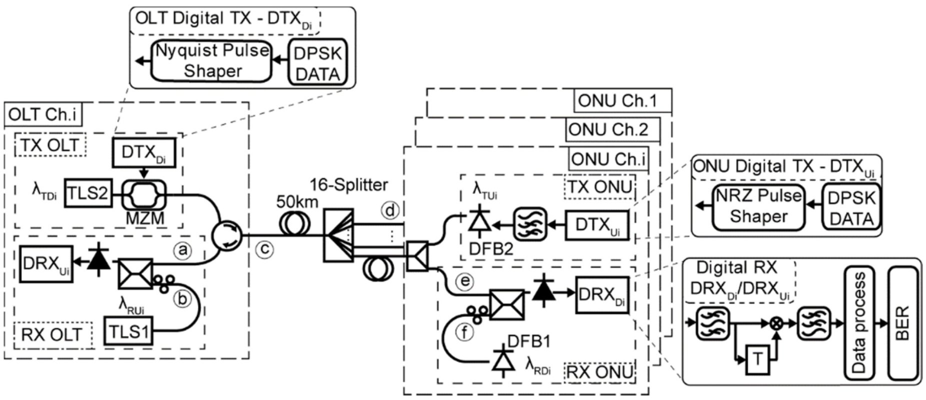

Fig. 2. Experimental setup for the evaluation of the optical link. P_{RX} at (a) and (e) points, P_{LO} at the (b) and (f) point and P_{TX} at (c) and (d) points.

The ONU transmitter consists of a DFB, which is direct-phase-modulated using its chirp through a previously equalized signal [7]. The cost-effective DFB used for the measurements presents a relative wide linewidth, in the range of 10MHz. The DFB emission wavelength is thermally tuned to achieve the channel spacing and flexible grid requirements inside the WDM channel. These requirements, fine tuning and long time stability, can be ensured using Proportional Integral Derivative (PID) thermal controllers with a ± 0.01°C resolution and stability. The used DFB frequency variation with temperature is 10GHz/°C, similar to other cost-effective DFBs [8], so the ± 0.01°C PID resolution will ensure a wavelength stability

#252375 Received 20 Oct 2015; revised 21 Dec 2015; accepted 22 Dec 2015; published 7 Jan 2016
(C) 2016 OSA 11 Jan 2016 | Vol. 24, No. 1 | DOI:10.1364/OE.24.000555 | OPTICS EXPRESS 557

around 100MHz. If higher stability is required, the PID controller may be upgraded using a low bandwidth photodiode with an etalon [9].

Both optical transmitters (OLT and ONU) use a Digital Transmitter (DTX) unit, where the data is differentially encoded and shaped to achieve maximum performance for the 1Gbps up and down data-streams. The transmitted symbols in the OLT Digital Transmitter (DTX_{Di}) are filtered using a Nyquist Pulse Shaper filter with 12-symbols filter length and zero roll-off factor. The transmitted symbols generated in the ONU Digital Transmitter (DTX_{Ui}) are bipolar Non Return to Zero (NRZ) coded and high-pass filtered to obtain the phase modulation of the laser [7, 10]. The DTX are implemented in MATLAB™ and the electrical signals are generated by a 12GSa/s Arbitrary Waveform Generator.

The link between the OLT and the ONUs is fully passive and it implemented by on 50Km of Standard Single Mode Fiber (SSMF) and a 16-splitter for sharing out the data to the users. It represents one of the PON sections shown in Fig. 1.

Both receivers are based on a single photodetector heterodyne detection configuration. In this configuration the received signal is coupled with the Local Oscillators (LO), mixed in the photodetector and filtered. The LO used in the OLT receiver is an external cavity TLS with similar characteristics to the one used for the transmitter, and as was pointed out for the OLT transmission, it can be substituted by a DFB presenting enough wavelength stability without BER penalty. Besides, the ONU uses the same DFB model for both: the receiver and transmitter. Both LOs have been configured to provide the same optical power of + 4.2dBm. The emission wavelength of these LOs is tuned $\Delta\lambda$ away from the received central wavelength of its uDWDM channel, being $\lambda_{RDi} = \lambda_{TDi} \pm \Delta\lambda$ at the ONU and $\lambda_{RUi} = \lambda_{TUi} \pm \Delta\lambda$ at the OLT. The coherent detection is highly dependent on the polarization difference between signal an LO, so we had to adequately control the polarization of the signal for our measurements, but our system is easily upgradeable to a polarization independent heterodyne receiver like the proposed in [11].

The received signal has been optically down-converted in the heterodyne detector to an Intermediate Frequency (IF) equal to the frequency shift between the LO and the central wavelength of the received signal ($\Delta\lambda$). 1GHz and 2GHz have been chosen as the heterodyne IFs because they represent a compromise between: a) an optimum separation between the 1Gbps signal and the LO to obtain the best BER performance (IF = $n \cdot Rb$, with n integer); and b) the achievement of the narrowest frequency slot for each user. The obtained IF signal is amplified and, digitalized using a 40GSa/s Digital Oscilloscope with a 2.5GHz electrical bandwidth. However, the signal can be digitalized with a lower sampling rate down to 10GSa/s without BER penalty. The first step in the digital processing is the bandpass filtering of the digitalized signal in order to reduce the noise and eliminate the adjacent channels and the non-heterodyned part of the received signal produced by the rest of the channels that are reaching the detector out of band of the heterodyne signal. The demodulation of the DPSK format, is made by multiplying the signal with the same signal delayed by one symbol and by lowpass filtering, Fig. 2. Finally, the bit error rate (BER) is calculated comparing the received data-stream with the transmitted one.

2.1 Experimental digital receiver filtering optimization

The digital filters inside each DRX have been optimized separately to maximize the sensitivity in the receivers. The Band Pass Filter (BPF) and Low Pass Filter (LPF) bandwidths at the ONU (DRX_{Di}) have been optimized to minimize the BER for the two different heterodyne frequencies (1GHz and 2GHz) for a received Nyquist-DPSK downlink signal of –48dBm. The central frequencies of the BPF are fixed to the heterodyne frequencies. The minimum BER, as shown by red crosses in Fig. 3, is achieved for a BPF bandwidth of 1.3GHz (IF = 1GHz) and 1.5GHz (IF = 2GHz), respectively. The minimum BER for the case of 1GHz IF is higher than the BER of the 2GHz case due to the reduction of the BPF bandwidth needed to eliminate the non-heterodyne signal that is closer to the signal of interest

#252375 Received 20 Oct 2015; revised 21 Dec 2015; accepted 22 Dec 2015; published 7 Jan 2016

for the 1GHz IF than in the 2GHz IF. On the other hand, the BER is minimum and stabilized for both heterodyne frequencies for LPF bandwidths higher than 1.25GHz in both cases as shown in Fig. 3.

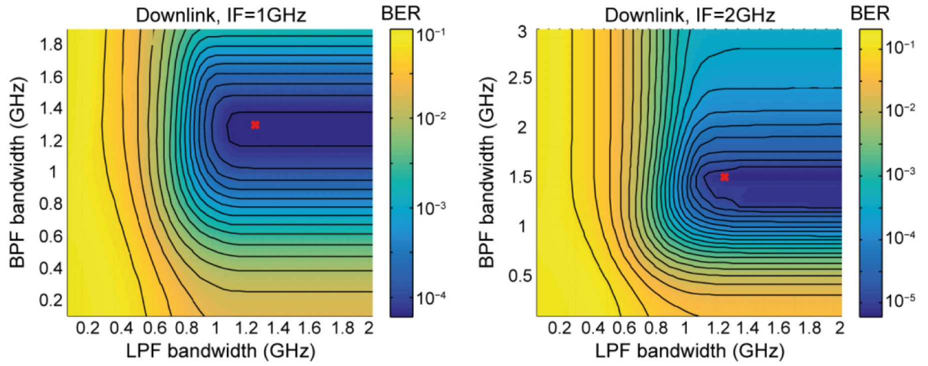

Fig. 3. Experimental results showing the optimization of digital BPF and LPF used in the Digital Receiver at the ONU (Nyquist-DPSK modulation) for 1GHz (left) and 2GHz (right) of intermediate frequency.

For the optimization of the OLT receiver (DRX_{Ui}) the BPF filter parameters have been investigated while the LPF bandwidth has been fixed to the same value than in the ONU Digital Receiver, 1.25GHz. Two BPF main parameters, the bandwidth and the low cut-off frequency, have been optimized to reduce the BER for the same two heterodyne IF frequencies (1GHz and 2GHz) at the same conditions of −48dBm NRZ-DPSK uplink signal at the receiver. As shown in Fig. 4, the optimum lower cut-off frequencies are 0.6GHz (IF = 1GHz) and 1.2GHz (IF = 2GHz), respectively. These optimum cut-off frequencies eliminate part of the main spectral lobe of the NRZ-DPSK signal (30% for IF = 1GHz and 10% for IF = 2GHz, respectively) but also remove almost completely the non-heterodyned signal, which can be greater than the useful signal, and scales up as the number of udWDM channels increases. The optimum BPF bandwidths are 1.6GHz and 2.3GHz, for 1GHz and 2GHz intermediate frequency respectively.

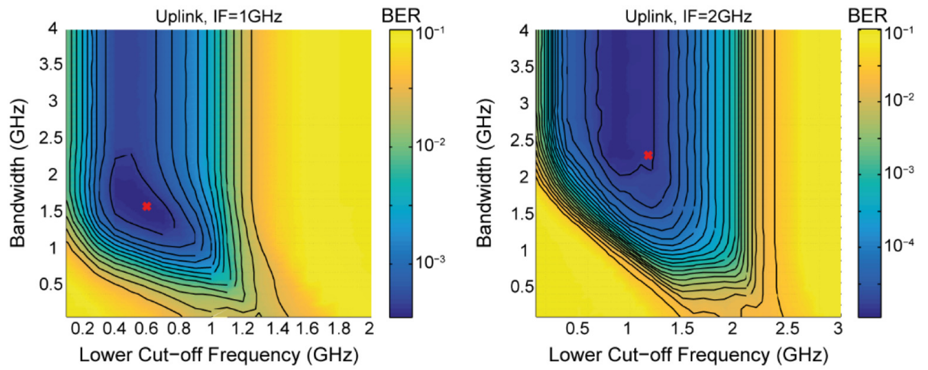

Fig. 4. Experimental results showing the optimization of digital BPF used in the Digital Receiver at the OLT (NRZ-DPSK modulation) for 1GHz (left) and 2GHz (right) of intermediate frequency.

#252375 Received 20 Oct 2015; revised 21 Dec 2015; accepted 22 Dec 2015; published 7 Jan 2016
(C) 2016 OSA 11 Jan 2016 | Vol. 24, No. 1 | DOI:10.1364/OE.24.000555 | OPTICS EXPRESS 559

3. Results

The performance of both links, downlink with Nyquist-DPSK modulation over MZM and uplink with NRZ-DPSK directly-modulated DFB, has been analyzed to proof the feasibility of the proposed flexible udWDM full-duplex optical link. The first analyzed parameter is the sensitivity of each link, which is defined as the minimum received power to ensure a minimum quality of the links. The second analysis focuses in the spectral separation of the uplink and downlink wavelengths, which determines their allocation inside the frequency slot. Both analyses have been performed for two IF heterodyne frequencies (1GHz and 2GHz).

3.1 Sensitivity

The sensitivity of both links has been defined as the minimum received power to ensure a 10^{-12} BER using a 7% overhead FEC, as recommended by ITU-T G.975.1 [12]. This FEC limit requires a maximum received BER of $2.2\cdot10^{-3}$.

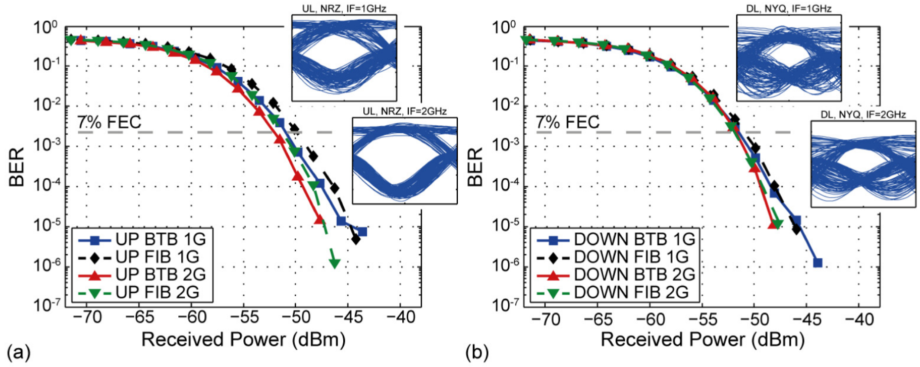

Fig. 5. BER versus received power for the two links in the OLT-ONU connection, uplink (left) and downlink (right), and for the two heterodyne frequencies (1GHz and 2GHz). Inlets: Eye diagrams for $P_{RX} = -36$dBm.

The back-to-back (BTB) downlink sensitivity is −52dBm with a heterodyne frequency of 2GHz, as shown in Fig. 5(b), and the sensitivity penalty when reducing the heterodyne frequency down to 1GHz is lower than 0.5dB. The interference of the non-heterodyned part of the received signal, affecting more significantly as commented before, generates this power penalty. The downlink is almost unaffected by the fiber transmission, as the power penalty of a transmission through 50km of ITU-T G.652.A SSMF [13] is below 0.5dB. This small dispersion power penalty is due to the narrow bandwidth of the Nyquist-DPSK modulation, around 1GHz for a 1Gbps data rate.

The BTB uplink sensitivity, as shown in Fig. 5(a), is the same than in the downlink (−52dBm) using a heterodyne IF of 2GHz and −51dBm when the heterodyne IF is 1GHz. The power penalty for reducing the intermediate frequency is 1dB because the optimized digital filters remove a greater part of the signal spectrum when the heterodyne IF is 1GHz than when it is 2GHz. The power penalty of 50km ITU-T G.652.A SSMF at the uplink is slightly higher than 1dB due to the wider spectrum transmitted through the NRZ-DPSK modulation.

3.2 Link separation / Frequency slot composition

The user channel is composed of two streams, downlink and uplink, which allocation inside the frequency slot has to ensure a null BER penalty due to the transmission Rayleigh backscattering in the receiver, e.g. the OLT transmitter should not affect the OLT receiver. This is usually avoided by separating the up and down wavelengths, but in our case we are trying to set them as close as possible following a udWDM scheme, so it is important to

#252375 Received 20 Oct 2015; revised 21 Dec 2015; accepted 22 Dec 2015; published 7 Jan 2016

11 Jan 2016 | Vol. 24, No. 1 | DOI:10.1364/OE.24.000555 | OPTICS EXPRESS 560

analyze this point. Moreover, the frequency slot composition is the same for all the users, so a downlink stream will be always between two uplinks and vice versa, see Fig. 1. Thus, the distribution of the links inside a frequency slot has also to ensure that the interference of the transmission Rayleigh backscattering of a stream does not introduce a BER penalty in its two adjacent streams.

The analysis of the BER penalty introduced by a transmitting link over its own receiver and the adjacent one has been studied for two different transmitter optical powers (0dBm and −6dBm). This analysis has been done using the most critical configuration for the backscattering of each link, placing a 50km-long SSMF spool in different locations, as shown in Fig. 6. This fiber is long enough to generate a maximum level of Rayleigh backscattering optical power, which is practically constant for optical fibers longer than 20 km [14]. The LO used in the receivers has been shifted down from the central frequency of the received link at two heterodyne IF 1GHz and 2GHz. As it is shown in Fig. 6, adjacent links are varied −8GHz to 6GHz from the central frequency of the 1Gbps link under BER analysis.

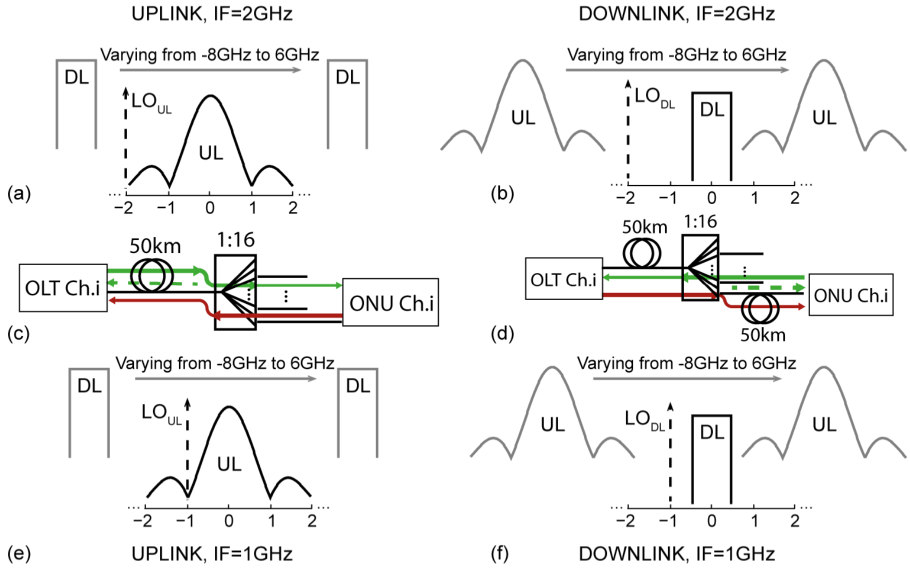

Fig. 6. Link separation setup (c, d), position of the received links and LOs and variation of the interference-backscattering link (a, b, e, f).

For the uplink characterization, the OLT is, simultaneously, receiving a −48dBm uplink transmitted by the ONU of the user channel Ch.i and transmitting the downlink of the same user channel Ch.i or of the adjacent user channel Ch.i ± 1. The worst network-configuration for this case, which is also the most common, is that one where a long feeder fiber (50km) is placed between the OLT and the 16-splitter (1:16), because the generated backscattering by the downlink will not be attenuated by the splitter, see Fig. 6(c). As shown in Fig. 7(a), there is a clear BER penalty when the + 0dBm downlink is placed in the frequency band between −6GHz and + 2GHz (8GHz) from the central frequency of the uplink. This frequency band must be avoided for the downlink. If the optical power transmitted by the downlink is reduced, both, BER penalty and banned frequency-band, are reduced (as shown in Table 1, where all the configurations are summarized). In fact, when the downlink optical transmitted power is −6dBm, it can be placed over this of the LO (at −2GHz) because the BER penalty is practically null. This special band is due to the narrow spectral bandwidth of the Nyquist-DPSK transmission used in the downlink (1GHz) and the optimal lower cut-off frequency of

#252375 Received 20 Oct 2015; revised 21 Dec 2015; accepted 22 Dec 2015; published 7 Jan 2016

the BPF for IF 2GHz (1.2GHz as commented previously), therefore effectively filtering out any Rayleigh backscattering interference. This reduction in the BER at the spacing of the LO wavelength decreases significantly, when the heterodyne frequency is 1GHz, see Fig. 7(c). In this case, the optimum lower cut-off frequency of the BPF for IF 1GHz of 0.6GHz does not filter out completely the Rayleigh backscattering interference of the Nyquist-DPSK downlink. In this case, the optimum lower cut-off frequency of the BPF for IF 1GHz of 0.6GHz does not filter out completely the Rayleigh backscattering interference of the Nyquist-DPSK downlink. Fortunately, the banned frequency band is also reduced, from −4GHz to + 2GHz (6GHz).

For the downlink characterization, the ONU is receiving a −48dBm downlink signal transmitted by the OLT while it is transmitting the uplink of the same user channel Ch.i. The worst network-configuration is that one presenting a long drop SSMF (50km) between the 16-splitter (1:16) and the ONU, as depicted in Fig. 6(d), significantly longer that typical PON deployments, hence covering worst conditions. In this case, the banned-band is higher than in the uplink case, between −6GHz and + 4GHz (10GHz) from the central frequency with a + 0dBm uplink, see Table 1, and the LO is placed at −2GHz position, see Fig. 7(b). Even more important is that now there is not a non-banned frequency band around the LO when the IF is 2GHz, where a clear reduction in the BER values can be seen although it is not enough. The reduction of the banned frequency band when the heterodyne frequency is 1GHz, see Fig. 7(d), also happens in the downlink case. The reason is that the Rayleigh backscattering interference signal, proportional to the spectrum of the uplink NRZ-DPSK directly-modulated DFB is significantly broader. Therefore, the BPF cannot properly filter out the inference signal, neither for IF = 2GHz, nor for IF = 1GHz. The case of the interference of the uplink of the adjacent ONU (Ch.i-1) has been tested but it is not shown because the interference with the interest ONU is null for both 0 and −6dBm optical powers. For clarifying, the uplink of the adjacent ONU (Ch.i-1) is attenuated by the 1:16 splitter and the Rayleigh backscattering generated at the 50Km feeder fiber is also attenuated again by the 1:16 splitter. Summarizing the Rayleigh backscattering arriving to ONU (Ch.i) due to uplink of the adjacent ONU (Ch.i-1) is fully negligible as it has been checked experimentally.

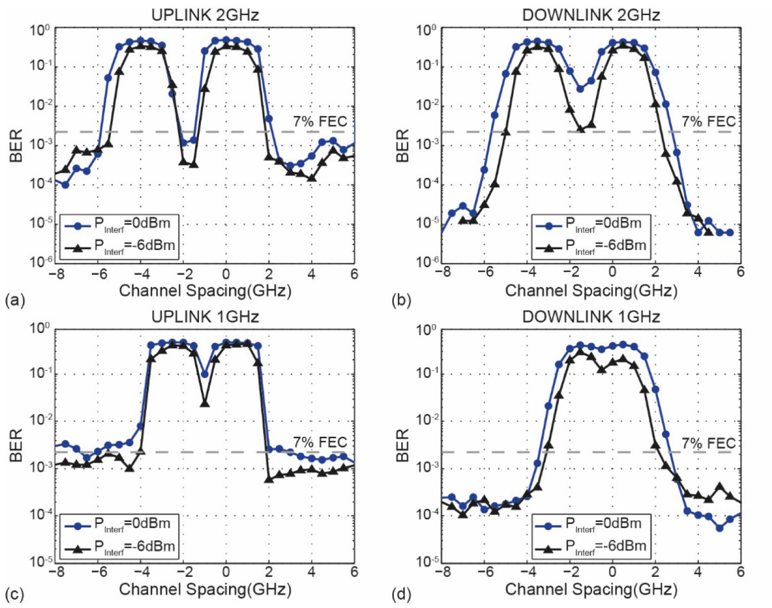

Fig. 7. BER penalty for different links: ONU downlink (a, c) and OLT uplink (b, d).

#252375 Received 20 Oct 2015; revised 21 Dec 2015; accepted 22 Dec 2015; published 7 Jan 2016

11 Jan 2016 | Vol. 24, No. 1 | DOI:10.1364/OE.24.000555 | OPTICS EXPRESS 562

In both links, the optical power reduction of the transmitted interference signal leads to a reduction of the banned frequency bands due to the reduction of the backscattering power, including the generated by the secondary lobs of the NRZ-BPSK.

Table 1. Banned frequency bands for the adjacent links. Referenced to the received signal central frequency.

Interference Transmitted Power	Downlink		Uplink	
	IF = 1GHz	IF = 2GHz	IF = 1GHz	IF = 2GHz
0dBm	−4GHz to 3.5GHz	−6GHz to 4GHz	−4GHz to 2GHz	−6GHz to 2GHz
−6dBm	−3.5GHz to 3.5GHz	−6GHz to 3.5GHz	−4GHz to 2GHz	−6GHz to −2.5GHz −1.5GHz to 2GHz

4. Discussion: channel distribution and power budget

Based on the previous analysis, it is possible to allocate the two links of each user channel in a 6.25GHz frequency slot for the two heterodyne frequencies used in this study, as shown in Fig. 8. In both cases, the transmitted optical power for all the links is fixed to −6dBm in order to obtain a channel allocation without BER penalties.

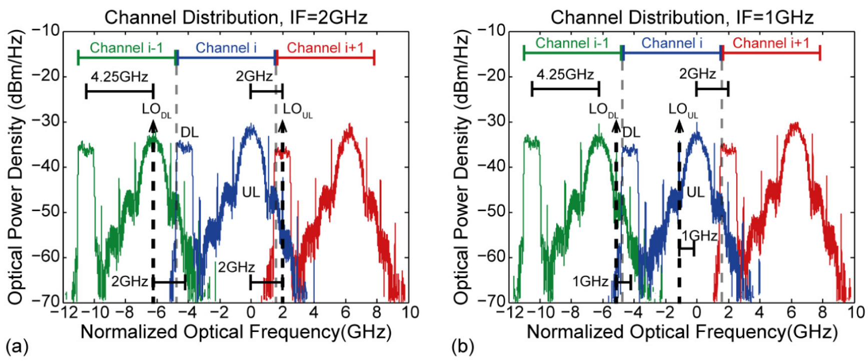

Fig. 8. Spectrum of three contiguous OLT-ONU channels. The central frequency corresponds to 1560.3nm.

When the heterodyne frequency is 2GHz, Fig. 8(a), the separation between the central frequency of the downlink and the uplink of the same channel is 4.25GHz. Moreover, the separation between the uplink and the downlink of adjacent channels is 2GHz. This link distribution has been done according to the channel separation results summarized at Table 1 and the non-interference between the Rayleigh backscattering of the uplink of the adjacent channel and the downlink. The LO used in the ONU is placed 2GHz below the central frequency of the downlink, while in the OLT the LO is 2GHz above the uplink central frequency, as shown in Fig. 8(a).

The channel composition, downlink and uplink position inside the frequency slot, is the same for both heterodyne intermediate frequencies. The only difference is the position of the local oscillators. As shown at Fig. 8(b), both LO are placed 1GHz below of the central frequency of their links.

Taking into account the limited transmission power for the links (−6dBm) and the sensitivity obtained in the previous section, the power budget of each link has been calculated for both heterodyne frequencies, Table 2. The best case for both links is to use a 2GHz heterodyne frequency, obtaining a power budget of 43dB for the downlink and 45dB for the uplink. This power budgets takes into account the 3dB of insertion losses of the splitter at the input of ONU and 1dB of the circulator used at the OLT, needed for separating both the uplink and the downlink. In the 1GHz heterodyne IF case, the power budget is 42.5dB for the downlink and 44dB for the uplink. The 3dB of insertion losses of the ONU input splitter can be reduced using an asymmetrical splitter. This is possible because there is a 12dB margin between the DFB emission power and the transmitter required power at the ONU output. Thus, an 80/20 splitter can be used at the ONU where the insertion losses for the receiver will be 0.97dB in this case and the uplink would become the limiting power budget.

Table 2. Receiver sensitivity and power budget for a 16 users PON.

	IF = 2GHz		IF = 1GHz	
Link	P_{RX}	Power Budget	P_{RX}	Power Budget
Uplink	−52dBm	45dB	−51dBm	44dB
Downlink	−52dBm	43dB	−51.5dBm	42.5dB

The power budget indicates than the best case for both links is achieved for the heterodyne frequency of 2GHz and the channel distribution and the LO allocation is the Fig. 8(a). This channel allocation allows that each full-duplex channel occupies a frequency slot of 6.25GHz.

The 100GHz (200GHz) WDM channel is proposed as the basic routing unit for the metro network and as the add/drop unit channel for the metro-access interface, which will require a 1:16 (1:32) power splitter for the last distribution range. In a non-routing scenario (a standard PON without OXCs and/or ROADMs) and a 2GHz heterodyne IF frequency, the power budget (Table 2) allows maximum reach distances between the OLT and the ONU in the range of 117Km for a 100GHz WDM channel (1:16 splitter with 13.8dB insertion loss) and 103Km for a 200GHz WDM channel (1:32 splitter with 17.2dB insertion loss). In a routing scenario, the maximum reach distance will vary between 30Km to 100Km depending on the dimension (number of ROADMs and OXCs) of the metro-access network. Therefore, the number of users per WDM channel will vary depending on the bandwidth availability of the grid. For example, for a fully flexgrid, the nodes will support 16 (32) users, while in case of implementing ROADMs and OXCs based on flat top optical filters with an availability of 75% of the bandwidth, a reduced number of final users, 12 (24), will be served.

5. Conclusion

The performance of full-duplex 1Gbps optical links for a cost-effective udWDM transmission with 6.25GHz frequency slots are demonstrated and optimized for cost-effective metro-access networks. The 1Gbps downlink, transmitted by the OLT, is based on Nyquist-DPSK implemented by a MZM, and has been optimized to a transmitted power of −6dBm, providing a sensitivity of −52dBm at the ONU receiver. The uplink, transmitted by the ONU, is based on a NRZ-DPSK directly-modulated DFB providing similar transmitted power of −6dBm and a sensitivity of −52dBm at the OLT receiver. Thus, a power budget of 43dB, including the 3dB ONU splitter, is accomplished. Significant cost reduction is achieved as the OLT and ONU receivers are based on single photodiode heterodyne detection with a DFB local oscillator that can be placed at 1 or 2GHz apart from the central frequency of the link. This single photodiode heterodyne receiver can be easily upgraded with a polarization independent one.

The experimental analysis of channel separation demonstrates the allocation of full-duplex 1Gbps optical links inside 6.25GHz frequency slots preserving the 43dB power budget by optimized channel spacing allocation. This allocation permits: 16 (32) users to be served for each 100GHz (200GHz) fully flexgrid WDM channel, in ranges of more than 100Km considering commercially available power splitter insertion losses; and coexistence at shorter reaches with future mesh 5G metro-access networks including ROADMs and OXCs.

#252375 Received 20 Oct 2015; revised 21 Dec 2015; accepted 22 Dec 2015; published 7 Jan 2016

Acknowledgments

This work was partially supported by the Diputación General de Aragón under grant T25, the Spanish MINECO projects muCORE (TEC2013-46917-C2-2-R) and SUNSET (TEC2014-59583-C2-1-R), Centro Universitario de la Defensa project SIRENA (CUD2013-05) and a FPU grant from MECD to the first author (FPU-13/00620).

#252375 Received 20 Oct 2015; revised 21 Dec 2015; accepted 22 Dec 2015; published 7 Jan 2016

3.2 Paper II

Cost-Effective Transceiver Based on an RSOA and a VCSEL for Flexible uDWDM Networks

J. A. Altabas, D. Izquierdo, J. A. Lazaro, and I. Garces, "Cost-Effective Transceiver Based on an RSOA and a VCSEL for Flexible uDWDM Networks," *IEEE Photonics Technology Letters*, vol. 28, no. 10, pp. 1111–1114, 2016

IEEE PHOTONICS TECHNOLOGY LETTERS, VOL. 28, NO. 10, MAY 15, 2016 1111

Cost-Effective Transceiver Based on an RSOA and a VCSEL for Flexible uDWDM Networks

Jose A. Altabas, David Izquierdo, Jose A. Lazaro, *Member, IEEE*, and Ignacio Garces, *Member, IEEE*

***Abstract*— A cost-effective transceiver for a 1-Gb/s full-duplex ultra-dense wavelength division multiplexing optical link is proposed for flexible metro-access and 5G networks. The transceiver is based on a vertical cavity surface emitting laser, which is used as the local oscillator for a heterodyne receiver and also feeds a phase-modulated reflective semiconductor optical amplifier (RSOA) transmitter. The modulation format used in the RSOA is a nonreturn-to-zero differential binary phase shift keying (DPSK) for the uplink, while the downlink is based on a Nyquist DPSK format. The central frequencies of the links are 2 GHz separated, and both links can be placed inside a 6.25-GHz frequency slot. The sensitivity of this transceiver is −43.5 dBm over a 50-km fiber.**

***Index Terms*— Coherent receiver, reflective semiconductor optical amplifiers, ultra dense wavelength division multiplexing, vertical cavity surface emitting lasers.**

I. Introduction

THE convergence of wireless and optical networks at the 5G scenario [1], combined with new streaming media and Internet of Things (IoT) services, are increasing the traffic of metropolitan and access networks. The evolution of these networks is converging to high capacity, all-optical merged-networks as the one shown in Fig. 1. In this context, flexible and coherent ultra-Dense Wavelength Division Multiplexing (uDWDM) metro-access networks are the most promising alternative to the current Time Division Multiplexing (TDM) optical networks due to its transparency and high spectral efficiency [2]. However, cost-effective devices have to be researched and developed in order to address the requirements of users and vendors [3].

This letter presents a cost-effective transceiver based on a continuous-emitting Vertical Cavity Surface Emitting Laser (VCSEL) [4], a phase-modulated Reflective Semiconductor Optical Amplifier (RSOA) [5] and a heterodyne coherent receiver. This transceiver allows a full-duplex 1Gbps channel inside a 6.25GHz frequency slot for a flexible uDWDM metro-access network with a sensitivity of −43.5dBm.

Manuscript received November 30, 2015; revised January 27, 2016; accepted February 15, 2016. Date of publication February 24, 2016; date of current version March 29, 2016. This work was supported in part by the CUD under Grant CUD2013-05:SIRENA, in part by the Spanish MINECO Projects muCORE under Grant TEC2013-46917-C2-2-R and SUNSET under Grant TEC2014-59583-C2-1-R within FEDER, and in part by the DGA under Grant T25. The work of J. A. Altabas was supported by the Spanish MECD under Grant FPU13/00620.

J. A. Altabas and I. Garces are with the Aragon Institute of Engineering Research, Universidad de Zaragoza, Zaragoza 50018, Spain (e-mail: jaltabas@unizar.es; ngarces@unizar.es).

D. Izquierdo is with Centro Universitario de la Defensa, Academia General Militar, Zaragoza 50090, Spain (e-mail: d.izquierdo@unizar.es).

J. A. Lazaro is with Universitat Politècnica de Catalunya, Barcelona 08034, Spain (e-mail: jose.lazaro@tsc.upc.edu).

Color versions of one or more of the figures in this letter are available online at http://ieeexplore.ieee.org.

Digital Object Identifier 10.1109/LPT.2016.2531789

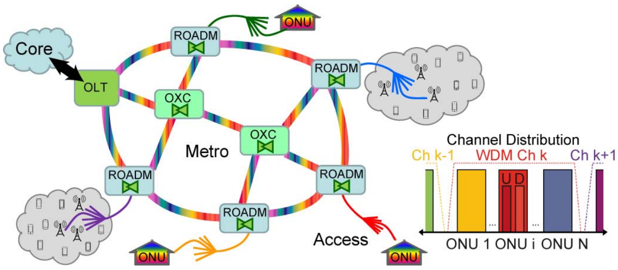

Fig. 1. All-optical 5G Metro-Access Network scenario. Inlet: proposed flexible uDWDM full-duplex channel distribution.

II. Setup

The proposed transceiver is used in the Optical Network Unit (ONU) of the 1Gbps symmetrical link setup shown in Fig. 2. The key-component of the transceiver is the VCSEL which is used simultaneously, using a 50/50 coupler, as Local Oscillator (LO) in the reception stage and as feeder in the transmission stage. In the transmission stage, the VCSEL feeds an RSOA using another 50/50 coupler and an isolator to avoid the instability of the VCSEL cavity due to RSOA backscattering. This VCSEL has 20MHz of linewidth and the wavelength stability is ±0.15GHz with a temperature stability of ±0.01°C. The RSOA, which is optical and electrically saturated with the VCSEL ($P_S = -5.5$dBm) and with the 125mA current bias, is modulated with 1Gbps Non Return to Zero Differential Binary Phase Shift Keying (NRZ-DPSK) with 54mA$_{p\text{-}p}$. The ONU transmitted power (P_{TX}) is −3dBm. The reception stage, that uses the VCSEL as LO ($P_{LO} = -5.5$dBm), is based on a single-photodiode heterodyne receiver [6] and can be easily upgraded to an independent polarization receiver [7].

The Optical Line Terminal (OLT) transceiver of this experimental setup is based on an external cavity Tunable Laser Source (TLS), located 2GHz shifted from the central wavelength of the ONU ($f_{OLT} = f_{ONU} - 2$GHz), which is used as feeder for a Mach-Zehnder Modulator (MZM) at the transmission stage and as LO at the receiver stage. The MZM is set at the null point and modulated with a 1Gbps Nyquist-DPSK format with 12-symbols filter length and zero roll-off factor. The OLT transmits the same power than the ONU,

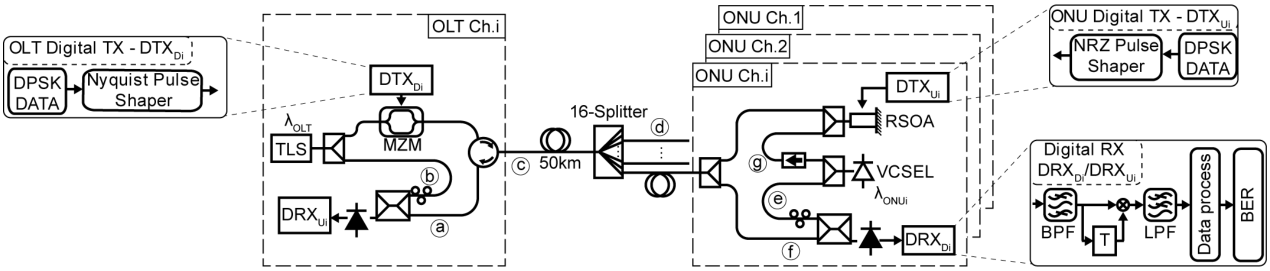

Fig. 2. Experimental setup for the evaluation of the optical link. P_{RX} at (a) and (e) points, P_{LO} at the (b) and (f) point, P_{TX} at (c) and (d) points and Ps at (g) point.

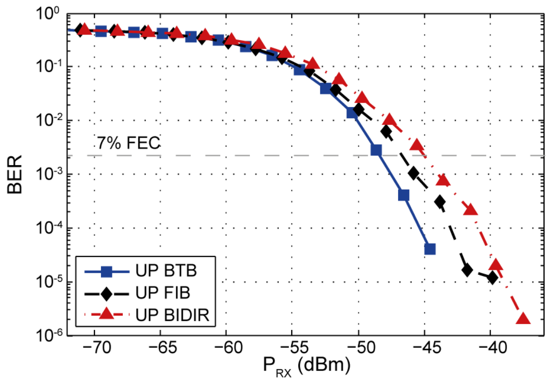

Fig. 3. BER vs received power for uplink for the BTB (UP BTB), fiber (UP FIB) and bidirectional connection (UP BIDIR).

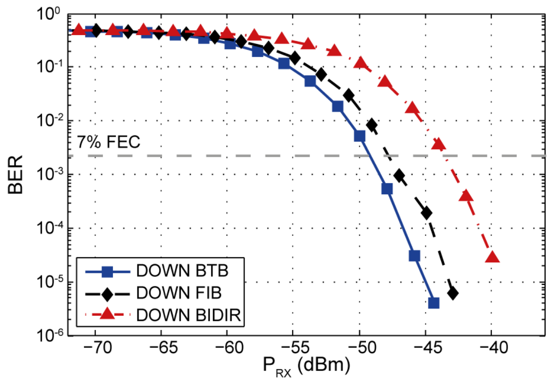

Fig. 4. BER vs. received power for downlink for the BTB (DOWN BTB), fiber (DOWN FIB) and bidirectional connection (DOWN BIDIR).

$P_{TX} = -3$dBm. The OLT receiver is the same configuration that is used at the ONU but with different LO source (TLS) and power ($P_{LO} = 0$dBm). In a real implementation, the OLT could be implemented using as much transceivers as users or share the OLT unit between several users and so reduce the cost [2], [8].

The transmitted signals for both transceivers are generated using a 12GS/s Arbitrary Waveform Generator (AWG) while the received signals are digitalized with a 40GS/s Digital Signal Oscilloscope (DSO) with 2.5GHz electrical bandwidth.

The optical channel is based on a 50Km Standard Single Mode Fiber (SSMF) and a 1:16 distribution splitter.

III. Results

The sensitivity, defined as the minimum received power to ensure a BER of $2.2 \cdot 10^{-3}$ without FEC and 10^{-12} with a 7% overhead FEC [9], has been evaluated for both links in three different scenarios. The uplink sensitivity for back-to-back (BTB) transmission is -48dBm while the power penalty due to a 50Km SSMF transmission is only 2dB, as shown in Fig. 3. The downlink sensitivity, shown in Fig. 4, is -49dBm for BTB transmission and the power penalty due to fiber transmission is 1.5dB. The bidirectional connection, when both links are transmitting simultaneously, increases the power penalties by 1dB (4dB) for the uplink (downlink). Consequently, the power budget in this one user scenario is 42dB (40.5dB) for the uplink (downlink), so distances upper 100Km will be reached [6]. Equal power budget can be achieved by P_{TX} / P_{LO} adjustment. A different OLT configuration, including additional users, could reduce the power budget.

The optical spectrum of the 1Gbps symmetrical link, shown in Fig. 5, was obtained with a BOSA High Resolution Optical Complex Spectrum Analyzer (HROCSA) from Aragon Photonics Labs. The central wavelength of both links are shifted 2GHz away from each other and the wavelength used for transmission is also used as LO for reception. The inlet of Fig. 5 shows the VCSEL spectrum used as light source in the proposed transceiver.

Fig. 5 can be used also to explain the asymmetrical power penalty in the bidirectional scenario. The backscattering of the downlink has a narrow bandwidth due to the Nyquist-DPSK modulation over one of the secondary lobes of the uplink spectrum and it can be easily electrically filtered with a small penalty in the OLT receiver. In contrast, the uplink (NRZ-DPSK) has a broad bandwidth and the backscattering generated by the secondary lobe introduces noise over all the downlink spectra, and it cannot be electrically removed. Thus, uplink has a lower power penalty than downlink in the full bidirectional channel scenario.

The uplink signal is generated with NRZ-DSPK modulated RSOA working as phase modulator. Therefore, transitions between symbols lie ideally on a constant amplitude circle at the IQ diagram. This transition between symbols implies

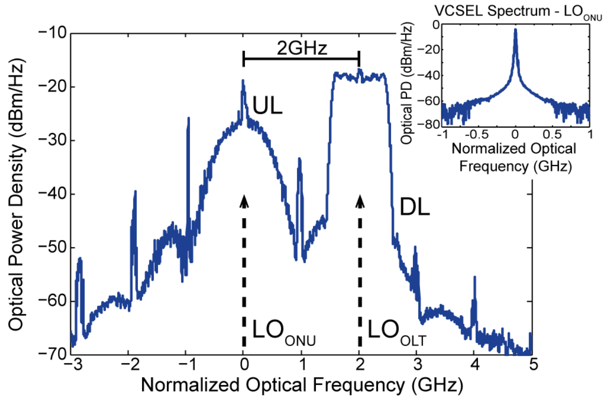

Fig. 5. Optical spectrum for both links of a single channel and the LO position of each link. The central frequency corresponds to 1523.58nm. Inlet: VCSEL Spectrum.

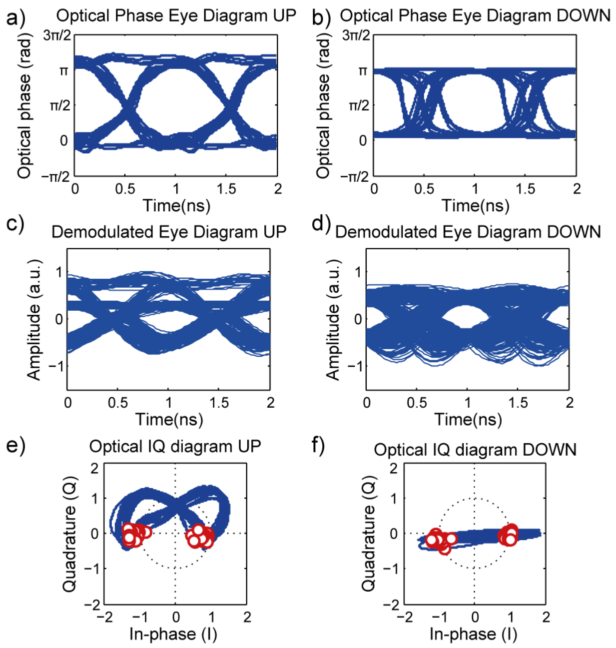

Fig. 6. Optical phase eye diagram from HROCSA (a and b), demodulated eye diagrams for $P_{RX} = -36$dBm (c and d) and optical IQ diagram from HROCSA (e and f) for uplink (a, c and e) and downlink (b, d and f).

a continuous phase variation, as can be seen at the optical phase eye diagram in Fig 6.a, obtained from the HROCSA. It can also be seen at the demodulated electrical eye diagram in Fig. 6.c, obtained from the implemented heterodyne receiver (Fig. 2). This eye diagram also shows a spread of the symbol amplitude caused by a residual amplitude modulation at RSOA. The optical IQ diagram from the HROCSA, shown at Fig. 6.e, confirms both phenomena. The continuous phase modulation of the RSOA is confirmed as the symbols transitions do not cross the IQ diagram origin, while the residual amplitude modulation generates transitions and symbols not laying on the amplitude constant circle.

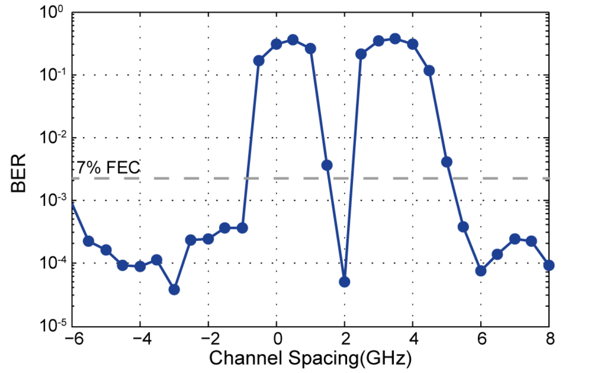

Fig. 7. Uplink BER at OLT while the OLT is transmitting the adjacent channel downlink.

The downlink signal is a Nyquist-DPSK over a MZM. In this case, the transitions between symbols cross the IQ diagram origin, Fig 6.f. The use of Nyquist pulse shaping introduces Inter Symbolic Interference (ISI) along the symbol period with the exception of the symbol center. Therefore, a noticeable temporal jitter at the optical phase transitions is measured Fig. 6.b. The demodulated eye diagram (Fig. 6.d), confirms this temporal jitter and shows that the signal maximum is not located in the optimal sampling point due to amplitude overshoots caused by the ISI. The optical IQ diagram (Fig. 6.f) confirms the transitions between symbols crossing the IQ diagram origin and the amplitude overshoots.

The interference between two adjacent channels has been analyzed when OLT is, simultaneously, receiving the uplink from ONU_i while transmitting the downlink to an adjacent $ONU_{i\pm1}$. In this scenario, the downlink backscattering of the adjacent channel will deteriorate the uplink BER depending on the frequency distance of the adjacent channel. This is the only case studied because in our proposed channel distribution, the uplink is always flanked with two downlinks (the one of its channel and the one of the adjacent channel) and the interference of an adjacent uplink on the downlink is not relevant due the reduction of the uplink backscattering by the 1:16 distribution splitter [6]. The BER overpass the 7% FEC limit for adjacent channel located in the range from -1GHz to 1.5GHz and 2.5GHz to 5.5GHz, as is shown Fig. 7. Therefore, frequency slots of 6.25GHz with null band guard [6] could be used for 1Gbps full-duplex link per user.

IV. Conclusion

A full-duplex 1Gbps cost-effective transceiver has been evaluated for its integration in an uDWDM link for flexible 5G metro-access networks. This transceiver is based on a single continuous-emitting VCSEL, a phase-modulated RSOA and a heterodyne receiver. In the full-duplex scenario, the sensitivity is -43.5dBm, so ranges of more than 100km can be reached. The uplink and the downlink are placed 2GHz away and the channels can be placed inside 6.25GHz frequency slots and grid.

REFERENCES

[1] M. Fiorani *et al.*, "Challenges for 5G transport networks," in *Proc. IEEE Int. Conf. ANTS*, New Delhi, India, Dec. 2014, pp. 1–6.

[2] H. Rohde *et al.*, "Coherent ultra dense WDM technology for next generation optical metro and access networks," *J. Lightw. Technol.*, vol. 32, no. 10, pp. 2041–2052, May 15, 2014.

[3] M. Presi, F. Bottoni, R. Corsini, G. Cossu, and E. Ciaramella, "All DFB-based coherent UDWDM PON with 6.25 GHz spacing and a >40 dB power budget," *IEEE Photon. Technol. Lett.*, vol. 26, no. 2, pp. 107–110, Jan. 15, 2014.

[4] J. B. Jensen, R. Rodes, A. Caballero, N. Cheng, D. Zibar, and I. T. Monroy, "VCSEL based coherent PONs," *J. Lightw. Technol.*, vol. 32, no. 8, pp. 1423–1433, Apr. 15, 2014.

[5] H. K. Shim, H. Mu, U. H. Hong, and Y. C. Chung, "A practical 10-Gb/s ultra-dense WDM PON," in *Proc. OECC/ACOFT*, Melbourne, VIC, Australia, Jul. 2014, pp. 289–290.

[6] J. A. Altabas, D. Izquierdo, J. A. Lazaro, A. Lerin, F. Sotelo, and I. Garces, "1 Gbps full-duplex links for ultra-dense-WDM 6.25 GHz frequency slots in optical metro-access networks," *Opt. Exp.*, vol. 24, no. 1, pp. 555–565, 2016.

[7] B. Glance, "Polarization independent coherent optical receiver," *J. Lightw. Technol.*, vol. 5, no. 2, pp. 274–276, Feb. 1987.

[8] C. Kottke *et al.*, "Coherent UDWDM PON with joint subcarrier reception at OLT," *Opt. Exp.*, vol. 22, no. 14, pp. 16876–16888, 2014.

[9] *ITU-T Recommendation, G.975.1*, 2004.

3.3 Paper III

Chirp-based direct phase modulation of VCSELs for cost-effective transceivers

J. A. Altabas, D. Izquierdo, J. A. Lazaro, and I. Garces, "Chirp-based direct phase modulation of VCSELs for cost-effective transceivers," *Optics Letters*, vol. 42, no. 3, pp. 583–586, 2017

Letter Vol. 42, No. 3 / February 1 2017 / *Optics Letters* **583**

Optics Letters

Chirp-based direct phase modulation of VCSELs for cost-effective transceivers

JOSE A. ALTABAS,[1,*] DAVID IZQUIERDO,[1,2] JOSE A. LAZARO,[3] AND IGNACIO GARCES[1]

[1]*Aragon Institute of Engineering Research, Universidad de Zaragoza, Mariano Esquillor, ed. I+D+I, E-50018 Zaragoza, Spain*
[2]*Centro Universitario de la Defensa, Academia General Militar, Carretera de Huesca s/n, E-50090 Zaragoza, Spain*
[3]*Universitat Politecnica de Catalunya, Jordi Girona 31, E-08034 Barcelona, Spain*
**Corresponding author: jaltabas@unizar.es*

Received 10 November 2016; revised 22 December 2016; accepted 6 January 2017; posted 6 January 2017 (Doc. ID 280562); published 27 January 2017

A 2.5 Gb/s differential binary phase-shift keying (DPSK) transmitter based on direct phase modulation of a vertical cavity surface emitting lasers (VCSEL) using its own chirp is proposed. The VCSEL, which has a wavelength of 1539.84 nm, has been characterized both statically and dynamically. The sensitivity of a single photodiode heterodyne receiver using the proposed 2.5 Gb/s VCSEL transmitter is −39.5 dBm. Thus, this transmitter is an extremely cost-effective solution for future access networks.

OCIS codes: (140.7260) Vertical cavity surface emitting lasers; (060.1660) Coherent communications.

https://doi.org/10.1364/OL.42.000583

The traffic demand over access networks is growing exponentially due to cloud computing based new services, the Internet of Things, and the convergence between wireless and optical communications in the new 5G paradigm [1]. Flexible ultra-dense wavelength division dultiplexing (uDWDM) metro-access networks using coherent detection are a promising solution for these convergent networks [2], but cost-effective transmitters have to be designed for better development and deployment of these networks. In recent years, some cost-effective devices have been proposed, as directly phase-modulated reflective semiconductor optical amplifiers [3,4], with or without remote pumping, and directly phase-modulated distributed feedback lasers (DFBs) [5,6] or intensity modulated vertical cavity surface emitting lasers (VCSELs) [7]. In addition, VCSELs have been tested as local oscillators (LOs) for heterodyne receivers [4,7]. VCSELs can reduce the transceiver cost for access networks because they are potentially the cheapest lasers that can be fabricated, and phase modulation may provide the power budget needed to deploy cost-effective transceivers.

In this Letter, we present a direct phase modulation of a VCSEL through the chirp of the laser. First, we obtained its static and dynamic parameters (frequency chirp) and used them to simulate its behavior and modulate its phase. A 2.5 Gb/s differential binary phase-shift keying (DPSK) has been achieved, and it has been demodulated by coherent heterodyne reception.

The static and dynamic (frequency chirp) parameters of a commercially available VCSEL from Raycan with thermal stabilization have been measured. The measured static parameters are the lasing threshold, the slope efficiency, and the wavelength and optical power in terms of the bias current and temperature.

The VCSEL static parameters have been obtained setting the VCSEL in a continuously emitting mode and varying the bias current and the temperature using the setup shown in Fig. 1. The laser threshold, the slope efficiency, and the emitting power in terms of the bias current and the temperature are measured with a power meter, while the wavelength is measured using a high-resolution complex optical spectrum analyzer (HRCOSA).

The lasing threshold is 1.399 mA, and the slope efficiency is 0.137 mW/mA, both at 25°C. The emitted wavelength in terms of the bias current, and the temperature is shown in Fig. 2. The variation of the wavelength with the temperature is −0.122 nm/°C and with the bias current is 0.527 nm/mA. In Fig. 2, the constant emitting power lines have been plotted in terms of the temperature and the bias current. The emitted wavelength can be tuned maintaining a constant optical power in such a way that, for example, a wavelength variation of 5 nm can be obtained with a constant emitting optical power of −1.5 dBm. Therefore, the emitted wavelength and optical power of the VCSEL can be tuned by adjusting both the temperature and the bias current.

The VCSEL dynamic parameter measured is the frequency chirp, defined as the dynamic shift of the operating optical frequency of the laser with the variation of the emitting optical power and, for modulation frequencies higher than the thermal response of the device. It can be described as [8]

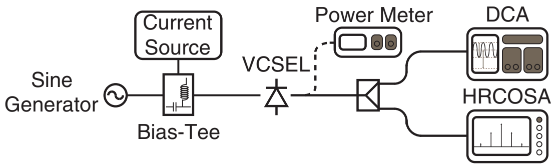

Fig. 1. Experimental setup for the VCSEL characterization.

0146-9592/17/030583-04 Journal

584 Vol. 42, No. 3 / February 1 2017 / Optics Letters Letter

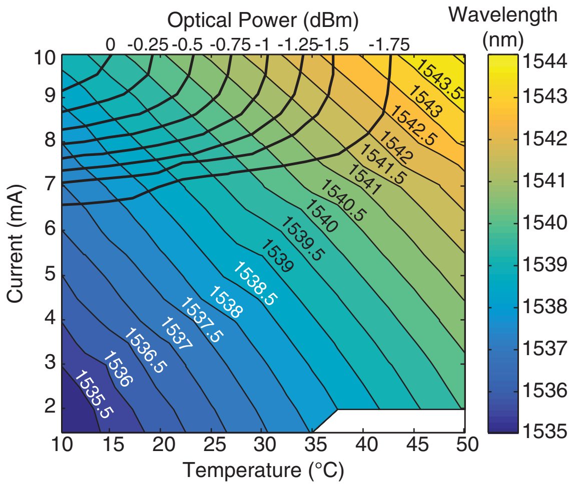

Fig. 2. VCSEL wavelength and constant power curves in terms of the bias current and the temperature.

$$\Delta\nu(t) = \frac{1}{2\pi}\frac{d\phi(t)}{dt} = \frac{\alpha}{4\pi}\left(\frac{1}{P(t)}\frac{dP(t)}{dt} + \kappa P(t)\right), \quad \textbf{(1)}$$

where $\Delta\nu(t)$ is the optical frequency shift, $\phi(t)$ is the instantaneous optical phase, and $P(t)$ is the instantaneous optical power. The transient chirp (α) is associated with the variation of the emitting optical power, and the adiabatic chirp (κ) is related to the instantaneous emitting optical power. These parameters have been characterized using the FM/AM method [9,10] which is based on the measurement of the residual phase to amplitude modulation when modulating a VCSEL with a sine signal of frequency (f) and a low-intensity modulation depth (m). The optical intensity output is:

$$I(t) = I_0(1 + m\cos(2\pi f t)) \quad \text{with } m \ll 1. \quad \textbf{(2)}$$

The optical carrier (with power I_0) and the two first-order sidebands (I_{+1} and I_{-1}) found in the spectrum are measured employing the HRCOSA, while the (m) is measured using a digital communication analyzer (DCA) oscilloscope, as can be seen in Fig. 1. The average optical power of the first-order sidebands ($\overline{I}_{\pm 1}$) allows us to obtain the ratio between residual phase modulation and amplitude modulation ($2p/m$) [8,9]:

$$\overline{I}_{\pm 1} = I_0\left(\frac{m}{4}\right)^2\left[1 + \left(\frac{2p}{m}\right)^2\right] \quad \text{with } m \ll 1, p \ll 1. \quad \textbf{(3)}$$

This ratio ($2p/m$) is related to α and κ [8]:

$$\frac{2p}{m} = \alpha\sqrt{1 + \left(\frac{f_c}{f}\right)^2} = \alpha\sqrt{1 + \left(\frac{\kappa}{2\pi f}I_0\right)^2}, \quad \textbf{(4)}$$

where f_c is the chirp frequency, which is the frequency when both chirp effects are equal [11].

In Fig. 3, the ratio $2p/m$ versus the modulation frequency for different bias currents (I_{bias}) is shown. The $2p/m$ ratio decreases with the modulation frequency, and it converges to the α value when the second factor under the square root of Eq. (4) tends to zero, i.e., at high modulation frequencies. The f_c and the α are obtained adjusting the experimental values to Eq. (4). The f_c increases linearly with the bias current, and it is used to obtain the κ factor through the relation shown in Eq. (4). The α

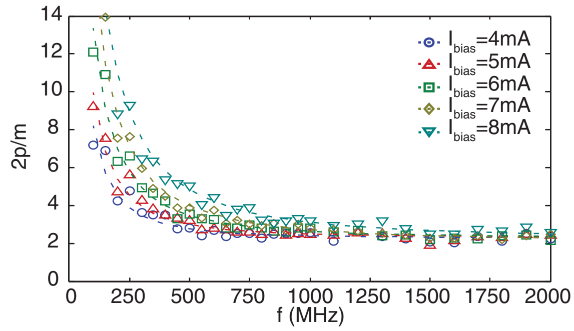

Fig. 3. Experimental $2p/m$ curves for different bias currents.

and the κ parameters are independent with the bias current. The α parameter is found to be 2.24 ± 0.1, and the κ parameter is 7.6 ± 0.8 GHz/mW.

The measured dynamic (frequency chirp) parameters are used to simulate the chirp and phase behavior and to develop a DPSK transmitter based on a directly phase-modulated VCSEL.

The experimental setup used to obtain a non-return-to-zero (NRZ) DPSK transmitter based on a directly phase-modulated VCSEL with an heterodyne receiver is shown in Fig. 4. Data have been encoded differentially in order to use a cost-effective receiver, but the transmitter can use nondifferential encoding. The VCSEL is a commercially available device from Raycan with thermal stabilization, exhibiting a relatively wide linewidth, higher than 10 MHz, and an electrical bandwidth of 4 GHz. The VCSEL is biased to a current of 8 mA and emits –1 dBm of optical power at 25°C. The thermal wavelength tuning of this VCSEL, previously described, allows a flexible wavelength allocation.

The pulse shaper for the VCSEL direct phase modulation consists of a sharp transition at the start of the symbol and an exponential decay after the symbol, which can be modeled with a first-order high-pass function with a cutoff frequency of 636.32 MHz and is shown in Fig. 5(a), where we have used a bit rate of 1.25 Gb/s for a better description of the chirp and phase behavior. The optical power signal [Fig. 5(a)] is distorted because of the arbitrary waveform generator electrical response and the VCSEL dynamic behavior.

This optical power signal has been acquired and used as the input for simulating the chirp of the VCSEL applying the parameters obtained previously. Figure 5(b) shows the frequency shift caused by the two terms of Eq. (1). The first term (transient chirp) is related to the variation of the optical power and the α parameter, and shows strong peaks and a small decay

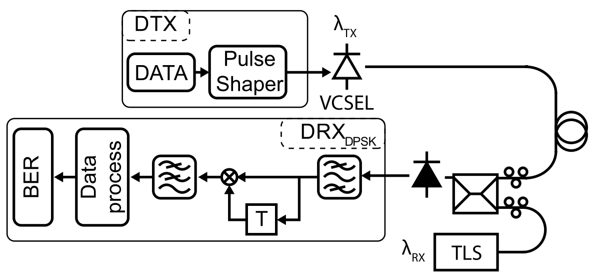

Fig. 4. Experimental setup of the proposed transmitter with heterodyne coherent reception.

Letter Vol. 42, No. 3 / February 1 2017 / *Optics Letters* 585

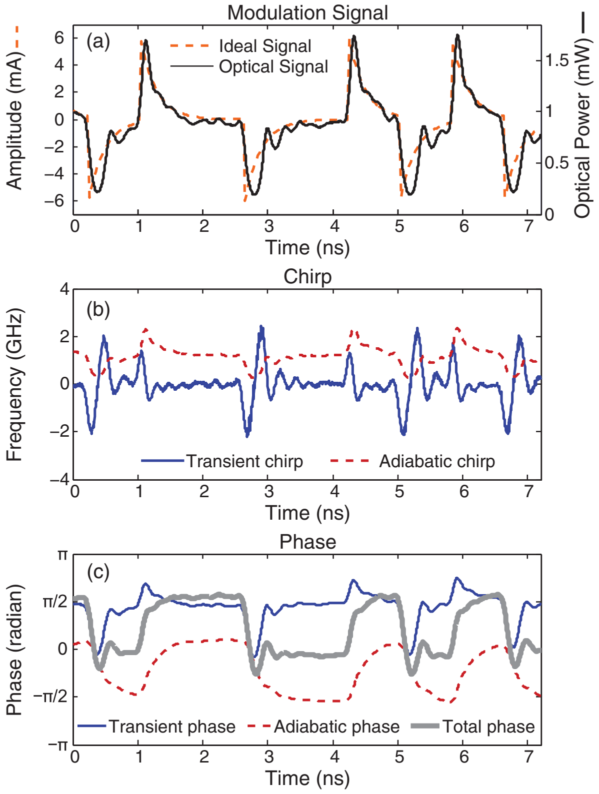

Fig. 5. (a) 1.25 Gb/s ideal pulse-shaping modulation signal and measured optical signal, simulated: (b) transient and adiabatic chirp, and (c) total phase and the generated phase by the transient and adiabatic chirps.

after it when the sharp transition happens. The second term (adiabatic chirp) is related to the value of the optical power and the κ parameter. This second term of the chirp follows mainly the modulation signal.

The optical phase variation generated by the laser frequency chirp is calculated from the integral of the frequency chirp equation [Eq. (1)] and is shown in Fig. 5(c). The optical phase change related to the transient chirp shows a sharp transition at the start of the symbol and then an exponential decay, similar to the modulation signal. The optical phase variation due to negative modulation pulses is stronger and sharper than that generated by the positive pulses, because they cause stronger transient chirp frequency shifts producing asymmetrical phase transitions. The optical phase change related to the adiabatic chirp presents a slow slope showing a charging capacitor behavior that contributes to the final value of the phase change. As both optical phase terms happen simultaneously, the total optical phase behavior is also asymmetrical. This can be seen in Fig. 5(c) as an undershoot at the start of the negative pulses.

Different optical phase variations can be obtained by a tight control of the amplitude and the exponential decay of the modulation signal. Therefore, different phase-shift keying (PSK) modulation schemes over a directly modulated VCSEL can be achieved. In this Letter, we have implemented a 2.5 Gb/s DPSK transmitter using just a direct modulation of the VCSEL. This value is near the maximum achievable transmission rate for this laser, taking into account the modulation signals needed to produce the phase modulation and the 4 GHz bandwidth of the device.

The receiver side for the detection of the generated signal is based on a heterodyne receiver with a single photodiode and a external cavity tunable laser source (TLS) as a LO with a linewidth smaller than 100 kHz and 0 dBm emitted optical power. This heterodyne receiver can be upgraded to a polarization independent receiver employing the technique described in [12]. The optical frequency of the LO is tuned 5 GHz away from that of the transmitter. In our experimental setup, the polarization of both signals (receiver signal and LO) was adjusted using manual polarization controllers. The received signal is electrically amplified and digitalized with a 40 GSa/s digital signal oscilloscope. After the digitalization, the signal is band-pass filtered with a FIR filter in order to reduce the noise as in [4]. Then the signal is delayed one symbol and multiplied by itself for the DPSK case. Finally, it is low-pass filtered with another FIR filter to demodulate the data.

The results of the 2.5 Gb/s DPSK employing a directly phase-modulated VCSEL are shown and compared with a 2.5 Gb/s DPSK implemented using a Mach–Zehnder modulator (MZM) and a TLS as the optical source and with a 2.5 Gb/s on-off keying (OOK) transmission implemented using this same VCSEL. In this later case, the receiver has to be modified after the first FIR filter to demodulate the received signal. The comparison is done in terms of spectrum shape and sensitivity, which is defined as the minimum received power below $\text{BER} = 2.2 \cdot 10^{-3}$, i.e., the 7% overhead FEC limit to ensure a BER of 10^{-12} [13].

Figure 6 shows the sensitivity of the three modulation formats in a back-to-back (btb) scenario. The proposed directly phase-modulated VCSEL sensitivity is −39.5 dBm. The DPSK over a MZM has a sensitivity of −45 dBm. Therefore, the proposed transmitter has a power penalty of 5.5 dB in comparison with the best performance transmitter (MZM with a TLS as a laser), which is a reasonable power penalty for the cost reduction obtained. The OOK using a VCSEL shows a sensitivity of −35.75 dBm, which means that the proposed transmitter improves the sensitivity in 2.75 dB. This improvement is achieved because the symbol distance is doubled in the phase

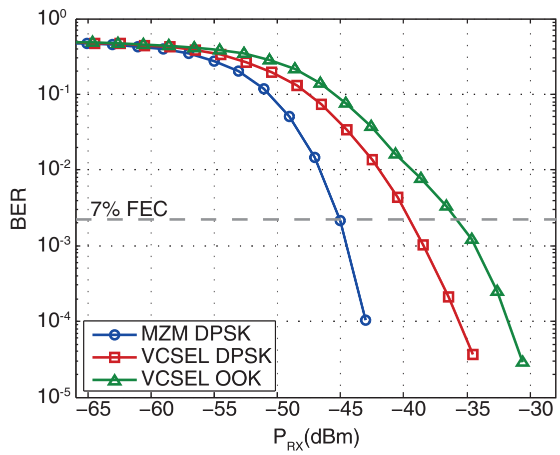

Fig. 6. BER versus received power for the MZM with DPSK, VCSEL with DPSK, and VCSEL with OOK for a btb scenario.

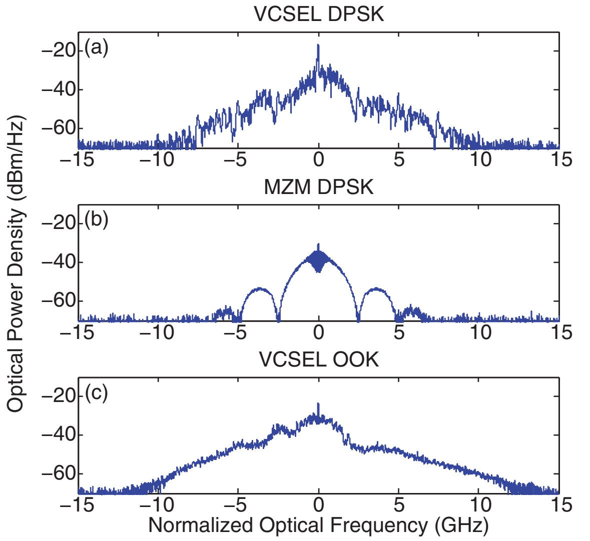

Fig. 7. Optical spectra for (a) 2.5 Gb/s DPSK with VCSEL, (b) 2.5 Gb/s DPSK with MZM, and (c) 2.5 Gb/s OOK with VCSEL. The central frequency corresponds to 1539.84 nm.

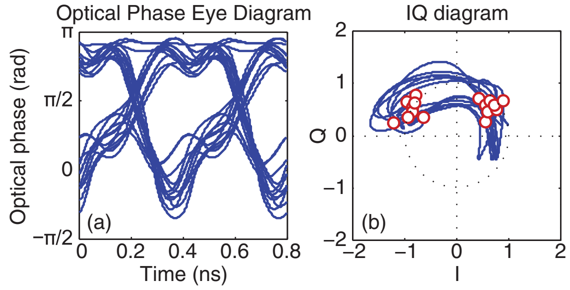

Fig. 8. 2.5 Gb/s DPSK with a directly phase-modulated VCSEL. Experimental optical: (a) phase eye diagram and (b) IQ diagram.

modulation (DPSK) with respect to the intensity modulation (OOK). The measured penalty of DPSK VCSEL sensitivity for 50 Km of single-mode fiber transmission is below 0.1 dB.

Figure 7 shows the optical spectra of the three compared signals obtained with a HRCOSA. The spectrum of 2.5 Gb/s DPSK implemented with our directly phase-modulated VCSEL is shown in Fig. 7(a). It has a sinc shape, typical of the NRZ signals, with a suppressed carrier, characteristic of the DPSK signals. The spectrum of 2.5 Gb/s DPSK over a MZM [Fig. 7(b)] has a similar shape and suppressed carrier. The DPSK with a MZM has a clearer shape than the DPSK directly modulated with a VCSEL because of the residual amplitude modulation in the later generated by the modulation pulse shape in the VCSEL. The spectrum of 2.5 Gb/s OOK over a VCSEL [Fig. 7(c)] has been widened with respect to the phase-modulated signal and the optical carrier nearly suppressed because of the uncontrolled chirp effect. Therefore, the utilization of a directly phase-modulated VCSEL allows us to reduce the employed optical spectrum.

The experimental optical phase eye diagram and IQ diagram obtained with a HRCOSA are shown in Fig. 8. The optical phase eye diagram [Fig. 8(a)] shows that the phase modulation varies approximately between 0 and π as is expected for a binary DPSK. The phase variation has been optimized to obtain the minimum BER, which is achieved through a phase shift close to π and the lowest penalty due to the residual amplitude modulation. Variations of the amplitude and the decay of the modulation signal will allow us to change the modulation levels in order to obtain higher-order modulation (M-PSK).

The experimental IQ diagram [Fig. 8(b)] shows a continuous phase modulation of the VCSEL because the signal is transiting around the unity circle of the IQ diagram. The transition between symbols does not match the IQ unity circle, as can be seen in Fig. 8(b), due to the residual amplitude modulation. Nevertheless, this residual amplitude modulation is small enough to obtain the desired DPSK signal.

In conclusion, this Letter presents the static and frequency chirp characterization of a VCSEL and, for the first time to the best of our knowledge, the VCSEL utilization as a phase modulation transmitter using its own chirp parameters. The directly phase-modulated VCSEL is employed to develop a 2.5 Gb/s DPSK cost-effective transmitter. The 2.5 Gb/s VCSEL transmitter is used to obtain a sensitivity of −39.5 dBm with a single photodiode heterodyne receiver. The sensitivity of the directly phase-modulated VCSEL has only a 5.5 dB power penalty, compared to a 2.5 Gb/s DPSK over MZM and a sensitivity improvement of 2.75 dB in relation to the 2.5 Gb/s OOK VCSEL. In addition, the 2.5 Gb/s DPSK VCSEL has promising characteristics such as transmitter tuneability by bias and temperature control, narrow spectrum, and a good-quality optical phase eye diagram. All these facts make this transmitter a promising cost-effective candidate for access networks.

Funding. Diputación General de Aragón (T25); Ministerio de Economía y Competitividad (MINECO) (TEC2013-46917-C2-2-R, TEC2014-59583-C2-1-R); Centro Universitario de la Defensa (CUD2013-05); MECD (FPU-13/00620).

REFERENCES

1. M. Fiorani, P. Monti, B. Skubic, J. Mårtensson, L. Valcarenghi, P. Castoldi, and L. Wosinska, in *IEEE International Conference on Advanced Networks and Telecommuncations Systems (ANTS)* (2014), pp. 1–6.
2. H. Rohde, E. Gottwald, A. Teixeira, J. D. Reis, A. Shahpari, K. Pulverer, and J. S. Wey, J. Lightwave Technol. **32**, 2041 (2014).
3. H. K. Shim, H. Kim, and Y. C. Chung, Opt. Express **22**, 29037 (2014).
4. J. A. Altabas, D. Izquierdo, J. A. Lazaro, and I. Garces, IEEE Photon. Technol. Lett. **28**, 1111 (2016).
5. R. S. Vodhanel, A. F. Elrefaie, M. Z. Iqbal, R. E. Wagner, J. L. Gimlett, and S. Tsuji, J. Lightwave Technol. **8**, 1379 (1990).
6. I. N. Cano, A. Lerin, V. Polo, and J. Prat, IEEE Photon. Technol. Lett. **26**, 973 (2014).
7. J. B. Jensen, R. Rodes, A. Caballero, N. Cheng, D. Zibar, and I. T. Monroy, J. Lightwave Technol. **32**, 1423 (2014).
8. L. Bjerkan, A. Royset, L. Hafskjaer, and D. Myhre, J. Lightwave Technol. **14**, 839 (1996).
9. A. Villafranca, J. Lasobras, and I. Garces, in *Spanish Conference on Electron Devices* (2007), pp. 173–176.
10. L. A. Neto, D. Erasme, N. Genay, P. Chanclou, Q. Deniel, F. Traore, T. Anfray, R. Hmadou, and C. Aupetit-Berthelemot, J. Lightwave Technol. **31**, 334 (2013).
11. S. Kobayashi, Y. Yamamoto, M. Ito, and T. Kimura, IEEE J. Quantum Electron. **18**, 582 (1982).
12. B. Glance, J. Lightwave Technol. **5**, 274 (1987).
13. I.-T. G.975.1, "Forward error correction for high bit-rate DWDM submarine systems" (2004).

3.4 Paper IV

Real-time 10Gbps Polarization Independent Quasicoherent Receiver for NG-PON2 Access Networks

J. A. Altabas, G. Silva Valdecasa, L. F. Suhr, M. Didriksen, J. A. Lazaro, I. Garces, I. Tafur Monroy, A. T. Clausen, and J. B. Jensen, "Real-Time 10 Gbps Polarization Independent Quasicoherent Receiver for NG-PON2 Access Networks," *Journal of Lightwave Technology*, vol. 37, no. 2, pp. 651–656, 2019

JOURNAL OF LIGHTWAVE TECHNOLOGY, VOL. 37, NO. 2, JANUARY 15, 2019 651

Real-Time 10 Gbps Polarization Independent Quasicoherent Receiver for NG-PON2 Access Networks

Jose A. Altabas, Guillermo Silva Valdecasa, Lau F. Suhr, Morten Didriksen, Jose A. Lazaro, *Member, IEEE*, Ignacio Garces, *Member, IEEE*, Idelfonso Tafur Monroy, *Senior Member, IEEE*, Anders T. Clausen, and Jesper B. Jensen

(Top-Scored Paper)

***Abstract*—In this paper, we propose and test experimentally a real-time 10 Gbps polarization independent quasicoherent receiver for NG-PON2 access networks. The proposed 10 Gbps quasicoherent receiver exhibits a sensitivity of −35.2 dBm after 40 km standard single mode fiber (SSMF) transmission with a commercial generic EML as transmitter. This sensitivity means a 14.9 dB improvement over a direct detection scheme with a photodiode after 40 km SSMF transmission. Therefore, the use of the proposed 10 Gbps quasicoherent receiver with the tested EML will provide a power budget of 35.64 dB (class E2) and a splitting ratio of 128 after the 40 km SSMF transmission. Finally, the proposed 10 Gbps quasicoherent receiver allows a colorless and optical filterless operation because wavelength selection is done by tuning the local oscillator wavelength and using electrical intermediate frequency filtering.**

***Index Terms*—Access network, coherent receiver, NG-PON2, PON, TWDM.**

Manuscript received June 29, 2018; revised September 14, 2018 and October 16, 2018; accepted October 19, 2018. Date of publication November 9, 2018; date of current version February 20, 2019. This work was supported in part by the Diputación General de Aragón under Grant T20_17R, in part by the Spanish MINECO projects FOANT (TEC2017-85752-R) and ALLIANCE (TEC2017-90034-C2-2-R) co-funded by FEDER, and in part by a MECD FPU under Grant (FPU-13/00620). This paper was presented in part at the Optical Fiber Communication Conference and Exposition, San Diego Convention Center, San Diego, CA, USA, March 2018. *(Corresponding author: Jose A. Altabas.)*

J. A. Altabas and I. Garces are with the Department of Electrical Engineering and Communications, Aragon Institute of Engineering Research, University of Zaragoza, Zaragoza 50018, Spain (e-mail: jaltabas@unizar.es; ngarces@unizar.es).

G. S. Valdecasa, L. F. Suhr, M. Didriksen, and J. B. Jensen are with the Bifrost Communications, Scion DTU, Kgs Lyngby 2800, Denmark (e-mail: gsv@bifrostcommunications.com; lasu@fotonik.dtu.dk; md@bifrostcommunications.com; jbj@bifrostcommunications.com).

J. A. Lazaro is with the School of Telecommunications Engineering, Polytechnic University of Catalonia, Barcelona 08034, Spain (e-mail: jose.lazaro@tsc.upc.edu).

I. T. Monroy is with the Institute for Photonics Integration, Eindhoven University of Technology, Eindhoven 5600, The Netherlands (e-mail: i.tafur.monroy@tue.nl).

A. T. Clausen is with the DTU Fotonik, Technical University of Denmark, Kgs Lyngby 2800, Denmark (e-mail: ancl@fotonik.dtu.dk).

Color versions of one or more of the figures in this paper are available online at http://ieeexplore.ieee.org.

Digital Object Identifier 10.1109/JLT.2018.2880361

I. Introduction

During the recent years, data traffic over optical access networks has grown exponentially. This data traffic growth will continue in the future because of the high bandwidth demand due to the expansion of current services such as streaming media, Internet of Things (IoT) and cloud computing; the development of new services using virtual and augmented reality technologies [1] and the convergence of wireless and optical access networks on the 5G paradigm [2].

In order to address the current and future data traffic requirements, the NG-PON2 standard for passive optical networks (PON) was recently released [3], [4]. The NG-PON2 standard is based on time and wavelength division multiplexing (TWDM) through four wavelength channels at a data rate of 10 Gbps per channel and providing an aggregated data rate of 40 Gbps.

The NG-PON2 standard has high demanding requirements for both network and devices in order to satisfy this growing user data traffic and the operators' necessities. The TWDM operation of NG-PON2 requires 10 Gbps colorless and tunable optical network units (ONU), as can be seen in Fig. 1. In addition, the NG-PON2 standard proposes optical distribution networks (ODN) with high splitting ratios, up to 256, and long transmission distances, up to 40 km. These high demanding technical requirements increase the cost of the ONU because of the necessity of using optical tunable filters, high sensitivity avalanche photodiodes (APD) [5], [6], optical amplifiers and high optical power and wavelength stable transmitting lasers.

Coherent technologies [7] have been researched during the recent years as a promising solution to satisfy these more and more demanding requirements of the optical access network. Cost-effective emitters have been proposed for coherent optical access networks as directly-phase modulated distributed feedback lasers (DFB) [8], [9], directly-phase modulated reflective semiconductor amplifiers (RSOA) [10], [11], intensity modulated vertical cavity surface emitting lasers (VCSEL) [12] or directly-phase modulated VCSELs [13]. In addition, several coherent receiver technologies have also been proposed and developed. These proposals have a special focus on polarization independence or polarization control as it is an issue for low

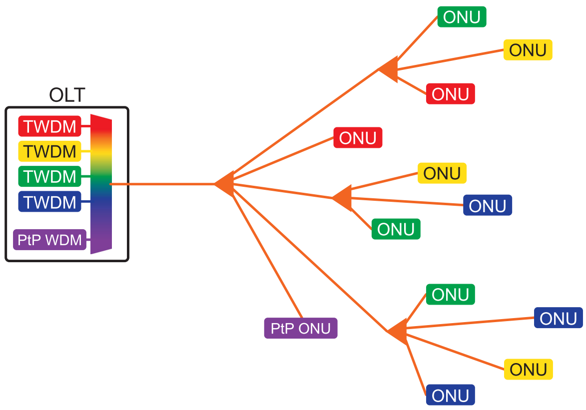

Fig. 1. NG-PON2 network.

cost coherent receivers. One of the first proposals was made by Glance [14] using a similar setup but designed for digital DPSK signals, when our proposal is managing analog signals. This same architecture has been proposed in other works for coherent optical access [15]. Other solutions based on different designs use 3 × 3 couplers [16], polarization scrambling at the transmitter [17] or Alamouti encoding at the transmitter side [18]. Additionally, coherent receivers for optical access networks demand as reduced as possible digital signal processing (DSP) [19], [20] after the optical reception in order to keep the ONU complexity as simple as possible.

This work proposes a real-time 10 Gbps polarization independent quasicoherent receiver for NG-PON2 access networks, extending and completing our previously published results presented in [21]. In particular, we will add to the previous results: the spectral characteristics of the source, the intermediate frequency shift for the receiver given the characteristics of the emitter, a comparison of the behaviour between the direct detection (DD) scheme and the quasicoherent receiver for back to back and 40 km links, and a discussion of the available power budget, addressing the performance of the receiver in terms of splitting ratio and the NG-PON2 class than can be fulfilled with it. We will see that the receiver allows an increase of its sensitivity in order to fulfil the NG-PON2 requirements without using APDs at the receiver or high power lasers at the transmitter and therefore achieving a cost effective receiver architecture adequate for the ONUs and the optical line terminals (OLTs) of a passive optical access network. In addition, the real-time 10 Gbps polarization independent quasicoherent receiver enables a colorless operation without expensive tunable optical filters and a real-time operation without additional DSP keeping a low complexity of the receiver.

II. Experimental Setup

The schematic of the real-time polarization independent 10 Gbps quasicoherent receiver is shown in Fig. 2 and denoted as Quasicoherent Receiver. Fig. 2 also shows the experimental setup employed to test the quasicoherent receiver.

The first part of the 10 Gbps receiver consists of a polarization maintaining (PM) optical coupler, which is used to combine the receiver signal and the local oscillator (LO). The LO is connected to the PM coupler in such a way that at the output the power is splitted at 50% in both principal polarization axes. The LO consists of an external cavity laser (ECL) with 100 kHz linewidth and −145 dB/Hz Relative Intensity Noise (RIN). The ECL was selected as LO because it eases the tuning of the emitting wavelength and its output optical power. We have also tested several Distributed Feedback (DFB) lasers as LO presenting linewidths up to ∼10 MHz and we have found that the sensitivity results are basically the same. These DFB lasers had also RIN values in the range of, or lower than −145 dB/Hz so the noise characteristics of the DFBs are similar to these of the ECL.

After the optical coupler, the signal and LO go through a polarization beam splitter (PBS) and are received using two high bandwidth photodiodes (PD). The LO wavelength (λ_{LO}) is shifted away a value of λ_{IF} from the signal wavelength (λ_{EML}) in order to downconvert the received signal to an intermediate frequency (IF) when the signal and LO are received with the PDs, as is depicted in the inset of Fig. 2. Two types of PDs have been employed in this article. The first analysis of the quasicoherent receiver has been made using two standard commercial PDs presenting an electrical bandwidth of 23 GHz, as the result presented on [21]. The sensitivity and the intermediate frequency shift measurements have been made employing two slightly better sensitivity commercial PDs with 33 GHz electrical bandwidth, but maintaining the same IF and measurement conditions. These new PDs will permit in the future to obtain higher intermediate frequencies thus allowing future increases in the available user bandwidth.

The received intermediate frequency signal is then downconverted to baseband, as is shown in Fig. 2, employing two 10 Gbps ultra-wideband envelope detectors (ED) [21], similar to the ones presented on [22] but designed to support 10 Gbps signals. After the downconversion of the signals to baseband, both signals are electrically added and then amplified. Finally, the Bit Error Rate (BER) is measured using a real-time BER test (BERT). Therefore, the 10 Gbps polarization independent quasicoherent receiver does not require any kind of digital signal processing (DSP) after the reception to measure its performance as is generally needed in heterodyne coherent receivers, allowing a simple real-time operation for a quasicoherent scheme.

The designed testbed consists of a 10 Gbps transmitter, 40 km of Standard Single Mode Fiber (SSMF) and a variable optical attenuator (VOA). The transmitter used to test the described real-time 10 Gbps polarization independent quasicoherent receiver is a commercial, 80 km-10 Gbps bandwidth external modulated laser (EML) emitting 0.44 dBm optical power. The transmitter is modulated with a 10 Gbps non-return to zero (NRZ) data signal coming from a pulse pattern generator (PPG). The optical spectrum of the transmitted signal is shown Fig. 3. We can see that the λ_{EML} is 1548.75 nm and the bandwidth at −15 dB ($\mathrm{BW}_{-15\,\mathrm{dB}}$) is 16.1 GHz. The inset of Fig. 3 shows the eye diagram of the transmitted signal and from it the extinction ratio is estimated to be 15.28 dB.

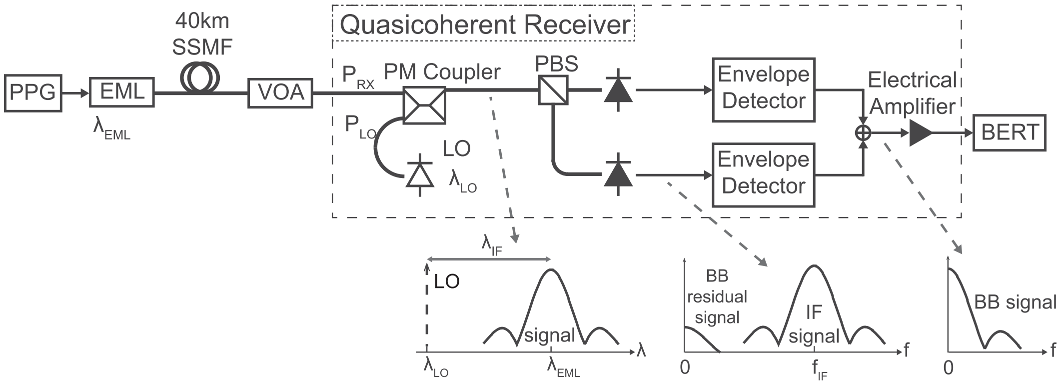

Fig. 2. Experimental setup. Insets: LO and signal spectrum schematic, heterodyne downconverted signal and baseband received signal.

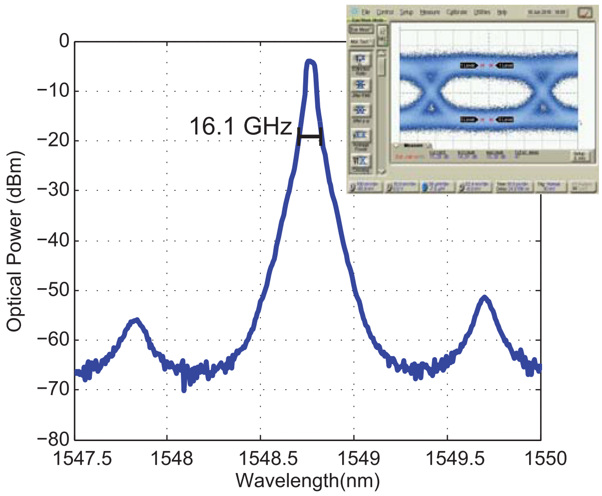

Fig. 3. Optical Spectrum of TX signal. Inset: Eye diagram of TX signal.

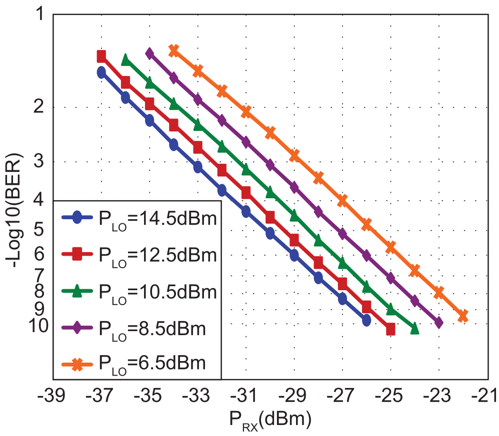

Fig. 4. BER versus received power for 10 Gbps quasicoherent receiver for different LO power.

Fig. 4 shows how the evolution of BER curves as a function of the received power (P_{RX}) for different LO optical powers (P_{LO}), similar to the measurements made in [1]. P_{LO} is varied from 6.5 dBm to 14.5 dBm in steps of 2 dB. The P_{LO} increment causes a reduction of the required P_{RX} to obtain a given BER value i.e., an improvement of the sensitivity of the 10 Gbps quasicoherent receiver. As the curves depicted in Fig. 4 are nearly parallel straight lines, the P_{RX} reduction is the same almost for any measured BER. For the first 2 dB of P_{LO} increase, the improvement of the sensitivity is around 1.25 dB. This improvement gets saturated after increasing the P_{LO} over 10.5 dBm and the required P_{RX} reduction falls approximately to 0.75 dB for the last 2 dB of P_{LO} increment. This behavior is compatible with a receiver limited by shot noise, which is going to be higher than the LO-RIN that will have a greater contribution to the overall noise as our receiver is not balanced. As a consequence of this characterization, the increment of 8 dB of the P_{LO} causes an accumulated P_{RX} reduction of 4 dB and therefore a P_{LO} of 14.5 dBm will be used because it provides the best BER value for any received optical power.

III. Results and Discussion

In this section, the performance of the 10 Gbps quasicoherent receiver is tested and discussed. The performance analysis is based on the receiver sensitivity, the maximum IF shift allowed by the quasicoherent receiver and its relation with the maximum spectral excursion (MSE) of the transmitters, and the achievable power budget.

The receiver sensitivity has been defined as the minimum received power with a maximum BER of 10^{-3}, which is the maximum allowed BER by the forward error correction (FEC) as stated on the NG-PON2 standard [4]. Fig. 5 shows the receiver sensitivity curves for the proposed quasicoherent receiver and a direct detection scheme (DD) for back-to-back (BTB) and for 40 km SSMF transmission. The DD reception is performed using a PD with the same features than these used in the quasicoherent receiver and the same electrical amplifier in order to have a useful comparison.

The receiver sensitivity exhibited by the 10 Gbps quasicoherent receiver is −35.2 dBm for BTB transmission. The quasicoherent receiver exhibits a null dispersion penalty after 40 km SSMF transmission, as it can be seen from figure 5, due to the

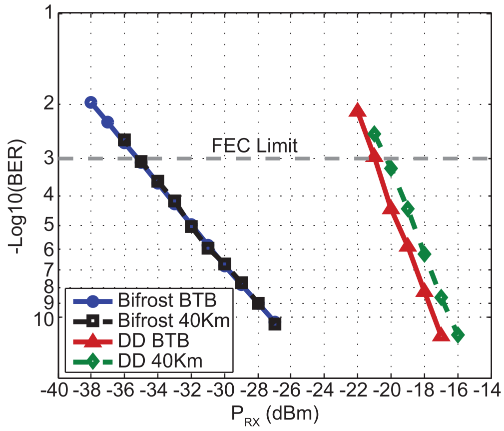

Fig. 5. BER vs. received power for 10 Gbps quasicoherent receiver and DD.

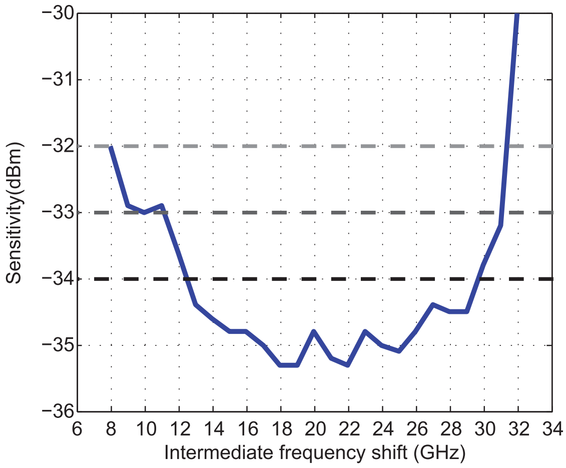

Fig. 6. Intermediate frequency shift for 10 Gbps quasicoherent receiver.

use of an EML in combination with the filtering characteristics of the envelope detector. The BTB receiver sensitivity with DD is -20.9 dBm and exhibits a dispersion penalty of 0.6 dB after 40 km SSMF transmission. Therefore, the proposed 10 Gbps real-time polarization independent quasicoherent receiver has a 14.3 dB sensitivity improvement in comparison with a DD scheme. This improvement increases to 14.9 dB when the dispersion penalty of 40 km SSMF transmission is included. Typical avalanche photodiodes (APD) only provide an improvement between 5 and 10 dB in comparison with the PDs [6], [7].

The maximum IF shift is defined as the maximum IF range that provides at least a target receiver sensitivity. This IF range varies due to the electrical bandwidth of the PDs, which in these measurements was of 33 GHz. Fig. 6 shows the receiver sensitivity of the 10 Gbps quasicoherent receiver for each IF generated after the PDs. The sweep of the IF has been done varying the LO wavelength and keeping the transmitter (TX) wavelength fixed for simplicity. These results would be the same if the TX wavelength was varied and the LO wavelength was kept fixed. The maximum IF shift for a receiver sensitivity of -34 dBm is 17.2 GHz. This maximum IF shift can be increased

TABLE I
MSE VALUES FOR UPSTREAM TRANSMITTERS AND QUASICOHERENT RECEIVER COMPATIBILITY

Channel Spacing	50 GHz	100 GHz
NG-PON2 requirement	±12.5 GHz	±20 GHz
Quasicoherent receiver with P_{RX} of -34dBm	±16.65 GHz	-
Quasicoherent receiver with P_{RX} of -32dBm	±19.75 GHz	±19.75 GHz

to 20 GHz with 1 dB of penalty and to 23.4G Hz with 2 dB of penalty as can be seen in Fig. 6.

The maximum spectral excursion (MSE) of a transmitter is defined as “the absolute difference between the nominal central frequency of the wavelength channel and the -15 dB point of the transmitted spectrum furthest from the nominal central frequency” [5]. Although the MSE is a parameter related to the transmitter, it is relevant for the 10 Gbps quasicoherent receiver because it may determine its colorless and optical filterless operation, which are desired characteristics for a NGPON2 receiver. In a PON architecture, the nominal central frequency or wavelength of the transmitter may change due to many different causes, being a burst transmitter one of them, and the bit rate and chirp characteristics of the transmitter will determine its $BW_{-15\text{ dB}}$. The 10 Gbps quasicoherent receiver allows a colorless operation by using the LO as the selector of the receiver wavelength channel, provided that the signal spectrum does not vary too much. The optical filterless operation of the 10 Gbps quasicoherent receiver is achieved because the LO downconverts the selected channel to IF and then the signal is electrically filtered, but an increase of the transmitter signal spectrum may cause an additional excursion of the IF. So, the proposed receiver design may avoid expensive optical tunable filters on the receiver to obtain a colorless operation, but clearly the maximum IF shift of the quasicoherent receiver is relevant in relation with the MSE of the transmitter.

The MSE sets a limit on the transmitter wavelength fluctuation because its value is the combination of its wavelength variation and the $BW_{-15\text{ dB}}$ of the transmitted signal. Therefore, the MSE value sets the maximum IF fluctuation allowed for the 10 Gbps quasicoherent receiver to operate as a colorless one. The NG-PON2 standard defines a MSE of ± 12.5 GHz for 50 GHz channel spacing and a MSE of ± 20 GHz for 100 GHz channel spacing. Therefore, the maximum IF shift is dependent on the sensitivity of the receiver but also on the variation of the spectrum of the transmitted signal, as it is important that the complete spectrum of the signal fits within the limits of the maximum IF shift of the receiver.

The MSE values defined within the NG-PON2 standard and the 10 Gbps quasicoherent receiver measured MSE compatibilities are summarized on Table I. The 10 Gbps quasicoherent receiver will provide a receiver sensitivity of -34 dBm being compatible with transmitters that have an MSE of ± 16.65 GHz. Therefore, the 10 Gbps quasicoherent receiver can operate with transmitters designed for 50 GHz channel spacing network on the NG-PON2 standard. If the required receiver sensitivity can drop to -32 dBm, the 10 Gbps quasicoherent receiver will be compatible with transmitters with a MSE of ± 19.75 GHz. This

TABLE II
POWER BUDGET, SPLITTING RATIO AND NG-PON2 CLASS SUMMARY

	Testing EML			Standard NG-PON2 TX		
	Power budget	Splitting ratio	NG-PON2 class	Power budget	Splitting ratio	NG-PON2 class
Quasicoherent receiver with the best sensitivity value	35.64 dB	128	E2	37.2 dB	128	E2
Quasicoherent receiver compatible with 50 GHz channel spacing	34.44 dB	64	E1	36 dB	128	E2
Quasicoherent receiver compatible with 100 GHz channel spacing	32.44 dB	64	N2	34 dB	64	E1
DD – PIN (as measured in this work)	21.34 dB	8	-	22.3 dB	16	-
DD – APD [23]	30.94 dB	32	N1	32.5 dB	64	N2

MSE value is close enough to the MSE requirement of the transmitters that operate with 100 GHz channel spacing of the NG-PON2 standard and so compatible with them.

An important parameter for NG-PON2 networks is the power budget of the link because it will determine the maximum reach and splitting ratio of the deployed network and so the profit that its exploitation will provide to the operator. In this case, we will define the power budget as the difference between the transmitted power and the receiver sensitivity after 40 km SSMF transmission. The dispersion penalty has been subtracted from the power budget in order to show just the allowed optical path losses. In the power budget calculation, the fiber attenuation is considered as 0.25 dB/km and the splitter losses are considered as 3.5 log2(M) dB with M being the splitting ratio [4].

We will discuss the obtainable power budget using the tested EML as the transmitter but also using typical NG-PON2 transmitters, which provide higher optical powers. These other transmitters have not been measured in this work, but their emitted optical power nominal values, as shown in the standard, have been used as a comparison.

The proposed 10 Gbps quasicoherent receiver and the EML employed for the setup are able to provide an optical power budget of 35.64 dB for a -35.2 dBm receiver sensitivity. This power budget allows to fulfill the requirements of E2 class of the standard. We will compare these values with the optically unfiltered PIN measured in figure 5 (DD-PIN), and also, for a more realistic comparison, with an APD-based optically filtered receiver [23], which presents a sensitivity of about -30.5 dBm. For the first case, if a DD-PIN scheme is used, the power budget drops to 21.44 dB and in this case it is not able to fulfill the required optical path losses (OPL) of any NG-PON2 class. If we consider the DD-APD receiver, the available power budget of 30.94 dB would fulfill the maximum OPL of NG-PON2 N1 class, which is 29 dB. In terms of splitting ratios, the proposed 10 Gbps quasicoherent receiver would allow a splitting ratio after 40 km SSMF transmission of 128, whereas the DD-PIN PIN would only allow a splitting ratio after 40 km SSMF transmission of 8, which would increase to 32 in the case of using the APD-based receiver.

The EML that we have used on the tests does not fulfill the emitting power requirements of the standard, which has a lower limit of $+2$ dBm. If a standardized NG-PON2 transmitter is employed, the minimum emitted optical power is $+2$ dBm. In this case, and considering only emitted optical power variations, the power budget provided by the proposed 10 Gbps coherent receiver would be of 37.2 dB after 40 km SSMF transmission. The combination of a standardized NG-PON2 transmitter with the proposed 10 Gbps quasicoherent receiver would fulfil the E2 class of the NG-PON2 standard and would allow a splitting ratio after 40 km SSMF transmission of 128, only 0.8 dB below the optical power necessary to obtain the logical NG-PON2 limit of 256 users. If this standardized NG-PON2 transmitter is received using DD-PIN, the optical power budget falls to 22.3 dB, which does not fulfil any NG-PON2 class and will only allow a splitting ratio after 40 km SSMF transmission of 16. If the DD-APD receiver is used, the N2 class can be fulfilled and the splitting ratio after 40 km SSMF transmission will increase to 64.

Therefore, the proposed 10 Gbps quasicoherent receiver improves the power budget in comparison with the tested DD scheme using a PIN and even with the one that can be expected using an APD-based receiver. This improvement is translated on the fulfillment of a higher NG-PON2 class and a larger splitting ratio after 40 km SSMF transmission.

These power budget values of the 10 Gbps quasicoherent receiver and the direct detection scheme for the testing EML and for a $+2$ dBm optical power standard NG-PON2 transmitter are summarized on Table II, showing the allowed splitting ratios and the NG-PON2 OPL class compatibility.

In a multiwavelength scenario, as is required for the NG-PON2 standard, the transmitted wavelengths can fluctuate in the range defined by the MSE as was stated previously. In addition, the maximum transmitted wavelength variation is related with the sensitivity of the proposed 10 Gbps quasicoherent receiver as we have analyzed before. Thus, the power budget in a multiwavelength scenario will also be related with the MSE and so with the channel spacing.

A channel spacing of 100 GHz imposes a sensitivity of -32 dBm because of the MSE requirements, as has been explained previously. So, the power budget with a channel spacing of 100 GHz will be of 32.44 dB with the testing EML and around 34 dB with a standardized NG-PON2 transmitter. These power budgets allow to fulfill the N2 and E1 classes, respectively, and they will allow splitting ratios of 64.

If the used channel spacing is 50 GHz, the sensitivity improves to -34 dBm and so the power budgets will be better. The power budget will be of 34.44 dB when the transmitter is the testing

EML and around 36 dB if a +2 dBm standardized NG-PON2 transmitter is used. Thus, the E1 and E2 classes are fulfilled with these respective power budgets allowing splitting ratios of 64 and 128 respectively.

IV. Conclusion

A real-time 10 Gbps polarization independent quasicoherent receiver for NG-PON2 access networks has been presented in this paper. This real-time quasicoherent reception technique is a promising technology for NG-PON2 access networks that allows to solve the most demanding requirements of the NG-PON2 standard.

The proposed 10 Gbps quasicoherent receiver shows a sensitivity of −35.2 dBm after 40 km SSMF transmission. This sensitivity provides an improvement of 14.3 dB in comparison with DD with a PD after the same 40 km SSMF transmission. In addition, it will be better even with the 5–10 dB of improvement that an APD would provide.

The 10 Gbps quasicoherent receiver sensitivity will allow a power budget of 35.64 dB when the testing EML is used or 37.2 dB when a standardized NG-PON2 transmitter would be used. These power budgets will allow to fulfill the E2 OPL class of the NG-PON2 standard, respectively, whereas direct detection with a PD will not fulfil any OPL classes of NG-PON standard. In addition, the power budgets of the 10 Gbps quasicoherent receiver will give rise to a splitting ratio of 128 in comparison with the 8 and 16, respectively, that will allow direct detection with a PD. Even if an APD is employed for direct detection, the 10 Gbps quasicoherent receiver will increase the splitting ratio at least by a factor 2.

In addition, the proposed 10 Gbps quasicoherent receiver allows a colorless and optical filterless operation, which is compatible with NG-PON2 transmitters. The colorless operation is possible due to the channel selection done using the tunability of LO and the electrical IF filtering. If the transmitter has a MSE compatible with 50 GHz channel spacing, the quasicoherent receiver will provide a sensitivity of −34 dBm. Whereas the provided sensitivity will be −32 dBm if the transmitter has a MSE compatible with a 100 GHz channel spacing.

In conclusion, the proposed real-time 10 Gbps polarization independent quasicoherent receiver is a promising receiver for NG-PON2 access networks increasing the available power budgets and allowing colorless and filterless operation compatible with NG-PON2 transmitters.

References

[1] Cisco Visual Networking Index: Global Mobile Data Traffic Forecast Update, pp. 2016–2021, 2017, White Paper.

[2] M. Ruffini, "Multidimensional convergence in future 5G networks," *J. Lightw. Technol.*, vol. 35, no. 3, pp. 535–549, Feb. 2017.

[3] J. S. Wey *et al.*, "Physical layer aspects of NG-PON2 standards-part 1: Optical link design [Invited]," *J. Opt. Commun. Netw.*, vol. 8, no. 1, pp. 33–42, Jan. 2016.

[4] Y. Luo *et al.*, "Physical layer aspects of NG-PON2 standards–Part 2: System design and technology feasibility [Invited]," *J. Opt. Commun. Netw.*, vol. 8, no. 1, pp. 43–52, Jan. 2016.

[5] J. C. Campbell, "Recent advances in telecommunications avalanche photodiodes," *J. Lightw. Technol.*, vol. 25, no. 1, pp. 109–121, Jan. 2007.

[6] M. Achouche *et al.*, "InGaAs communication photodiodes: from low- to high-power-level designs," *IEEE Photon. J.*, vol. 2, no. 3, pp. 460–468, Feb. 2010.

[7] M. S. Erkilinç *et al.*, "Bidirectional wavelength-division multiplexing transmission over installed fibre using a simplified optical coherent access transceiver," *Nature Commun.*, vol. 8, Oct. 2017, Art. no. 1043.

[8] J. A. Altabas *et al.*, "1 Gbps full-duplex links for ultra-dense-WDM 6.25 GHz frequency slots in optical metro-access networks," *Opt. Express*, vol. 24, no. 1, pp. 555–565, Jan. 2016.

[9] I. N. Cano, A. Lerín, and J. Prat, "DQPSK directly phase modulated DFB for flexible coherent UDWDM-PONs," *IEEE Photon. Technol. Lett.*, vol. 28, no. 1, pp. 35–38, Jan. 2016.

[10] J. A. Altabas *et al.*, "Cost-Effective transceiver based on an RSOA and a VCSEL for flexible uDWDM networks," *IEEE Photon. Technol. Lett.*, vol. 28, no. 10, pp. 1111–1114, May 2016.

[11] H. K. Shim *et al.*, "A practical 10-Gb/s ultra-dense WDM PON," in *Proc. OptoElectron. Commun. Conf. Australian Conf. Optical Fibre Technol.*, Melbourne, VIC, Australia, Jul. 2014, pp. 289–290.

[12] J. B. Jensen *et al.*, "VCSEL based coherent PONs," *J. Lightw. Technol.*, vol. 32, no. 8, pp. 1423–1433, Apr. 2014.

[13] J. A. Altabas *et al.*, "Chirp-based direct phase modulation of VCSELs for cost-effective transceivers," *Opt. Lett.*, vol. 42, no. 3, pp. 583–586, Feb. 2017.

[14] B. Glance, "Polarization independent coherent optical receiver," *J. Lightw. Technol.*, vol. LT-5, no. 2, pp. 274–276, Feb. 1987.

[15] I. N. Cano *et al.*, "Simplified polarization diversity heterodyne receiver for 1.25 Gb/s cost-effective udWDM-PON," in *Proc. Opt. Fibre Commun.*, 2014, p. W4G.2.

[16] E. Ciaramella, "Polarization-Independent receivers for Low-Cost coherent OOK systems," *IEEE Photon. Technol. Lett.*, vol. 26, no. 6, pp. 548–551, Mar. 2014.

[17] I. N. Cano *et al.*, "Polarization independent single-PD coherent ONU receiver with centralized scrambling in udWDM-PONs," in *Proc. Eur. Conf. Opt. Commun.*, Cannes, France, Sep. 2014, pp. 1–3.

[18] M. S. Faruk *et al.*, "Technology requirements for an alamouti-coded 100 Gb/s digital coherent receiver using 3 × 3 couplers for passive optical networks," *IEEE Photon. J.*, vol. 10, no. 1, pp. 1–13, Feb. 2018.

[19] L. Xue *et al.*, "50-Gb/s TDM-PON based on 10G-class devices by optics-simplified DSP," in *Proc. Opt. Fibre Commun. Conf.*, San Diego, CA, USA, Mar. 2018, pp. 1–3.

[20] R. Ferreira *et al.*, "Demonstration of Nyquist UDWDM-PON with digital signal processing in real-time," in *Proc. Opt. Fibre Commun. Conf.*, San Diego, CA, USA, Mar. 2015, pp. 1–3.

[21] J. A. Altabas *et al.*, "Real-time 10 Gbps polarization independent quasicoherent receiver for NG-PON2 access networks," in *Proc. Opt. Fibre. Commun.*, San Diego, CA, USA, Mar. 2018, pp. 1–3.

[22] B. Cimoli *et al.*, "An ultra-wideband schottky diode based envelope detector for 2.5 Gbps signals," in *Proc. 46th Eur. Microw. Conf.*, London, U.K., 2016, pp. 277–280.

[23] Y. Luo *et al.*, "Time- and wavelength-division multiplexed passive optical network (TWDM-PON) for Next-Generation PON stage 2 (NG-PON2)," *J. Lightw. Technol.*, vol. 31, no. 4, pp. 587–593, Feb. 2013.

Authors' biographies not available at the time of publication.

3.5 Paper V

25Gbps Quasicoherent Receiver for Beyond NG-PON2 Access Networks

J. A. Altabas, L. F. Suhr, G. Silva Valdecasa, J. A. Lazaro, I. Garces, J. B. Jensen, and A. T. Clausen, “25Gbps Quasicoherent Receiver for Beyond NG-PON2 Access Networks,” in *2018 European Conference on Optical Communication (ECOC)*, (Rome, Italy), p. We2.70, 2018

25Gbps Quasicoherent Receiver for Beyond NG-PON2 Access Networks

Jose A. Altabas[(1)], Lau F. Suhr[(2)], Guillermo Silva Valdecasa[(2)], Jose A. Lazaro[(3)], Ignacio Garces[(1)], Jesper B. Jensen[(2)] , Anders T. Clausen[(4)]

[(1)] Aragon Institute of Engineering Research (I3A), Universidad de Zaragoza, Mariano Esquillor, ed. I+D+I, E-50018, Zaragoza, Spain, jaltabas@unizar.es
[(2)] Bifrost Communications, Scion DTU, Akademivej Bygnig 381, 2800 Kgs Lyngby, Denmark
[(3)] Universitat Politècnica de Catalunya (UPC), Jordi Girona 31, E-08034, Barcelona, Spain
[(4)] DTU Fotonik, Technical University of Denmark (DTU), Ørsteds Plads, 2800 Kgs. Lyngby, Denmark

Abstract *A 25Gbps quasicoherent receiver with simple DSP has been experimentally validated for 25G access networks. It exhibits a sensitivity of -24.7dBm after 20km SSMF and duobinary decoding and provides a power budget of 25.7dB.*

Introduction

Data traffic over access networks has been exponentially growing during the recent years and it will continue growing due to highly demanding new services such as streaming media, Internet of Things (IoT), cloud computing or virtual and augmented reality[1] and the 5G convergence of wireless and optical networks.

The NG-PON2 standard was released[2] to address this data traffic growth and deal with the short term requirements of the users. It is based on time and wavelength division multiplexing (TWDM) with a channel bit rate of 10 Gbps per wavelength. However, the exponential growth of traffic demand pushes research to study the next generation of access network in order to meet mid and long term user requirements. This next generation of access networks will be based on 25 Gbps data rate per wavelength but employing the same 10 Gbps based devices in order to keep a reduced cost system[3].

Recently, coherent and quasicoherent access networks[4] have arisen as a feasible technology to address these high demanding requirements. They allow to increase the data rate, the receiver sensitivity, the splitting ratio and the optical fibre transmission length. Moreover, they also allow a filterless wavelength demultiplexing, which is necessary for keeping the TWDM concept. All these improvements can be achieved without a significant cost increment, and different cost-effective devices[3,4,5] have been developed.

In this article, we propose and experimentally validate a 25 Gbps quasicoherent receiver for beyond NG-PON2 access networks. The proposed receiver allows to increase the receiver sensitivity and a filterless wavelength demultiplexing using a low complexity digital signal processing based on a simple equalizer.

Experimental setup

Fig. 1 shows the schematic of the 25 Gbps quasicoherent receiver, denoted as Bifrost Quasicoherent Receiver, and the experimental setup. Fig. 1 also depicts the simple digital signal processing applied to the received data.

The proposed 25 Gbps quasicoherent receiver with polarization independent operation[4] consists of an optical coupler, which is fed by the received signal and a local oscillator (LO), followed by a polarization beam splitter (PBS) and two 33 GHz bandwidth photodiodes (PD). The LO is an external cavity laser to ease wavelength adjustment and with an emitting power of 14.5 dBm. The LO wavelength (λ_{LO}=1554.58 nm) is shifted away from the received signal wavelength (λ_{EML}=1554.44 nm) to downconvert the 25 Gbps received signal to an intermediate frequency (IF) of 18 GHz. The two resulting 25 Gbps IF signals are then downconverted to baseband employing two envelope detectors (ED) based on ultra-wideband Schottky diodes designed for 10 Gbps signals, similar to the ones shown in[4]. The 33 GHz PDs are needed even with the 10 Gbps ED due to wavelength fluctuation allowed in NG-PON2. The two

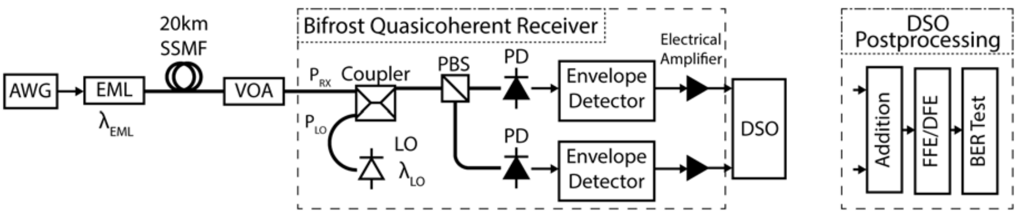

Fig. 1: Experimental Setup.

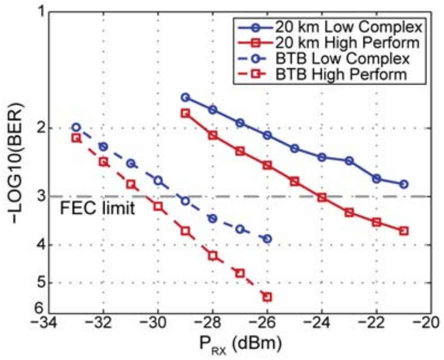

Fig. 2: BER versus received power for 25 Gbps Bifrost Receiver with NRZ decoding.

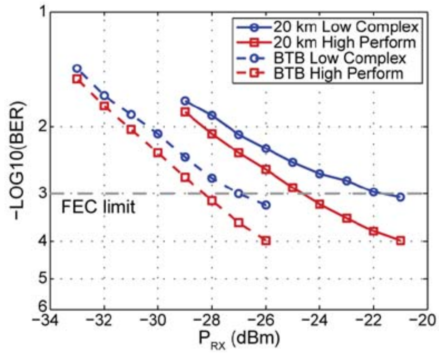

Fig. 3: BER versus received power for 25 Gbps Bifrost Receiver with duobinary decoding.

25 Gbps baseband signals are amplified and then digitalized using an 80 GS/s Digital Storage Oscilloscope (DSO).

After digitalization of the data, a simple digital signal processing is applied. First, both signals are added in order to complete the polarization independent process. This procedure has been done digitally for experimental simplicity but it can be done using analog electronics and reducing the digital acquisition process to only one signal[4]. A feed-forward equalization (FFE) and a decision feedback equalization (DFE) is then used to obtain either an equalized NRZ signal or an equalized duobinary signal. We have tested two different equalizations, the first one consisting of 41 tap FFE and 21 tap DFE and denoted as high performance equalizer, and the second one consisting of 15 tap FFE and 6 tap DFE and denoted as low complexity equalizer. All mentioned taps use T/2 spacing, both utilizing the least-mean squares algorithm. Finally, the data is decoded either as NRZ or as duobinary and the BER test is performed.

The experimental setup feeding the Bifrost quasicoherent receiver consists of a 30 GHz externally modulated laser (EML) with a modulated emission power of +1 dBm and an extinction ratio (ER) of 8 dB, 20 km of standard single mode fibre (SSMF) and a variable optical attenuator (VOA). The EML is modulated with a 25 Gbps non-return-to-zero (NRZ) PRBS generated with a 65 GS/s arbitrary waveform generator (AWG). The AWG is employed to emulate a transmitter subsystem with a combined bandwidth of 18.5 GHz.

Results

The sensitivity is defined as the minimum received power for a BER of 10^{-3} to justify the use of the same forward error code already used on NG-PON2[2]. Fig. 2 shows the sensitivity curves for NRZ decoding and Fig. 3 shows the sensitivity curves for duobinary decoding. Both figures present curves for both equalizers (the high performance equalizer and the low complexity equalizer) and for different link distances: back-to-back (BTB), and 20 km SSMF transmission. Fig. 4 shows the eye diagrams after the high performance equalizer with NRZ and duobinary decoding for both link distances.

The high performance equalizer shows a BTB sensitivity of -30.5 dBm with NRZ decoding, as can be seen on Fig. 2. This BTB sensitivity drops to -28.5 dBm when duobinary decoding is used, as can be seen on Fig. 3. This BTB penalty is due to additional amplitude level, seen on Fig 4.

The 20 km SSMF sensitivity with the high performance equalizer is -24 dBm with NRZ decoding and -24.7 dBm with duobinary decoding, as Fig. 2 and Fig. 3 show respectively. The dispersion penalty is smaller with duobinary decoding because of the reduced spectrum of duobinary signals.

If the complexity of the equalization is reduced, the BTB sensitivity is now of -29.2 dBm with NRZ decoding and -27 dBm with duobinary decoding. Therefore, the low complexity equalization causes around 1.5 dB penalty on the BTB sensitivities. The duobinary decoding with the low complexity equalization keeps a similar penalty of about 2 dB as with the high performance equalization, caused by a worse eye diagram quality.

In the case of using low complexity equalizer, the dispersion penalty for 20 km SSMF transmission causes the NRZ signal to be unrecoverable with 10^{-3} FEC, as the BER is never better than this threshold, as shown in Fig. 2. However, the duobinary decoding allows the BER curve to go below the FEC threshold, as can be seen on Fig. 3. This is due to a smaller dispersion penalty of duobinary signals relative to NRZ signals. Thus, the 20 km SSMF sensitivity is -22 dBm with duobinary decoding. However, in

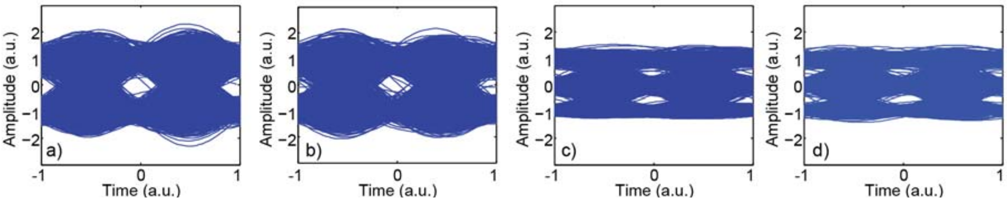

Fig. 4: Eye diagrams with high performance equalization. NRZ: a) BTB, b) 20 km SSMF; Duobinary: c) BTB, d) 20 km SSMF.

this case, the equalization complexity reduction leads to a 2.7 dB penalty.

Consequently, both decoding techniques will be valid for 20 km SSMF transmission when the high performance equalizer is employed but duobinary decoding will be preferred because of the slightly better sensitivity. In the case of the low complexity equalizer, the duobinary decoding will be required for the 20 km SSMF transmission, which is necessary for 25 Gbps access network.

Furthermore, the proposed 25 Gbps quasicoherent receiver with duobinary decoding and the EML employed on the test will provide a remaining power budget after 20 km SSMF transmission of 25.7 dB with the high performance equalizer and 23 dB with the low complexity equalizer. Therefore, it will allow a splitting ratio of 64 and 32, respectively, after 20 km of SSMF transmission.

In the case of employing an EDFA/SOA amplified transmitter, as it can be used at the optical line terminator (OLT), +10 dBm launched power can be easily achieved. Thus, the power budgets after the 20 km SSMF transmission will be 34.7 dB and 32 dB for high performance and low complexity equalization respectively. The splitting ratio after the 20 km SSMF will then increase to 256 for both equalizers.

In addition to the high sensitivity provided by the proposed 25 Gbps quasicoherent receiver, it allows a colourless and filterless operation: the LO wavelength can be tuned to receive a desired channel allowing a colourless operation and the optical heterodyne reception downconverts the optical channel selected by the LO to the IF frequency where it will be electrically filtered. Thus, the proposed 25 Gbps quasicoherent receiver can select a specific optical channel without tuneable optical filters on a multiwavelength scenario, as could be a 100G (4x25G) NGPON2-like access network.

Alternatively, the colourless operation of the 25 Gbps quasicoherent receiver also enables operation with low dispersion wavelengths in the O-band. In this situation, the NRZ decoding could be employed with a low dispersion penalty leading to a sensitivity similar to the measured BTB sensitivity. The provided splitting ratio would be similar to the one obtained in C-band because of the higher fibre attenuation in the O-band.

Conclusions

A 25 Gbps quasicoherent receiver has been proposed and experimentally tested exhibiting a BTB sensitivity of -28.5 dBm (-27 dBm) with a high performance (low complexity) equalizer, and duobinary decodification. After 20 km SSMF transmission, the sensitivity will be -24.7 dBm and -22 dBm, respectively.

Therefore, the power budget after 20 km SSMF transmission is 25.7 dB and 23 dB when a +1 dBm emitted optical power EML is employed as the transmitter, which means a splitting ratio of 64 and 32, respectively. This ratio can be increased using higher output power emitters.

NRZ decoding provides a higher BTB sensitivity (-30.5 dBm and -29.2 dBm, respectively) but also a high dispersion penalty. Thus, NRZ could be interesting in a lower dispersion, though higher losses, band.

In conclusion, the proposed 25 Gbps quasicoherent receiver is an attractive candidate for beyond NG-PON2 access networks, as a single wavelength 25G-PON and especially, due to its colourless and filterless operation, as a multiwavelength 100G-PON (4x25G).

Acknowledgements

This work was partially supported by the Diputación General de Aragón under grant T20_17R, the Spanish MINECO projects FOANT (TEC2017-85752-R) and ALLIANCE (TEC2017-90034-C2-2-R) co-funded by FEDER, and a MECD FPU grant (FPU-13/00620).

References

[1] Cisco Visual Networking Index: Global Mobile Data Traffic Forecast Update, 2016–2021, White Paper.

[2] J. S. Wey et al., "Physical layer aspects of NG-PON2 standards-Part 1: Optical link design [Invited]," IEEE/OSA J. Opt. Commun. Networking, Vol. **8**, no. 1, p. 33 (2016).

[3] D. T. van Veen et al., "Proposals for Cost-Effectively Upgrading Passive Optical Networks to a 25G Line Rate," J. Lightwave Technol. Vol. **35**, no. 6, p. 1180 (2017).

[4] J. A. Altabas et al., "Real-time 10Gbps Polarization Independent Quasicoherent Receiver for NG-PON2 Access Networks," Proc. OFC, Th1A3, San Diego (2018).

[5] J. A. Altabas et al., "Chirp-based direct phase modulation of VCSELs for cost-effective transceivers," Opt. Lett., Vol. **42**, p.583 (2017).

Chapter 4

Report

4.1 Research objectives

The main objective of the thesis is to investigate, develop, implement and test new coherent transmitters and receivers for the next generation optical access networks. The main goals of this research are to increase the capacity, reach and number of users of the current networks together with the reduction of the cost of deployment (CAPEX) and operation (OPEX) of these future optical access networks. In order to achieve this goal, the following specific objectives have been established:

- Study the feasibility of cost-effective transmitters, such as DFB, RSOA and VCSEL, for directly phase modulation in order to increase the spectral efficiency and reach of the optical access networks.
- Analyze the feasibility of single PD heterodyne receivers for optical access networks, exploring different configurations and optimizing their parameters.
- Evaluate the feasibility of using bidirectional links for uDWDM optical access networks, which allows to increase their overall capacity.
- Investigate real-time quasi-coherent receivers to be used in the optical access networks and compatible with NG-PON2 standard.
- Explore the feasibility of using bandwidth limited quasi-coherent receivers for optical access networks beyond the NG-PON2 standard.

4.2 Methodology

In line with the research objectives and the work presented as a compendium in this thesis, the methodology section is divided in three subsections: directly-phase modulated transmitters, single PD heterodyne receivers for DPSK signals and quasi-coherent receivers.

In the directly-phase modulated transmitters subsection (subsection 4.2.1), the technique to generate DPSK signal over a DFB, RSOA and VECSL is described. Additionally, the technique for the generation of Nyquist-DPSK with a MZM is also explained.

In single PD heterodyne receivers for DPSK signals and quasi-coherent receivers subsections (subsection 4.2.2 and subsection 4.2.3), it will be presented the techniques for reception of DPSK and IM signals with cost-effective coherent receivers.

4.2.1 Directly-phase modulated transmitters

Directly-phase modulated transmitters have shown a high interest during the recent years, as it was pointed out in subsection 2.2.3. In this subsection, the direct-phase modulation of a DFB, a RSOA and a VCSEL is described conceptually, theoretically and experimentally.

The phase modulation of lasers (DFB and VCSEL) is related with their instantaneous frequency shifts, also named as chirp. The modulation of the bias current of a laser causes a modulation of its output power. If the laser is emitting in its linear regime, the emitted optical power will be proportional to the modulation current. In addition, its emitting wavelength (or frequency) will also change when it is modulated. The instantaneous frequency shift or chirp follows the Equation 4.1 for modulation frequencies higher than the device thermal response [142].

$$\Delta\nu(t) = \frac{1}{2\pi}\frac{\mathrm{d}\phi(t)}{\mathrm{d}t} = \frac{\alpha}{4\pi}\left(\frac{1}{P(t)}\frac{\mathrm{d}P(t)}{\mathrm{d}t} + \kappa P(t)\right) \tag{4.1}$$

where $\Delta\nu(t)$ is the instantaneous frequency shift, $\phi(t)$ is the instantaneous optical phase, and $P(t)$ is the instantaneous optical power. α and κ are the transient and adiabatic chirp parameters, which are intrinsic to the employed laser. α is related with the emitted optical power variation and κ is related with instantaneous emitted optical power.

Equation 4.1 shows that choosing an adequate modulation signal, the instantaneous frequency shift can be controlled and so the instantaneous optical phase.

As a first approach to directly-phase modulation over lasers, a DFB was chosen. This type of laser is broadly used in optical access networks for directly-amplitude modulation. In addition, some previous work about directly-phase modulation over DFBs have been performed by [110, 113] in the previous years. They proposed to use a NRZ signal filtered with a carefully chosen capacitor.

The first step to direct phase modulation of a DFB is the selection and characterization of the DFB to use, in our case the DFB JDSU CQF915/1839. This DFB has a linewidth in the range of 10 MHz, which is adequate for its later reception in a coherent receiver. The current vs. optical power is shown in Figure 4.1. This figure shows the threshold current, which is 15 mA, and the slope efficiency of the linear region, which is 0.0483 W/A. In order to avoid the saturation and damage region, the bias current will be limited to 200 mA. Another important feature of this DFB is that contains a thermistor and Peltier cell integrated inside of its packing. This thermistor and Peltier cell will allow to control the operational temperature of the DFB and then its nominal emitting wavelength, which is an important requirement for receiving coherent signals.

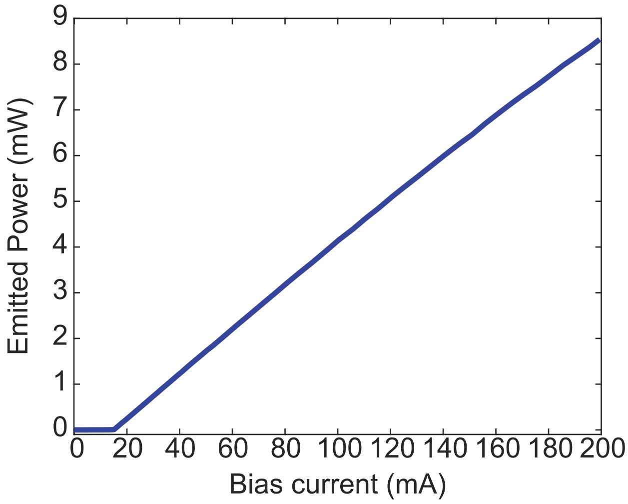

Figure 4.1: Current vs. optical power of JDSU CQF915/1839.

After the laser selection, the procedure proposed in [113], named as equalization of the laser, is performed. In order to do it, a simple printed circuit board (PCB) is designed, as shown in Figure 4.2. This PCB includes a capacitor and a resistor. The resistor is 27 Ω, which allows to adapt the input impedance of the laser to 50 Ω, since the internal resistor of the DFB is around 23 Ω. The capacitance was selected in order to equalize the signal for the direct-phase modulation. Finally, the chosen capacitance was 1 pF, which provides a minimum bit error rate (BER) for DPSK modulation and also, shows a typical DPSK spectrum.

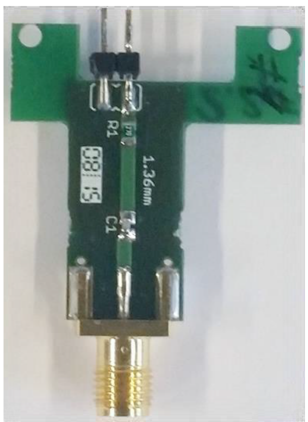

Figure 4.2: Photo of the equalization board of the DFB.

The spectrum of a square shaped DPSK has two main features that allow to confirm its correct modulation when the high resolution optical spectrum, shown in Figure 4.3, is analyzed. On the one hand, the square shaped time domain causes a typical sinc shaped spectrum, similar to the one that was obtained. On the other hand, the DPSK exhibits a suppressed optical carrier, as it can be also seen in Figure 4.3.

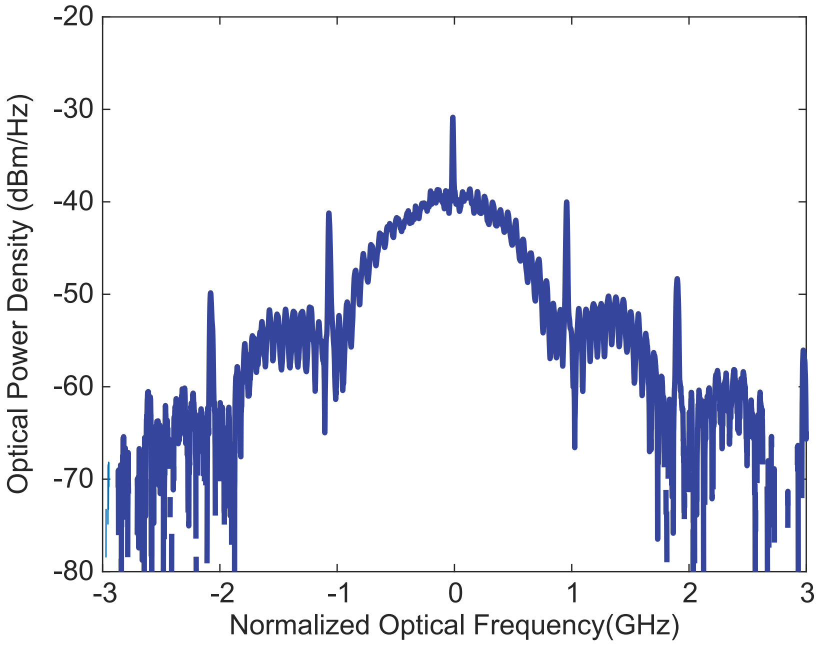

Figure 4.3: 1 Gbps DPSK with a directly phase-modulated DFB high resolution optical spectrum.

This technique was employed in the article of the compendium section 3.1 [1] and in the contributions [12, 13, 15, 16, 37].

After the successful directly phase modulation of a DFB and with the experience obtained there, it was decided to apply the concept of directly phase modulation over a VCSEL. VCSELs emit less optical power, are less stable and spectrally broader than DFBs, but they present the advantage of a reduced cost and a lower energy consumption.

The directly phase modulation of the VCSEL has been performed using a tailored pulse shape signal that allows to employ the chirp equation 4.1 to induce the desired phase changes.

As with the previous laser, the first step is selecting and characterizing a suitable VCSEL for directly phase modulation. In this case, the Raycan VCSEL RC33xxx1-F was selected, which has an approximated linewidth of 20 MHz. The VCSEL linewidth, which can be seen in the inlet of Figure 4.4, is bigger than the DFB one but it still is good enough to be received with the coherent receptor presented later. Figure 4.4 shows the current threshold, which is 1.4 mA and the efficiency slope, which is 0.137 W/A.

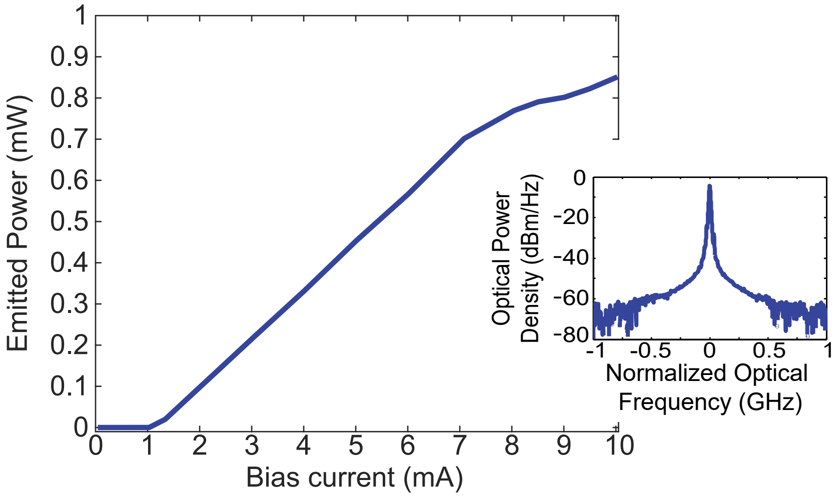

Figure 4.4: Current vs. optical power of Raycan VCSEL RC33xxx1-F for 25 °C. Inlet: Optical spectrum of VCSEL.

The use of this VCSEL as a transmitter of a coherent link requires its emitting wavelength to be controlled and kept stable. This VCSEL includes an integrated thermistor and a Peltier cell for temperature control, which is the most important parameter to control the VCSEL wavelength. In addition, the VCSEL wavelength is also extremely sensitive to the bias current, so a very stable current source (Thorlabs LDC200CV) must be used.

The direct phase modulation of a VCSEL using a tailored pulse shaper requires the accurate characterization of the chirp parameters, α and κ, of Equation 4.1. These parameters are obtained employing the frequency modulation/amplitude modulation (FM/AM) method [143, 144]. The experimental setup required for this method is depicted in Figure 4.5 and consists of a tone generator, a high resolution complex optical spectral analyzer (HRCOSA) and a digital communication analyzer oscilloscope (DCA).

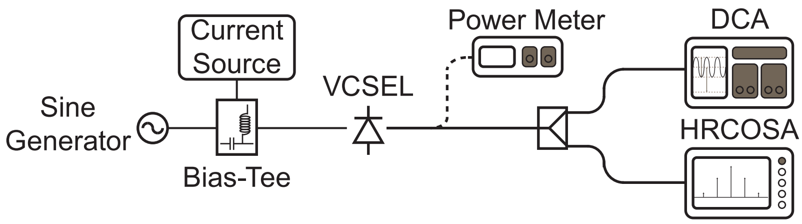

Figure 4.5: Experimental setup for chirp parameters characterization.

Using the experimental setup described in Figure 4.5 and the technique described deeply on section 3.3, the parameters α, f_c and κ for different bias currents can be obtained.

The obtained κ parameter is plotted in Figure 4.6 in comparison with the I_{bias}. This figure allows to confirm that α and κ are independent of the bias current, while the f_c increases linearly

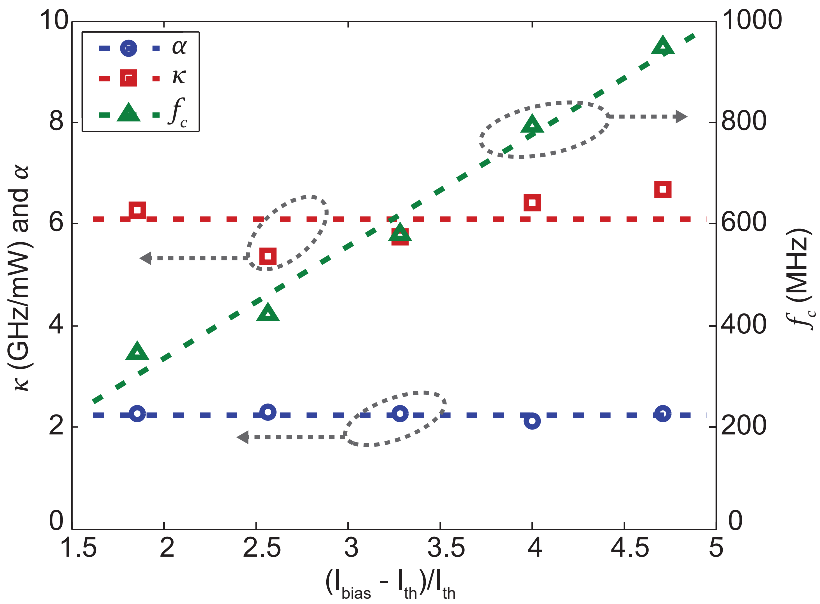

Figure 4.6: α, f_c and κ vs. different bias currents.

with it. Finally, Figure 4.6 shows that the α parameter is 2.24 ± 0.1 and the κ parameter is $7.6 \pm 0.8 GHz/W$ for the Raycan VCSEL RC33xxx1-F.

After obtaining the chirp parameters, Equation 4.1 can be used for simulating the chirp behavior and so the phase of the signal depending on the pulse shape of the modulating signal. This simulation was as a preliminary test for choosing the pulse shape and it was done assuming that the VCSEL was working in the linear regime, i.e. assuming that it was not going to saturate for high currents neither to suffer from clipping for low currents.

The used modulation signal and the measured optical modulation at the output of the VCSEL are shown in Figure 4.7.a. The measured optical modulation was introduced in the Equation 4.1 obtaining the chirp behavior shown in Figure 4.7.b. As it was expected, the adiabatic contribution has the same shape than the optical power signal scaled by a factor $\frac{\alpha\kappa}{4\pi}$. On the other hand, the transient chirp has a derivative shape with a different scaling factor when the pulse is positive than when it is negative. The different scaling factor is related with $P(t)$ term as denominator, which reduces the transient chirp contribution when the power increases in the positive pulses.

Finally, Figure 4.7.c shows the phase behavior and the contribution of the transient and the adiabatic chirp independently. In this figure, it can be seen that the phase modulation follows the behavior of the adiabatic contribution, whereas the transient chirp mainly contributes to increase the sharpness of the transitions.

The measured optical phase eye diagram and the measured optical IQ diagram is shown in Figure 4.8. These diagrams matched with the behavior predicted by the simulation.

Additionally, the high resolution optical spectrum, shown in Figure 4.9, allows to confirm

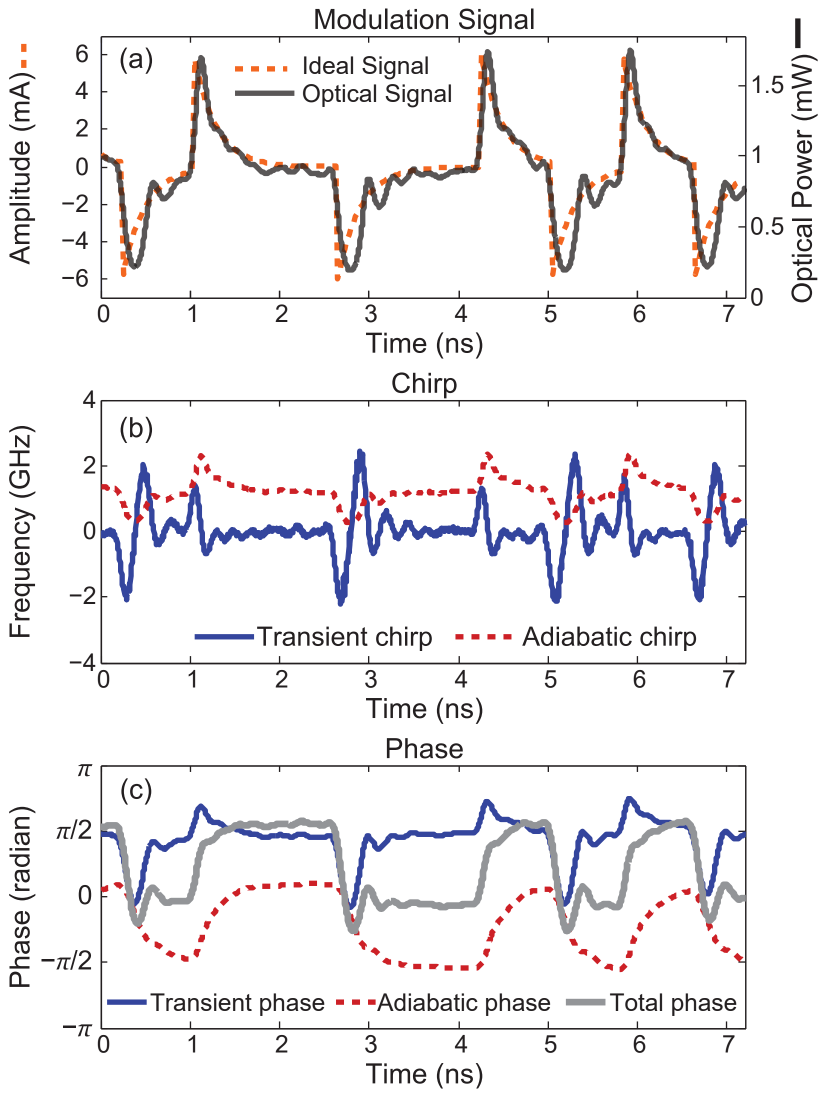

Figure 4.7: (a) 1.25 Gbps ideal pulse-shaping modulation signal and measured optical signal, simulated: (b) transient and adiabatic chirp, and (c) total phase and the generated phase by the transient and adiabatic chirps.

the phase modulation through it characteristic sinc shape and suppressed carrier of a squared shaped DPSK for 1.25 Gbps and 2.5 Gbps.

This technique has been employed in the article of the compendium section 3.3 [3], in the appendix section B.2 [7] and in the contributions [30, 36, 37].

Another approach for phase modulation in cost-effective transmitters is the phase modulation of RSOAs. The theory behind of a phase modulation of a RSOA is different than for DFBs or VCSELs.

The RSOA is an amplifier and so it is based on a gain material which converts the input bias current into optical gain. For the phase modulation of a RSOA, it is necessary to modify the refractive index of its gain material to induce phase changes over the pump carrier. The

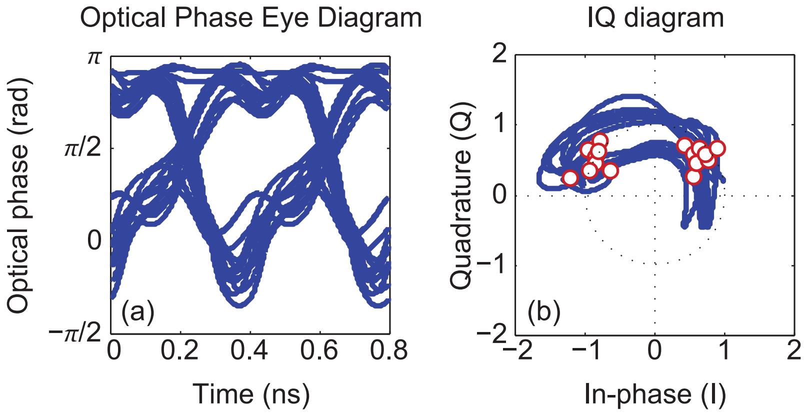

Figure 4.8: 2.5 Gbps DPSK with a directly phase-modulated VCSEL: (a) Optical phase eye diagram and (b) Optical IQ diagram.

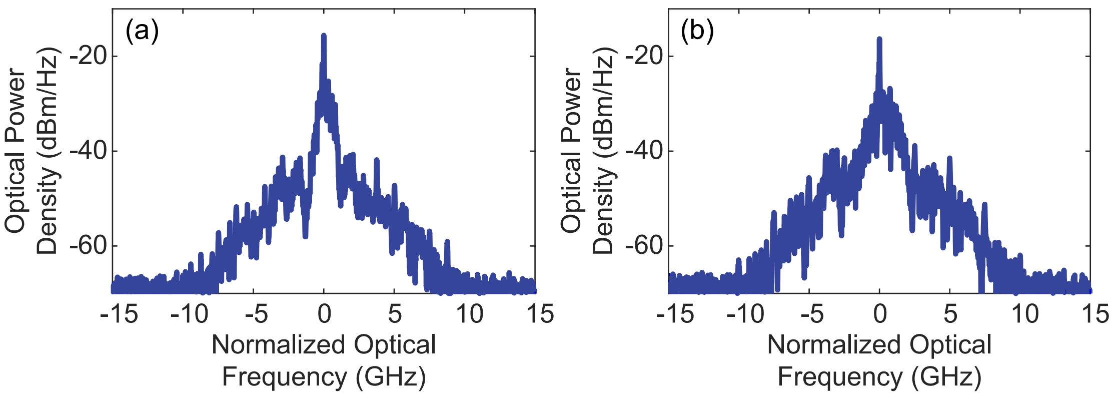

Figure 4.9: 1.25 Gbps (a) and 2.5 Gbps (b) DPSK with a directly phase-modulated VCSEL high resolution optical spectrum.

refractive index of a gain material is related with the number of electronic carriers. The electronic carriers are provided by the bias current and removed by the amplification of the light. Therefore, if the bias current is modified, the number of electronic carriers will be modified and so the refractive index. This variation of the refractive index of the RSOA gain material causes the phase change that we are looking for. The main issue associated with the variation of the bias current, and so the electronic carriers, is that they are also related with the optical gain of the RSOA. Thus, the phase modulation will cause an undesired intensity modulation. In order to avoid the intensity modulation, the RSOA has to be biased to a saturation point, i.e. to a bias current where the gain material is unable to convert all the electronic carriers in photons. Therefore, the variation of the bias current in this point will cause a variation of the electronic carriers of the gain material and so in the refractive index but not in its optical gain.

Previously to this work, several research projects have been developed studying the phase modulation of a RSOA [114, 115]. The required pump for the RSOA of these previous works is based on either remote pump using DFBs or multi-tone lasers or local pump with DFBs. In our work, we proposed to use a VCSEL as the pump for RSOA.

The RSOA selected for this modulation was a CIP SOA-RL-OEC-1550, with an optical gain of 20 dB and a saturation optical output power of 3 dBm. The selected pump VCSEL was the same used for directly phase modulation, i.e. Raycan VCSEL RC33xxx1-F, but transmitting in continuous wave mode. The transmitter setup is shown in Figure 4.10. The RSOA is pumped through a coupler in order to have a second output for the output signal. The VCSEL requires an insulator before the coupler in order to avoid the instability caused by the reflected signal. This design has been chosen instead of a circulator considering the cost and the potential integrability of the transmitter. Additionally, the VCSEL has a coupler at the output to reuse its emitted signal as LO for the receiver.

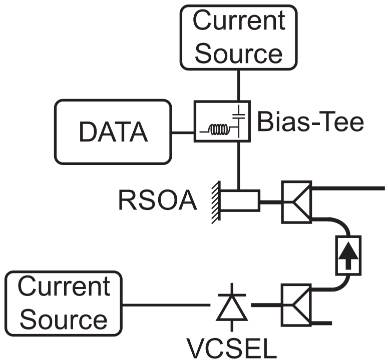

Figure 4.10: RSOA-VCSEL transmitter setup.

The optical power after the insulator is -5.5 dBm, which is high enough to saturate the RSOA after the input coupler with a bias current of 125 mA. This bias current is modulated with a NRZ pulse shaping signal. The modulation signal will cause the phase shifts required to obtain the directly phase modulation but presenting a reduced intensity modulation as it is operating in the saturation regime.

The modulation amplitude is 54 mA_{pp} and it was adjusted through the minimization of the received BER. The phase eye diagram and the IQ diagram, shown in Figure 4.11, are used to confirm the phase modulation of the RSOA pumped with a VCSEL and they also are used for a fine adjustment of the modulation amplitude. In the IQ diagram, the transition between the symbols shows that there is some residual intensity modulation, but it is small enough for a modulation of this type.

Finally, the sinc shape and suppressed carrier of the high resolution optical spectrum, shown in Figure 4.12, confirm the phase modulation of the RSOA pumped with a VCSEL. The carrier suppression is not completely due to the small residual intensity modulation.

This technique has been employed in the article of the compendium section 3.2 [2] and in the appendix section B.1 [6] and in the contributions [16, 37].

A Nyquist-DPSK signal over a MZM was also performed with AVANEX PowerBit F-10

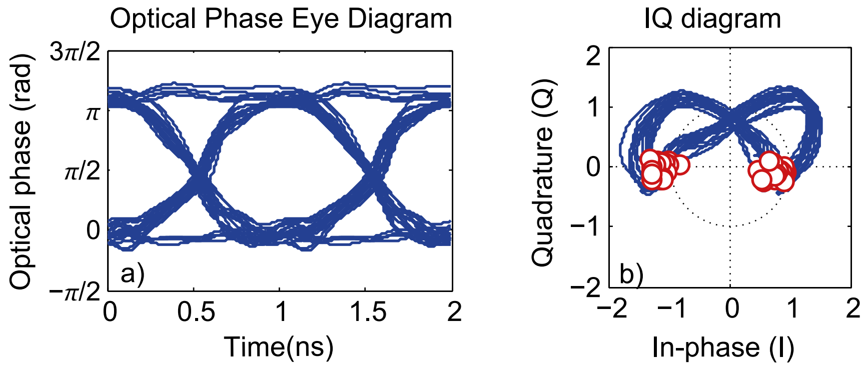

Figure 4.11: 1 Gbps DPSK with a directly phase-modulated RSOA pumped with a VCSEL. Experimental optical: (a) phase eye diagram and (b) IQ diagram.

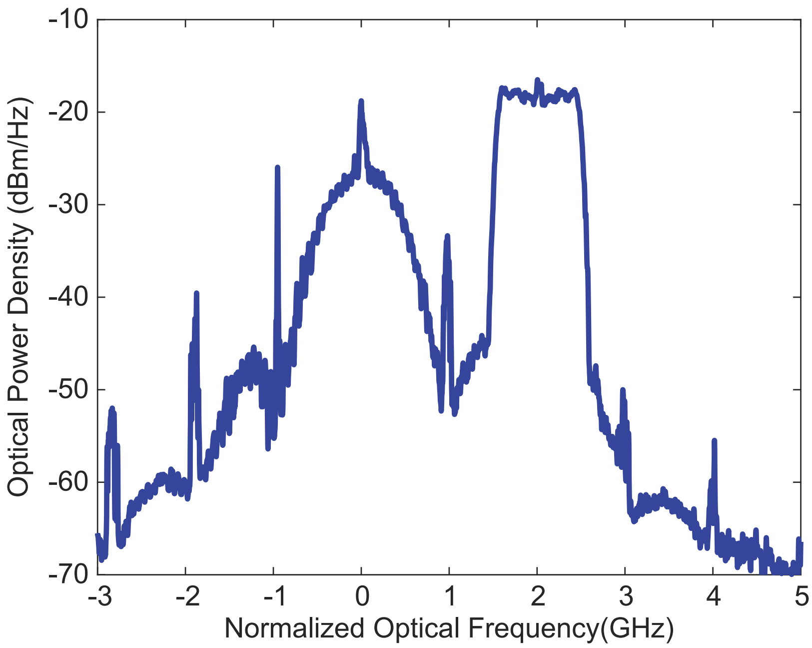

Figure 4.12: 1 Gbps DPSK with a directly phase-modulated RSOA pumped with a VCSEL high resolution optical spectrum and 1 Gbps Nyquist-DPSK over a MZM separated by 2 GHz.

MZM for comparison with the direct phase modulations presented here and to use it as a downlink signal in the uDWDM bidirectional channels. The Nyquist-DPSK over MZM optical spectrum depicted in Figure 4.12 has two main features: squared shape and suppressed carrier. The squared shape is caused by the Nyquist pulse shaper or raised cosine pulse shaper with $\beta = 0$ as it is expected. A suppressed carrier is obtained by the DPSK modulation, as it was described for the rest of the DPSK transmitters detailed in this section, which are independent of the pulse shaper.

This technique has been employed in the articles of the compendium section 3.1 [1] and section 3.2 [2], in the appendixes section B.1 [6], section B.2 [7], in the article [9] and in the contributions [6, 12–16, 34, 37].

4.2.2 Single PD heterodyne receivers for DPSK signals

Optical coherent receivers have been developed during years for the most complex and profitable optical telecommunication networks, e.g. long-haul and submarine links. In this section, a single PD heterodyne receiver for DPSK signals as a cost-effective solution for coherent access networks will be described.

The single PD heterodyne receiver is a modification of the most basic coherent receiver presented on subsection 2.2.3, which is based on an optical coupler and balanced PDs. This receiver consists of an optical coupler but using only one single PD, as can be seen on Figure 4.13.

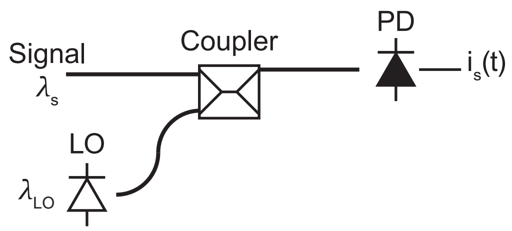

Figure 4.13: Single PD heterodyne receiver.

For a heterodyne operation, the LO wavelength has to be spaced from the optical carrier signal at least the signal bandwidth (BW). Therefore, the output signal after the PD will follow the Equation 4.2, which similar to the Equation 2.12.

$$i_s(t) = \eta \left| \vec{E} \right|^2 = \eta \left(\underbrace{\frac{1}{2}|E_{LO}|^2}_{LO\ DD} + \underbrace{\frac{1}{2}|E_S(t)|^2}_{Signal\ DD} + \underbrace{|E_S(t)|\,|E_{LO}|\sin(2\pi\Delta f t + \Delta\phi(t))}_{Signal-LO\ beating} \right) \tag{4.2}$$

The DD components, described in Equation 4.2, can interfere with the signal-LO beating and degrade the link performance. This can be avoided by employing a sufficiently high intermediate frequency ($\Delta\omega$) and a high pass filter for the signal DD. This technique is achievable because the DD signal is always in baseband, whereas the spectral position of the signal-LO beating depends on the wavelength difference between the received signal and the LO, as is described in Figure 4.14 and Equation 4.2. The main drawback of this technique is that a high electrical bandwidth PD is required, which will increase the cost of the system when high data rates are transmitted. If the frequency difference ($2\pi\Delta f$) is reduced to the theoretical bandwidth limit ($2\pi\Delta f = BW$), the signal-LO beating and the DD signal will overlap giving rise to a degradation of the link. In this case, some techniques as the Kramers-Kronig (KK) receiver [145,146] or the signal-signal beating interference (SSBI) cancellation [146,147] should be implemented after the signal digitalization.

In this work, the KK receiver and the SSBI cancellation have been discarded because of their high computational cost. The fist alternative, i.e. sufficient bandwidth of the with a high pass filter is feasible because low-data rate signals will be employed in a uDWDM access network environment.

Therefore, after the PD, the signal $i_s(t)$ has to be band pass filtered, in order to remove the DD terms and reduce the received noise. The filtered signal $i_{BPF}(t)$ is described on Equation 4.3.

$$i_{BPF}(t) = \underbrace{BPF\{i_s(t)\}}_{Band\ Pass\ Filter} = \eta\,|E_S(t)|\,|E_{LO}|\sin(2\pi\Delta ft + \Delta\phi(t)) \tag{4.3}$$

After the band pass filter (BPF) and, as part of the demodulation of the DPSK signal, the current received symbol is multiplied by the previous one, as it is described on Equation 4.4.

$$\begin{aligned} i_*(t) &= i_{BPF}(t) * i_{BPF}(t - T_s) = \\ &= \eta^2\,|E_S(t)|\,|E_{LO}|\sin(2\pi\Delta ft + \Delta\phi(t)) * \\ &* |E_S(t - T_s)|\,|E_{LO}|\sin(2\pi\Delta f\,(t - T_s) + \Delta\phi(t - T_s)) \end{aligned} \tag{4.4}$$

Assuming that the $|E_S(t)| = |E_S(t - T_s)|$ because the amplitude of phase signal is independent of the symbol, it can be rewritten as:

$$\begin{aligned} i_*(t) = \eta^2 \frac{|E_S(t)|^2\,|E_{LO}|^2}{2} &[\cos(2\pi\Delta fT_s + \Delta\phi(t) - \Delta\phi(t - T_s)) + \\ &+ \cos(2\pi 2\Delta ft - 2\pi 2\Delta fT_s + \Delta\phi(t - T_s) + \Delta\phi(t) - \Delta\phi(t - T_s))] \end{aligned} \tag{4.5}$$

Finally, the multiplied signal $i_*(t)$ is low pass filtered in order to remove the second harmonic and the obtained signal is described as follows:

$$i_{LPF}(t) = \underbrace{LPF\{i_*(t)\}}_{Low\ Pass\ Filter} = \eta^2 \frac{|E_S(t)|^2\,|E_{LO}|^2}{2} \cos(2\pi\Delta fT_s + \Delta\phi(t) - \Delta\phi(t - T_s)) \tag{4.6}$$

The $i_{LPF}(t)$ can be reordered as Equation 4.7.

$$\begin{aligned} i_{LPF}(t) = \eta^2 \frac{|E_S(t)|^2\,|E_{LO}|^2}{2} &[\cos(2\pi\Delta fT_s) * \cos(\Delta\phi(t) - \Delta\phi(t - T_s)) - \\ &- \sin(2\pi\Delta fT_s) * \sin(\Delta\phi(t) - \Delta\phi(t - T_s))] \end{aligned} \tag{4.7}$$

Equation 4.7 shows that $\Delta f T_s = n, n \in \mathbb{Z}$ is needed in order to maximize an output proportional to the phase difference between symbols as we can seen in Equation 4.8.

$$i_o(t) = \eta^2 \frac{|E_S(t)|^2 |E_{LO}|^2}{2} \cos(\Delta\phi(t) - \Delta\phi(t - T_s)) \tag{4.8}$$

The demodulation procedure described with the Equation 4.3 is depicted in Figure 4.14.

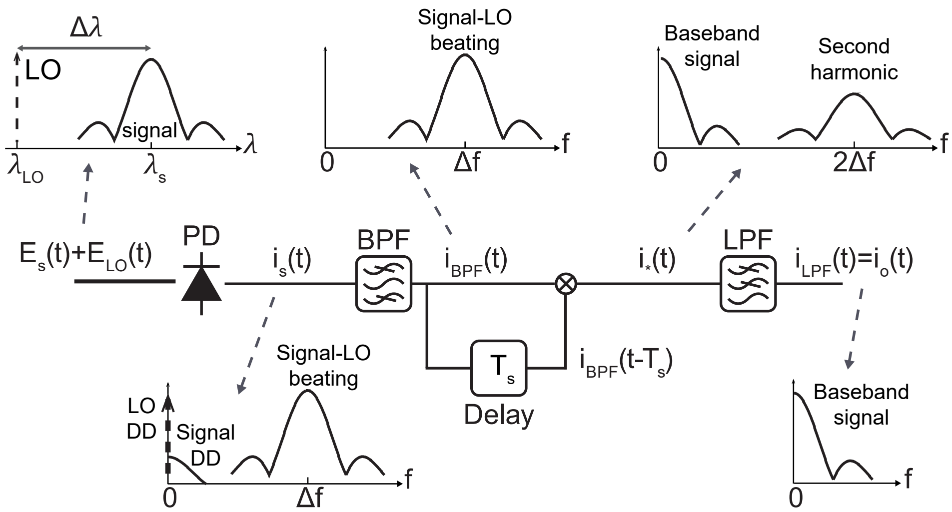

Figure 4.14: DPSK demodulation diagram with a single PD heterodyne receiver and the electrical spectra at the different demodulation stages.

The filter design of the DPSK receiver, shown in Figure 4.14, is important for maximizing the sensitivity of the receiver. The cut-off frequencies of the the bandpass and lowpass filters are optimized analysing the BER variation for a determined received power. In [1], this technique was employed to optimize the receiver sensitivity doing a deep analysis of the filter BW requirements for 1 Gbps DPSK in a bidirectional link. This work will be commented on section 4.3.

One of the main problems of this receiver, as it is for all the coherent receivers, is the polarization dependency, but in this case it can be solved using the technique presented in [134]. The single PD heterodyne receiver has to be modified as is shown in Figure 4.15.

This polarization independent DPSK heterodyne receiver introduces a PBS after the coupler and a second PD after the PBS. The LO has to be aligned at 45 degrees respecting to the PBS axis in order to split the LO power equally between the two PDs. The input optical fields of both PDs are described by Equations 4.9 and 4.10.

$$\vec{E}_x(t) = \frac{1}{\sqrt{2}} \left[\frac{1}{\sqrt{2}} j \, |E_{LO}| \, e^{j(\omega_{LO} t + \phi_{LO}(t) + \delta_{LO})} + \cos(\theta) \, |E_S(t)| \, e^{j(\omega_S t + \phi_S(t) + \delta_S)} \right] \tag{4.9}$$

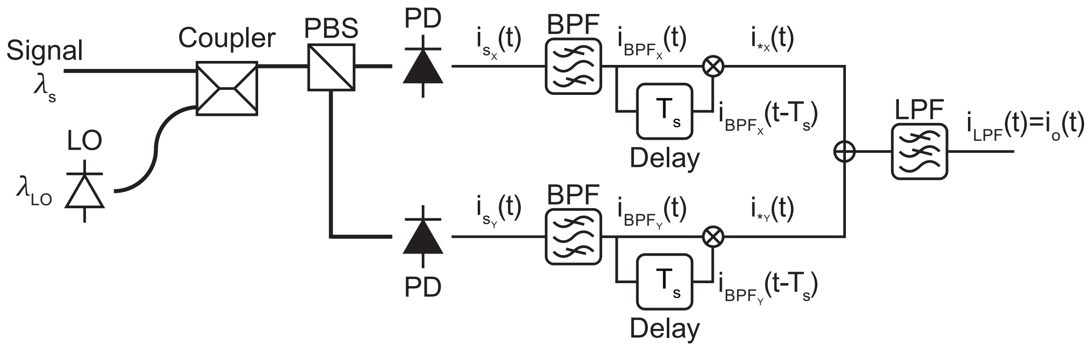

Figure 4.15: Polarization independent DPSK heterodyne receiver.

$$\vec{E}_y(t) = \frac{1}{\sqrt{2}} \left[\frac{1}{\sqrt{2}} j \left| E_{LO} \right| e^{j(\omega_{LO} t + \phi_{LO}(t))} + \sin(\theta) \left| E_S(t) \right| e^{j(\omega_S t + \phi_S(t))} \right] \tag{4.10}$$

where θ is the alignment angle of signal polarization in comparison with the PBS axis, δ_{LO} is the phase difference between the polarization components of the LO in the axes X and Y and δ_S is the phase difference between the polarization axes of the signal. These optical fields are received with the PDs and the generated photocurrents are described by Equations 4.11 and 4.12.

$$i_{s_x}(t) = \eta_x \left| \vec{E}_x \right|^2 = \eta_x \Bigg(\underbrace{\frac{1}{4} |E_{LO}|^2}_{LO\ DD} + \underbrace{\frac{1}{2} \cos^2(\theta) |E_S(t)|^2}_{Signal\ DD} + \\ + \underbrace{\frac{\cos(\theta)}{\sqrt{2}} \left| E_S(t) \right| \left| E_{LO} \right| \sin(2\pi \Delta f t + \Delta\phi(t) + \Delta\delta)}_{Signal-LO\ beating} \Bigg) \tag{4.11}$$

$$i_{s_y}(t) = \eta_y \left| \vec{E}_y \right|^2 = \eta_y \Bigg(\underbrace{\frac{1}{4} |E_{LO}|^2}_{LO\ DD} + \underbrace{\frac{1}{2} \sin^2(\theta) |E_S(t)|^2}_{Signal\ DD} + \\ + \underbrace{\frac{\sin(\theta)}{\sqrt{2}} \left| E_S(t) \right| \left| E_{LO} \right| \sin(2\pi \Delta f t + \Delta\phi(t))}_{Signal-LO\ beating} \Bigg) \tag{4.12}$$

where η_x and η_y are the responsivity of each PD, and in the following I will consider them equal, $\eta_x = \eta_y = \eta$. These both photocurrents are band pass filtered and they will be described as:

$$i_{BPF_x}(t) = BPF\left\{i_{s_x}(t)\right\} = \eta\frac{\cos(\theta)}{\sqrt{2}}\left|E_S(t)\right|\left|E_{LO}\right|\sin(2\pi\Delta f t + \Delta\phi(t) + \Delta\delta) \tag{4.13}$$

$$i_{BPF_y}(t) = BPF\left\{i_{s_y}(t)\right\} = \eta\frac{\sin(\theta)}{\sqrt{2}}\left|E_S(t)\right|\left|E_{LO}\right|\sin(2\pi\Delta f t + \Delta\phi(t)) \tag{4.14}$$

As in the single PD heterodyne receiver version, the current received symbol is multiplied by the previous one in each signal independently as is described by Equations 4.15 and 4.16, where we also assume that $|E_S(t)| = |E_S(t - T_s)|$.

$$\begin{aligned} i_{*_x}(t) &= i_{BPF_x}(t) * i_{BPF_x}(t - T_s) = \\ &= \eta^2\frac{\cos^2(\theta)}{2}\left|E_S(t)\right|^2\left|E_{LO}\right|^2\sin(2\pi\Delta f t + \Delta\phi(t) + \Delta\delta) * \\ &* \sin(2\pi\Delta f\,(t - T_s) + \Delta\phi(t - T_s) + \Delta\delta) \end{aligned} \tag{4.15}$$

$$\begin{aligned} i_{*_y}(t) &= i_{BPF_y}(t) * i_{BPF_y}(t - T_s) = \\ &= \eta^2\frac{\sin^2(\theta)}{2}\left|E_S(t)\right|^2\left|E_{LO}\right|^2\sin(2\pi\Delta f t + \Delta\phi(t)) * \\ &* \sin(2\pi\Delta f\,(t - T_s) + \Delta\phi(t - T_s)) \end{aligned} \tag{4.16}$$

Now, both signals are added and then low pass filtered:

$$\begin{aligned} i_{LPF}(t) &= LPF\left\{i_{*_x}(t) + i_{*_y}(t)\right\} = \eta^2\frac{\left|E_S(t)\right|^2\left|E_{LO}\right|^2}{4} * \\ &* \underbrace{\left[\cos^2(\theta) + \sin^2(\theta)\right]}_{=1}\cos(2\pi\Delta f T_s + \Delta\phi(t) - \Delta\phi(t - T_s)) \end{aligned} \tag{4.17}$$

As in the single PD heterodyne receiver version, $\Delta f T_s = n, n \in \mathbb{Z}$ is needed and therefore, the same output signal is obtained, which is proportional to the phase difference between symbols, as can be seen in Equation 4.18.

$$i_o(t) = \eta^2\frac{\left|E_S(t)\right|^2\left|E_{LO}\right|^2}{4}\cos(\Delta\phi(t) - \Delta\phi(t - T_s)) \tag{4.18}$$

This technique has been employed in the articles of the compendium section 3.1 [1], section 3.2 [2] and section 3.3 [3] and in the appendixes section B.1 [6], section B.2 [7], in the article [9] and in the contributions [15, 16, 30, 36, 37].

4.2.3 Quasi-coherent receiver

The receiver presented in the previous subsection is based on a single PD heterodyne receiver for DPSK signals. A similar approach of receiver can be employed for IM signals. In this subsection, the heterodyne receiver for IM signals will be analysed in its polarization independent version. In the following, it will be named as quasi-coherent receiver, denoting that the setup is a coherent-line one but the signals are modulated just in intensity, not in phase.

The optical components of the quasi-coherent receiver are the same than for the receiver presented in the previous subsection, as can be seen in Figure 4.16. Therefore, the photocurrents generated by the PDs are the same than in the previous section, i.e. Equation 4.11 and Equation 4.12. From these equations, it can be extracted that DD components can interfere with the signal-LO beating. In order to avoid a degradation of the performance of the quasi-coherent receiver, the band pass filters have to be placed after the PDs. They will remove the DD components without removing the signal-LO beating component, as long as the intermediate frequency ($\Delta\omega$) is high enough. After the band pass filters, the signals also follow the Equations 4.13 and 4.14 of the receiver studied in the previous subsection.

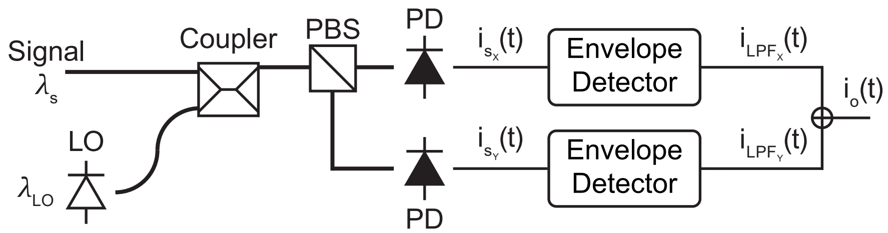

Figure 4.16: Polarization independent quasi-coherent receiver.

Then, the signal-LO beating component will be downconverted using the envelope detector. The theoretical envelope detector, which is usually employed in digital signal processing, consists of a square function and a low pass filter, as can be seen in Figure 4.17.a. After the squaring, the different polarization signals follow the Equations 4.19 and 4.20.

$$\begin{aligned} i_{square_x}(t) &= {i_{BPF_x}}^2(t) = \\ &= \eta^2 \frac{\cos^2(\theta)}{2} \left|E_S(t)\right|^2 \left|E_{LO}\right|^2 \sin^2(2\pi\Delta f t + \Delta\phi(t) + \Delta\delta) = \\ &= \eta^2 \frac{\cos^2(\theta)}{2} \left|E_S(t)\right|^2 \left|E_{LO}\right|^2 \left[\frac{1}{2} - \frac{\cos(2(2\pi\Delta f t + \Delta\phi(t) + \Delta\delta))}{2}\right] \end{aligned} \tag{4.19}$$

$$
\begin{aligned}
i_{square_y}(t) &= {i_{BPF_y}}^2(t) = \\
&= \eta^2 \frac{\sin^2(\theta)}{2} |E_S(t)|^2 |E_{LO}|^2 \sin^2(2\pi\Delta f t + \Delta\phi(t)) = \\
&= \eta^2 \frac{\sin^2(\theta)}{2} |E_S(t)|^2 |E_{LO}|^2 \left[\frac{1}{2} - \frac{\cos(2(2\pi\Delta f t + \Delta\phi(t)))}{2}\right]
\end{aligned} \tag{4.20}
$$

The square function downconverts the signal to baseband but also generates a second component at the double carrier frequency. The low pass filter will remove the second harmonic and the downcoversion will be totally performed. These low pass filtered signals are described as:

$$
i_{LPF_x}(t) = LPF\left\{i_{square_x}(t)\right\} = \eta^2 \frac{\cos^2(\theta)}{4} |E_S(t)|^2 |E_{LO}|^2 \tag{4.21}
$$

$$
i_{LPF_y}(t) = LPF\left\{i_{square_y}(t)\right\} = \eta^2 \frac{\sin^2(\theta)}{4} |E_S(t)|^2 |E_{LO}|^2 \tag{4.22}
$$

Finally, both low pass filtered signals are added and the transmitted signal is recovered as:

$$
\begin{aligned}
i_o(t) = i_{LPF_x}(t) + i_{LPF_y}(t) &= \eta^2 \frac{|E_S(t)|^2 |E_{LO}|^2}{4} \underbrace{\left[\cos^2(\theta) + \sin^2(\theta)\right]}_{=1} = \\
&= \eta^2 \frac{|E_S(t)|^2 |E_{LO}|^2}{4}
\end{aligned} \tag{4.23}
$$

In order to provide a real-time operation to the quasi-coherent receiver, an analog envelope detector was developed. This analog envelope detector consists of Schottky diodes and a low-pass filter, as can be seen in Figure 4.17.b.

The Schottky diode rectifies the signals produced by the PDs at an intermediate frequency (IF), which are defined by Equations 4.19 and 4.20. The rectification is a non-linear process that generates the baseband and high order components in similar way than the square function. After the rectification using Schottky diodes, high order components are filtered with the low pass filter.

Both signals must be added after the low pass filters to ensure the polarization independent operation of the quasi-coherent receiver. In order to simplify the real-time operation, one of the Schottky diodes envelope detector is designed to obtain an inverted signal, so the addition can be done by employing a differential amplifier.

After the addition, an equalizer can be applied as in [5], specifically a feed forward equalizer (FFE)/decision feedback equalizer (DFE) was applied.

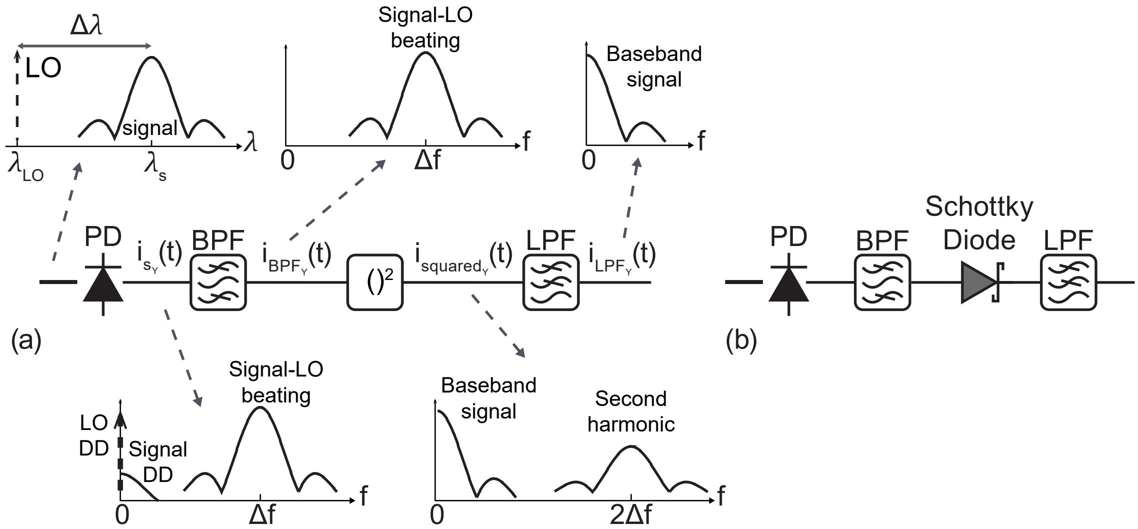

Figure 4.17: Theoretical envelope detector (a), analog implementation of envelope detector (b). Electrical spectra at the different demodulation stages for (a).

The FFE/DFE equalizer consists in two equalization parts, as is shown in Figure 4.18. The first part (FFE) is a linear filter, which is fed by the input signal and removes the precursor ISI [148]. The second part (DFE) uses the decided symbols to feed a second linear filter and remove the postcursor ISI that the FFE cannot remove [148].

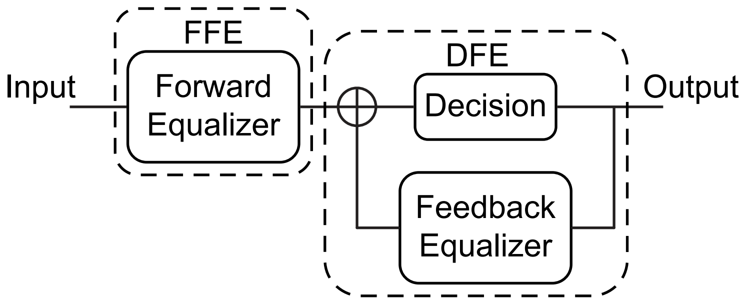

Figure 4.18: FFE/DFE equalizer schematic.

This technique has been employed in the articles of the compendium section 3.4 [4] and section 3.5 [5], in the article [11] and in the contributions [22, 27, 30, 32, 39].

4.3 Main contributions

The main results of this thesis can be divided into two principal lines of research: phase modulated uDWDM access networks, including bidirectional links, and intensity modulated optical access networks for NG-PON2 and beyond.

4.3.1 Phase modulated uDWDM access networks

In this subsection, I will present the main results obtained using the techniques presented in the subsection 4.2.1 and subsection 4.2.2 and publish in the section 3.1 [1], section 3.2 [2], section 3.3 [3], section B.1 [6], section B.2 [7], in the article [9], and the conference contributions [12–16, 30, 34, 36, 37].

First, I will present the results for the different links regardless the link configuration that will be lately employed. Therefore, I will present different types of links based on different directly-phase modulated transmitters with single PD heterodyne receivers.

The first link consists of a directly-phase modulated DFB as the transmitter and a single PD heterodyne receiver. This link has a data rate of 1 Gbps using a NRZ-DPSK codification.

The bandwidth of the digital filters of the receiver was extensively studied for two different LO frequency positions and so two different intermediate frequencies (IF) after the PD, with results shown in Figure 4.19. The LO frequency positions are placed 1 GHz and 2 GHz respecting to the signal carrier.

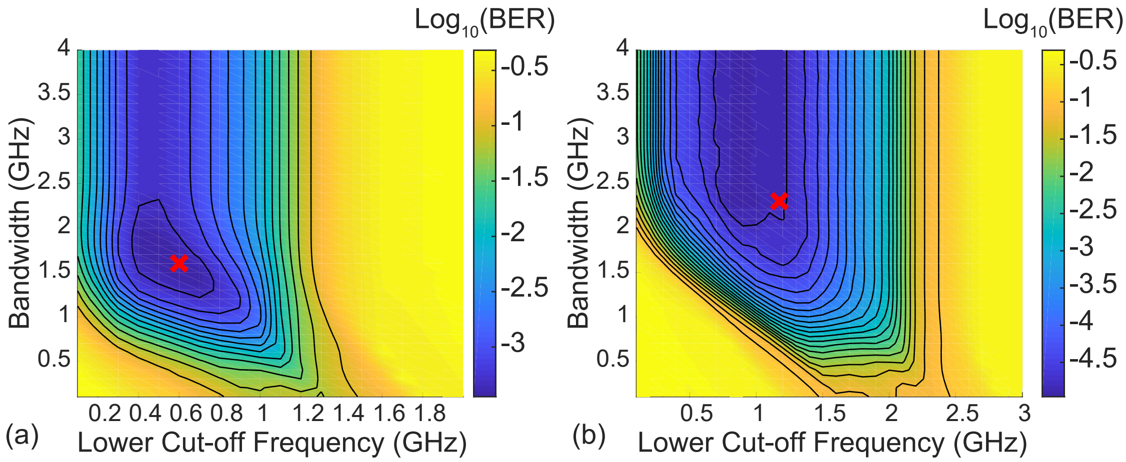

Figure 4.19: Bandwidth and lower cut-off frequency optimization of digital BPF for IF = 1 GHz (a) and IF = 2 GHz (b).

Figure 4.19 allows to obtain the lower cut-off frequency and the bandwidth of the BPF. The lower cut-off frequency is 0.6 GHz for an IF of 1 GHZ and 1.2 GHz for an IF of 2 GHZ. The bandwidth is 1.6 GHz for an IF of 1 GHz and 2.3 GHz for an IF of 2 GHZ. The best BER results were obtained with a LPF bandwidth equal to 1.25 GHz.

Using these parameters, the BER vs. received power curves are shown in Figure 4.20 for optical back-to-back (BTB) and for a transmission over a 50 km of standard single mode fiber (SSMF).

The sensitivity is -51 dBm with a IF of 1 GHz and -52 dBm with a IF of 2 GHz. The penalty due to 50 km SSMF transmission is approximately 1 dB for both IF. This sensitivity, the transmitted power and the transmission penalty leads to a remarkable power budget of 51 dB for IF = 2 GHz. This power budget will allow to have a splitting ratio of 1024 after 50 km of SSMF transmission, assuming 0.25 dB/km as the fiber attenuation and $3.5\log_2(N)$ dB for the splitting ratio (N).

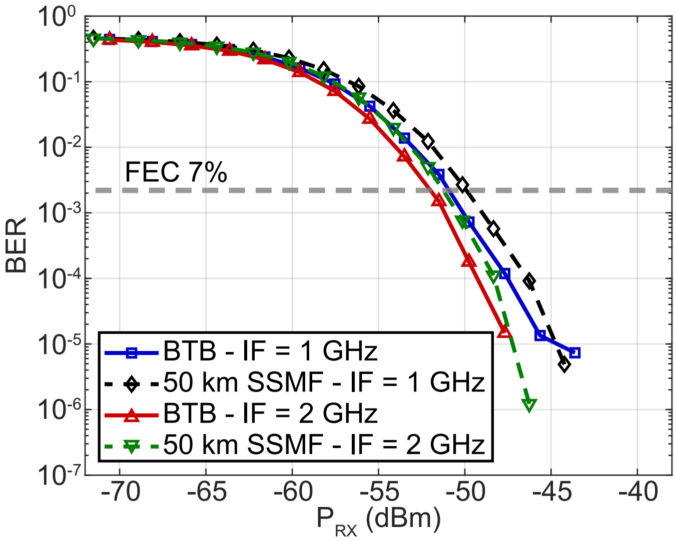

Figure 4.20: Sensitivity for 1 Gbps link based on directly-phase modulated DFB and a single PD heterodyne receiver for an IF of 1 GHz and 2 GHz.

The second link consists of a directly-phase modulated RSOA pumped with a VCSEL as transmitter and a single PD heterodyne receiver. This link was presented on section 3.2 [2]. This is link also has a data rate of 1 Gbps.

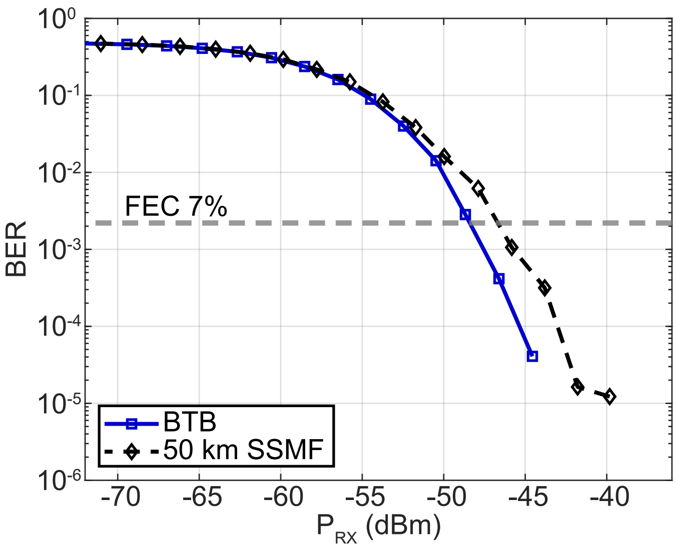

Figure 4.21: Sensitivity for 1 Gbps link based on directly-phase modulated RSOA pumped with a VCSEL and a single PD heterodyne receiver.

The BER vs. received power curves for optical BTB and for 50 km SSMF transmission is shown in Figure 4.21.

The BTB sensitivity is -48 dBm and it exhibits a 50 km SSMF transmission penalty of 2 dB. Therefore, this link exhibits a power budget of 46 dB. This power budget will allow to transmit through 50 km of SSMF with an splitting ratio of 512, assuming 0.25 dB/km as the fiber attenuation and $3.5 \log_2(N)$ dB for the splitting ratio (N).

The last link consists of directly-phase modulated VCSEL as transmitter and a single PD heterodyne receiver. This link was presented for a data rate of 2.5 Gbps on section 3.3 [3] and for a data rate of 1.25 and 2.5 Gbps on section B.2 [7].

The VCSEL transmitted power is -1 dBm. The LO is an external cavity laser (ECL) with emitted power of 0 dBm. The LO frequency position is 2.5 GHz for 1.25 Gbps data rate and 5 GHz for 2.5 Gbps, i.e. the double of the data rate. The BPF and LPF are obtained following a similar analysis than in the results obtained in [1]. The LPF has a bandwidth of 1.5 GHz for 1.25 Gbps and 4 GHz for 2.5 Gbps. The BPF has a lower cut-off frequency of 1.5 GHz for 1.25 Gbps and 3.7 GHz for 2.5 Gbps and bandwidth of 2 GHz for 1.25 Gbps and 4 GHz for 2.5 Gbps.

Figure 4.22 shows the BER vs. received power for the optical BTB of the directly-phase modulated link for both data rates.

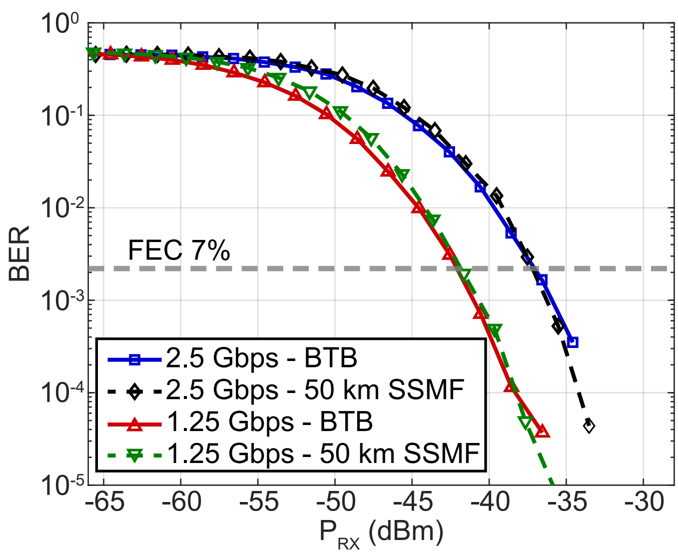

Figure 4.22: Sensitivity for 1.25 Gbps - 2.5 Gbps link based on directly-phase modulated VCSEL and a single PD heterodyne receiver.

The sensitivity of the link is -42.5 dBm for 1.25 Gbps and -39.5 dBm for 2.5 Gbps. The transmission penalty due to transmission through 50 km SSMF is below 0.1 dB for both data rates. The power budget will be -41.5 dB for 1.25 Gbps and -38.5 dB for 2.5 Gbps. Therefore, the splitting ratio after 50 km SSMF can be 256 for 1.25 Gbps and 128 for 2.5 Gbps.

In Table 4.1, the data rate, transmitted power, sensitivity, transmission penalty, power budget and splitting ratio of the different links with directly phase modulated transmitters (DFB, RSOA+VCSEL and VCSEL) and single PD heterodyne receivers are summarized.

Table 4.1: Summary of the links with different directly-phase modulated transmitters and single PD heterodyne receivers.

	DFB section 3.1 [1, 15]	RSOA+VCSEL section 3.2 [2]	VCSEL section B.2 [7]	VCSEL section 3.3 [3] section B.2 [7]
Data Rate	1 Gbps	1 Gbps	1.25 Gbps	2.5 Gbps
TX Power	0 dBm	0 dBm	-1 dBm	-1 dBm
LO Power	+4.2 dBm	0 dBm	0 dBm	0 dBm
Sensitivity	-52 dBm	-48 dBm	-42.5 dBm	-39.5 dBm
Transmission Penalty	1 dB	2 dB	0.1 dB	0.1 dB
Power Budget	51 dB	46 dB	41.5 dB	38.5 dB
Splitting ratio	1024	512	256	128

It was also studied links where the transmitter was formed by a laser and a MZM, which is modulated with a Nyquist pulse shaped DPSK, and a single PD heterodyne receiver with different types of LO. Using this transmitter, it was been able to obtain the results shown in Table 4.2, which in general are better than those made using the directly phase modulated sources. The use of Nyquist pulse shaped DPSK signals made that the spectra of the signals were narrow enough to be used in uDWDM applications.

Table 4.2: Summary of the links with Nyquist-DPSK over a MZM with single PD heterodyne receivers with different LOs.

	DFB section 3.1 [1, 15]	VCSEL section 3.2 [2]	VCSEL section B.2 [7]	VCSEL section B.2 [7]
Data Rate	1 Gbps	1 Gbps	1.25 Gbps	2.5 Gbps
TX Power	0 dBm	0 dBm	-1 dBm	-1 dBm
LO Power	+4.2 dBm	-5.5 dBm	-0.14 dBm	-0.14 dBm
Sensitivity	-52 dBm	-49 dBm	-4 dBm	-3 dBm
Transmission Penalty	0.5 dB	1.5 dB	0.1 dB	0.1 dB
Power Budget	51.5 dB	42 dB	47.76 dB	43.26 dB
Splitting ratio	2048	256	1024	256

Therefore, using the transmitter and receivers commented before, two combinations were implemented to obtain bidirectional channels in narrow frequency slots. The first bidirectional channel consists of a 1Gbps uplink based on directly phase modulated DFB with single PD heterodyne receiver with a ECL as LO and a 1 Gbps downlink based on Nyquist-DPSK over MZM with a single PD heterodyne receiver with a DFB as LO. This bidrectional link was presented on section 3.1 [1] and on [15] and the experimental setup is presented on Figure 4.23.

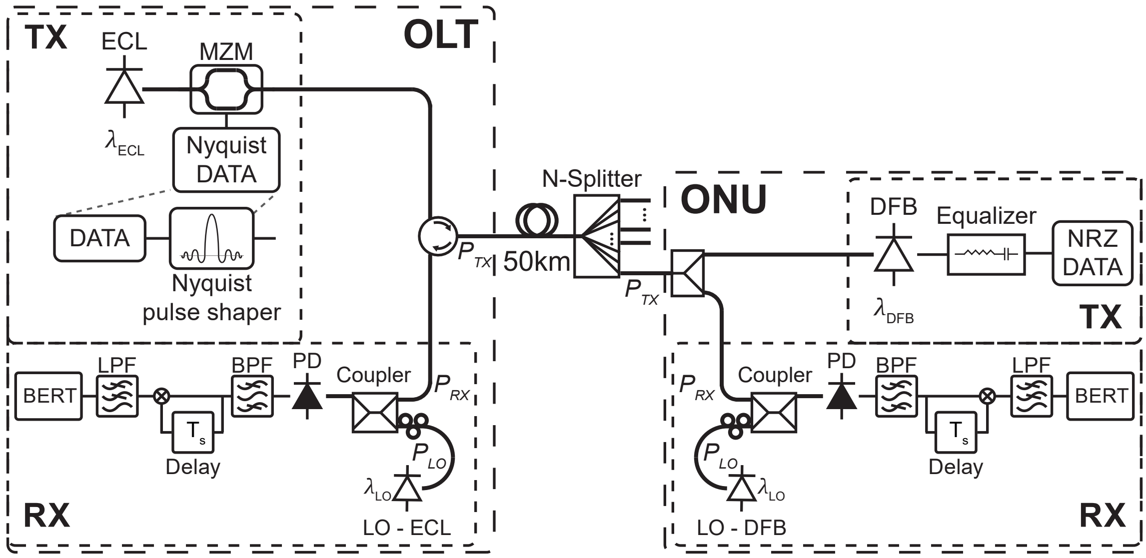

Figure 4.23: Experimental setup for bidirectional link based on 1 Gbps uplink based on directly-phase modulated DFB and a single PD heterodyne receiver with ECL as LO and a 1 Gbps downlink based on Nyquist-DPSK over MZM with a single PD heterodyne receiver with a DFB as LO.

The LO frequency position will be 1 GHz away from the signal carrier because it ensures a possible link distribution in a narrow frequency slot with a determined transmitted power, as was analyzed on section 3.1. The transmitted power will determine the power penalty of the opposite link due to Rayleigh backscattering interference. This was shown in section 3.1 and it will be show in Figure 4.24.

Therefore, the transmitted power that ensures no-penalty due to bidirectional transmission for both uplink and downlink is -6 dBm. This value corresponds to the transmitted power after the circulator in the downlink and after the power splitter in the uplink. The frequency position of the both links and the LOs is shown in Figure 4.25.

The links and LOs frequency positions to ensure no-penalty due to bidirectional transmission allow to design a frequency slot of 6.25 GHz where 1 Gbps will be transmitted to each direction. As there is no-penalty due to bidirectional transmission, the sensitivities will be equivalent to the unidirectional links. Therefore, the sensitivity of the uplink will be -51 dBm and the sensitivity of the downlink will be -52 dBm. The 50 km SSMF transmission penalty is still 0.5 dB for the downlink and 1 dB for the uplink.

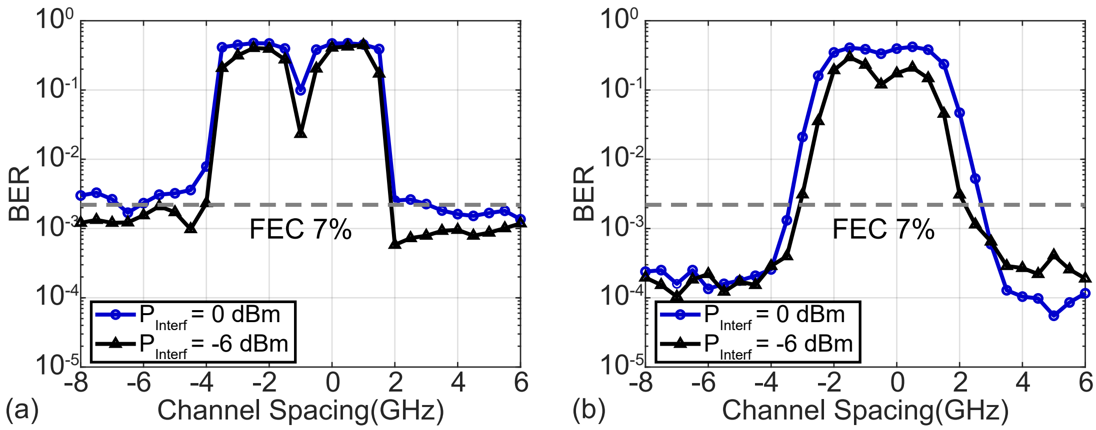

Figure 4.24: BER penalty for bidirectional transmission for the uplink (a) and downlink (b) with directly-phase modulated DFB uplink and Nyquist-DPSK over MZM downlink.

These sensitivities, transmission penalties and transmission powers lead to a power budget of 42 dB for the downlink and 42.5 dB for the uplink. As the downlink is more limiting, 42 dB will be the combined power budget of the frequency slot. This power budget will allow a splitting ratio of 256, assuming a fiber attenuation of 0.25 dB/km and a splitter losses of $3.5\log_2(N)$ dB.

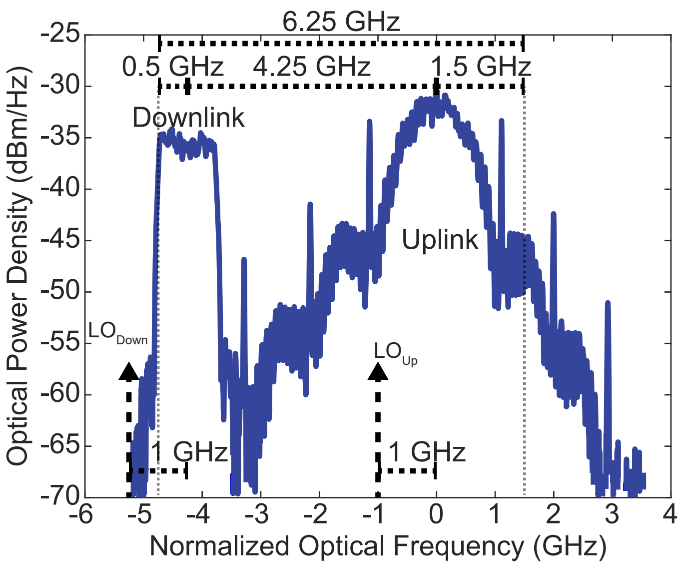

Figure 4.25: Spectra of both links and the LO positions for the bidirectional link based on directly-phase modulated DFB uplink and Nyquist-DPSK over MZM downlink.

The second bidirectional channel consists of a 1Gbps uplink based on directly phase modulated RSOA pumped by a VCSEL with single PD heterodyne receiver with a ECL as LO and a 1 Gbps downlink based on Nyquist-DPSK over MZM with a single PD heterodyne receiver with a VCSEL as LO. This bidirectional link was presented on section 3.2 [2] and in section B.1 [6] and the experimental setup is presented on Figure 4.26.

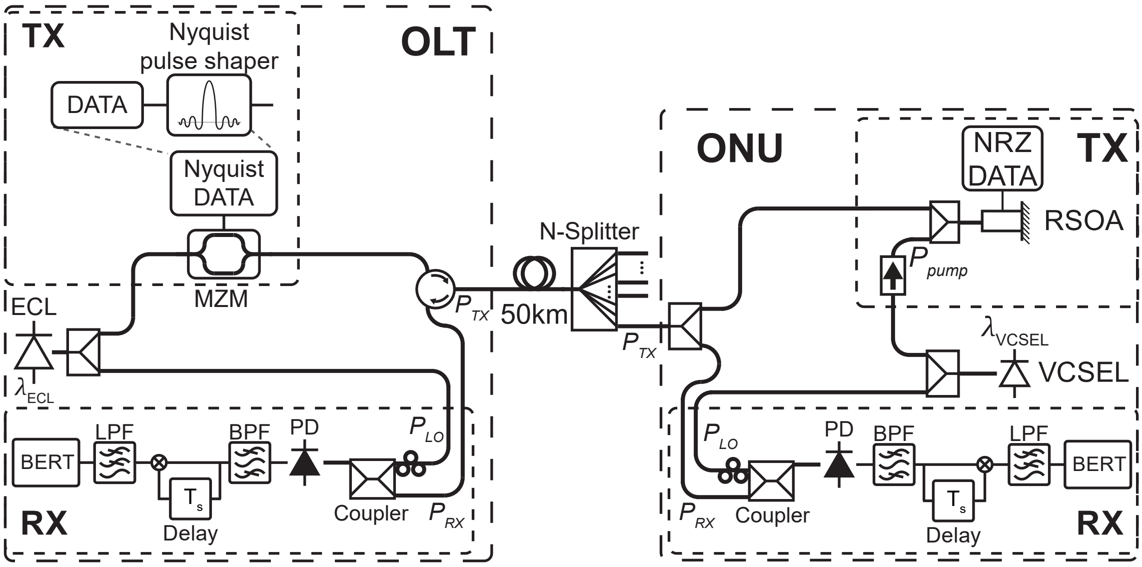

Figure 4.26: Experimental setup for bidirectional link based on 1 Gbps uplink based on directly-phase modulated RSOA pumped by a VCSEL and a single PD heterodyne receiver with ECL as LO and a 1 Gbps downlink based on Nyquist-DPSK over MZM with a single PD heterodyne receiver with a VCSEL as LO.

In this link, the distance between the channels is fixed to 2 GHz because the same VCSEL is used to pump the RSOA for generating the uplink signal and as LO for receiving the downlink signal. The position of the next adjancent channels and the LO for the uplink was done analyzing the BER degradation due to the Rayleigh backscattering, as can be seen in Figure 4.27. The transmitted powers for this analysis are -3 dBm for both links, considering the transmitted power after the circulator in the downlink and after the power splitter in the uplink.

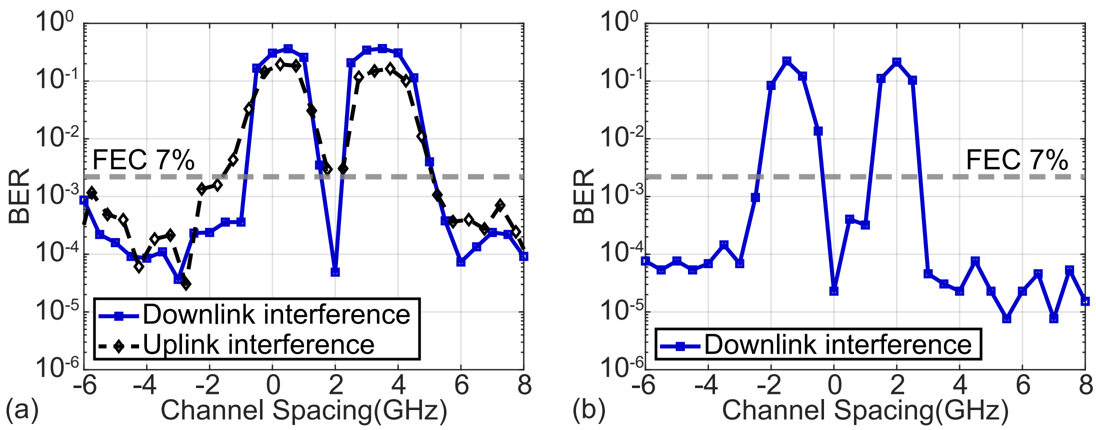

Figure 4.27: BER penalty for bidirectional transmission for the uplink (a) and downlink (b) with directly-phase modulated RSOA pumped with a VCSEL uplink and Nyquist-DPSK over MZM downlink.

The interference analysis will lead to a frequency slot of 5 GHz. The sensitivity is -49 dBm for the downlink and -48 dBm for the uplink, as they were shown in the unidirectional links. The 50 km SSMF transmission penalty is 1.5 dB for the downlink and 2 dB for the uplink. However, the bidirectional transmission introduces an additional penalty due to the fixed distance between the two links. This bidirectional penalty is 4 dB for the downlink and 1 dB for the uplink. This can be seen in Figure 4.28.

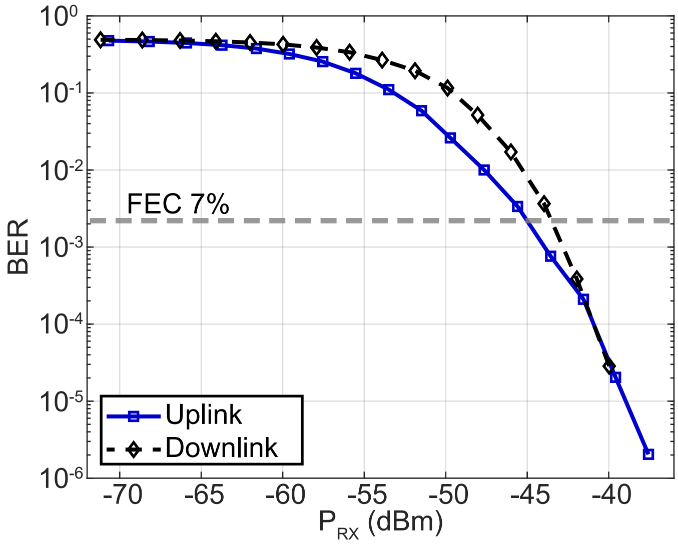

Figure 4.28: Sensitivity for bidirectional link based on 1 Gbps uplink based on directly-phase modulated RSOA pumped by a VCSEL and a single PD heterodyne receiver with ECL as LO and a 1 Gbps downlink based on Nyquist-DPSK over MZM with a single PD heterodyne receiver with a VCSEL as LO.

Therefore, the power budgets will be 37 dB for the downlink and 40.5 dB for the uplink, including the losses of the circulator (1.5 dB) in the uplink and the power splitter (3.5 dB) in the downlink. The limiting power budget of the frequency slot is the downlink power budget, so 37 dB will be the power budget of this frequency slot. This power budget leads to a splitting ratio of 128, considering a fiber attenuation of 0.25 dB/km and a splitter losses of $3.5\log_2(N)$ dB.

In Table 4.3, the frequency slot, data rate, transmitted power, sensitivity, transmission penalty, bidirectional penalty, power budget and splitting ratio of the bidirectional link are summarized.

Table 4.3: Summary of the bidirectional links.

	DFB section 3.1 [1,15]		RSOA+VCSEL section 3.2 [2], section B.1 [6]	
	uplink	downlink	uplink	downlink
Frequency Slot	6.25 GHz		5 GHz	
Data Rate	1 Gbps	1 Gbps	1 Gbps	1 Gbps
TX Power	-6 dBm	-6 dBm	-3 dBm	-3 dBm
Sensitivity	-51 dBm	-52 dBm	-48 dBm	-49 dBm
Transmission Penalty	1 dB	0.5 dB	2 dB	1.5 dB
Bidirectional Penalty	1.5 dB (circulator)	3.5 dB (splitter)	1 dB + 1.5 dB (circulator)	4 dB + 3.5 dB(splitter)
Power Budget	42 dB		37 dB	
Splitting ratio	256		128	

4.3.2 Intensity modulated optical access networks for NG-PON2 and beyond

This subsection shows the main results obtained using the technique presented in the subsection 4.2.3 and publish in the section 3.4 [4], section 3.5 [5], in the article [11] and in the contributions [22,27,30,32,39].

The main contribution of this part has been the characterization of the polarization independent quasicoherent receiver for data rates of 10 Gbps and 25 Gbps. First, the 10 Gbps quasicoherent receiver with real-time operation using an analog envelope detector will be presented. Second, the 25 Gbps quasicoherent receiver, which uses an equalizer after the envelope detector and so its real-time operation has not been yet tested, will be presented.

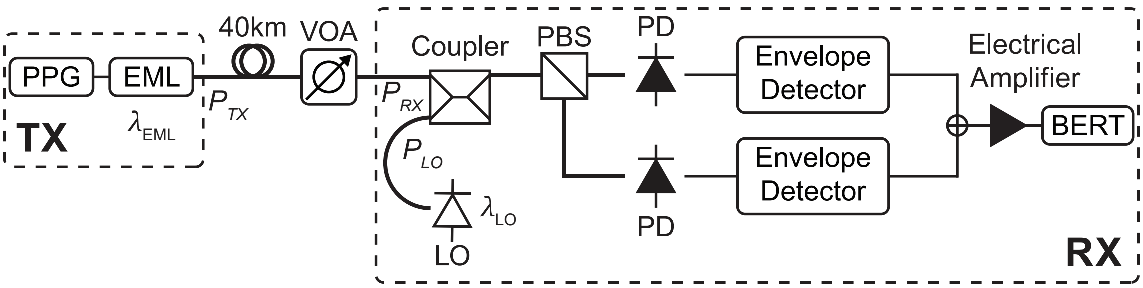

Figure 4.29: Experimental setup for 10 Gbps quasicoherent receiver .

The 10 Gbps quasicoherent receiver was presented on section 3.4 [4] and in [22], and it is shown in Figure 4.29 with the experimental setup used for testing the receiver. The transmitted signal is a NRZ-IM signal generated using a EML.

Using this experimental setup, the effect of varying the LO power was analyzed. Figure 4.30 shows the BER vs. received power curves for different LO powers. The sensitivity is defined as the minimum received power for a pre-forward error correction (FEC) BER of 10^{-3}, which is the specified limit for pre-FEC BER in the NG-PON2 standard.

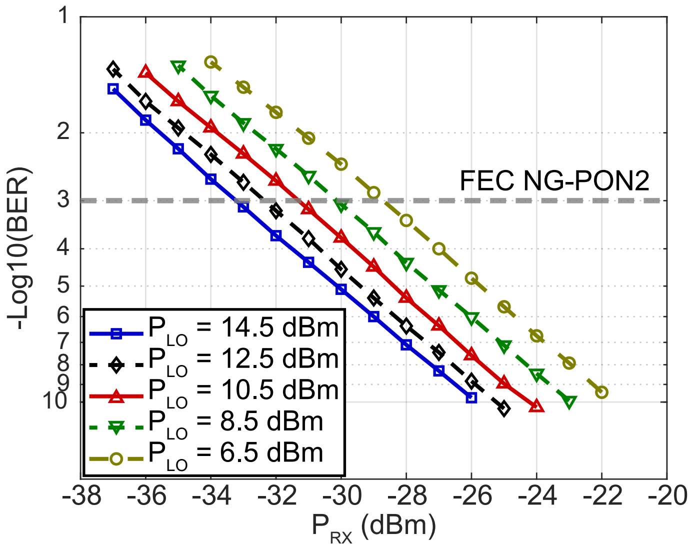

Figure 4.30: BER vs. received power curves for different LO powers.

The increment of the LO power in 2 dB cause an improvement of 1.25 dB in the sensitivity of the receiver until the LO power reach the 10.5 dBm. After this LO power, the improvement falls 0.75 due to the shot noise limited PDs. The best sensitivity is obtained with the maximum LO power that does not damage the PDs. Therefore, the LO power used in the following results will be 14.5 dBm.

The BER vs. received power curves for optical BTB and 40 km SSMF is shown Figure 4.31 for quasicoherent receiver and for direct detection.

The BTB sensitivity of the quasicoherent receiver is -35.2 dBm and no transmission penalty due to the 40 km SSMF transmission. The DD sensitivity is -20.9 dBm for BTB and its 40 km SSMF transmission penalty is 0.6 dB. This means that the quasicoherent receiver presents an improvement of 14.3 dB in comparison with a DD receiver, which increases to 14.6 dB if the transmission penalties are considered.

Therefore, the power budget of the quasicoherent receiver is 35.64 dB with the transmitter used in the experimental setup. Therefore, it fulfills the requirement of the E2 class of the NG-PON2 standard and allows a splitting ratio of 128 after 40 km SSMF transmission, considering 0.25 dB/km as the SSMF attenuation and $3.5\log_2(N)$ dB for the losses of the power splitter. In section 3.4 [4], this calculus was also performed considering a NG-PON2 compatible transmitter.

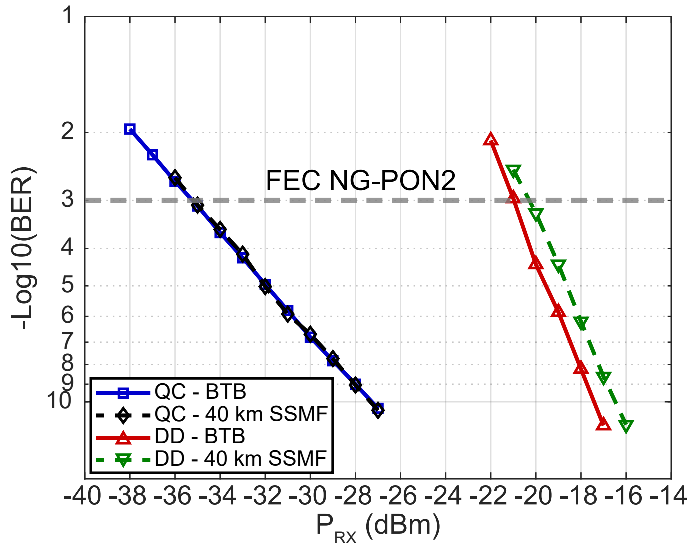

Figure 4.31: BER vs. received power curves for 10 Gbps quasicoherent receiver (QC) and direct detection (DD).

In the case of a DD based receiver, the power budget is 21.34 dB, which does not allow to fulfill the requirements of any of the classes of the NG-PON2, and a splitting ratio as low as 8.

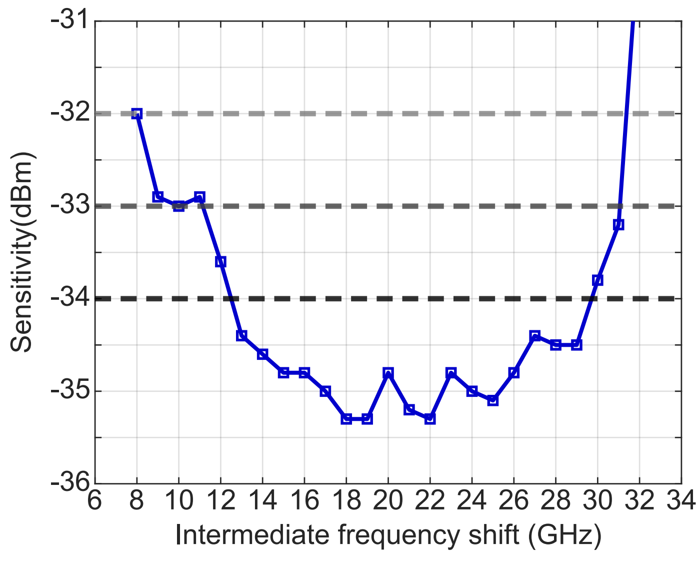

Figure 4.32: Sensitivity vs. intermediate frequency for 10 Gbps quasicoherent receiver.

NG-PON2 standard was designed to be a multiwavelength TDM or TWDM, so the receiver must be able to support signals that fluctuates in the assigned wavelength channel. The NG-PON2 standard defines the maximum spectral excursion (MSE) of the transmitter as the ”absolute difference between the nominal central frequency of the wavelength channel and the

-15 dB point of the transmitted spectrum furthest from the nominal frequency". The MSE for channel spacing of 50 GHz is ± 12.5 GHz and for a channel spacing of 100 GHz is ± 20 GHz. The transmitter has -15 dB bandwidth of 16.1 GHz. Therefore, the receiver needs to be able to receive signals that can fluctuate 8.9 GHz in the case of a channel spacing of 50 GHz and 23.9 GHz in the case of a channel spacing of 100 GHz.

The maximum IF variation that ensures a sensitivity of -34 dBm is 17.2 GHz, while 20 GHz is the maximum variation for a sensitivity of -33 dBm and 23.4 GHz for a sensitivity of -32 dBm. Therefore, the quasicoherent receiver is compatible with a channel spacing of 50 GHz with a sensitivity of -34 dBm and compatible with a channel spacing of 100 GHz with sensitivity of -32 dBm.

The 25 Gbps quasicoherent receiver was presented on section 3.5 [5]. The experimental setup used for testing the 25Gbps quasicoherent receiver is the same than before, but it has to be adapted to the data rate increment.

After the quasicoherent receiver, the signal is digitalized and an equalizer is applied. Two different equalizers have been used in this experiment. The first one consists of 41 FFE taps and 21 DFE taps, denoted in the following as high performance equalizer, and the second one consists of 15 FFE taps and 6 DFE taps, which will be named as low complexity equalizer. Both equalizers use the least-mean square algorithm with T/2 spaced taps and are trained to converge to the original NRZ signal or to a duobinary signal.

The BER vs. received power curves for optical BTB and 20 km SSMF are shown in Figure 4.33 with the quasicoherent receiver for both equalizers converging to NRZ signal.

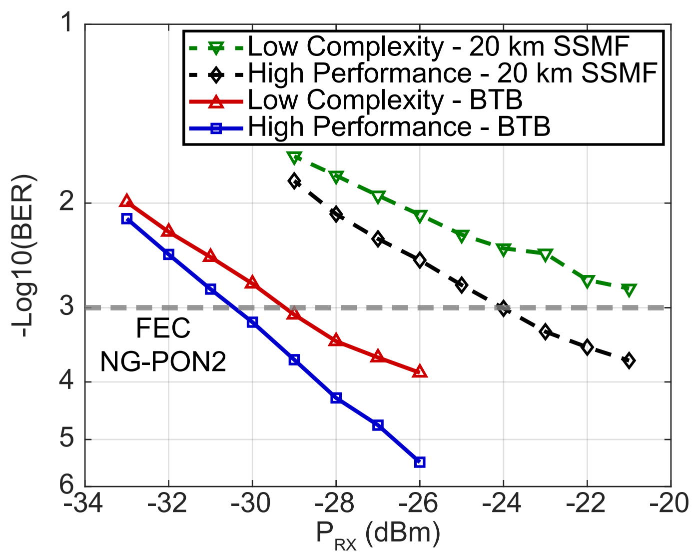

Figure 4.33: BER vs. received power curves for 25 Gbps quasicoherent receiver with NRZ detection.

The quasicoherent receiver with the high performance equalizer provides a BTB sensitivity of -30.5 dBm and it suffers a 20 km SSMF transmission penalty of 6.5 dB. The BTB sensitivity of the low complexity equalizer quasicoherent receiver is -29.2 dBm and there is not any measured power where the BER is below the FEC limit. Therefore, only the quasicoherent receiver with the high performance equalizer converging to NRZ will be possible for 20 km SSMF transmission and it will have a power budget of 25 dB. This power budget allows a splitting ratio of 32 after 20 km of SSMF transmission.

The BER vs. received power curves for optical BTB and 20 km SSMF are shown in Figure 4.34 with the quasicoherent receiver for both equalizers converging to a duobinary signal.

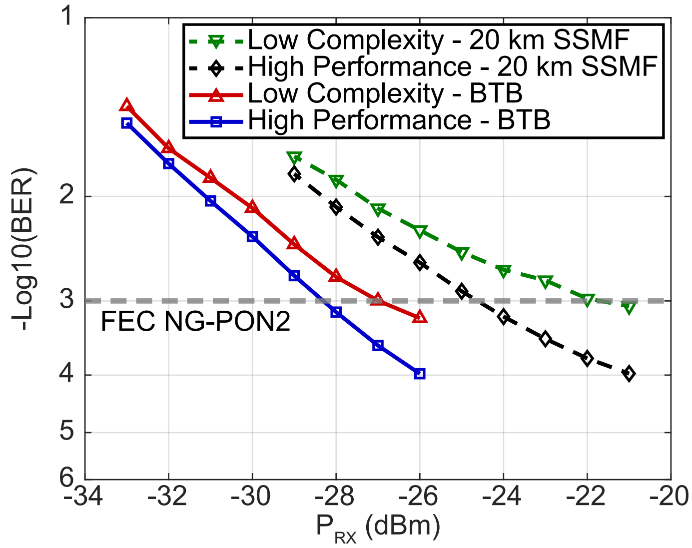

Figure 4.34: BER vs. received power curves for 25 Gbps quasicoherent receiver with duobinary detection.

The high performance equalizer quasicoherent receiver with duobinary convergence has a BTB sensitivity of -28.5 dBm and a 20 km SSMF transmission penalty of 3.8 dB. The low complexity equalizer quasicoherent receiver BTB sensitivity is -27 dBm and its 20 km SSMF transmission penalty will be 5 dB. The duobinary convergence allows to use both equalizers for 20 km SSMF transmission. Therefore, the high performance equalizer quasicoherent receiver has a power budget of 25.7 dB and the low complexity equalizer quasicoherent receiver has a power budget of 25 dB. The quasicoherent receiver with any of the equalizers will allow a splitting ratio of 32 after 20 km SSMF transmission when the equalizers converge to a duobinary signal.

In Table 4.4, the data rate, transmitted power, sensitivity, transmission penalty, power budget, splitting ratio and equalization of the quasicoherent receivers and the links achieved with them are summarized.

Table 4.4: Summary of the quasicoherent receivers.

	section 3.4 [4, 22]	section 3.5 [5]	section 3.5 [5]	section 3.5 [5]
Data Rate	10 Gbps	25 Gbps	25 Gbps	25 Gbps
Transmitted Power	+0.44 dBm	+1 dBm	+1 dBm	+1 dBm
Sensitivity	-35.2 dBm	-30.5 dBm	-28.5 dBm	-27 dBm
Transmission Penalty	0 dB (40 km)	6.5 dB (20km)	3.8 dB (20km)	5 dB (20km)
Power Budget	35.64 dB	25 dB	25.7 dB	23 dB
Splitting ratio	128	32	32	32
Equalization (FFE/DFE T/2)	NO	NRZ FFE 41 taps DFE 21 taps	duobinary FFE 41 taps DFE 21 taps	duobinary FFE 15 taps DFE 6 taps

Chapter 5

Conclusions

In this thesis, receivers and transmitters for the next generation of optical access networks have been investigated and developed. In order to address the requirements of these future optical access networks, i.e. long reach, high number of users, high capacity and low latency, while keeping the cost as low as possible, this thesis has been focused in two different passive optical networks approaches, uDWDM and NG-PON2 and beyond access networks.

uDWDM techniques based on ultra narrow channels over frequency slots of 12.5 GHz or 6.25 GHz, which are assigned exclusively to final user, have been investigated. This concept is known as lambda-to-the-user and usually provides a relative low capacity link, in the range of 1 Gbps, 1.25 Gbps or 2.5 Gbps, but completely dedicated to that specific user. The NG-PON2 and beyond access networks follow the path of the current deployed standards, which employ TDM over IM signals in the links between the central offices and the users. The NG-PON2 and beyond networks increase the data rate to 10 Gbps or 25 Gbps from the current data rates of 1.25 Gbps or 2.5 Gbps. Additionally, they introduce the concept of TWDM, where the users are multiplexed on time and wavelength at the same time.

Directly phase modulated transmitters have been researched and developed in this thesis in order to address the requirements of uDWDM PONs. Specifically, three directly phase modulated transmitters have been studied: a 1 Gbps transmitter based on a DFB; a 1 Gbps transmitter based on a RSOA pumped by a VCSEL; and a 1.25 - 2.5 Gbps transmitter based on a VCSEL. These directly phase modulated transmitters will allow to increase the capacity of the network, because using phase modulation, transmitters can send the same or more data rate in a much more compact spectrum while keeping a reduced cost. Additionally, a single PD heterodyne receiver for DPSK signals has been implemented and the performance of different types of laser (DFB and VCSEL) as alternative LO have been analyzed. This type of receiver allows to select a single channel in a uDWDM network without optical filters and allows to increase the reach and the number of users of the network due to the coherent amplification. The combination of this directly phase transmitters with the single PD heterodyne receiver allows to obtain power budgets as high as 38.5 dB and 51 dB that support splitting ratios between

128 and 1024. Therefore, the feasibility of using directly phase modulated DFBs, RSOAs and VCSELs combined with single PD heterodyne receivers has been demonstrated and they can be strong candidates for the future uDWDM access networks.

A 1 Gbps link using a directly phase modulated DFB or RSOA pumped by a VCSEL has been used as the uplink of bidirectional channels. A Nyquist-DPSK signal generated by a MZM has been used as the downlink of this bidirectional channel. These bidirectional channels will allow to obtain a 1 Gbps full-duplex link between the central office and the user with frequency slots as narrow as 6.25 GHz or 5 GHz. The 1.25 - 2.5 Gbps directly phase modulated VCSEL provides a high data rate for uDWDM in a compact spectrum with the cheapest transmitter. These bidirectional channels provide power budgets of 42 dB and 37 dB for the DFB and RSOA respectively therefore supporting splitting ratios of 256 and 128, respectively. It has been then proven, the feasibility of bidirectional links in ultra narrow frequency slots, as well as their capability of increasing the overall capacity of the future uDWDM access networks.

A 10 Gbps quasicoherent receiver has been developed in order to address the requirements of the NG-PON2 standard. The quasicoherent receiver uses coherent amplification in order to increase the receiver sensitivity of IM signals, achieving a power budget of 35.64 dB. This will allow to increase the reach and splitting ratio of the network, specifically for 40 km and 128 users with 10 Gbps per wavelength. The quasicoherent receiver also allows multiwavelength operation without the necessity of optical filtering. The multiwavelength operation is a requirement for the NG-PON2 access networks, where four wavelengths are multiplexed with a data rate of 10 Gbps per wavelength. Therefore, the quasicoherent receiver has been developed and tested in this thesis, becoming an attractive candidate for NG-PON2 networks.

A 25 Gbps quasicoherent receiver combined with an FFE/DFE equalizer has been presented to address the requirements of the beyond NG-PON2 networks. This receiver allows to transmit in C-band with enough sensitivity, thanks to the coherent amplification, and with remarkable reach, overcoming the chromatic dispersion. The 25 Gbps quasichorent receiver will provide power budgets higher than 23 dB after 20 km SSMF transmissions, which means that it will be able to provide up to 32 users. The capacity of multiwavelength operation in the C-band of the quasicoherent receiver will allow to use this receiver in DWDM networks following the path of NG-PON2 but at a higher data rate. Therefore, the combination between the quasicoherent receiver and the FFE/DFE equalizer has been tested and shows promising results for the networks beyond NG-PON2.

Finally, directly phase modulated transmitters (DFB, RSOA pumped by VCSEL and VCSEL) combined with single PD heterodyne receivers are perfect candidates for the future uDWDM passive optical networks addressing the lambda-to-the-user concept. The quasicoherent receiver is the perfect receiver to address the demanding requirements of the NG-PON2 standard and opens the door to the DWDM networks for beyond NG-PON2 networks at data rates higher than 25 Gbps.

Bibliography

[1] J. A. Altabas, D. Izquierdo, J. A. Lazaro, A. Lerin, F. Sotelo, and I. Garces, "1Gbps full-duplex links for ultra-dense-WDM 6.25GHz frequency slots in optical metro-access networks," *Optics Express*, vol. 24, no. 1, pp. 555–565, 2016.

[2] J. A. Altabas, D. Izquierdo, J. A. Lazaro, and I. Garces, "Cost-Effective Transceiver Based on an RSOA and a VCSEL for Flexible uDWDM Networks," *IEEE Photonics Technology Letters*, vol. 28, no. 10, pp. 1111–1114, 2016.

[3] J. A. Altabas, D. Izquierdo, J. A. Lazaro, and I. Garces, "Chirp-based direct phase modulation of VCSELs for cost-effective transceivers," *Optics Letters*, vol. 42, no. 3, pp. 583–586, 2017.

[4] J. A. Altabas, G. Silva Valdecasa, L. F. Suhr, M. Didriksen, J. A. Lazaro, I. Garces, I. Tafur Monroy, A. T. Clausen, and J. B. Jensen, "Real-Time 10 Gbps Polarization Independent Quasicoherent Receiver for NG-PON2 Access Networks," *Journal of Lightwave Technology*, vol. 37, no. 2, pp. 651–656, 2019.

[5] J. A. Altabas, L. F. Suhr, G. Silva Valdecasa, J. A. Lazaro, I. Garces, J. B. Jensen, and A. T. Clausen, "25Gbps Quasicoherent Receiver for Beyond NG-PON2 Access Networks," in *2018 European Conference on Optical Communication (ECOC)*, (Rome, Italy), p. We2.70, 2018.

[6] J. A. Altabas, D. Izquierdo, J. Lazaro, and I. Garces, "1Gbps full-duplex 5GHz frequency slots uDWDM flexible Metro/Access Networks based on VCSEL-RSOA transceiver," in *2016 OptoElectronics and Communications Conference - International Conference on Photonics in Switching (OECC/PS)*, (Niigata, Japan), pp. WA1–5, 2016.

[7] J. A. Altabas, D. Izquierdo, J. A. Lazaro, and I. Garces, "1.25-2.5Gbps cost-effective transceiver based on directly phase modulated VCSEL for flexible access networks," in *2017 Optical Fiber Communications Conference and Exhibition (OFC)*, (Los Angeles, CA, USA), p. Th1K.4, 2017.

[8] R. Puerta, S. Rommel, J. A. Altabas, L. Pyndt, R. Idrissa, A. K. Sultanov, J. J. Vegas Olmos, and I. Tafur Monroy, “Multiband carrierless amplitude/phase modulation for ultra-wideband high data rate wireless communications,” *Microwave and Optical Technology Letters*, vol. 58, no. 7, pp. 1603–1607, 2016.

[9] S. Sarmiento, J. A. Altabas, D. Izquierdo, I. Garces, S. Spadaro, and J. A. Lazaro, “Cost-Effective DWDM ROADM Design for Flexible Sustainable Optical Metro–Access Networks,” *Journal of Optical Communications and Networking*, vol. 9, no. 12, pp. 1116–1124, 2017.

[10] J. A. Altabas, S. Rommel, R. Puerta, D. Izquierdo, J. I. Garces, J. A. Lazaro, J. J. V. Olmos, and I. T. Monroy, “Nonorthogonal Multiple Access and Carrierless Amplitude Phase Modulation for Flexible Multiuser Provisioning in 5G Mobile Networks,” *Journal of Lightwave Technology*, vol. 35, no. 24, pp. 5456–5463, 2017.

[11] S. Sarmiento, J. A. Altabas, S. Spadaro, and J. A. Lazaro, “Experimental Assessment of 10 Gbps 5G Multicarrier Waveforms for High-Layer Split u-DWDM-PON-Based Fronthaul,” *Journal of Lightwave Technology*, vol. 37, no. 10, pp. 2344–2351, 2019.

[12] J. A. Altabas, J. A. Lazaro, F. Sotelo, and I. Garces, “Experimental Demonstration of Bandwidth Reduction using Nyquist Shaped PSK for Flexible udWDM,” in *2015 Conference on Lasers and Electro-Optic (CLEO: 2015)*, (San Jose, CA, USA), p. JTh2A.70, 2015.

[13] J. A. Altabas, F. Sotelo, J. A. Lazaro, and I. Garces, “Experimental Bandwidth Optimization for Flexible PON Using Nyquist Shaped PSK,” in *2015 Conference on Lasers and Electro-Optics Europe - European Quantum Electronics Conference (CLEO/Europe-EQEC)*, (Munich, Germany), pp. CI–2.4 SUN, 2015.

[14] J. A. Altabas, P. Arribas, D. Izquierdo, F. Sotelo, A. Lerin, J. M. Fabrega, J. A. Lazaro, I. Garces, and G. Junyent, “Survey of Faster-Than-Nyquist for Flexible Passive Optical Networks,” in *2015 International Conference on Transparent Optical Networks (ICTON)*, (Budapest, Hungary), p. Mo.D1.3, 2015.

[15] J. A. Altabas, D. Izquierdo, F. Sotelo, I. Garces, J. A. Lazaro, A. Lerin, S. Spadaro, and G. Junyent, “Experimental demonstration of flex-grid udWDM with 6.25GHz full-duplex frequency slots for Metro/Access & Data Centers,” in *2015 International Conference on Photonics in Switching (PS)*, (Florence, Italy), p. SC3, 2015.

[16] J. A. Altabas, D. Izquierdo, A. Pascual, S. Sarmiento, J. A. Lazaro, I. Garces, and A. Villafranca, “Design of flexible udWDM Metro-Access Network Devices assisted by High

Resolution Complex Spectroscopy," in *2016 International Conference on Transparent Optical Networks (ICTON)*, (Trento, Italy), p. Tu.D2.5, 2016.

[17] J. A. Lazaro, S. Spadaro, J. Perello, J. Gene, J. A. Altabas, A. Pages, D. Careglio, P. Barlet-Ros, A. Cabellos, and J. Sole-Pareta, "SUNSET: Sustainable network infrastructure enabling the future Digital Society," in *2016 International Conference on Transparent Optical Networks (ICTON)*, (Trento, Italy), p. Tu.C3.3, 2016.

[18] S. Sarmiento, R. Montero, J. A. Altabas, D. Izquierdo, F. Agraz, A. Pages, J. Perello, J. Gene, M. Alonso, A. Pascual, I. Garces, S. Spadaro, and J. A. Lazaro, "SDN-enabled flexible optical node designs and transceivers for sustainable metro-access networks convergence," in *2016 International Conference on Transparent Optical Networks (ICTON)*, (Trento, Italy), p. Th.A1.4, 2016.

[19] J. A. Altabas, D. Izquierdo, A. Lopez, M. A. Losada, J. Mateo, J. A. Lazaro, and I. Garces, "MultiCAP modulation for high spectral efficiency transmission over SI-POF," in *2017 Conference on Lasers and Electro-Optics Europe - European Quantum Electronics Conference (CLEO/Europe-EQEC)*, (Munich, Germany), pp. CI–4.5 SUN, 2017.

[20] L. Nadal, J. M. Fabrega, J. A. Altabas, D. Izquierdo, F. J. Vilchez, M. S. Moreolo, J. A. Lazaro, and I. Garces, "Transparent service delivery in elastic metro/access networks with cost-effective programmable transceivers," in *2017 International Conference on Transparent Optical Networks (ICTON)*, (Girona, Spain), p. Tu.C2.5, 2017.

[21] J. A. Altabas, S. Rommel, R. Puerta, D. Izquierdo, I. Garces, J. A. Lazaro, J. J. Vegas Olmos, and I. Tafur Monroy, "Non-Orthogonal Multiple Access and Carrierless Amplitude Phase Modulation for 5G Mobile Networks," in *2017 European Conference on Optical Communication (ECOC)*, (Gothenburg, Sweden), p. Tu.1.B.2, 2017.

[22] J. A. Altabas, G. Silva Valdecasa, M. Didriksen, J. A. Lazaro, I. Garces, I. Tafur Monroy, and J. B. Jensen, "Real-time 10Gbps polarization independent quasicoherent receiver for NG-PON2 access networks," in *2018 Optical Fiber Communications Conference and Exhibition (OFC)*, (San Diego, CA, USA), p. Th1A.3, 2018.

[23] J. A. Lazaro, M. Coves, S. Sarmiento, J. A. Altabas, and A. Lerin, "5G Connected Vehicles Supported by Optical Fiber Access," in *2018 International Conference on Transparent Optical Networks (ICTON)*, (Bucharest, Romania), p. Mo.B5.3, 2018.

[24] J. A. Altabas, D. Izquierdo, M. A. Losada, J. Clemente, S. Sarmiento, J. Mateo, J. A. Lazaro, and I. Garces, "Experimental demonstration of multiband CAP modulation for

SI-POF links," in *2018 International Conference on Plastic Optical Fibers (POF)*, (Seattle, WA, USA), p. P19, 2018.

[25] S. Sarmiento, A. Gran, J. A. Altabas, M. Scalabroni, S. Spadaro, I. Garces, and J. A. Lazaro, "Experimental Assessment of 5-10Gbps 5G Multicarrier Waveforms with Intensity-Modulation Direct-Detection for PONs," in *2018 Photonics in Switching and Computing (PSC)*, (Limassol, Cyprus), p. Fr1C.5, 2018.

[26] J. Clemente, D. Izquierdo, P. J. Reyes-Iglesias, A. Ortega-Monux, J. A. Altabas, I. Molina-Fernandez, G. Wanguemert-Perez, J. de Oliva-Rubio, and I. Garces, "Experimental Demonstration of Colorless Operation of an Integrated 120 Coherent Receiver," in *2018 European Conference on Optical Communication (ECOC)*, (Rome, Italy), p. We3H.2, 2018.

[27] D. Izquierdo, J. A. Altabas, P. Millan, J. Clemente, J. A. Lazaro, S. Rommel, R. Puerta, J. J. Vegas Olmos, I. Tafur Monroy, and I. Garces, "Non-Orthogonal Multiple Access based on Carrierless Amplitude Phase format for coherent PON flexible resource provisioning," in *2019 Conference on Lasers and Electro-Optics Europe - European Quantum Electronics Conference (CLEO/Europe-EQEC)*, (Munich, Germany), pp. CI–P.15 SUN, 2019.

[28] S. Sarmiento, J. A. Altabas, S. Spadaro, and J. A. Lazaro, "From 4.2Gbps Asymmetrical Clipping (ACO)-OFDM to 8.7Gbps Layered ACO-FBMC with Intensity-Modulation Direct-Detection for PONs," in *2019 Conference on Lasers and Electro-Optics Europe - European Quantum Electronics Conference (CLEO/Europe-EQEC)*, (Munich, Germany), pp. CI–P.13 SUN, 2019.

[29] S. Sarmiento, J. M. Delgado Mendinueta, J. A. Altabas, S. Spadaro, S. Shinada, H. Furukawa, J. J. Vegas Olmos, J. A. Lazaro, and N. Wada, "Experimental Investigation of 50–90 Gb/s IM-DD NOMA-CAP Modulation for Short Range Optical Transmission Applications," in *2019 OptoElectronics and Communications Conference (OECC) - International Conference on Photonics in Switching and Computing (PSC)*, (Fukuoka, Japan), pp. TuF3–5, 2019.

[30] J. A. Altabas, D. Izquierdo, J. Clemente, S. Sarmiento, G. Silva Valdecasa, M. Squartecchia, L. F. Suhr, O. Gallardo, A. Lopez, M. Á. Losada, J. Mateo, J. B. Jensen, J. A. Lazaro, and I. Garces, "Advanced Technologies for Coherent Access Networks," in *2019 International Conference on Transparent Optical Networks (ICTON)*, (Agnes, France), p. Th.B1.4, 2019.

[31] S. Sarmiento, J. M. Delgado Mendinueta, J. A. Altabas, S. Spadaro, S. Shinada, H. Furukawa, J. J. Vegas Olmos, J. A. Lazaro, and N. Wada, "Optical power budget enhancement in 50 Gb/s IM-DD PONs with NOMA CAP modulation and SOA-based amplification," in *2019 International Conference on Transparent Optical Networks (ICTON)*, (Agnes, France), p. We.D1.3, 2019.

[32] D. Izquierdo, J. A. Altabas, J. Clemente, P. Millan, J. A. Lazaro, S. Rommel, R. Puerta, J. J. Vegas Olmos, I. Tafur Monroy, and I. Garces, "Flexible resource provisioning of coherent PONs based on Non-Orthogonal Multiple Access and CAP signals," in *2019 European Conference on Optical Communication (ECOC)*, (Dublin, Ireland), p. M.1.F.3, 2019.

[33] S. Sarmiento, J. M. Delgado Mendinueta, J. A. Altabas, S. Spadaro, S. Shinada, H. Furukawa, J. J. Vegas Olmos, J. A. Lazaro, and N. Wada, "Split-Enabled 490 Gb/s Optical Interconnect with Direct Detection NOMA-CAP and 7-core Multi-Core Fibre," in *2019 European Conference on Optical Communication (ECOC)*, (Dublin, Ireland), p. P32, 2019.

[34] J. A. Altabas, P. Arribas, F. Sotelo, D. Izquierdo, J. A. Lazaro, and I. Garces, "Analysis of Advanced Coherent Modulation Formats for Optical Flexible Metro-Access Networks," in *2015 IX Reunión Española de Optoelectrónica (OPTOEL)*, (Salamanca, Spain), pp. PO–SIII–34, 2015.

[35] J. D. Sarmiento-Merenguel, A. Ortega-Moñix, R. Hallir, C. A. Alonso-Ramos, P. Reyes-Iglesias, I. Molina-Fernandez, I. Garces-Gregorio, and J. A. Altabas-Navarro, "Monolithically integrated DP-QPSK receiver without polarization beam splitters," in *2015 IX Reunión Española de Optoelectrónica (OPTOEL)*, (Salamanca, Spain), pp. PO–SII–23, 2015.

[36] D. Izquierdo, R. Martinez, J. A. Altabas, and I. Garces, "Transceptor Sintonizable de Coste Reducido Basado en VCSEL para Redes Opticas udWDM Flexibles Metropolitanas y de Acceso," in *2016 IV Congreso Nacional de I+D en Defensa y Seguridad (DESE I+D)*, (San Javier, Spain), pp. II–B–157, 2016.

[37] J. A. Altabas, D. Izquierdo, M. Chueca, C. Seron, J. Cebollada, S. Sarmiento, J. A. Lazaro, and I. Garces, "Transceptores ópticos coherentes para las redes ópticas de acceso futuras," in *2017 X Reunión Española de Optoelectrónica (OPTOEL)*, (Santiago de Compostela, Spain), pp. S.1–055, 2017.

[38] G. Ramos, J. A. Altabas, D. Izquierdo, A. Lopez, M. A. Losada, J. Clemente, S. Sarmiento, J. Mateo, J. A. Lazaro, and I. Garces, "Bit and Power Loaded Multiband

Carrierless Amplitude Phase Modulation for High Capacity POF Links," in *2019 XI Reunión Española de Optoelectrónica (OPTOEL)*, (Zaragoza, Spain), p. SP3.COM04, 2019.

[39] D. Izquierdo, J. A. Altabas, J. Clemente, P. Millan, J. A. Lazaro, S. Rommel, R. Puerta, J. J. Vegas Olmos, I. Tafur Monroy, I. Salinas, and I. Garces, "Distribución flexible de recursos en redes PON coherentes combinando NonOrthogonal Multiple Access y formatos CAP," in *2019 XI Reunión Española de Optoelectrónica (OPTOEL)*, (Zaragoza, Spain), p. SP3.COM06, 2019.

[40] J. A. Altabas, S. Sarmiento, and J. A. Lazaro, "Passive Optical Networks: Introduction," in *Wiley Encyclopedia of Electrical and Electronics Engineering* (J. G. Webster, ed.), pp. 1–20, John Wiley & Sons, Inc., 2018.

[41] J. A. Altabas Navarro, I. Tafur Monroy, S. Rommel, R. Puerta, J. J. Vegas Olmos, D. Izquierdo Nuñez, J. I. Garces Gregorio, and J. A. Lazaro Villa, "WO2018138254 -Constellation Multiplexing and Non-Orthogonal Multiple Access Based on Carrierless Amplitude Phase Modulation," 2018.

[42] Z. Franco, F. Sotelo, S. Gómez-De Pedro, J. A. Altabas, M. Puyol, D. Izquierdo, J. Alonso, and I. Garcés, "Nanosecond fluorescence lifetime low-cost system for sensor applications," in *2014 Transfrontier Meeting of Sensors and Biosensors (TMSB)*, (Barcelona, Spain), 2014.

[43] Z. Franco, F. Sotelo, S. Gómez-De Pedro, J. A. Altabas, M. Puyol, D. Izquierdo, J. Alonso, and I. Garcés, "Nanosecond fluorescence lifetime low-cost sensor," in *2014 IEEE Sensors*, (Valencia. Spain), pp. A1L–B.3, 2014.

[44] J. A. Lazaro, J. Gonzalez, J. A. Altabas, and A. Lerin, "Graphene Silicon ring resonators for wavelength routers in Photonic Network-on-Chip," in *2015 Conference on Lasers and Electro-Optics Europe - European Quantum Electronics Conference (CLEO/Europe-EQEC)*, (Munich, Germany), pp. JSIV–2.4 SUN, 2015.

[45] Z. Franco, F. Sotelo, S. Gomez-de Pedro, J. A. Altabas, M. Puyol, D. Izquierdo, J. Alonso, and I. Garces, "Low-cost measurement system for nanosecond fluorescence lifetime sensors," in *2015 IX Reunión Española de Optoelectrónica (OPTOEL)*, (Salamanca, Spain), pp. PO–SIII–18, 2015.

[46] J. A. Lazaro, J. Gonzalez, J. A. Altabas, and A. Lerin, "Graphene Silicon ring resonators for wavelength routers in Photonic Network-on-Chip," in *2015 International Conference on Transparent Optical Networks (ICTON)*, (Budapest, Hungary), p. Th.B5.2, 2015.

[47] J. A. Lazaro Villa, A. Lerin de la Santisima Trinidad, and J. A. Altabas Navarro, "ES2597577 - Device and System for Modulating the Phase of an Optical Signal, Based on Graphene and/or Carbon-Based Nanostructured Materials," 2017.

[48] J.-X. Cai, H. G. Batshon, M. V. Mazurczyk, O. V. Sinkin, S. Member, D. Wang, M. Paskov, C. R. Davidson, S. Member, W. W. Patterson, A. Turukhin, M. A. Bolshtyansky, D. G. Foursa, and S. Member, "51.5 Tb/s Capacity over 17,107 km in C+L Bandwidth Using Single-Mode Fibers and Nonlinearity Compensation," *Journal of Lightwave Technology*, vol. 36, no. 11, pp. 2135–2141, 2018.

[49] G. Rademacher, R. S. Lu, B. J. Puttnam, and T. A. Eriksson, "159 Tbit/s C+L Band Transmission over 1045 km 3-Mode Graded-Index Few-Mode Fiber," *2018 Optical Fiber Communications Conference and Exhibition (OFC)*, p. Th4C.4, 2018.

[50] D. Soma, Y. Wakayama, S. Beppu, S. Sumita, and T. Tsuritani, "10.16 Peta-bit/s Dense SDM/WDM transmission over Low-DMD 6-Mode 19-Core Fibre across C+L Band," in *2017 European Conference on Optical Communication (ECOC)*, (Gothenburg, Sweden), p. Th.PDP.A.1, 2017.

[51] S. L. I. Olsson, J. Cho, and S. Chandrasekhar, "Record-High 17.3-bit/s/Hz Spectral Efficiency Transmission over 50 km Using Probabilistically Shaped PDM 4096-QAM," in *2018 Optical Fiber Communications Conference and Exhibition (OFC)*, (San Diego, CA, USA), p. Th4C.5, 2018.

[52] J. Renaudier, A. C. Meseguer, A. Ghazisaeidi, P. Tran, R. R. Muller, and R. Brenot, "First 100-nm Continuous-Band WDM Transmission System with 115Tb/s Transport over 100km Using Novel Ultra-Wideband Semiconductor Optical Amplifiers," in *2017 European Conference on Optical Communication (ECOC)*, (Gothenburg, Sweden), p. Th.PDP.A.3, 2017.

[53] R. Muñoz, R. Vilalta, R. Casellas, R. Martínez, T. Szyrkowiec, A. Autenrieth, V. López, and D. López, "SDN/NFV orchestration for dynamic deployment of virtual SDN controllers as VNF for multi-tenant optical networks," in *2015 Optical Fiber Communications Conference and Exhibition (OFC)*, (Los Angeles, CA, USA), p. W4J.5, 2015.

[54] Z. Liu, J. Zhang, L. Bai, and Y. Ji, "Joint Jobs Scheduling and Routing for Metro-Scaled Micro Datacenters over Elastic Optical Networks," in *2018 Optical Fiber Communications Conference and Exhibition (OFC)*, (San Diego, CA, USA), p. M2E.3, 2018.

[55] L. Velasco, L. Gifre, F. Paolucci, and F. Cugini, "First Experimental Demonstration of Autonomic Slice Networking," in *2017 Optical Fiber Communications Conference and Exhibition (OFC)*, (Los Angeles, CA, USA), p. Th5A.3, 2017.

[56] C. F. Lam, ed., *Passive Optical Networks*. Elsevier, 2007.

[57] G. Keiser, ed., *FTTX concepts and applications*. John Wiley & Sons, Inc, 2006.

[58] F. Effenberger, D. Cleary, O. Haran, G. Kramer, R. D. Li, M. Oron, and T. Pfeiffer, "An introduction to PON technologies," *IEEE Communications Magazine*, vol. 45, no. 3, pp. 17–25, 2007.

[59] B. Schrenk, F. Laudenbach, R. Lieger, T. Lorunser, P. Bakopoulos, A. Poppe, M. Stierle, H. Avramopoulos, and H. Leopold, "Passive ROADM Flexibility in Optical Access with Spectral and Spatial Reconfigurability," *IEEE Journal on Selected Areas in Communications*, vol. 33, no. 12, pp. 2837–2846, 2015.

[60] ITU-T, "G.9802 Multiple-wavelength passive optical networks (MW-PONs)," 2015.

[61] ITU-T, "G.989 40-Gigabit-capable passive optical networks (NG-PON2): Definitions, abbreviations and acronyms," 2015.

[62] ITU-T, "G.694.1 Spectral grids for WDM applications: DWDM frequency grid," 2012.

[63] S. Smolorz, H. Rohde, P. Ossieur, C. Antony, P. D. Townsend, B. Baekelandt, X. Z. Qiu, S. Appathurai, H. Krimmel, A.-l. Germany, and B. Labs, "Next generation access networks: PIEMAN and beyond," in *2009 International Conference on Photonics in Switching (PS)*, (Pisa, Italy), pp. 196–199, 2009.

[64] G. Talli, C. W. Chow, P. Townsend, R. Davey, T. D. Ridder, X.-z. Qiu, P. Ossieur, H.-g. Krimmel, D. Smith, I. Lealman, A. Poustie, S. Randel, and H. Rohde, "Integrated Metro and Access Network: PIEMAN," in *2007 European Conference on Networks & Optical Communications (NOC)*, (Stockholm, Sweden), pp. 493–500, 2007.

[65] J. A. Lázaro, V. Polo, C. Bock, M. Omella, and J. Prat, "Remotely Amplified SARDANA : Single-fibre-tree Advanced Ring-based Dense Access Network Architecture," in *2006 European Conference on Optical Communication (ECOC)*, (Cannes, France), pp. 1–3, 2006.

[66] J. A. Lázaro, R. I. Martínez, V. Polo, C. Arellano, and J. Prat, "Hybrid Dual-fiber-Ring with Single-fiber-Trees Dense Access Network Architecture using RSOA-ONU," in *2007 Optical Fiber Communications Conference and Exhibition (OFC)*, (Anaheim, CA, USA), p. OTuG2, 2007.

[67] A. Lovri, S. Aleksi, J. A. Lazaro, G. M. T. Beleffi, F. Bonada, J. Prat, and A. L. J. Teixeira, "Influence of Broadcast Traffic on Energy Efficiency of Long-Reach SARDANA

Access Network," in *2011 Optical Fiber Communications Conference and Exhibition (OFC)*, (Los Angeles, CA, USA), p. OThB5, 2011.

[68] B. Schrenk, J. A. Lazaro, D. Klonidis, F. Bonada, F. Saliou, V. Polo, E. Lopez, Q. T. Le, P. Chanclou, L. Costa, A. Teixeira, S. Chatzi, I. Tomkos, G. M. Beleffi, D. Leino, R. Soila, S. Spirou, G. De Valicourt, R. Brenot, C. Kazmierski, and J. Prat, "Demonstration of a remotely dual-pumped long-reach PON for flexible deployment," *Journal of Lightwave Technology*, vol. 30, no. 7, pp. 953–961, 2012.

[69] K. Prince, T. B. Gibbon, R. Rodes, E. Hviid, C. I. Mikkelsen, C. Neumeyr, M. Ortsiefer, E. Rönneberg, J. Rosskopf, P. Öhlén, E. I. De Betou, B. Stoltz, E. Goobar, J. Olsson, R. Fletcher, C. Abbott, M. Rask, N. Plappert, G. Vollrath, and I. T. Monroy, "GigaWaM - Next-generation WDM-PON enabling gigabit per-user data bandwidth," *Journal of Lightwave Technology*, vol. 30, no. 10, pp. 1444–1454, 2012.

[70] M. Iglesias Olmedo, L. Suhr, K. Prince, R. Rodes, C. Mikkelsen, E. Hviid, C. Neumeyr, G. Vollrath, E. Goobar, P. Öhlén, and I. T. Monroy, "Gigabit Access Passive Optical Network Using Wavelength Division Multiplexing - GigaWaM," *Journal of Lightwave Technology*, vol. 32, no. 22, pp. 4285–4293, 2014.

[71] M. Forzati, A. Bianchi, J. Chen, K. Grobe, B. Lannoo, C. M. Machuca, J.-C. Point, B. Skubic, S. Verbrugge, E. Weis, L. Wosinska, and D. Breuer, "Next-Generation Optical Access Seamless Evolution: Concluding Results of the European FP7 Project OASE," *Journal of Optical Communications and Networking*, vol. 7, no. 2, pp. 109–123, 2015.

[72] K. Wang, C. M. Machuca, L. Wosinska, P. J. Urban, A. Gavler, K. Brunnstrom, and J. Chen, "Techno-Economic Analysis of Active Optical Network Migration Toward Next-Generation Optical Access," *Journal of Optical Communications and Networking*, vol. 9, no. 4, pp. 327–341, 2017.

[73] C. Mas Machuca, M. Kind, K. Wang, K. Casier, M. Mahloo, and J. Chen, "Methodology for a Cost Evaluation of Migration Toward NGOA Networks," *Journal of Optical Communications and Networking*, vol. 5, no. 12, pp. 1456–1466, 2013.

[74] M. Mahloo, J. Chen, L. Wosinska, A. Dixit, B. Lannoo, D. Colle, and C. Machuca, "Toward reliable hybrid WDM/TDM passive optical networks," *IEEE Communications Magazine*, vol. 52, no. 2, pp. 14–23, 2014.

[75] M. Ruffini, L. Wosinska, M. Achouche, J. Chen, N. Doran, F. Farjady, J. Montalvo, P. Ossieur, B. O'Sullivan, N. Parsons, T. Pfeiffer, X. Z. Qiu, C. Raack, H. Rohde,

M. Schiano, P. Townsend, R. Wessaly, X. Yin, and D. Payne, "DISCUS: An end-to-end solution for ubiquitous broadband optical access," *IEEE Communications Magazine*, vol. 52, no. 2, pp. 24–32, 2014.

[76] M. Ruffini, M. Achouche, A. Arbelaez, R. Bonk, A. D. Giglio, N. J. Doran, M. Furdek, R. Jensen, J. Montalvo, N. Parsons, T. Pfeiffer, L. Quesada, C. Raack, H. Rohde, M. Schiano, G. Talli, P. Townsend, R. Wessaly, L. Wosinska, X. Yin, and D. B. Payne, "Access and metro network convergence for flexible end-to-end network design [invited]," *Journal of Optical Communications and Networking*, vol. 9, no. 6, pp. 524–535, 2017.

[77] G. Talli, F. Slyne, S. Porto, D. Carey, N. Brandonisio, A. Naughton, P. Ossieur, S. McGettrick, C. Blumm, M. Ruffini, D. Payne, R. Bonk, T. Pfeiffer, N. Parsons, and P. Townsend, "SDN Enabled Dynamically Reconfigurable High Capacity Optical Access Architecture for Converged Services," *Journal of Lightwave Technology*, vol. 35, no. 3, pp. 550–560, 2017.

[78] B. R. Rofoee, G. Zervas, Y. Yan, N. Amaya, and D. Simeonidou, "Flexible and adaptive optical metro networking on fixed/flex grid exploiting hybrid time/frequency for shared resource allocation," in *2012 European Conference on Optical Communication (ECOC)*, (Amsterdam, The Netherlands), p. Tu.3.D.5, 2012.

[79] G. Vall-Llosera, A. Rafel, N. Parkin, M. Angelou, D. Klonidis, I. Cano, M. Presi, G. Papastergiou, I. Tomkos, J. Prat, and E. Ciaramella, "COCONUT cost, power consumption and migration analysis: A route towards NG-PON3," in *2015 International Conference on Transparent Optical Networks (ICTON)*, (Budapest, Hungary), p. Mo.D2.1, 2015.

[80] M. Artiglia, R. Corsini, M. Presi, F. Bottoni, G. Cossu, and E. Ciaramella, "Coherent Systems for Low-Cost 10 Gb / s Optical Access Networks," *Journal of Lightwave Technology*, vol. 33, no. 15, pp. 3338–3344, 2015.

[81] I. N. Cano, A. Lerin, V. Polo, and J. Prat, "Simplified polarization diversity heterodyne receiver for 1.25Gb/s cost-effective udWDM-PON," in *2014 Optical Fiber Communications Conference and Exhibition (OFC)*, (San Francisco, CA, USA), p. W4G.2, 2014.

[82] V. Houtsma and D. V. Veen, "Bi-Directional 25G/50G TDM-PON with Extended Power Budget Using 25G APD and Coherent Detection," *Journal of Lightwave Technology*, vol. 36, no. 1, pp. 122–127, 2018.

[83] K. Fukuchi, T. Ono, and Y. Yano, "10 Gbit/s-120 km standard fiber transmission employing a novel optical phase-encoded intensity modulation for signal spectrum com-

pression," in *1997 Optical Fiber Communications Conference and Exhibition (OFC)*, (Dallas, TX, USA), p. ThH3, 1997.

[84] H. Kim, C. X. Yu, and D. T. Neilson, "Demonstration of optical duobinary transmission system using phase modulator and optical filter," *IEEE Photonics Technology Letters*, vol. 14, no. 7, pp. 1010–1012, 2002.

[85] J. J. Vegas Olmos, L. F. Suhr, B. Li, and I. Tafur Monroy, "10 Gbps Five Levels Polibinary Signaling for Short Range and Access Networks," in *2013 Asia Communications and Photonics Conference and International Conference on Information Photonics and Optical Communications (ACP/IPOC)*, (Beijing, China), p. AW4G.3, 2013.

[86] A. G. Reza and J. K. K. Rhee, "30-Gb/s PAM-8 Transmission with Directly-Modulated Laser using Machine Learning Equalizer," in *2018 Asia Communications and Photonics Conference (ACP)*, (Hangzhou, China), p. Su3C.5, 2018.

[87] T. Xu, Z. Li, J. Peng, A. Tan, Y. Song, Y. Li, J. Chen, and M. Wang, "Decoding of 10-G Optics-Based 50-Gb/s PAM-4 Signal Using Simplified MLSE," *IEEE Photonics Journal*, vol. 10, no. 4, pp. 1–8, 2018.

[88] N. Cvijetic, "OFDM for next-generation optical access networks," *Journal of Lightwave Technology*, vol. 30, no. 4, pp. 384–398, 2012.

[89] N. Cvijetic, "OMG3 OFDM in Optical Access Networks," in *2011 Optical Fiber Communications Conference and Exhibition (OFC)*, (Los Angeles, CA, USA), p. OMG3, 2011.

[90] Q. Zhuge, M. Morsy-Osman, M. E. Mousa-Pasandi, X. Xu, M. Chagnon, Z. A. El-Sahn, C. Chen, and D. V. Plant, "Single channel and WDM transmission of 28 Gbaud zero-guard-interval CO-OFDM," *Optics Express*, vol. 20, no. 26, pp. B439–B444, 2012.

[91] A. J. Lowery and L. Du, "All-optical OFDM transmitter design using AWGRs and low-bandwidth modulators," *Optics Express*, vol. 19, no. 17, pp. 15696–15704, 2011.

[92] S. Y. Jung, S. M. Jung, and S. K. Han, "I/Q channel separated baseband OFDM optical transmission using orthogonal polarizations in IM/DD system," *Journal of Lightwave Technology*, vol. 32, no. 13, pp. 2392–2398, 2014.

[93] L. Chen, B. Krongold, and J. Evans, "Performance analysis for optical OFDM transmission in short-range IM/DD systems," *Journal of Lightwave Technology*, vol. 30, no. 7, pp. 974–983, 2012.

[94] F. Barrami, Y. Le Guennec, E. Novakov, J. M. Duchamp, and P. Busson, “A novel FFT/IFFT size efficient technique to generate real time optical OFDM signals compatible with IM/DD systems,” in *2013 European Microwave Conference EuMC)*, (Nuremberg, Germany), pp. 01–29, 2013.

[95] A. Aldhaibani, S. Aljunid, H. Fadhil, and A. Matsafar, “Dispersion compensation in optical SSB-OFDM transmission over 288 km using direct detection technique,” in *2015 International Conference on Intelligent Systems, Modelling and Simulation (ISMS)*, (Langkawi, Malaysia), pp. 680–682, 2015.

[96] S. D. Dissanayake, S. Member, J. Armstrong, and S. Member, “Comparison of ACO-OFDM , DCO-OFDM and ADO-OFDM in IM / DD Systems,” *Journal of Lightwave Technology*, vol. 31, no. 7, pp. 1063–1072, 2013.

[97] F. Yang, Y. Sun, and J. Gao, “Adaptive LACO-OFDM with Variable Layer for Visible Light Communication,” *IEEE Photonics Journal*, vol. 9, no. 6, p. 7907908, 2017.

[98] G. Nauryzbayev, M. Abdallah, and H. Elgala, “Outage of SEE-OFDM VLC-NOMA networks,” *IEEE Photonics Technology Letters*, vol. 31, no. 2, pp. 121–124, 2019.

[99] I. Cano, X. Escayola, V. Polo, M. Santos, and J. Prat, “Sign labeled OFDM with intensity-modulation direct detection for PONs,” in *2012 European Conference on Optical Communication (ECOC)*, (Amsterdam, The Netherlands), p. P6.04, 2012.

[100] K. Kanonakis, I. Tomkos, H. G. Krimmel, F. Schaich, C. Lange, E. Weis, J. Leuthold, M. Winter, S. Romero, P. Kourtessis, M. Milosavljevic, I. N. Cano, and J. Prat, “An OFDMA-based optical access network architecture exhibiting ultra-high capacity and wireline-wireless convergence,” *IEEE Communications Magazine*, vol. 50, no. 8, pp. 71–78, 2012.

[101] M. Wieckowski, J. B. Jensen, I. Tafur Monroy, J. Siuzdak, and J. P. Turkiewicz, “300 Mbps transmission with 4.6 bit/s/Hz spectral efficiency over 50 m PMMA POF link using RC-LED and multi-level carrierless amplitude phase modulation,” in *2011 Optical Fiber Communications Conference and Exhibition and (OFC)*, (Los Angeles, CA, USA), p. NTuB, 2011.

[102] G. H. Im, D. D. Harman, G. Huang, A. V. Mandzik, M. H. Nguyen, and J. J. Werner, “51.84 Mb/s 16-CAP ATM LAN Standard,” *IEEE Journal on Selected Areas in Communications*, vol. 13, no. 4, pp. 620–632, 1995.

[103] J. G. Proakis, M. Salehi, N. Zhou, and X. Li, *Communication Systems Engineering*. PrenticeHall, 1994.

[104] M. I. Olmedo, T. Zuo, J. B. Jensen, Q. Zhong, X. Xu, S. Popov, and I. T. Monroy, "Multiband carrierless amplitude phase modulation for high capacity optical data links," *Journal of Lightwave Technology*, vol. 32, no. 4, pp. 798–804, 2014.

[105] R. Puerta, S. Rommel, J. J. V. Olmos, and I. T. Monroy, "Up to 35 Gbps ultra-wideband wireless data transmission links," in *2016 International Symposium on Personal, Indoor and Mobile Radio Communications (PIMRC)*, (Valencia, Spain), p. WeD7.2, 2016.

[106] R. Puerta, M. Agustin, L. Chorchos, J. Tonski, J. R. Kropp, N. Ledentsov, V. A. Shchukin, N. N. Ledentsov, R. Henker, I. T. Monroy, J. J. V. Olmos, and J. P. Turkiewicz, "Effective 100 Gb/s IM/DD 850-nm Multi- and Single-Mode VCSEL Transmission Through OM4 MMF," *Journal of Lightwave Technology*, vol. 35, no. 3, pp. 423–429, 2017.

[107] G. P. Agrawal, *Fiber-Optic Communication Systems*. John Wiley & Sons, Inc., 2012.

[108] K. Kikuchi, "Fundamentals of Optical Fiber Communications," *Journal of Lightwave Technology*, vol. 34, no. 1, pp. 157–178, 2016.

[109] R. S. Vodhanel, A. F. Elrefaie, M. Z. Iqbal, R. E. Wagner, J. L. Gimlett, and S. Tsuji, "Performance of Directly Modulated DFB Lasers in 10-Gb/s ASK, FSK, and DPSK Lightwave Systems," *Journal of Lightwave Technology*, vol. 8, no. 9, pp. 1379–1386, 1990.

[110] R. S. Vodhanel, "5 Gbit/s Direct Optical DPSK Modulation of a 1530-nm DFB Laser," *IEEE Photonics Technology Letters*, vol. 1, no. 8, pp. 218–220, 1989.

[111] J. Franklin, L. Kil, D. Mooney, D. Mahgerefteh, X. Zheng, Y. Matsui, K. Mccallion, F. Fan, and P. Tayebati, "Generation of RZ-DPSK using a Chirp-Managed Laser (CML)," in *2008 Optical Fiber Communications Conference and Exhibition (OFC)*, (San Diego, CA, USA), p. JWA67, 2008.

[112] I. N. Cano, A. Lerin, V. Polo, and J. Prat, "Flexible D(Q)PSK 1.25-5 Gb/s UDWDM-PON with directly modulated DFBs and centralized polarization scrambling," in *2015 European Conference on Optical Communication (ECOC)*, (Valencia. Spain), p. Th.1.3.7, 2015.

[113] I. N. Cano, A. Lerín, V. Polo, and J. Prat, "Direct phase modulation DFBs for cost-effective ONU transmitter in udWDM PONs," *IEEE Photonics Technology Letters*, vol. 26, no. 10, pp. 973–975, 2014.

[114] K. Y. Cho, U. H. Hong, A. Agata, T. Sano, Y. Horiuchi, H. Tanaka, M. Suzuki, and Y. C. Chung, "10-Gb/s, 80-km reach RSOA-Based WDM PON employing QPSK signal and self-homodyne receiver," in *2012 Optical Fiber Communications Conference and Exhibition (OFC)*, (Los Angeles, CA, USA), p. OW1B1, 2012.

[115] K. Y. Cho, U. H. Hong, A. Agata, T. Sano, M. Suzuki, and Y. C. Chung, "Electronic phase equalization technique for 10-Gb/s RSOA-based coherent WDM PON," in *2012 Opto-Electronics and Communications Conference (OECC)*, (Busan, Korea), pp. 3A1–1, 2012.

[116] J. J. Martínez, J. I. Garcés Gregorio, A. López Lucia, A. Villafranca Velasco, J. C. Aguado, and M. Á. Losada Binué, "Novel WDM-PON architecture based on a spectrally efficient IM-FSK scheme using DMLs and RSOAs," *Journal of Lightwave Technology*, vol. 26, no. 3, pp. 350–356, 2008.

[117] I. Garces, J. C. Aguado, J. J. Martinez, A. Lopez, A. Villafranca, and M. A. Losada, "Analysis of narrow-FSK downstream modulation in colourless WDM PONs," *Electronics Letters*, vol. 43, no. 8, pp. 471 – 472, 2007.

[118] J. B. Jensen, R. Rodes, A. Caballero, N. Cheng, D. Zibar, and I. T. Monroy, "VCSEL based coherent PONs," *Journal of Lightwave Technology*, vol. 32, no. 8, pp. 1423–1433, 2014.

[119] G. Jacobsen, "Performance of heterodyne DM-DPSK systems with thight IF filtering," *Electronics Letters*, vol. 28, no. 3, pp. 254–256, 1992.

[120] M. T. Core and H. H. Tan, "BER for optical heterodyne DPSK receivers using delay demodulation and integration detection," *IEEE Transactions on Communications*, vol. 50, no. 1, pp. 21–30, 2002.

[121] X. Liu, A. H. Gnauck, X. Wei, J. Hsieh, C. Ai, and V. Chien, "Athermal optical demodulator for OC-768 DPSK and RZ-DPSK signals," *IEEE Photonics Technology Letters*, vol. 17, no. 12, pp. 2610–2612, 2005.

[122] S. Yamazaki and K. Emura, "Feasibility Study on QPSK Optical-Heterodyne Detection System," *Journal of Lightwave Technology*, vol. 8, no. 11, pp. 1646–1653, 1990.

[123] J. Zhang, J. Yu, Z. Dong, N. Chi, X. Li, and G. K. Chang, "Nonlinear compensation and inter-channel crosstalk suppression for 4x160.8Gb/s DWDM PDM-QPSK signal with heterodyne coherent detection," in *2013 Optical Fiber Communications Conference and Exhibition (OFC)*, p. JW2A.43, 2013.

[124] N. Ye, M. Gleeson, H. Yang, H. Zhang, B. Roycroft, K. Thomas, A. Gocalinska, E. Pelucchi, Z. Li, D. Richardson, H. Chen, A. M. Koonen, W. Jia, J. Zhao, F. G. Gunning, F. Peters, and B. Corbett, "Demonstration of 90 optical hybrid at 2 μm wavelength range based on 4x4 MMI using diluted waveguide," in *2014 European Conference on Optical Communication (ECOC)*, (Cannes, France), p. P.2.14, 2014.

[125] M. Lu, A. Bhardwaj, A. Sivananthan, L. A. Johansson, H. Park, E. Bloch, M. J. Rodwell, and L. A. Coldren, "A widely-tunable integrated coherent optical receiver using a phase-locked loop," in *2011 IEEE Photonic Society 24th Annual Meeting*, p. ThL4, 2011.

[126] E. Torrengo, V. Ferrero, and S. Camatel, "A 20-Gb/s quadrature phase-shift-keying real-time coherent system based on a subcarrier optical phase-locked loop," *IEEE Photonics Technology Letters*, vol. 21, no. 18, pp. 1296–1298, 2009.

[127] M. Lu, H. C. Park, E. Bloch, A. Sivananthan, J. S. Parker, Z. Griffith, L. A. Johansson, M. J. Rodwell, and L. A. Coldren, "An integrated 40 Gbit/s optical costas receiver," *Journal of Lightwave Technology*, vol. 31, no. 13, pp. 2244–2253, 2013.

[128] C. Xie, P. J. Winzer, G. Raybon, A. H. Gnauck, B. Zhu, T. Geisler, and B. Edvold, "Colorless coherent receiver using 3x3 coupler hybrids and single-ended detection," *Optics Express*, vol. 20, no. 2, pp. 1164–1171, 2011.

[129] P. Runge, F. Ganzer, G. Zhou, R. Zhang, A. Seeger, M. Schell, P. J. Reyes-Iglesias, D. Pérez-Galacho, A. Ortega-Moñux, and I. Molina-Fernández, "Monolithic integrated InP receiver chip for coherent phase sensitive detection in the C- and L-band for colorless WDM applications," in *European Conference on Optical Communication, ECOC*, (Cannes, France), p. P.2.2, 2014.

[130] B. Koch, R. Noé, V. Mirvoda, D. Sandel, V. Filsinger, and K. Puntsri, "40-krad/s polarization tracking in 200-Gb/s PDM-RZ-DQPSK transmission over 430 km," *IEEE Photonics Technology Letters*, vol. 22, no. 9, pp. 613–615, 2010.

[131] L. E. Nelson, Y. Pan, M. Birk, R. Isaac, C. Rasmussen, M. Givehchi, and B. Mikkelsen, "WDM performance and multiple-path interference tolerance of a real-time 120 Gbps pol-mux QPSK transceiver with soft decision FEC," in *2012 Optical Fiber Communications Conference and Exhibition (OFC)*, (Los Angeles, CA, USA), p. NTh1I.5, 2012.

[132] M. S. Erkilinc, D. Lavery, K. Shi, B. C. Thomsen, R. I. Killey, S. J. Savory, and P. Bayvel, "Comparison of low complexity coherent receivers for UDWDM-PONs (λ-to-the-User)," *Journal of Lightwave Technology*, vol. 36, no. 16, pp. 3453–3464, 2018.

[133] M. Erkılınç, D. Lavery, P. Bayvel, R. Killey, S. Savory, and C. Schubert, "Coherent ONU Designs for 50 Gb/s/λ PON," in *2019 Optical Fiber Communications Conference and Exhibition (OFC)*, (San Diego, CA, USA), p. Th3F.5, OSA, 2019.

[134] B. Glance, "Polarization Independent Coherent Optical Receiver," *Journal of Lightwave Technology*, vol. 5, no. 2, pp. 274–276, 1987.

[135] M. Kavehrad and B. S. Glance, "Polarization-Insensitive Frequency Shift Keying Optical Heterodyne Receiver Using Discriminator Demodulation," *Journal of Lightwave Technology*, vol. 6, no. 9, pp. 1386–1394, 1988.

[136] T. E. Darcie, B. Glance, K. Gayliard, J. R. Talman, B. L. Kasper, and C. A. Burrus, "Polarisation-diversity receiver for coherent FSK communications," *Electronics Letters*, vol. 23, no. 25, pp. 1369–1371, 1987.

[137] E. Ciaramella, "Polarization-independent receivers for low-cost coherent OOK systems," *IEEE Photonics Technology Letters*, vol. 26, no. 6, pp. 548–551, 2014.

[138] J. Tabares, V. Polo, and J. Prat, "Polarization-Independent Heterodyne DPSK Receiver Based on 3x3 Coupler for Cost-Effective udWDM-PON," in *2017 Optical Fiber Communications Conference and Exhibition (OFC)*, (Los Angeles, CA, USA), p. Th1K.3, OSA, 2017.

[139] I. N. Cano, A. Lerin, V. Polo, and J. Prat, "Polarization independent single-PD coherent ONU receiver with centralized scrambling in udWDM-PONs," in *2014 European Conference on Optical Communication (ECOC)*, (Cannes, France), p. P.7.12, 2014.

[140] M. S. Erkilinç, D. Lavery, K. Shi, B. C. Thomsen, P. Bayvel, R. I. Killey, and S. J. Savory, "Polarization-insensitive single-balanced photodiode coherent receiver for long-reach WDM-PONs," *Journal of Lightwave Technology*, vol. 34, no. 8, pp. 2034–2041, 2016.

[141] M. S. Erkilinc, D. Lavery, R. Maher, M. Paskov, B. C. Thomsen, P. Bayvel, R. I. Killey, and S. J. Savory, "Polarization-insensitive single balanced photodiode coherent receiver for passive optical networks," in *2015 European Conference on Optical Communication (ECOC)*, p. Th.1.3.3, 2015.

[142] L. Bjerkan, A. Røyset, L. Hafskjær, and D. Myhre, "Measurement of laser parameters for simulation of high-speed fiberoptic systems," *Journal of Lightwave Technology*, vol. 14, no. 5, pp. 839–850, 1996.

[143] A. Villafranca, J. Lasobras, and I. Garces, “Precise characterization of the frequency chirp in directly modulated DFB lasers,” in *2007 Spanish Conference on Electron Devices*, (Madrid, Spain), p. P3.10, 2007.

[144] L. Anet Neto, D. Erasme, N. Genay, P. Chanclou, Q. Deniel, F. Traore, T. Anfray, R. Hmadou, and C. Aupetit-Berthelemot, “Simple estimation of fiber dispersion and laser chirp parameters using the downhill simplex fitting algorithm,” *Journal of Lightwave Technology*, vol. 31, no. 2, pp. 334–342, 2013.

[145] A. Mecozzi, C. Antonelli, and M. Shtaif, “Kramers – Kronig receivers,” *Advances is Optics and Photonics*, vol. 11, no. 3, pp. 480–517, 2019.

[146] C. Sun, D. Che, and W. Shieh, “Comparison of chromatic dispersion sensitivity between kramers-kronig and SSBI iterative cancellation receiver,” in *2018 Optical Fiber Communications Conference and Exhibition (OFC)*, (San Diego, CA, USA), p. W4E4, 2018.

[147] W. R. Peng, S. Chi, B. Zhang, X. Wu, A. E. Willner, and K. M. Feng, “Spectrally Efficient Direct-Detected OFDM Transmission Incorporating a Tunable Frequency Gap and an Iterative Detection Techniques,” *Journal of Lightwave Technology*, vol. 27, no. 24, pp. 5723–5735, 2009.

[148] M. Q. Le, P. J. Hurst, and J. P. Keane, “An Adaptive Analog Noise-Predictive,” *IEEE Journal of Solid-State Circuits*, vol. 37, no. 2, pp. 105–113, 2002.

[149] ITU-T, “G.983.1 Broadband optical access systems based on Passive Optical Networks (PON),” 2005.

[150] ITU-T, “G.983.2 ONT management and control interface specification for B-PON,” 2005.

[151] ITU-T, “G.983.3: A Broadband Optical Access System with Increased Service Capability by Wavelength Allocation,” 2001.

[152] ITU-T, “G.983.4 A broadband optical access system with increased service capability using dynamic bandwidth assignment,” 2001.

[153] ITU-T, “G.983.5 A broadband optical access system with enhanced survivability,” 2002.

[154] ITU-T, “G.984.1 Gigabit-capable passive optical networks (GPON): General characteristics,” 2008.

[155] ITU-T, “G.984.2 Gigabit-capable Passive Optical Networks (GPON): Physical Media Dependent (PMD) layer specification,” 2003.

[156] ITU-T, "G.984.3 Gigabit-capable passive optical networks (G-PON): Transmission convergence layer specification," 2014.

[157] ITU-T, "G.984.4 Gigabit-capable Passive Optical Networks (G-PON): ONT management and control interface specification," 2008.

[158] ITU-T, "G.984.5 Gigabit-capable Passive Optical Networks (G-PON): Enhancement band," 2007.

[159] ITU-T, "G.984.6 Gigabit-capable passive optical networks (GPON): Reach extension," 2008.

[160] ITU-T, "G.984.7 Gigabit-capable passive optical networks (GPON): Long reach," 2010.

[161] ITU-T, "G.987 10-Gigabit-capable passive optical network (XG-PON) systems: Definitions, abbreviations and acronyms," 2012.

[162] ITU-T, "G.987.1 10-Gigabit-capable passive optical networks (XG-PON): General requirements," 2016.

[163] ITU-T, "G.987.2 10-Gigabit-capable passive optical networks (XG-PON): Physical media dependent (PMD) layer specification," 2016.

[164] ITU-T, "G.987.3 10-Gigabit-capable passive optical networks (XG-PON): Transmission convergence (TC) layer specification," 2014.

[165] ITU-T, "G.987.4 10 Gigabit-capable passive optical networks (XG-PON): Reach extension," 2012.

[166] ITU-T, "G.988 ONU management and control interface (OMCI) specification," 2017.

[167] ITU-T, "G.989.1 40-Gigabit-capable passive optical networks (NG-PON2): General requirements," 2013.

[168] ITU-T, "G.989.2 40-Gigabit-capable passive optical networks 2 (NG-PON2): Physical media dependent (PMD) layer specification," 2014.

[169] ITU-T, "G.989.3 40-Gigabit-capable passive optical networks (NG-PON2): Transmission convergence layer specification," 2015.

[170] ITU-T, "G.9807.1 10-Gigabit-capable symmetric passive optical network (XGS-PON)," 2016.

[171] ITU-T, "G.9807.2 10 Gigabit-capable passive optical networks (XG(S)-PON): Reach extension," 2017.

[172] Communications Industry Researchers (CIR), "Current and Future Markets for PON, the Evolution to NG-PON Technology: 2017-2026," tech. rep., 2017.

[173] IEEE, "802.3ah-2004 Media Access Control Parameters, Physical Layers, and Management Parameters for Subscriber Access Networks," 2004.

[174] IEEE, "802.3bk-2013 Physical Layer Specifications and Management Parameters for Extended Ethernet Passive Optical Networks," 2013.

[175] IEEE, "802.3av-2009 Physical Layer Specifications and Management Parameter for 10 Gb/s Passive Optical Networks," 2009.

[176] S. Gorshe and J. Mandin, "Introduction to IEEE 802.3av 10Gbit/s Ethernet Passive Optical Networks (10G EPON)," tech. rep., 2009.

[177] IEEE, "802 . 3 Industry Connections Feasibility Assessment for the Next Generation of EPON," no. March, 2015.

[178] C. Knittle, "IEEE 100 Gb / s EPON," in *2016 Optical Fiber Communications Conference and Exhibition (OFC)*, (Anaheim, CA, USA), p. Th1I.6, 2016.

[179] ITU-T, "G.suplement 64 PON transmission technologies above 10 Gbit/s per wavelength," vol. 64, 2018.

List of Acronyms

- 100G-EPON - 100 Gbps Ethernet passive optical network
- 10G-EPON - 10 Gigabit Ethernet passive optical network
- 1G-EPON - 1 Gigabit Ethernet passive optical network
- 25G-EPON - 25 Gbps Ethernet passive optical network
- 40G-EPON - 40 Gbps Ethernet passive optical network
- 50G-EPON - 50 Gbps Ethernet passive optical network
- ACO-OFDM - Asymmetrical clipped optical orthogonal frequency division multiplexing
- AES - Advanced encryption standard
- AO-OFDM - All-optical orthogonal frequency division multiplexing
- APD - Avalanche photodiode
- A-PON - Asynchronous transfer mode passive optical network
- APS - Automatic protection switching
- ATM - Asynchronous transfer mode
- AWG - Arrayed waveguide grating
- BER - Bit error rate
- BPF - Band pass filter
- BTB - Back-to-back
- CAP - Carrierless amplitude phase modulation
- CAPEX - Cost of deployment
- CD - Chromatic dispersion
- CO - Central office
- COCONUT - Cost-effective coherent ultra-dense-WDM-PON for lambda-to-the-user access networks
- CO-OFDM - Coherent optical orthogonal frequency division multiplexing
- CP - Cyclic prefix
- CPRI - Common public radio interface
- CWDM - Coarse wavelength division multiplexing
- DB - Duobinary
- DBA - Dynamic bandwidth allocation

- DC - Direct current
- DCA - Digital communication analyzer oscilloscope
- DCO-OFDM - Direct current biased optical orthogonal frequency division multiplexing
- DD - Direct detection
- DFB - Distributed feedback laser
- DFE - Decision feedback equalizer
- DISCUS - The distributed core for unlimited bandwidth supply for all users and services
- DML - Direct modulated laser
- DMT - Discrete multitone
- DPSK - Differential phase shift keying
- DSP - Digital signal processing
- DWDM - Dense wavelength division multiplexing
- DWDM-PON - Dense wavelength division multiplexing passive optical network
- EAM - Electro-absorption modulator
- ECL - External cavity laser
- EDB - Electrical duobinary
- EDFA - Erbium doped fiber amplifier
- EML - Externally modulated laser
- EU - European Union
- FEC - Forward error correction
- FFE - Feed forward equalizer
- FM/AM - Frequency modulation/amplitude modulation
- FSAN - Full service access networks
- FTTA - Fiber-to-the-antenna
- FTTB - Fiber-to-the-business
- FTTC - Fiber-to-the-curb
- FFTH - Fiber-to-the-home
- FTTN - Fiber-to-the-neighborhood
- FFTO Fiber-to-the-office
- FTTP - Fiber-to-the-premises
- FTTU - Fiber-to-the-user
- FTTx - Fiber-to-the-x
- GEM - G-PON encapsulation mode
- GFP - Generic framing procedure
- GigaWaM - Giga bit access passive optical network using wavelength division multiplexing
- G-PON - Gigabit-capable passive optical network

- GTC - G-PON transmission convergence
- HRCOSA - High resolution complex optical spectral analyzer
- I - In-phase
- IEEE - Institute of electrical and electronics engineers
- IF - Intermediate Frequency
- iFFT - Inverse fast Fourier transform
- IM - Intensity modulation
- IM/DD - Intensity modulation/direct detection
- IM/DD-OFDM - Intensity modulation/direct detection orthogonal frequency division multiplexing
- IoT - Internet of things
- ISI - Intesymbolic interference
- ITU-T - International telecommunication union - telecommunication standardization sector
- KK - ramers-Kronig
- LACO-OFDM - Layered asymmetrical clipped optical orthogonal frequency division multiplexing
- LO - Local oscillator
- LPF - Low pass filter
- LR-PON - Long reach passive optical network
- MGY - Modulated grating Y-branch laser
- MPCP - Multipoint control protocol
- MSE - Maximum spectral excursion
- MW-PON - Multiple-wavelength passive optical network
- MZM - Mach-Zehnder Modulator
- NFV - Network function virtualization
- NG-EPON - Next generation Ethernet passive optical network
- NGOA - Next generation optical access
- NG-PON2 - 40 Gigabit-capable passive optical network
- NRZ - Non-return to zero
- OAM - Operations, administration, and maintenance
- OASE - Optical access seamless evolution
- ODB - Optical duobinary
- ODN - Optical distribution network
- OFDM - Orthogonal frequency division multiplexing
- OFDMA - Orthogonal frequency division multiple access
- OLT - Optical line terminator

- OMCI - ONU Management and Control Interface
- ONU - Optical network unit
- OOB - Out-of-band
- OOC - Out-of-channel
- OOK - On-off keying
- OPEX - Cost of operation
- OPL - Optical path loss
- OPLL - Optical phase-locked loop
- OSNR - Optical signal-to-noise ratio
- OTL - Optical trunk line
- PAM - Pulse amplitude modulation
- PAPR - Peak to average power ratio
- PBS - Polarization beam splitter
- PCB - Printed circuit board
- PD - Photodiode
- PDM - Physical media dependent
- PIEMAN - Photonic integrated extended metro and access network
- PLL - Phase-locked loop
- PLOAM - Physical layer operation, administration and maintenance
- PON - Passive optical network
- PSK - Phase shift keying
- PTBC - Polarization-time block code
- PtMP - Point-to-multipoint
- PtP - Point-to-point
- Q - Quadrature
- QAM - Quadrature amplitude modulation
- QoS - Quality of service
- RC - Raised cosine
- RM - Remote node
- RRC - Root raised cosine
- RRU - Radio remote unit
- RS - Reed-Solomon
- RSOA - Reflective semiconductor optical amplifier
- SARDANA - Scalable advanced ring-based passive dense access network architecture
- SDM - Spatial division multiplexing
- SDN - Software defined network
- SEE-OFDM - Spectral and energy efficent orthogonal frequency division multiplexing

- SOA - Semiconductor optical amplifier
- SSBI - Signal-signal beating interference
- SSMF - Standard single mode fiber
- TC - Transmission convergence
- TDMA - Time division multiple access
- TDM-PON - Time division multiplexing passive optical network
- TWDMA Time and wavelength-division multiple access
- TWDM-PON - Time and wavelength division multiplexing passive optical network
- uDWDM - Ultra-dense wavelength division multiplexing
- VCSEL - Vertical cavity surface emitting laser
- WDM - Wavelength division multiplexing
- WDMA - Wavelength division multiple access
- WDM-PON - Wavelength division multiplexing passive optical network
- WR-ODN - Wavelength-routed optical distribution network
- WR-WDM - Wavelength routed wavelength division multiplexing
- WS-ODN - Wavelength-selected optical distribution network
- WS-WDM - Wavelength selected wavelength division multiplexing
- XGEM - XG-PON encapsulation mode
- XG-PON - 10 Gigabit-capable passive optical network
- XGS-PON - 10 Gigabit-capable symmetric passive optical network
- XGTC - XG-PON transmission convergence

List of Figures

2.1 Current telecommunication networks. 10
2.2 FTTx concept. 11
2.3 TDM-PON network: (a) downlink, (b) uplink. 13
2.4 WDM-PON network: (a) downlink, (b) uplink. 14
2.5 TWDM-PON network: (a) downlink, (b) uplink. 15
2.6 Difference between coarse and dense WDM-PON. 16
2.7 PIEMAN. [64] 17
2.8 SARDANA. [66] 17
2.9 GigaWaM. [70] 18
2.10 OASE. [71] 18
2.11 DISCUS. [76] 19
2.12 Difference between DWDM and uDWDM PON. 19
2.13 COCONUT. [81] 20
2.14 Duobinary. 21
2.15 NRZ, EDB, ODB and PAM-4 optical power eye diagrams and spectrum with R_b data rate. 22
2.16 M-PSK and M-QAM constellations. 23
2.17 OFDM block diagram. 24
2.18 Real OFDM: Hermitian. 25
2.19 OFDMA. 26
2.20 Time and frequency response of the multiCAP filters. 27
2.21 IQ modulator. 28
2.22 Dual-polarization IQ modulator. 28
2.23 Coherent receiver based on 2x2 optical coupler. 29
2.24 Heterodyne, homadyne and intradyne electrical spectra. 30
2.25 Heterodyne electical and digital receiver part. 31
2.26 Phase-diversity homodyne coupler (90º hybrid). 31
2.27 Digital signal processing of a coherent intradyne receiver. 32
2.28 Coherent 3x3 receiver (120º hybrid). 33

2.29 Polarization-diversity intradyne coupler (90º hybrid). 34
2.30 Digital signal processing of a coherent polarization-diversity intradyne receiver. 35
2.31 Ciaramella receiver. 35

4.1 Current vs. optical power of JDSU CQF915/1839. 83
4.2 Photo of the equalization board of the DFB. 83
4.3 1 Gbps DPSK with a directly phase-modulated DFB high resolution optical spectrum. 84
4.4 Current vs. optical power of Raycan VCSEL RC33xxx1-F for 25 ºC. Inlet: Optical spectrum of VCSEL. 85
4.5 Experimental setup for chirp parameters characterization. 85
4.6 α, f_c and κ vs. different bias currents. 86
4.7 (a) 1.25 Gbps ideal pulse-shaping modulation signal and measured optical signal, simulated: (b) transient and adiabatic chirp, and (c) total phase and the generated phase by the transient and adiabatic chirps. 87
4.8 2.5 Gbps DPSK with a directly phase-modulated VCSEL: (a) Optical phase eye diagram and (b) Optical IQ diagram. 88
4.9 1.25 Gbps (a) and 2.5 Gbps (b) DPSK with a directly phase-modulated VCSEL high resolution optical spectrum. 88
4.10 RSOA-VCSEL transmitter setup. 89
4.11 1 Gbps DPSK with a directly phase-modulated RSOA pumped with a VCSEL. Experimental optical: (a) phase eye diagram and (b) IQ diagram. 90
4.12 1 Gbps DPSK with a directly phase-modulated RSOA pumped with a VCSEL high resolution optical spectrum and 1 Gbps Nyquist-DPSK over a MZM separated by 2 GHz. 90
4.13 Single PD heterodyne receiver. 91
4.14 DPSK demodulation diagram with a single PD heterodyne receiver and the electrical spectra at the different demodulation stages. 93
4.15 Polarization independent DPSK heterodyne receiver. 94
4.16 Polarization independent quasi-coherent receiver. 96
4.17 Theoretical envelope detector (a), analog implementation of envelope detector (b). Electrical spectra at the different demodulation stages for (a). 98
4.18 FFE/DFE equalizer schematic. 98
4.19 Bandwidth and lower cut-off frequency optimization of digital BPF for IF = 1 GHz (a) and IF = 2 GHz (b). 99
4.20 Sensitivity for 1 Gbps link based on directly-phase modulated DFB and a single PD heterodyne receiver for an IF of 1 GHz and 2 GHz. 100

4.21 Sensitivity for 1 Gbps link based on directly-phase modulated RSOA pumped with a VCSEL and a single PD heterodyne receiver. 100
4.22 Sensitivity for 1.25 Gbps - 2.5 Gbps link based on directly-phase modulated VCSEL and a single PD heterodyne receiver. 101
4.23 Experimental setup for bidirectional link based on 1 Gbps uplink based on directly-phase modulated DFB and a single PD heterodyne receiver with ECL as LO and a 1 Gbps downlink based on Nyquist-DPSK over MZM with a single PD heterodyne receiver with a DFB as LO. 103
4.24 BER penalty for bidirectional transmission for the uplink (a) and downlink (b) with directly-phase modulated DFB uplink and Nyquist-DPSK over MZM downlink. 104
4.25 Spectra of both links and the LO positions for the bidirectional link based on directly-phase modulated DFB uplink and Nyquist-DPSK over MZM downlink. 104
4.26 Experimental setup for bidirectional link based on 1 Gbps uplink based on directly-phase modulated RSOA pumped by a VCSEL and a single PD heterodyne receiver with ECL as LO and a 1 Gbps downlink based on Nyquist-DPSK over MZM with a single PD heterodyne receiver with a VCSEL as LO. 105
4.27 BER penalty for bidirectional transmission for the uplink (a) and downlink (b) with directly-phase modulated RSOA pumped with a VCSEL uplink and Nyquist-DPSK over MZM downlink. 105
4.28 Sensitivity for bidirectional link based on 1 Gbps uplink based on directly-phase modulated RSOA pumped by a VCSEL and a single PD heterodyne receiver with ECL as LO and a 1 Gbps downlink based on Nyquist-DPSK over MZM with a single PD heterodyne receiver with a VCSEL as LO. 106
4.29 Experimental setup for 10 Gbps quasicoherent receiver 107
4.30 BER vs. received power curves for different LO powers. 108
4.31 BER vs. received power curves for 10 Gbps quasicoherent receiver (QC) and direct detection (DD). 109
4.32 Sensitivity vs. intermediate frequency for 10 Gbps quasicoherent receiver. . . . 109
4.33 BER vs. received power curves for 25 Gbps quasicoherent receiver with NRZ detection. 110
4.34 BER vs. received power curves for 25 Gbps quasicoherent receiver with duobinary detection. 111

A.1 Wavelength plan standards. 150

List of Tables

4.1 Summary of the links with different directly-phase modulated transmitters and single PD heterodyne receivers. 102
4.2 Summary of the links with Nyquist-DPSK over a MZM with single PD heterodyne receivers with different LOs. 102
4.3 Summary of the bidirectional links. 107
4.4 Summary of the quasicoherent receivers. 112

A.1 B-PON OPL class. 150
A.2 Launch powers, sensitivities and overloads for B-PON OPL classes. 151
A.3 G-PON OPL class. 152
A.4 Launch powers, sensitivities and overloads for G-PON OPL classes. 152
A.5 XG-PON OPL class 154
A.6 Launch powers, sensitivities and overloads for XG-PON OPL classes. 154
A.7 NG-PON2 OPL class 156
A.8 Launch powers, sensitivities and overloads for TWDM NG-PON2 OPL classes without preamplifier (Type A) and with preamplifier (Type B) in the OLT. . . . 157
A.9 XGS-PON OPL class 159
A.10 Launch powers, sensitivities and overloads for XGS-PON OPL classes. 160
A.11 1G-EPON OPL class 160
A.12 Launch powers, sensitivities and maximum receive power for 1G-EPON classes. 161
A.13 10G-EPON OPL class 162
A.14 Launch powers, sensitivities and maximum receive power for 10G-EPON classes. 163

Appendix A

PON standards

A.1 ITU-T

The full service access networks (FSAN) group was formed in 1995 for generating a common framework for access networks and since that moment it has released the following five standards for optical access networks and currently is working in the futures standards.

A.1.1 B-PON

The FSAN group proposed a standard to ITU-T based on asynchronous transfer mode (ATM) protocol for PON in 1998. This standard was called ATM-PON or A-PON. Afterwards, the standard was renamed to Broadband PON or B-PON [56], due to the inclusion of other services, as broadcast video or Ethernet services, over the PON. The B-PON standard was updated in 2005 and some of the previous recommendations were merged [149–153].

B-PON proposes downlink rates of 155.52, 622.08 and 1244.16 Mbps and uplink rates of 155.52 and 622.08 Mbps. B-PON uses TDM for downlink and TDMA for uplink for multiplexing the different ONUs and a DBA mechanism is implemented in order to optimize the usage of the network. The TDM and TDMA have been shown in Figure 2.3.

The B-PON standard is based on ATM transport protocols which are formed by the physical media dependent (PDM) layer, the Transmission convergence (TC) layer and the ATM protocols. The PDM layer contains the modulation schemes for downlink and uplink and TC layer manages the distrusted access to the uplink. Each TDM or TDMA time slots contain ATM or physical layer operation, administration and maintenance (PLOAM) cells. The communication between OLT and ONUs is based on ATM virtual circuits, which are able to implement different levels of quality of service (QoS). Additionally, optional services can be included as advanced encryption standard (AES) or automatic protection switching (APS).

B-PON defines three optical path loss (OPL) classes for the ODN, enlisted in Table A.1, with differential OPL of 15 dB for all of them. These OPL classes together with the different

Table A.1: B-PON OPL class.

	Class A	Class B	Class C
Min loss	5 dB	10 dB	15 dB
Max loss	20 dB	25 dB	30 dB

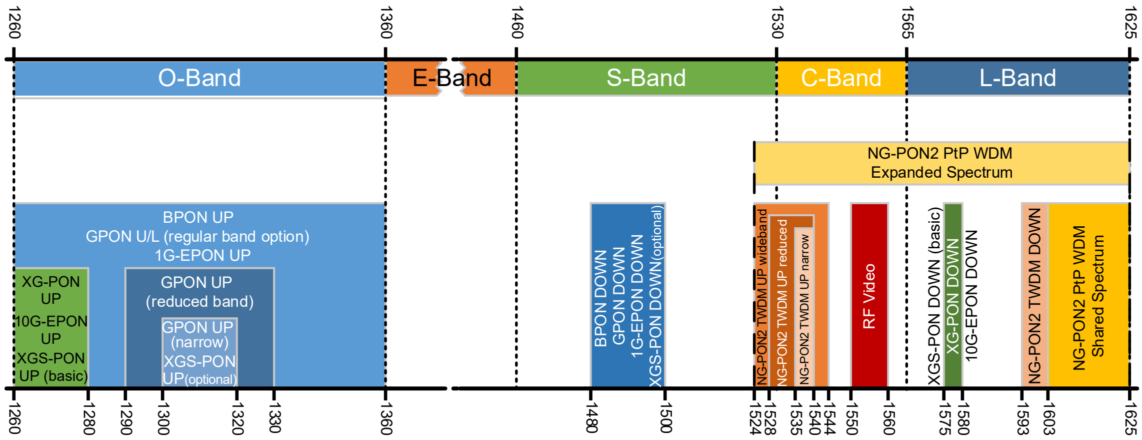

Figure A.1: Wavelength plan standards.

data rates define a set of mean launch power and receiver sensitivities and overloads, which are shown in Table A.2. The maximum physical reach of B-PON is 20 km. The downlink wavelength should be at the range of 1480-1500 nm and the uplink wavelength should be at the range of 1260-1360 nm, as can be seen in Figure A.1. In addition, B-PON defines the possibility of analog video broadcasting, which has assigned the wavelength range of 1539-1565 nm.

The B-PON standard is based on the following ITU recommendation:

- G.983.1 - Broadband optical access systems based on Passive Optical Networks (PON). This recommendation was published on 1998 and reviewed on 2005.

- G.983.2 - ONT management and control interface specification for B-PON. This recommendation was published on 2002 and reviewed on 2005 merging it with the old recommendations G.983.6 (2002), G.983.7 (2001), G.983.8 (2003), G.983.9 (2004) and G.983.10 (2004).

- G.983.3 - A broadband optical access system with increased service capability by wavelength allocation. This recommendation was published on 2001.

- G.983.4 - A broadband optical access system with increased service capability using dynamic bandwidth assignment. This recommendation was published on 2001.

- G.983.5 - A broadband optical access system with enhanced survivability. This recommendation was published on 2002.

Table A.2: Launch powers, sensitivities and overloads for B-PON OPL classes.

			Min mean launch power	Max mean launch power	Minimum sensitivity	Minimum overload
Downlink	155 Mbps	Class B	-4 dBm	+2 dBm	-30 dBm	-8 dBm
		Class C	-2 dBm	+4 dBm	-33 dBm	-11 dBm
	622 Mbps	Class A	-7 dBm	-1 dBm	-28 dBm	-6 dBm
		Class B	-2 dBm	+4 dBm	-28 dBm	-6 dBm
		Class C	-2 dBm	+4 dBm	-33 dBm	-11 dBm
	1244 Mbps	Class A	-4 dBm	+1 dBm	-25 dBm	-4 dBm
		Class B	+1 dBm	+6 dBm	-25 dBm	-4 dBm
		Class C	+5 dBm	+9 dBm	-26 dBm	-4 dBm
Uplink	155 Mbps	Class B	-4 dBm	+2 dBm	-30 dBm	-8 dBm
		Class C	-2 dBm	+4 dBm	-33 dBm	-11 dBm
	622 Mbps	Class A	-6 dBm	-1 dBm	-27 dBm	-6 dBm
		Class B	-1 dBm	+4 dBm	-27 dBm	-6 dBm
		Class C	-1 dBm	+4 dBm	-32 dBm	-11 dBm

A.1.2 G-PON

The FSAN group developed a new standard for addressing the necessities of PON with higher rates, diversity of services and a more efficient bandwidth use employing a variable length of packages. This new standard was called Gigabit-capable PON or G-PON and was released on 2003 [154–160]. One of the goals of this standard is the compatibility with the previous standards. The rates supported in this standard are 1244 Mbps and 2488 Mbps at the downlink and 155.52 Mbps, 622.08 Mbps, 1244 Mbps and 2488 Mbps at the uplinks and it can work in symmetrical or asymmetrical mode.

This standard uses the G-PON transmission convergence (GTC) layer framing which provides different functions as transport multiplexing between the OLT and the ONUs, PLOAM functions, DBA interface, ONU ranging and registration or FEC (Reed-Solomon (255,223)) and downlink data encryption as optional function. ATM and G-PON encapsulation mode (GEM) operational modes are supported in the G-PON standard. GEM is the common mode and is similar to generic framing procedure (GFP). The GEM encapsulation with segmentation capability allows TDM circuits. TDM is used for downlink and TDMA for the uplink. The required switching laser timing is 13 ns.

G-PON keeps the three OPL classes for the ODN defined on B-PON and adds 2 new OPL classes. These five OPL classes are enlisted in Table A.3 and all of them have a differential OPL of 15 dB. The combination of the OPL classes and the different data rates define a set

Table A.3: G-PON OPL class.

	Class A	Class B	Class B+	Class C	Class C+
Min loss	5 dB	10 dB	13 dB	15 dB	17 dB
Max loss	20 dB	25 dB	28 dB	30 dB	32 dB

of mean launch power and receiver sensitivities and overloads. G-PON keeps the same set of these parameter than for B-PON for the downlink with 1244 Mbps and for the uplink with 155 Mbps and 622 Mbps, and so they can be consulted on Table A.2. The G-PON standard adds the set of these parameters for downlink with 2488 Mbps and for the uplink with 1244 Mbps. In addition, it defines the set of parameters for uplink with 155 Mbps and class A, whose was not defined on B-PON. All the new set of these parameter are shown in Table A.4.

Table A.4: Launch powers, sensitivities and overloads for G-PON OPL classes.

			Min mean launch power	Max mean launch power	Minimum sensitivity	Minimum overload
Downlink	2488 Mbps	Class A	0 dBm	+4 dBm	-21 dBm	-1 dBm
		Class B	+5 dBm	+9 dBm	-21 dBm	-1 dBm
		Class B+	+1.5 dBm	+5 dBm	-27 dBm	-8 dBm
		Class C	+3 dBm (+8 dBm) [b]	+7 dBm (+12 dBm) [b]	-28 dBm (-23 dBm) [b]	-8 dBm (-3 dBm) [b]
		Class C+	+3 dBm	+7 dBm	-30 dBm	-8 dBm
Uplink [a]	155 Mbps	Class A	-6 dBm	0 dBm	-27 dBm	-5 dBm
	1244 Mbps	Class A	-3 dBm (-7 dBm) [c]	+2 dBm (-2 dBm) [c]	-24 dBm (-28 dBm) [c]	-3 dBm (-7 dBm) [c]
		Class B	-2 dBm	+3 dBm	-28 dBm	-7 dBm
		Class B+	+0.5 dBm	+5 dBm	-28 dBm	-8 dBm
		Class C	+2 dBm	+7 dBm	-29 dBm	-8 dBm
		Class C+	+0.5 dBm	+5 dBm	-32 dBm	-12 dBm

[a] The specification of 2488 Mbps uplink is not defined on G-PON standard.
[b] Considering future transmitters based on DFB+SOA.
[c] Considering receivers based on APD.

The maximum physical reach supported by this standard is 20 km with a split ratio of 1:64 (considering also a maximum reach of 60km or a split ratio of 1:128 for future necessities). The maximum differential reach considered by the standard is 20 km. G-PON also standardized the possibility of LR-PON compatible with at least class B+. These LR-PONs have a reach extender placed after a first optical trunk line (OTL). This reach extender can be an optical amplifier or an optical-electrical-optical regenerator. The LR-PONs allow to have a minimum physical reach of 40km with 40km of differential reach.

The downlink wavelength range is 1480-1500 nm. The uplink wavelength range are 1260-1360 nm for regular band option (using Fabry-Perot lasers), 1290-1330 nm for reduced band option (using ordinary DFB laser) and 1300-1320 nm for narrow band option (using wavelength selected lasers, i.e lasers that operates at ITU grid wavelength). The video broadcasting should be at wavelength range of 1550-1560 nm. Figure A.1 shows the overview of the wavelength assignment.

The G-PON standard is based on the following ITU recommendation:

- G.984.1 - Gigabit-capable passive optical networks (G-PON): General characteristics. This recommendation was published on 2003 and reviewed on 2008.
- G.984.2 - Gigabit-capable Passive Optical Networks (G-PON): Physical Media Dependent (PMD) layer specification. This recommendation was published on 2003.
- G.984.3 - Gigabit-capable passive optical networks (G-PON): Transmission convergence layer specification. This recommendation was published on 2004 and reviewed on 2014 including several amendments.
- G.984.4 - Gigabit-capable passive optical networks (G-PON): ONT management and control interface specification. This recommendation was published on 2004 and reviewed on 2014.
- G.984.5 - Gigabit-capable passive optical networks (G-PON): Enhancement band. This recommendation was published on 2007 and reviewed on 2014.
- G.984.6 - Gigabit-capable passive optical networks (G-PON): Reach extension. This recommendation was published on 2008.
- G.984.7 - Gigabit-capable passive optical networks (G-PON): Long reach. This recommendation was published on 2010.

A.1.3 XG-PON

The FSAN group released the standard 10Gigabit-capable Passive Optical Network (XG-PON) in 2010 in order to address the 10 Gbps communications over PON [161–166]. XG-PON originally proposed two standardized options: XG-PON1, which supports a 10 Gbps downlink and 2.5G b/s uplink and a future development XG-PON2, which supports a symmetrical 10 Gbps PON. Lately, XG-PON1 option was named as XG-PON because XG-PON2 option has finally become in an independent standard, XGS-PON, and it will be described later.

XG-PON has to coexist with the previous standard, G-PON. XG-PON use a G-PON like frames and protocols for allowing the coexistence between both standards and also it shall support Ethernet frames. The XG-PON protocol is divided on physical medium layer, TC layer and the path layer. The framing sublayer is called XG-PON transmission convergence (XGTC) and the path layer and encapsulation method is called XG-PON encapsulation mode (XGEM). XGEM allows individual traffic flows, fragmentation and data privacy. The used FEC in this standard is a RS (255,223). XG-PON downlink is based on TDM, and XG-PON uplink is burst oriented and employs TDMA to allow the access to the common medium.

The maximum physical reach of this standard is between 20 km and 60 km, with a maximum differential reach of 40 km (DD40) but also working with 20 km (DD20). The split ratio of XG-PON has to be 1:64 and considering future upgrades to 1:128 and 1:256.

Table A.5: XG-PON OPL class

	Class N1	Class N2	Class E1	Class E2
Min loss	14 dB	16 dB	18 dB	20 dB
Max loss	29 dB	31 dB	33 dB	35 dB

The uplink wavelength range is 1260-1280 nm and the downlink wavelength range is 1575-1580 nm, as shown in Figure A.1. XG-PON defines a new OPL classes, enlisted on Table A.5. The nominal classes (N1 and N2) are based on the previous classes B+ and C+, while the extended classes (E1 and E2) are newly developed. As in the previous standards, the OPL classes provides a set of parameters (mean launch power and receiver sensitivities and overloads) for both data rates and they are enlisted on Table A.6.

Table A.6: Launch powers, sensitivities and overloads for XG-PON OPL classes.

				Min mean launch power	Max mean launch power	Minimum sensitivity	Minimum overload
Downlink	10 Gbps	Class N1		+2 dBm	+6 dBm	-28 dBm	-8 dBm
		Class N2	N2a	+4 dBm	+8 dBm	-28 dBm	-8 dBm
			N2b	+10.5 dBm	+12.5 dBm	-21.5 dBm	-3.5 dBm
		Class E1		+6 dBm	+10 dBm	-28 dBm	-8 dBm
		Class E2	E2a	+8 dBm	+12 dBm	-28 dBm	-8 dBm
			E2b	+14.5 dBm	+16.5 dBm	-21.5 dBm	-3.5 dBm
Uplink	2.5 Gbps	Class N1		+2 dBm	+7 dBm	-27.5 dBm	-7 dBm
		Class N2		+2 dBm	+7 dBm	-29.5 dBm	-9 dBm
		Class E1		+2 dBm	+7 dBm	-31.5 dBm	-11 dBm
		Class E2		+2 dBm	+7 dBm	-33.5 dBm	-13 dBm

The XG-PON standard is based on the following ITU recommendation:

- G.987 - 10-Gigabit-capable passive optical network (XG-PON) systems: Definitions, abbreviations and acronyms. This recommendation was published on 2010 and reviewed on 2012.
- G.987.1 - 10-Gigabit-capable passive optical networks (XG-PON): General requirements. This recommendation was published on 2010 and reviewed on 2016.
- G.987.2 - 10-Gigabit-capable passive optical networks (XG-PON): Physical Media Dependent (PMD) layer specification. This recommendation was published on 2010 and reviewed on 2016.
- G.987.3 - 10-Gigabit-capable passive optical networks (XG-PON): Transmission Convergence (TC) layer specification. This recommendation was published on 2010 and reviewed on 2014.
- G.987.4 - 10-Gigabit-capable passive optical networks (XG-PON): Reach extension. This recommendation was published on 2012.
- G.988 - ONU Management and Control Interface (OMCI) specification. This recommendation was published on 2010 and reviewed on 2012.

A.1.4 NG-PON2

The FSAN group proposed a new standard called 40-Gigabit-capable passive optical network (NG-PON2) and ITU released in 2015 [61, 167–169]. The NG-PON2 standard is able to aggregated multiple services as residential and business access networks or mobile backhaul networks.

The NG-PON2 standard proposes two types of links: TWDM links and PtP WDM links. TWDM NG-PON2 links consist in 4 or 8 TWDM channels with rates of 2.5 or 10 Gbps for the uplink and the downlink. PtP WDM channels can support three line rate classes: class 1 with a line rate of 1.25 Gbps, class 2 with a line rate of 2.5 Gbps and class 3 with a line rate between 6.144 and 11.09 Gbps. The rate line class is selected depending on the P2P WDM client requirements, e.g. if the link has to support a common public radio interface (CPRI) option 2, the selected line rate class will be the number 1 because it requires 1.2288 Gbps, but if it has to support a CPRI option 6 or option 8, the selected line rate class will be the number 3 because they will require 6.144 and 10.1376 Gbps, respectively.

As it also happened in G-PON and XG-PON, the compatibility and coexistence with the previous standards is an important requirement. The NG-PON2 transmission convergence layer is the protocol layer of NG-PON2, including all the functionalities required for TWDM systems, as DBA, and for PtP WDM systems. The NG-PON2 standard also considers the use of FEC, employing the RS(248,232), which is a truncated version of RS(255,239), for the 2.5 Gbps links and the RS(248,216), which is a truncated version of RS(255,223), for the 10 Gbps links.

Table A.7: NG-PON2 OPL class

	TWDM and PtP WDM PON				PtP WDM PON	
	Class N1	Class N2	Class E1	Class E2	Class L1	Class L2
Min loss	14 dB	16 dB	18 dB	20 dB	8 dB	16 dB
Max loss	29 dB	31 dB	33 dB	35 dB	17 dB	25 dB

The NG-PON2 standard considers a physical reach distance of at least 40 km, denoted as DD40, but with the possibility of operating with a physical reach of 20 km, denoted as DD20. The standard also contemplates the possibility of reaching 60km with a differential fiber distance of 40 km. In an extend reach scenario the maximum distance can be up to 100 km employing reach extenders. On the other hand, the NG-PON2 standard has to be able to work with a split ratio up to 1:256, but not simultaneously with the higher physical reach distances. The PtP WDM PON can support two types of ODN: wavelength-selected ODN (WS-ODN) and wavelength-routed ODN (WR-ODN). WS-ODN uses tunable filters allowing selecting the channel at the ONU, which is the option required on the TWDM PON and ensures the compatibility with legacy PON systmes, and the WR-ODN uses wavelength splitters at ODN to routing the channels. In addition, colorless ONUs are required for an operation cost reduction. The OPL classes for NG-PON2 have been summarized on Table A.7. The NG-PON 2 standard has kept the OPL classes proposed by the XG-PON standard with a maximum differential OPL of 15 dB for TWDM and PtP WDM ODN and has added two new OPL classes with a maximum differential OPL of 9 dB for PtP WDM PON for low loss WR-PON. The OPL classes provides a set of parameters (mean launch power and receiver sensitivities and overloads) for both data rates and they are enlisted on Table A.8. In addition, The NG-PON2 standard has considered to provide a set of parameter for two types of upstream links: without preamplifier (type A) and with preamplifier (type B) at the OLT. Type A links would require more powerful ONUs and type B links would need more sensitive OLT. The set of parameter for the low loss classes L1 and L2 are nor enlisted and can be consulted in [168].

In addition, NG-PON2 defines three types of wavelength tuning time classes: Class 1 requires less than 10 μs of tuning time; class 2 requires between 10 and 25 μs of tuning time; and class 3 requires between 25 μs and 1 s of tuning time. Class 3 devices are usually based on thermal effects. Class 2 devices will allow sub-50 μs protection and class 1 will enable future dynamic bandwidth and wavelength allocation. NG-PON2 introduces requirements on crosstalk

Table A.8: Launch powers, sensitivities and overloads for TWDM NG-PON2 OPL classes without preamplifier (Type A) and with preamplifier (Type B) in the OLT.

		Class		Min mean launch power	Max mean launch power	Minimum sensitivity	Minimum overload
Downlink	2.5 Gbps	N1		0 dBm	+4 dBm	-30 dBm	-10 dBm
		N2		+2 dBm	+6 dBm	-30 dBm	-10 dBm
		E1		+4 dBm	+8 dBm	-21.5 dBm	-3.5 dBm
		E2		+6 dBm	+10 dBm	-28 dBm	-8 dBm
	10 Gbps	N1		+3 dBm	+7 dBm	-28 dBm	-7 dBm
		N2		+5 dBm	+9 dBm	-28 dBm	-7 dBm
		E1		+7 dBm	+11 dBm	-28 dBm	-7 dBm
		E2		+9 dBm	+11 dBm	-28 dBm	-9 dBm
Uplink	2.5 Gbps	N1	Type A	+4 dBm	+9 dBm	-26 dBm	-5 dBm
			Type B	0 dBm	+5 dBm	-30 dBm	-9 dBm
		N2	Type A	+4 dBm	+9 dBm	-28 dBm	-7 dBm
			Type B	0 dBm	+5 dBm	-32 dBm	-11 dBm
		E1	Type A	+4 dBm	+9 dBm	-30.5 dBm	-9 dBm
			Type B	0 dBm	+5 dBm	-34.5 dBm	-13 dBm
		E2	Type A	+4 dBm	+9 dBm	-32.5 dBm	-11 dBm
			Type B	0 dBm	+5 dBm	-36.5 dBm	-15 dBm
	10 Gbps	N1	Type A	+4 dBm	+9 dBm	-26 dBm	-5 dBm
			Type B	+2 dBm	+7 dBm	-28 dBm	-7 dBm
		N2	Type A	+4 dBm	+9 dBm	-28 dBm	-7 dBm
			Type B	+2 dBm	+7 dBm	-30 dBm	-9 dBm
		E1	Type A	+4 dBm	+9 dBm	-30.5 dBm	-9 dBm
			Type B	+2 dBm	+7 dBm	-32.5 dBm	-11 dBm
		E2 [a]	Type B	+4 dBm	+9 dBm	-32.5 dBm	-11 dBm

[a] The specification of 10 Gbps class E2 type A uplink is not defined on TWDM NG-PON2 standard.

because it uses wavelength multiplexing. The out-of-channel (OOC) interference penalty has to be less than 1 dB for the upstream and less than 0.1 dB for the downstream [168]. The out-of-band (OOB) interference penalty has to be less than 0.1 dB for both directions [168].

In NG-PON2, the wavelength stability requirements have been defined using the MSE in order to prevent a power leaking between channels and to ensure that the links operate property inside their own channels. The channel spacing of the TWDM downstream is 100 GHz and the MSE is ± 20 GHz. The channel spacing of the TWDM upstream can be in the range of 50–200 GHz and the MSE will be different for each of them. A channel spacing of 50GHz requires a MSE of ± 12.5 GHz, a channel spacing of 100 GHz requires MSE of ± 20 GHz, and a channel spacing of 200 GHz requires MSE of ± 25 GHz. The laser switching on/off can cause a short-term spectral excursion, which also have to be considered in the MSE requirements. The wavelength calibration accuracy of the TX tunable laser of the ONUs defines three categories: sufficient calibration, loose calibration, and no calibration. If the laser is not calibrated, they can be out of the MSE limit and wavelength-locking systems have to be implemented.

The wavelength range for TWDM downstream is 1596–1603 nm and for the TWDM upstream is 1524–1544 nm for wideband option, 1528–1540 nm for reduced option and 1535–1540 nm for the narrow option, as shown in Figure A.1. In the case of P2P WDM up/downstream, the wavelength range is 1524–1625 nm for the expanded spectrum option and 1603–1625 nm for the shared spectrum option.

This standard supports multiple wavelengths and has enough flexibility for the adaptation to the future necessities on the 100G and beyond age.

The NG-PON2 standard is based on the following ITU recommendation:

- G.989 - 40-Gigabit-capable passive optical networks (NG-PON2): Definitions, abbreviations and acronyms. This recommendation was published on 2015.
- G.989.1 - 40-Gigabit-capable passive optical networks (NG-PON2): General requirements. This recommendation was published on 2013 and reviewed on 2016.
- G.989.2 - 40-Gigabit-capable passive optical networks 2 (NG-PON2): Physical Media Dependent (PMD) layer specification. This recommendation was published on 2014.
- G.989.3 - 40-Gigabit-capable passive optical networks (NG-PON2): Transmission convergence layer specification. This recommendation was published on 2015.

A.1.5 XGS-PON

The FSAN group has been developing the XG-PON2 of the XG-PON standard (subsection A.1.3) as an independent standard named as XGS-PON standard [170, 171] since 2013. The XGS-PON acronym means 10-Gigabit- Capable Symmetric Passive Optical Network and it was released in 2016. The industry [172] is considering this standard as an intermediate step between the current access networks and the deployment of the NG-PON2 networks (subsection A.1.4), because this standard has also been designed for providing access services for residential and business and for mobile backhauling and the NG-PON2 technologies are not completely available yet.

As the previous standards, the XGS-PON standard protocol is divided on the physical dependent medium layer, the transmission convergence (TC) layer and the path layer. The TC layer is subdivided on the PON transmission sublayer and the adaptation sublayer, and allows implementing DBA. In this standard the path layer corresponds with the XGEM encapsulation layer. The downlink implements TDM for multiplexing the different ONUs and the upstream implements TDMA for allowing the access to the different ONUs to the common medium. Also, the FEC is implemented, specifically Reed–Solomon (255,223).

The minimum split ratios for XGS-PON should be 1:64 for ensuring the coexistence with G-PON, but the operators have shown interest on split ratios of 1:128 and 1:256. In addition, XGS-PON has to support at least 20 km of fiber reach but also the XGS-PON standard have to support a fiber reach of 60 km, to allow the coexistence with XG-PON. The required maximum differential reach is 40 km but working with steps of 20 km (DD20 and DD40).

The XGS-PON standard proposes two wavelength sets: basic and optional. The basic wavelength range is the same as in XG-PON (downlink =1575–1580 nm, uplink=1260–1280 nm). In order to support XGS-PON and legacy XG-PON ONUs in the basic wavelength set, dual-rate upstream TDMA and TDM at the downstream is used, and so the OLT has to support dual line-rates (2.5 and 10 Gbps). If the basic wavelength set is used, the legacy GPON ONUs coexistence is direct. The optional wavelength set is the same as the narrow uplink range and the downlink range of G-PON (downlink= 1480–1500 nm, uplink=1300–1320 nm). In the optional range, legacy G-PON ONU is not supported and legacy XG-PONs are supported with wavelength multiplexing. Both wavelength sets can be used simultaneously.

Table A.9: XGS-PON OPL class

	Basic wavelength set				Optional wavelength set	
	Class N1	Class N2	Class E1	Class E2	Class B+	Class C+
Min loss	14 dB	16 dB	18 dB	20 dB	13 dB	17 dB
Max loss	29 dB	31 dB	33 dB	35 dB	28 dB	32 dB

The OPL of XGS-PON depends on the wavelength set selected, as can be seen in Table A.9. If the basic wavelength set is used, the OPL is the same than in the XG-PON standard. In the case of using the optional wavelength set, the OPL is the same than in the G-PON standard. The XGS-PON OPL classes also generates a set of parameters (mean launch power and receiver sensitivities and overloads) for both wavelength sets and they can be consulted on Table A.10.

The XGS-PON standard is based on the following ITU recommendation:

- G.9807.1 - 10-Gigabit-capable symmetric passive optical network (XGS-PON). This recommendation was published on 2016.

- G.9807.2 - 10 Gigabit-capable passive optical networks (XG(S)-PON): Reach extension. This recommendation was published on 2017.

Table A.10: Launch powers, sensitivities and overloads for XGS-PON OPL classes.

			Class	Min mean launch power	Max mean launch power	Minimum sensitivity	Minimum overload
Downlink	10 Gbps	Basic wavelength set [a]	N1	+2 dBm	+5 dBm	-28 dBm	-9 dBm
			N2	+4 dBm	+7 dBm	-28 dBm	-9 dBm
			E1	+6 dBm	+9 dBm	-28 dBm	-9 dBm
		Optional wavelength set	B+	+2 dBm	+5 dBm	-27 dBm	-8 dBm
			C+	+6 dBm	+9 dBm	-27 dBm	-8 dBm
Uplink	10 Gbps	Basic wavelength set [a]	N1	+4 dBm	+9 dBm	-26 dBm	-5 dBm
			N2	+4 dBm	+9 dBm	-28 dBm	-7 dBm
			E1	+4 dBm	+9 dBm	-30 dBm	-9 dBm
		Optional wavelength set	B+	+3 dBm	+8 dBm	-26 dBm	-5 dBm
			C+	+3 dBm	+8 dBm	-30 dBm	-9 dBm

[a] The specification of class E2 uplink is not defined on XGS-PON standard.

A.2 IEEE

A.2.1 1G-EPON

The institute of electrical and electronics engineers (IEEE) standardization group defined in 2004 the 1G-EPON standard with the IEEE Standard 802.3ah-2004, Media Access Control Parameters, Physical Layers, and Management Parameters for Subscriber Access Networks [173]. Lately, the IEEE stancadrization group amended the standard for extend reach with the IEEE Standard 802.3bk-2013, Physical Layer Specification and Management Parameters for Extended Ethernet Passive Optical Networks [174].

Table A.11: 1G-EPON OPL class

	1000BASE-PX10-U/D		1000BASE-PX20-U/D		1000BASE-PX30-U/D	1000BASE-PX40-U/D
	U [a]	D [a]	U [a]	D [a]		
Min fiber reach	10 km		20 km		20 km	20 km
Min loss	5 dB		10 dB		15 dB	18 dB
Max loss	20 dB	19.5 dB	24 dB	23.5 dB	29 dB	33 dB

[a] The max loss specification is different for the uplink (U) and for the donwlink (D).

The 1G-EPON consists in PON with symmetrical 1 Gbps transmission rate. The minimum split ratio for 1G-EPON is 1:16 increasing to 1:32 or 1:64 depending on the class and the reach distances varies between 10 km and 20 km depending on the class, as can be seen in Table A.11. The wavelength allocation ranges are 1480–1500nm for downlink and 1260–1360nm for uplink band option. The power budgets for 1G-EPON also depends on the class, and they are enlisted on Table A.11. In addition, these power budget classes also defines a set of parameters (mean launch power and receiver sensitivities and maximum average power) enlisted on Table A.12. The required laser on/off timing is 512 ns.

Table A.12: Launch powers, sensitivities and maximum receive power for 1G-EPON classes.

	Min mean launch power	Max mean launch power	Minimum sensitivity	Max mean receive power
1000BASE-PX10-D	-3 dBm	+2 dBm	-24 dBm	-1 dBm
1000BASE-PX20-D	+2 dBm	+7 dBm	-27 dBm	-6 dBm
1000BASE-PX30-D	+3 dBm	+7 dBm	-29.78 dBm	-9.38 dBm
1000BASE-PX40-D	+4 dBm	+10 dBm	-32 dBm	-12 dBm
1000BASE-PX10-U	-1 dBm	+4 dBm	-24 dBm	-3 dBm
1000BASE-PX20-U	-1 dBm	+4 dBm	-24 dBm	-3 dBm
1000BASE-PX30-U	+0.62 dBm	+5.62 dBm	-27 dBm	-8 dBm
1000BASE-PX40-U	+2 dBm	+6 dBm	-30 dBm	-8 dBm

The 1G-EPON protocol is a multipoint control protocol (MPCP), which coordinates the communication between the OLT and ONUs in a shared PON medium, and it is similar to the PtP Ethernet. 1G-EPON upstream works in a burst mode, that is, TDMA. 1G-EPON downstream has a continuous signal stream and clock synchronization and the ONU use a loop timing for the upstream burst mode transmission obtaining the clock from the downstream received signal. The 1G-EPON uses 8B/10B code line (8 data bits encoded as 10 line bits) that produces a DC balanced output and easy clock recovery but it needs to increase the symbol rate to 1.25 Gbps in order to deliver a 1 Gbps of data. The FEC is an optional option and it uses a Reed–Solomon (255,239). If the vendors are interested, 1G-EPON can implement DBA; operations, administration, and maintenance (OAM) sublayer; encryption and protection mechanisms, but it is not specified at the standard.

A.2.2 10G-EPON

The IEEE standardization group standardized a new standard IEEE Standard 802.3av-2009, Physical Layer Specifications and Management Parameters for 10 Gbps Passive Optical Networks (10GEPON) in 2009 [175, 176] . This standard was also amended with the IEEE Standard 802.3bk-2013, Physical Layer Specification and Management Parameters for Extended Ethernet Passive Optical Networks [174] in 2013.

Table A.13: 10G-EPON OPL class

	10GBASE-PR10-U/D [a]	10GBASE-PR20-U/D [a]	10GBASE-PR30-U/D [a]	10GBASE-PR40-U/D [a]
Min fiber reach	10 km	20 km	20 km	20 km
Min loss	5 dB	10 dB	15 dB	18 dB
Max loss	20 dB	24 dB	29 dB	33 dB

[a] The same specification for 10/1GBASE-PRX10/U/D, 10/1GBASE-PRX20/U/D, 10/1GBASE-PRX30/U/D and 10/1GBASE-PRX40/U/D, respectively.

The 10G-EPON standard considers a symmetrical 10G/10G transmission rate PON (class PR) and asymmetrical 10G/1G transmission rate PON (class PRX) with 10 Gbps downlink and 1 Gbps uplink. The power budget for 10G-PON depends on the class, as is shown in Table A.13. The split ratios considered at this standard are 1:16, 1:32 and 1:64 and minimum reach distances of 10 or 20 km depending on the class as shown in Table A.13. The required laser switching timing is 512 ns. The wavelength ranges in order to maintain the coexistence with 1G-EPON are 1260–1280nm for the uplink of 10 Gbps, 1260–1360nm for uplink of 1 Gbps and 1575–1580nm for the downlink. In Table A.14, the set of parameters (mean launch power and receiver sensitivities and maximum average power) of the different classes are enlisted.

The coexistence between 10G-EPON and 1G-EPON in the downlink is solved using WDM multiplexing because their wavelength bands are not overlapped. In the case of the upstream, both standard bands are overlapped and a dual-rate burst receiver and dual rate DBA have to be used, moving all the coexistence issues to the electrical domain. The 10G-EPON protocol is a modified MPCP, which orchestrate the communication between OLT and ONU. The 10G-EPON uses 64B/66B code line, which produces less overhead than the 8B/10B code line of 1G-EPON, and so the symbol rate has to be 10.3125 Gbps for delivering a 10 Gbps of data. In 10G-EPON, the FEC is mandatory and it uses a Reed–Solomon (255,223).

Table A.14: Launch powers, sensitivities and maximum receive power for 10G-EPON classes.

		Min mean launch power	Max mean launch power	Minimum sensitivity	Max average receive power
10 Gbps [a]	10/1GBASE-PRX10-D 10GBASE-PR10-D	+2 dBm	+5 dBm	-24 dBm	-1 dBm
	10/1GBASE-PRX20-D 10GBASE-PR20-D	+5 dBm	+9 dBm	-28 dBm	-6 dBm
	10/1GBASE-PRX30-D 10GBASE-PR30-D	+2 dBm	+5 dBm	-28 dBm	-6 dBm
	10/1GBASE-PRX40-D 10GBASE-PR40-D	+5 dBm	+9 dBm	-29 dBm	-9 dBm
	10/1GBASE-PRX10-U 10GBASE-PR10-U	-1 dBm	+4 dBm	-20.5 dBm	0 dBm
	10/1GBASE-PRX20-U 10GBASE-PR20-U	-1 dBm	+4 dBm	-20.5 dBm	0 dBm
	10/1GBASE-PRX30-U 10GBASE-PR30-U	+4 dBm	+9 dBm	-28.5 dBm	-10 dBm
	10/1GBASE-PRX40-U 10GBASE-PR40-U	+6 dBm	+9 dBm	-29.5 dBm	-9 dBm

[a] The specification of the 1Gbps uplinks are the same than on 1G-EPON (Table A.12)

A.3 Future standard PON

Currently, IEEE and ITU-T are working in the next generation PON or beyond 10 Gbps PON generation. IEEE started the study group in 2014 in order to consider the next EPON standard: IEEE Standard 802.3ca, Next Generation Ethernet Passive Optical Network (NG-EPON) [177, 178] and ITU-T study group has recently published the series G-supplement 64 [179], entitled as PON transmission technologies above 10 Gbps per wavelength. Both study groups are fed from the recent research of the beyond 10 Gbps PON era and are showing the path where the next research should contribute.

The ITU-T future standard, also called 25G/50G/100G-PON, will consider both single wavelength operation with TDM and TDMA and multiwavelength operation with flexible TDM and wavelength allocation. This future standard stablishes symmetrical nominal rates per channel of 25 Gbps, 50 Gbps or higher and asymmetrical nominal rates per channels with 25 Gbps and 50 Gbps for the downstream and 10 Gbps, 25 Gbps and 50 Gbps for the upstream. The NG-EPON standard will consider a multiwavelength EPON with an aggregate capacity of at least 40 Gbps (40G-EPON) in both directions and the possibility of extending the aggregated capacity to 100 Gbps (100G-EPON). Also, a single-wavelength EPON is considered with symmetric rates of at least 25 Gbps (25G-EPON) or a downstream rate of 25 Gbps and an upstream rate of 10 Gbps (25/10G-EPON).

Both standards have to ensure the coexistence with the previous standards. Therefore, the ITU-T future standard has to be compatible with the OPL classes B+, N1, N2, C+ and E1 with a maximum fiber distance of at least 20 km. In addition, it has to be compatible with 1:32 and 1:64 splitting ratios. In the case of the NG-EPON, it has to be compatible with a reach distance of at least 20km and a differential reach of at least 10 km. If the loss budget is a PR10, the split ratio has to be 1:16 and the reach distance has to be at least 10 km. If the loss budget is a PR20, the split ratio has to be 1:32 and the reach distance has to be at least 10 km. If the loss budget is a PR30, the split ratio has to be 1:32 and the reach distance has to be at least 20 km. If the loss budget is a PR40, the split ratio has to be 1:64 and the reach distance has to be at least 20 km. In addition, the coexistence of the NG-EPON with its previous standards will require a triple-rate burst receiver at the OLT depending on the legacy 1G-EPON and 10G-EPON ONUs that could be in the ODN.

Both standards consider to use NRZ as a modulation because it has been the most commonly employed, but also multilevel modulation schemes as electrical duobinary in transmission and reception or only in reception, optical duobinary, PAM-4 or OFDM. In addition, using WS-ODN and WR-ODN as ODN are under consideration.

The wavelength plan for NG-EPON is under discussion and there are four possible plans for the wavelength allocation:

- Plan A: The downstream is placed at 1550-1560 nm (C-band) and the upstream is placed at 1530–1540 nm (C-band).
- Plan B: The downstream is placed at 1480–1500 nm (S-band) and the upstream is placed at 1530–1540 nm (C-band).
- Plan C: The downstream is placed at 1595–1605 nm (L-band) and the upstream is placed at 1530–1540 nm (C-band).
- Plan D: The downstream is placed at 1550–156 0nm (C-band) and the upstream is placed at 1340–1360 nm (O-band).

The wavelength plan of the ITU-T future standards is less developed but also is considering to use different combinations of O-band, S-band, C-band and L-band as in the case of NG-EPON.

Appendix B

Additional published works

B.1 Paper I

1Gbps full-duplex 5GHz frequency slots uDWDM flexible Metro/Access Networks based on VCSEL-RSOA transceiver

J. A. Altabas, D. Izquierdo, J. Lazaro, and I. Garces, "1Gbps full-duplex 5GHz frequency slots uDWDM flexible Metro/Access Networks based on VCSEL-RSOA transceiver," in *2016 OptoElectronics and Communications Conference - International Conference on Photonics in Switching (OECC/PS)*, (Niigata, Japan), pp. WA1–5, 2016

WA1-5 OECC/PS2016

1Gbps Full-Duplex 5GHz Frequency Slots uDWDM Flexible Metro/Access Networks Based on VCSEL-RSOA Transceiver

Jose A. Altabas[1,*], David Izquierdo[1,2], Jose A. Lazaro[3], and Ignacio Garces[1]
[1]Grupo de Tecnologías Fotónicas (GTF), Aragon Institute of Engineering Research (I3A), Universidad de Zaragoza, Mariano Esquillor ed. I+D+i, Zaragoza, 50018, Spain
[2]Centro Universitario de la Defensa (CUD), Academia General Militar, Carretera de Huesca s/n, Zaragoza, 50090,
[3]Grupo de Comunicaciones Ópticas (GCO), Universitat Politècnica de Catalunya, Jordi Girona 31, Barcelona, 08034, Spain
[*]jaltabas@unizar.es

Abstract: *1Gbps full-duplex 5GHz frequency slot is proposed for uDWDM Flexible Metro-Access Networks. The cost-effective ONU transceiver is based on VCSEL as LO for coherent reception and seed for phase-modulated RSOA, providing 40.5dB of power budget.*
Keywords: *Coherent communications; uDWDM; Phase modulation; Vertical Cavity Surface Emitting Lasers*

I. Introduction

New multimedia and cloud services, the deployment of Internet of Things (IoT) and the convergence between optical and wireless communications at the 5G paradigm [1] are pushing up the traffic demand at metro and access optical networks. These networks are converging and evolving to all-optical high-capacity flexible networks as the one shown in Fig. 1. Flexible ultra Dense Wavelength Division Multiplexing (uDWDM) metro-access networks using coherent techniques are being proposed as an efficient solution for this growing demand [2]. These networks require cost-effective devices, including coherent transceivers, for multiplexing several users inside a DWDM channel [3].

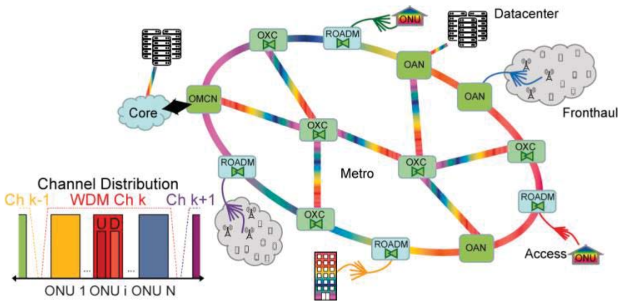

Fig. 1. Flexible 5G Metro-Access Network scenario. OMCN: Optical Metro-Core Node, OAN: Optical Aggregation Node, ROADM: Reconfigurable Optical Add-Drop Node, OXC: Optical Cross-connect, ONU: Optical Network Unit. Inlet: proposed flexible uDWDM full-duplex channel distribution.

In this paper, it is presented a full-duplex 1Gbps flexible uDWDM channel for its use in Passive Optical Networks (PON) implemented in scenarios as the one shown in Fig. 1. This channel is based on a novel cost-effective transceiver used at the Optical Network Unit (ONU) consisting on a Vertical-Cavity Surface-Emitting Laser (VCSEL) and a phase-modulated Reflective Semiconductor Optical Amplifier (RSOA) [3]. The VCSEL is used both as a seed source for the RSOA, and as Local Oscillator (LO) [4] for a single-detector heterodyne receiver. In addition, the downlink generated at the Optical Aggregation Node (OAN) uses an externally modulated laser with Nyquist shaped Differential Binary Phase Shift Keying (DPSK) for addressing the spectral efficiency required on the flexible uDWDM metro-access PON. We will show that the combination of cost-effective devices and spectrally efficient modulation formats allows a full-duplex 1Gbps communication in a 5GHz frequency slot, achieving a distribution of 10 user channels inside a 50GHz WDM ITU-T grid.

II. Setup

The experimental setup is shown in Fig. 2. The ONU transceiver is based on a single low-cost free-running VCSEL. The transmitter uses half of the optical power generated by the VCSEL to seed a RSOA which is directly phase-modulated with a Non Return to Zero (NRZ) DPSK signal. The RSOA phase modulation is achieved by means of its own frequency chirp. The transceiver uses a 2:1 coupler and an isolator to inject the VCSEL seeding light into the RSOA and to couple the resulting modulated signal to the output fiber. The single-detector heterodyne coherent receiver at the ONU uses as LO part of the VCSEL output power (P_{LO}=-5.5dBm). This receiver can be easily upgraded to an independent polarization solution [5]. The input and output at the ONU transceiver are separated using a 50/50 coupler.

The OAN emitter is a 100kHz linewidth external cavity Tunable Laser Source (TLS) which is tuned 2GHz apart from the VCSEL central wavelength. The optical power from the TLS is split to use it as light source for the OAN transmitter and as LO for the coherent receiver (P_{LO} = 0dBm). The downlink is generated by a Mach Zehnder Modulator (MZM) biased at the null transmission point using a Nyquist-shaped DPSK modulation format. The receiver is based on the same single-detector heterodyne configuration used in the ONU. Uplink and downlink at the OAN transceiver port are separated using a circulator. The OAN transmitter can be cost-effectively implemented using a unique external modulator to generate the downlink of several users as shown in [6].

The optical power outputs at both transceivers (ONU and OAN) are -3dBm. The PON has been implemented using 50Km of Standard Single Mode Fiber (SSMF) and a 1:16 distribution splitter to share out the data to the ONUs.

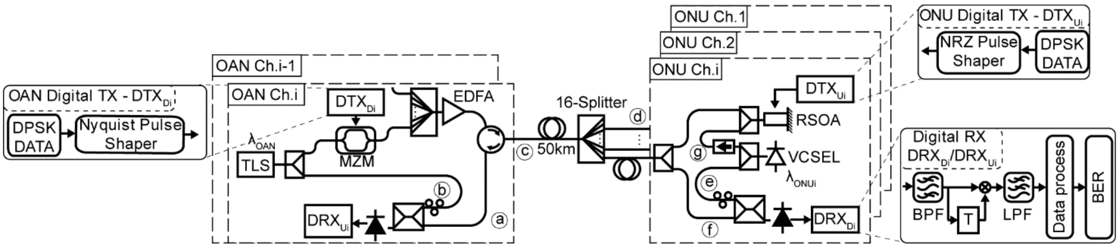

Fig. 2. Experimental setup for the evaluation of the optical link. P_{RX} at (a) and (e) points, P_{LO} at the (b) and (f) points, P_{TX} at (c) and (d) points, P_S at (g) point. (h) VCSEL spectrum

The Digital Transmitters (DTX_{Di}/DTX_{Ui}) are implemented using Mathworks Matlab™ and digitally generated with a 12 GS/s Arbitrary Waveform Generator. The data at both transmitters is encoded differentially to simplify the reception side and reduce the phase noise at the coherent receivers. The OAN DTX_{Di} is based on a raised cosine pulse shaper with 12-symbols length and zero roll-off factor and the ONU DTX_{Ui} encodes the signal with NRZ pulses. The received signals are digitalized at the Digital Receivers (DRX_{Di}/DRX_{Ui}) with a 40GS/s Real Time Oscilloscope with an electrical bandwidth of 2.5GHz. The digitalized received signals are bandpass filtered with a central frequency (f_c) of 2GHz and bandwidth (BW) of 1.5GHz at the ONU and f_c=2.35GHz and BW=2.3GHz at the OAN in order to reduce the noise [7]. Then, the filtered signals are demodulated multiplying them by the previous symbol and filtered with 1.25GHz cut-off frequency lowpass filters.

III. Results

The sensitivity with bidirectional transmission, which is the minimum received power to ensure a BER of $2.2\cdot10^{-3}$ without FEC and 10^{-12} with a 7% overhead FEC [8], is -45dBm for the uplink and -43.5dBm for the downlink, as can be seen in Fig. 3. The resulting power budget for the uplink is 42dB and 40.5dB for the downlink. These power budgets may allow to reach distances higher than 100Km with a 1:16 distribution splitter, or higher than 50Km with splitting ratios greater than 1:128.

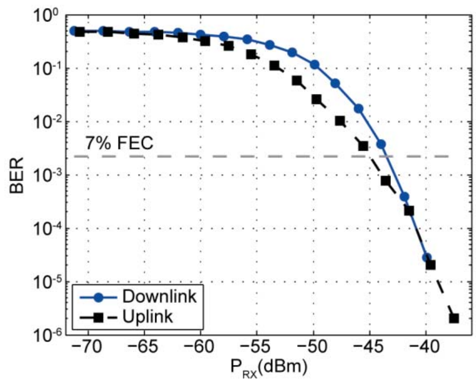

Fig. 3. BER vs received power for downlink and up link with 50Km fiber and bidirectional connection.

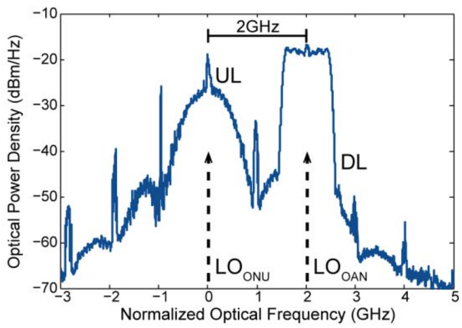

Fig. 4. Optical spectrum for both links of a single user channel and LO position of each link. The central frequency corresponds to the central emission wavelength of the VCSEL (1539.8nm).

The 1Gbps symmetrical channel optical spectrum is shown in Fig. 4 and it was obtained with a High Resolution Complex Optical Spectrum Analyzer (HRCOSA) from Aragon Photonics Labs which also was used for optimizing the RSOA phase modulation. On the center is the RSOA phased modulated uplink (UL) signal and on the right, the Nyquist shaped downlink (DL) signal. The separation between links (UL and DL) at the channel is 2GHz due to the wavelength reuse at the ONU.

The backscattering interference of an adjacent channel downlink with the main channel uplink at the OAN restricts the adjacent downlink central wavelength. As shown in Fig. 5, OAN BER curve, this central wavelength cannot be placed in the ranges from -1GHz to 1.5GHz and from 2.5GHz to 5GHz relative to the VCSEL wavelength. The adjacent channel downlink also interferences with the main channel downlink at the ONU and, as is shown in ONU BER curve at Fig. 5, it cannot be placed either in the range from -2.5GHz to -0.5GHz and from 1.5GHz to 2.5GHz. Thus, the adjacent channel downlink cannot be placed from -2.5GHz to 5GHz relative to the VCSEL wavelength.

The adjacent channel uplink allocation has not to interfere with the main channel uplink at the OAN, and, as is shown in Fig.6, it cannot be placed in the range of -2GHz to 4.5GHz. The backscattering of the adjacent channels uplinks will not interfere with the main channel downlink at the ONU because of the distribution splitter attenuation [7].

Thus, taking into account these measurements, the adjacent channel (Ch.i-1) uplink can be placed at -3GHz and the adjacent channel (Ch.i+1) downlink at 5GHz, when the main channel (Ch.i) downlink is placed at 0GHz and the uplink at 2GHz. These channels distribution results in a channel separation or frequency slot as small as 5GHz, allowing the allocation of 10 user channels inside a 50GHz WDM channel.

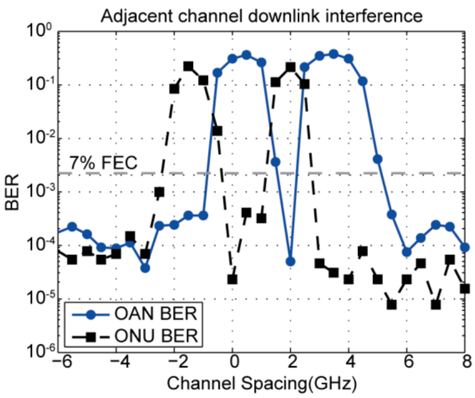

Fig. 5. BER degradation due to the adjacent channel downlink spectral position. Zero frequency corresponds to the VCSEL wavelength

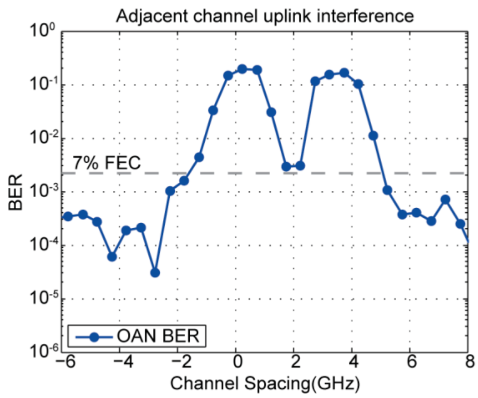

Fig. 6. BER degradation due to the adjacent channel uplink spectral position. Zero frequency corresponds to the VCSEL wavelength

IV. CONCLUSIONS

The performance of cost-effective 1Gbps full-duplex links in uDWDM flexible 5G Metro-Access Networks is shown. The 1Gbps downlink is based on Nyquist-DPSK over a MZM. The 1Gbps uplink consists of NRZ-DPSK directly phase modulated RSOA seeded with a VCSEL. Both receivers are based on single photodiode heterodyne detection with a LO (VCSEL in ONU and TLS in OAN). The power budget is around 40.5dB for bidirectional uDWDM channels for the proposed cost-effective RSOA-VCSEL transceiver and compatible with a record minimum frequency slot of 5GHz. Thus, 10 users can be allocated inside a 50GHz ITU channels and the flexible 5G Metro-Access Network could reach distances greater than 100Km with 1:16 splitter or greater than 50Km with 1:128 splitter.

ACKNOWLEDGMENT

This work was supported in part by the DGA under grant T25, the Spanish MINECO projects muCORE (TEC2013-46917-C2-2-R) and SUNSET (TEC2014-59583-C2-1-R) co-funded by FEDER, Centro Universitario de la Defensa project CUD2013-05: SIRENA and FPU grant from MECD to the first author (FPU 13/00620).

REFERENCES

[1] M. Fiorani, et al., "Challenges for 5G transport networks", in *Proc. ANTS*, New Delhi. India, Dec. 2014, pp. 1-6.
[2] H. Rohde, et al., "Coherent Ultra Dense WDM technology for Next Generation Optical Metro and Access Networks", J. Lightw. Technol., vol. 32, no. 10, pp. 2041-2052, 2014
[3] J. A. Altabas, et al., "Cost-effective Transceiver based on a RSOA and a VCSEL for Flexible uDWDM Networks", Photonics Technol. Lett. Feb. 2016, accepted
[4] J. B. Jensen, et al., "VCSEL Based Coherent PONs", J. Lightw. Technol., vol. 32, no. 8, pp. 1423-1433, 2014
[5] B. Glance, "Polarization independent coherent optical receiver", *J. Lightw. Technol.*, vol. 5, no. 2, pp. 274-276, 1987.
[6] C. Kottke, et al., "Coherent UDWDM PON with joint subcarrier reception at OLT", *Opt. Express*, vol.22, no. 14, pp.16876-16888, 2014.
[7] J. A. Altabas, et al., "1Gbps full-duplex links for ultra-dense-WDM 6.25GHz frequency slots in optical metro-access networks" Opt. Express, vol. 24, no.1, 555-565, 2016
[8] ITU-T Recommendation, G.975.1 (2004).

B.2 Paper II

1.25-2.5Gbps Cost-Effective Transceiver Based on Directly Phase Modulated VCSEL for Flexible Access Networks

J. A. Altabas, D. Izquierdo, J. A. Lazaro, and I. Garces, "1.25-2.5Gbps cost-effective transceiver based on directly phase modulated VCSEL for flexible access networks," in *2017 Optical Fiber Communications Conference and Exhibition (OFC)*, (Los Angeles, CA, USA), p. Th1K.4, 2017

Th1K.4.pdf OFC 2017 © OSA 2017

1.25-2.5Gbps Cost-Effective Transceiver Based on Directly Phase Modulated VCSEL for Flexible Access Networks

Jose A. Altabas[1], David Izquierdo[1,2], Jose A. Lazaro[3], Ignacio Garces[1]

[1]Aragon Institute of Engineering Research, Universidad de Zaragoza, Mariano Esquillor, ed. I+D+I, E-50018, Zaragoza, Spain
2 Centro Universitario de la Defensa, Academia General Militar, Carretera de Huesca s/n, E-50090, Zaragoza, Spain
3 Universitat Politècnica de Catalunya, Jordi Girona 31, E-08034, Barcelona, Spain
jaltabas@unizar.es

Abstract: A 1.25-2.5Gbps cost-effective transceiver based on DPSK directly phase modulated VCSEL and a heterodyne receiver with a VCSEL as LO is proposed. The proposed transmitter sensitivity is -43.5dBm for 1.25Gbps and -40.5dBm for 2.5Gbps.

OCIS codes: (140.7260) Vertical cavity surface emitting lasers; (060.5060) Phase modulation

1. Introduction

The traffic demand over the access networks is growing exponentially due to new streaming media, cloud computing, Internet of Things (IoT) and the convergence between wireless and optical communications in the new 5G paradigm [1]. Cost-effective Optical Network Units (ONU) have to be developed in order to address the necessities of the new access networks requirements. In the recent years, some cost effective devices have been proposed, using directly phase modulated Reflective Semiconductor Optical Amplifiers (RSOA) [2], Distributed Feedback lasers (DFB) [3] and intensity modulated (IM) Vertical Cavity Surface Emitting Lasers (VCSEL) [4].

In this work, we present a 1.25Gbps and 2.5Gbps low cost ONU transceiver based on Differential Binary Phase-Shift Keying (DPSK) over a directly phase modulated VCSEL as the transmitter and a heterodyne single photodiode receiver with VCSEL as Local Oscillator (LO). VCSELs are potentially the cheapest laser that can be fabricated, so they may reduce the cost of the ONU transmitters.

2. Experimental Setup

Fig. 1 shows the experimental setup used in our work. The proposed ONU transceiver is based on a directly phase modulated VCSEL combined with a testbed Optical Line Termination (OLT). Digital Transmitter (DTX), where the pulse shaper will vary depending on the experiment and Receiver (DRX), which will be different depending on the transmitter modulation, are also shown. We will also use a reference On-Off Keying (OOK) intensity modulated VCSEL (IM VCSEL) as a comparison for the directly phase modulated ONU transmitter.

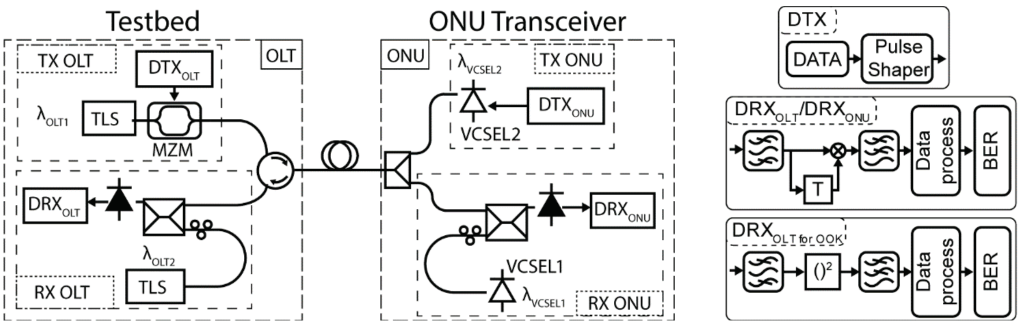

Fig. 1. Experimental setup of the proposed ONU Transceiver based on a directly phase modulated VCSEL TX and a heterodyne RX with a VCSEL as LO. DTX and DRX for the proposed ONU transceiver, the IM VCSEL and the Testbed OLT are also depicted.

The proposed ONU transceiver consists of a directly phase modulated VCSEL as transmitter and a heterodyne receiver with VCSEL as LO. Both VCSELs are from Raycan, exhibiting thermal stabilization, a relatively wide linewidth, higher than 10MHz, and an electrical bandwidth of 4GHz. The transmitter VCSEL is biased to a current of 8mA and emits -1dBm optical power. The wavelength of this VCSEL can be thermally tuned in a range of 5nm allowing the flexible wavelength allocation of the transceiver. The 1.25Gbps and 2.5Gbps DPSK data-streams are encoded and pulse shaped at the Digital Transmitter (DTX). The pulse shaper for the phase modulated transmitter is based on a sharp transition at the start of the symbol and a fast exponential decay in the rest of the symbol. This modulation shape in the input current produces an instantaneous frequency shift at the VCSEL spectrum because of its chirp, causing a rotation of the optical phase of the signal and achieving a directly phase modulation of the optical

978-1-943580-23-1/17/$31.00 ©2017 Optical Society of America

signal. This modulation shape also generates a short residual intensity modulation of the optical signal. The amplitude of the modulation signal has been optimized to obtain a phase rotation of π radians. The DTX for the reference ONU, based on an IM VCSEL, uses a NRZ pulse shaper, and the DTX of the testbed OLT uses a Nyquist pulse shaper combined with DPSK modulation at the MZM. All these signals are digitally generated at 12GSa/s using an Arbitrary Waveform Generator (AWG).

The proposed ONU receiver is based on single photodetector heterodyne detection with a VCSEL as LO, as can be seen in Fig. 1. The receiver VCSEL is biased to 9.5mA and emits -0.14dBm. The LO and the signal are coupled at the photodiode using an optical coupler and a polarization controller. These heterodyne receivers are easily upgradeable to a polarization insensible heterodyne receiver [5]. The LO used in the testbed receiver is an external cavity laser (ECL) with a linewidth smaller than 100kHz adjusted to the same emitting power of -0.14dBm. The wavelength of the LO is tuned 2.5 GHz away from this of the transmitter in the 1.25Gbps case and 5GHz in the case of the 2.5Gbps.

The received signal is amplified and then digitalized with a 40GSa/s Digital Signal Oscilloscope. The DRX for the digitalized signal is, first, a bandpass FIR filter in order to eliminate the possible adjacent channels and reduce the noise. The filtered signal is then multiplied by itself delayed one symbol in case of the DPSK modulation and squared in case of the IM modulation. Finally the signal is lowpass filtered with FIR filter to obtain the transmitted data, as shown in Fig 1.

3. Results

The sensitivity has been defined as the minimum received power with a maximum BER of $2.2 \cdot 10^{-3}$. This is the BER limit recommended by ITU-T G.975.1[6] to ensure 10^{-12} BER using a 7% overhead FEC. The sensitivity of the proposed directly phase modulated VCSEL transmitter with the testbed heterodyne receiver has been measured and compared with the case of IM VCSEL transmitter as reference, as can be seen in Fig. 2. In addition, the power penalty of using a cost-effective VCSEL as LO instead of using ECL in the heterodyne receiver is shown in Fig. 3.

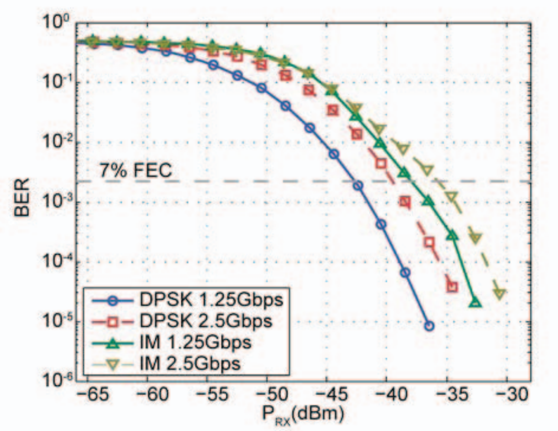

Fig. 2. BER versus received power for the proposed transmitter (DPSK directly phase modulated VCSEL) and the reference transmitter (IM VCSEL), for 1.25Gbps (solid) and 2.5Gbps (dashed).

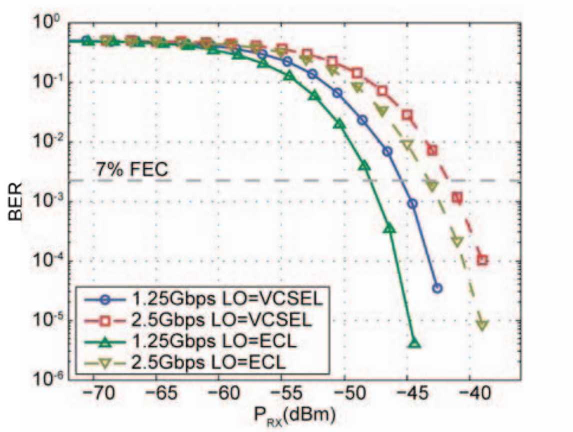

Fig. 3. BER versus received power for the receiver using the proposed VCSEL as LO and the reference ECL as LO, for 1.25Gbps (solid line) and 2.5Gbps (dashed line).

Fig.2 shows that the sensitivity of the proposed directly phase modulate VCSEL transmitter is -43.5dBm with a rate of 1.25Gbps and -40.5dBm with a rate of 2.5Gbps. The sensitivity reference IM VCSEL transmitter is -38dBm for the rate of 1.25Gbps and -35.5dBm for the rate of 2.5Gbps. Thus, the penalty of using a common IM VCSEL with heterodyne reception instead of the using the proposed directly phase modulated VCSEL with heterodyne reception is 5.5dB in the case of a rate of 1.25Gbps and 5dB in the case of a rate of 2.5Gbps. Therefore, the proposed transmitter allows increasing the power budget of the link.

The sensitivity of the testbed generated Nyquist-DPSK using the VCSEL as LO in the heterodyne receiver of the ONU transceiver is -48dBm for 1.25Gbps and -43.5dBm for 2.5Gbps, as can be seen in Fig. 3. If the LO is an ECL, the sensibility for 1.25Gbps is -45.5dBm, and -41.5dBm for 2.5Gbps. Thus, the power penalty of using a VCSEL instead of an ECL is 2.5dB for 1.25Gbps and 2dB for 2.5Gbps. This power penalty is small and admissible due to the cost reduction of using a VCSEL instead of an ECL.

Fig.4 shows the optical spectra of the NRZ-DPSK implemented with our directly phase modulated VCSEL, the NRZ-IM over a VCSEL and the Nyquist-DPSK over a MZM. Fig. 5 shows obtain the optical phase eye diagram and the IQ diagram of the NRZ-DPSK over our directly phase modulated VCSEL. These results have been obtained using a High Resolution Complex Optical Spectrum Analyzer (HRCOSA).

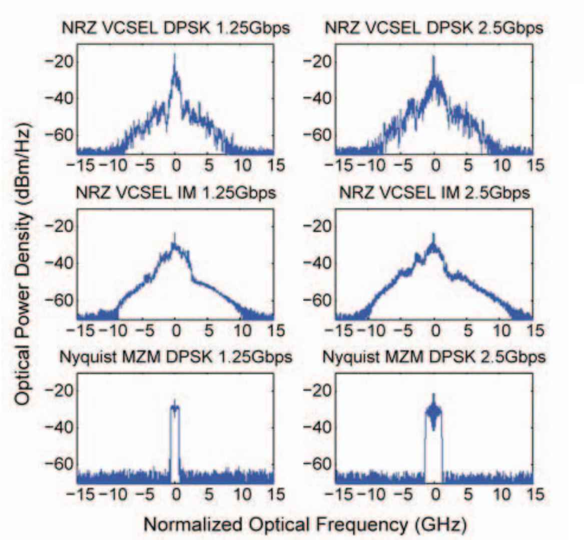

Fig. 4. Optical Spectra for NRZ-DPSK directly phase modulated VCSEL (top), for NRZ-IM VCSEL (middle) and Nyquist-DPSK MZM (bottom); for 1.25Gbps (left) and for 2.5Gbps (right). The central frequency corresponds to 1539.84nm

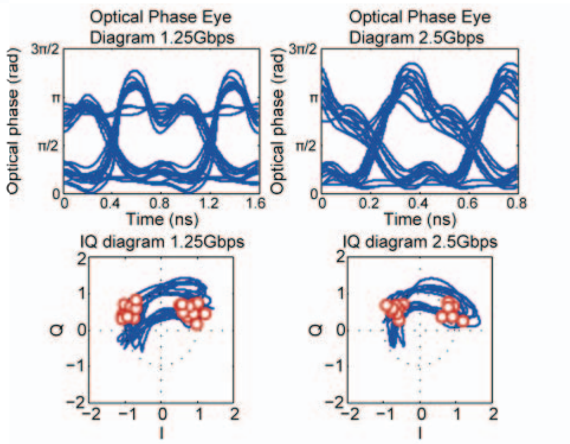

Fig. 5. Directly phase modulated VCSEL optical phase eye diagram (top) and optical IQ diagram (bottom); for 1.25Gbps (left) and for 2.5Gbps (rigth).

The directly phase modulated VCSEL spectra shows a clear NRZ shape for both 1.25Gbps and 2.5Gbps rates where the secondary lobes are attenuated due to the electrical bandwidth of the VCSEL. The IM VCSEL spectra at both rates have been broadened and distorted because of the laser chirp. Therefore, the IM VCSEL transceiver requires more optical spectrum than the directly phase modulated VCSEL in order to stablish a communication without crosstalk. The Nyquist-DPSK over a MZM, employed as the input signal at the ONU heterodyne receiver, shows the typical rectangular spectra of this kind of modulation.

The optical phase eye diagram confirms the π radians rotation between the symbols. The optical IQ diagram shows the VCSEL continuous phase modulation because the symbols transitions do not cross the IQ diagram origin and some residual amplitude modulation because these transitions do not lay on the amplitude constant circle.

4. Conclusion

This paper presents a 1.25Gbps-2.5Gbps flexible and cost effective ONU transceiver based on DPSK directly phase modulated VCSEL transmitter and heterodyne receiver with a VCSEL as LO. The VCSEL transmitter presents a sensitivity of -43.5dBm for 1.25Gbps and -40.5dBm for 2.5Gbps using a single photodiode heterodyne receiver. The DPSK directly phase modulated VCSEL transmitter sensitivity has an improvement of 5-5.5dB compared with an IM VCSEL with the same type of receiver. The receiver uses a VCSEL as LO instead of ECL with just a 2-2.5dB of power penalty. In addition, the optical spectrum, the optical phase eye diagram and the optical IQ diagram of the transmitted signal show that a DPSK directly phase modulated VCSEL link can be obtained and presents a more compact spectrum than an IM modulated VCSEL one.

5. References

[1] M. Fiorani, P. Monti, B. Skubic, J. Martensson, L. Valcarenghi, P. Castoldi, and L. Wosinska, “Challenges for 5G transport networks,” in 2014 IEEE International Conference on Advanced Networks and Telecommunications Systems (ANTS), New Delhi (2014), pp. 1-6.
[2] H. K. Shim, H. Mu, U. H. Hong, and Y. C. Chung, "A practical 10-Gb/s ultra-dense WDM PON", in 2014 OptoElectronics and Communication Conference and Australian Conference on Optical Fibre Technology, Melbourne (2014), pp. 289-290.
[3] R. S. Vodhanel, A. F. Elrefaie, M. Z. Iqbal, R. E. Wagner, J. L. Gimlett, and S. Tsuji, “Performance of directly modulated DFB lasers in 10-Gb/s ASK, FSK, and DPSK lightwave systems,” Journal of Lightwave Technology, Vol. 8, no. 9, pp. 1379–1386 (1990).
[4] J. B. Jensen, R. Rodes, A. Caballero, N. Cheng, D. Zibar, and I. T. Monroy, "VCSEL based coherent PONs," Journal of Lightwave Technology, Vol. 32, no. 8, pp. 1423-1433 (2014).
[5] B. Glance, "Polarization independent coherent optical receiver," Journal of Lightwave Technology, Vol. 5, no. 2, pp. 274-276, (1987).
[6] ITU-T Recommendation, G.975.1 (2004).

Appendix C

Description of Compendium Articles

1. J. A. Altabas, D. Izquierdo, J. A. Lazaro, A. Lerin, F. Sotelo, and I. Garces, "1Gbps full-duplex links for ultra-dense-WDM 6.25GHz frequency slots in optical metro-access networks," *Optics Express*, vol. 24, no. 1, pp. 555–565, 2016

   - Impact factor: 3.307 (2016)
   - Thematic area: OPTICS
   - Authors contribution: The contribution of the PhD student consists of the generation of the idea. The PhD student also worked on the design of the directly phase modulation of a DFB in collaboration with D. Izquierdo and supported by A. Lerin. After that, the PhD student, in collaboration with D. Izquierdo and F. Sotelo, designed and performed the experiments that allow to validate the direct phase modulation of the DFB and its integration in a bidirectional link. Later, the PhD student, in collaboration with D. Izquierdo, J. A. Lazaro and I. Garces, processed the results to obtain the optimum uplink and downlink position and extracted the conclusions. Finally, the PhD student wrote the article in collaboration with the rest of the authors.

2. J. A. Altabas, D. Izquierdo, J. A. Lazaro, and I. Garces, "Cost-Effective Transceiver Based on an RSOA and a VCSEL for Flexible uDWDM Networks," *IEEE Photonics Technology Letters*, vol. 28, no. 10, pp. 1111–1114, 2016

   - Impact factor: 2.375 (2016)
   - Thematic area: ENGINEERING, ELECTRICAL & ELECTRONIC; OPTICS; PHYSICS, APPLIED
   - Authors contribution: The contribution of the PhD student consists of the generation of the idea in collaboration with the rest of the authors. The PhD student also worked on the design of the directly phase modulation of a RSOA pumped by a VCSEL and the reuse of the VCSEL as LO in collaboration with D. Izquierdo. After

that, the PhD student, in collaboration with D. Izquierdo, designed and performed the experiments that allow to validate the direct phase modulation of the RSOA and its integration in a bidirectional link. Later, the PhD student, in collaboration with D. Izquierdo, J. A. Lazaro and I. Garces, processed the results to obtain the optimum uplink and downlink position and extracted the conclusions. Finally, the PhD student wrote the article in collaboration with the rest of the authors.

3. J. A. Altabas, D. Izquierdo, J. A. Lazaro, and I. Garces, "Chirp-based direct phase modulation of VCSELs for cost-effective transceivers," *Optics Letters*, vol. 42, no. 3, pp. 583–586, 2017

    - Impact factor: 3.589 (2017)
    - Thematic area: OPTICS
    - Authors contribution: The contribution of the PhD student consists of the generation of the idea in collaboration with the rest of the authors. The PhD student also worked on the design of the directly phase modulation of a VCSEL in collaboration with D. Izquierdo. After that, the PhD student, in collaboration with D. Izquierdo, designed and performed the experiments that allow to validate the direct phase modulation of the VCSEL and its integration in a bidirectional link. Later, the PhD student, in collaboration with D. Izquierdo, J. A. Lazaro and I. Garces, processed the results to obtain the optimum uplink and downlink position and extracted the conclusions. Finally, the PhD student wrote the article in collaboration with the rest of the authors.

4. J. A. Altabas, G. Silva Valdecasa, L. F. Suhr, M. Didriksen, J. A. Lazaro, I. Garces, I. Tafur Monroy, A. T. Clausen, and J. B. Jensen, "Real-Time 10 Gbps Polarization Independent Quasicoherent Receiver for NG-PON2 Access Networks," *Journal of Lightwave Technology*, vol. 37, no. 2, pp. 651–656, 2019

    - Impact factor: 3.652 (2017*) *2019 JCR impact factor has not been published yet
    - Thematic area: ENGINEERING, ELECTRICAL & ELECTRONIC; OPTICS; TELECOMMUNICATIONS
    - Authors contribution: The contribution of the PhD student consists of the generation of the idea in collaboration with the rest of the authors. After that, the PhD student designed and performed the experiments that allow to validate the quasicoherent receiver. Later, the PhD student, in collaboration with J. B. Jensen, processed the

results to obtain the optimum uplink and downlink position and extracted the conclusions. Finally, the PhD student wrote the article in collaboration with the rest of the authors.

5. J. A. Altabas, L. F. Suhr, G. Silva Valdecasa, J. A. Lazaro, I. Garces, J. B. Jensen, and A. T. Clausen, "25Gbps Quasicoherent Receiver for Beyond NG-PON2 Access Networks," in *2018 European Conference on Optical Communication (ECOC)*, (Rome, Italy), p. We2.70, 2018

    - Impact factor: Conference contribution
    - Thematic area: Conference contribution
    - Authors contribution: The contribution of the PhD student consists of the generation of the idea in collaboration with the rest of the authors. After that, the PhD student designed and performed the experiments that allow to validate the quasicoherent receiver in colaboration with L. F. Suhr. Later, the PhD student, in collaboration with L. F. Suhr and J. B. Jensen, processed the results to obtain the optimum uplink and downlink position and extracted the conclusions. Finally, the PhD student wrote the article in collaboration with the rest of the authors.